Intracellular delivery of RNA therapeutics with lipid nanoparticles

Erik Oude Blenke

The printing of this thesis was financially supported by:

Utrecht Insitute for Pharmaceutical Sciences (UIPS), Utrecht, The Netherlands

Lipoid GmbH, Ludwigshafen, Germany

Intracellular delivery of RNA therapeutics with lipid nanoparticles
Erik Oude Blenke

Department of Pharmaceutics, Utrecht Institute for Pharmaceutical Sciences (UIPS), Faculty of Science, University of Utrecht, Netherlands

ISBN: 978-94-6295-582-0

Cover
Installation 'Forest of Light', by British artist Bruce Munro. Picture by Branden Camp. Exhibition in Atlanta Botanical Garden, GA, USA. 2015

Lay-out
Erik Oude Blenke

Printed by
Proefschriftmaken.nl || Uitgeverij BoxPress

© Erik Oude Blenke, 2017

The research leading to this thesis has received support from the Innovative Medicines Initiative Joint Undertaking under grant agreement n° 115363 resources of which are composed of financial contribution from the European Union's Seventh Framework Programme (FP7/2007-2013) and EFPIA companies' in kind contribution.

Intracellular delivery of RNA therapeutics with lipid nanoparticles

Intracellulaire afgifte van RNA therapeutica met behulp van lipide nanodeeltjes

(met een samenvatting in het Nederlands)

Proefschrift

ter verkrijging van de graad van doctor aan de Universiteit Utrecht op gezag van de rector magnificus, prof.dr. G.J. van der Zwaan, ingevolge het besluit van het college voor promoties in het openbaar te verdedigen op woensdag 25 januari 2017 des middags te 2.30 uur

door

Erik Oude Blenke

geboren op 31 oktober 1987

te Eindhoven

Promotor:
Prof. dr. G. Storm

Copromotoren:
Dr. E. Mastrobattista
Dr. N.I. Martin

**“A person’s character isn’t determined by how he or she enjoys victory,
but rather how he or she endures defeat.” - *House of Cards***

Table of contents

Chapter 1

General Introduction

RNA interference and RNAi therapeutics

RNA interference (RNAi) exploits the endogenous microRNA (miRNA) pathway by introducing short RNA molecules that induce highly specific silencing of protein expression by degradation of its messenger RNA (mRNA). Sequence homology allows for the highly specific targeting and cleavage of complementary mRNA in the cytoplasm of the cell, inhibiting protein expression. By simply changing the target sequence, virtually every protein can be silenced, with the only exception maybe of those proteins that are involved in the miRNA pathway itself. RNAi has proven to be a valuable research tool and has helped to elucidate the role and function of many genes and pathways and validate many drug targets, by systematically knocking down single genes and studying the subsequent effects. Also, the finding that RNA molecules are not merely the dogmatic step between DNA and protein, but are in fact important regulators of gene expression, has fundamentally changed our understanding of the genome, disease and evolution. For this discovery Andrew Fire and Craig Mello were awarded the 2006 Nobel Prize in Physiology or Medicine, already eight years after their initial publication [1].

The field has moved rapidly since then and one of the most captivating directions is the application of RNAi to treat human disease. In theory, every gene and thereby protein can be silenced, including the previously 'undruggable' ones. The sequence homology based silencing promised high specificity and low off-target effects and treatment could even be personalized to patient-specific mutations. In the early days, it was considered a one-size-fits-all treatment, where only the target sequence had to be changed to treat any disease or patient. Unfortunately though, RNA therapeutics are the typical 'nightmare example' of a macromolecular drug that has high potential but is extremely difficult to deliver, due to their large size and the many negative charges.

By far the most important class of RNAi therapeutics are siRNAs, double stranded RNA (dsRNA) molecules that typically consist of 21 base pairs. Through their complete homology to the target gene, they activate the formation of the RNA induced silencing complex (RISC) in the cytosol to degrade the corresponding host mRNA, resulting in inhibition of transcription [2]. See Figure 1.1. Only the guide strand is loaded into the RISC while the other, the passenger strand is degraded, but it was shown by Fire and Mello that the RNAi effect is substantially potentiated if dsRNA is administered instead of the anti-sense guide strand alone. From an evolutionary point, this is likely because dsRNA signals viral presence which requires a potent inactivating response [3]. However, recent advances demonstrated that with chemical modifications to the backbone, the potency of single stranded siRNAs (ss-siRNAs) can be increased a 100-fold to also induce complete target degradation by the RISC [4,5].

MicroRNAs are the naturally occurring dsRNA activators of the miRNA pathway that are transcribed from the genome in the nucleus. After being transferred to the cytosol, they are processed in the same way as siRNAs and also loaded into the RISC. However, because they have incomplete homology with the target mRNA, they only cause the RISC to temporarily repress the target rather than degrading it.

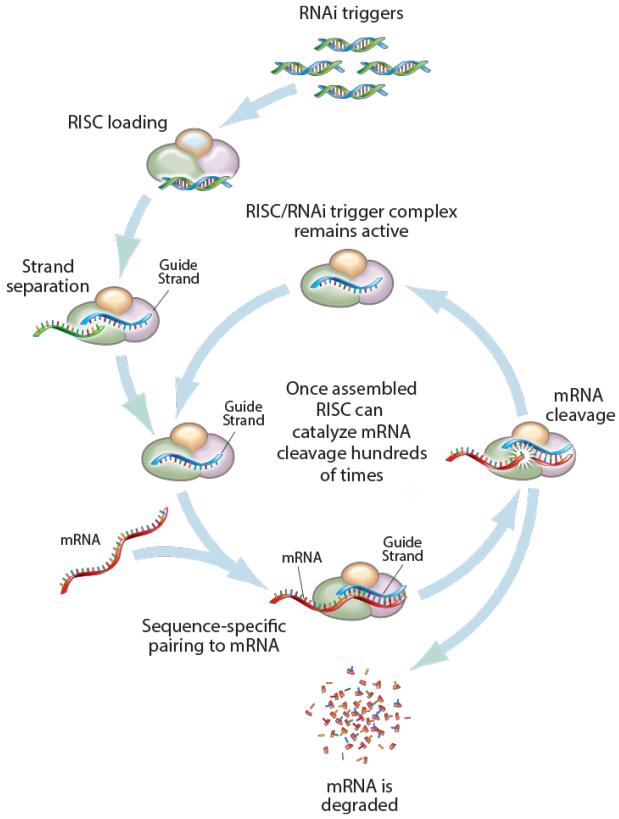

Figure 1.1 | Schematic representation of RNA interference with siRNAs
After introduction into the cytosol of the target cell, the double stranded siRNA is loaded into the RNA induced silencing complex (RISC) . Once loaded in the RISC, the 'passenger strand' is degraded and only the guide strand that has complementarity with the target sequence is used to hybridize with the target mRNA. This induces degradation of the mRNA and a single siRNA molecule can catalyze cleavage of hundreds to thousands of mRNA molecules. Almost every mRNA sequence can be targeted, by simply changing the sequence of the siRNA. Figure reproduced from http://arrowheadpharma.com/science/

From an evolutionary point of view, this process was likely put into place as a mechanism to fine-tune the expression of endogenous mRNAs. Alterations in this process can lead to disease and many disease phenotypes have an underlying cause in miRNA dysregulation. Interestingly, depending on the disease, miRNAs can be either the target for e.g. an siRNA or anti-miR to silence it, or be the therapeutic modality itself to restore the function, as it was found that both the over- as well as the under-expression of certain miRNAs can lead to disease [6,7].

Another class of RNAs that are now also emerging as RNA therapeutics are short antisense oligonucleotides (ASOs), which consist of only a single antisense strand. They also sterically block the target gene in a sequence dependent manner, but have a much broader range of effects, such as guiding cellular machinery to pre-mRNA or mRNA to direct alternative splicing or to fine-tune protein expression using other pathways than the miRNA pathway [8,9].

The attractive feature of RNA-like drug molecules, is that all RNAi triggers are structurally the same and that the sequence can be changed without significantly altering their physicochemical properties, pharmacokinetics and biodistribution profile. Endogenous mRNAs and miRNAs can also be used as therapeutics, but these are much larger than siRNAs and ASOs and may have therefore even lower access to their intracellular site of action.

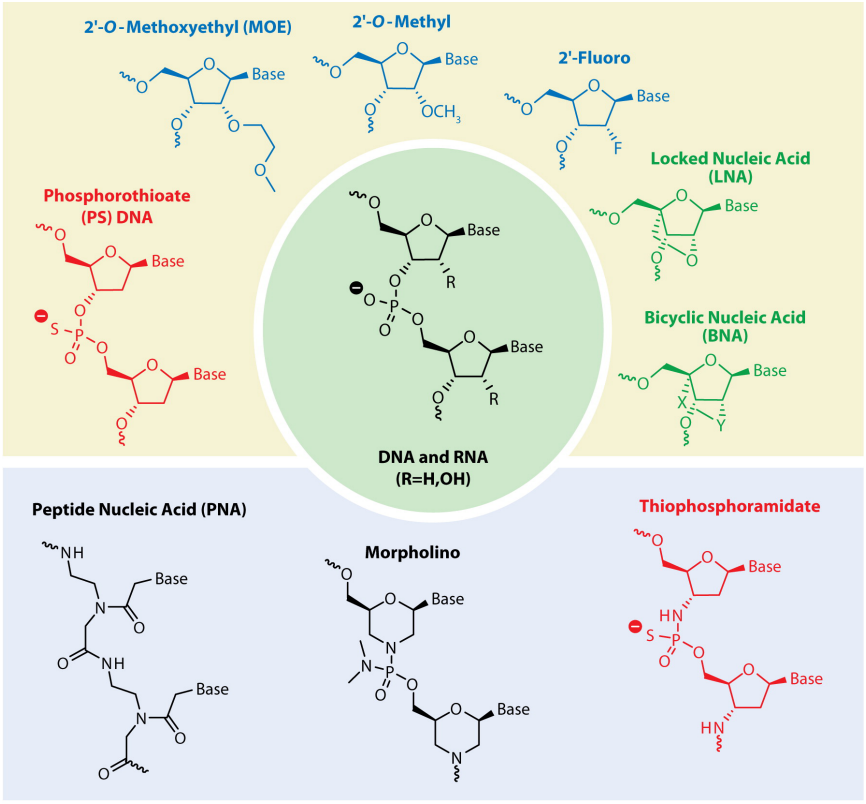

Figure 1.2 | Common RNA backbone modifications
The RNA backbone can be modified at the 2'O position of the ribose moiety or by changing the bonds between the nucleosides. All modifications aim to make the molecule more stable and resistant to nucleases, but the position of the modification within the RNA molecule is important, as it can also inhibit its function in silencing complexes such as the RISC. Figure reproduced from REF. [9].

Apart from their large size and high negative charge, RNA molecules have the unfavorable characteristic of being susceptible to degradation by nucleases in the bloodstream and their half-life after intravenous administration is only a few minutes [9,10]. Furthermore, administration of dsRNA can stimulate the innate immune system and induce an inflammatory interferon response [3]. Chemical modifications to the backbone of short RNAs can improve their enzymatic resistance and reduce immunogenicity. Common modifications include 2'-O-methyl or 2'-fluoro substitutions and the use of phosphorothioate bonds instead of the natural phosphodiester (see Figure 1.2) [3,9,10]. Although ribose modifications increase the stability, it was found

that the position of the modification within the RNA molecule is important, as it may also lead to loss of function because the molecule is no longer recognized by e.g. the RISC. Furthermore, some modifications may induce other, non-specific off-target effects [10]. Phosphorothioate bonds enhance the resistance against nucleases and induce serum protein binding after intravenous administration. This inhibits the rapid renal excretion of the siRNA but still, only very few of the modifications have significantly improved target cell penetration [10,11]. An exception to this rule is the work by Steven Dowdy's lab where siRNAs were reversibly charge-neutralized to increase circulation time and stability, although a targeting ligand was still needed to promote more efficient cellular uptake [12]. So in general, RNA molecules require delivery technology to increase cellular uptake and transport to their intracellular site of action [11,13].

Delivery technology

Delivery systems for systemic administration of RNA therapeutics have been subject of investigation for decades now. Including the efforts on plasmid DNA delivery in the early days, there is more than thirty years of literature [14,15]. The approach over these thirty years has been fairly common, as will be briefly outlined here. In nature, viruses are very efficient in delivering their genomes and viral vectors are in fact also very capable of delivering RNA constructs, but are generally regarded as immunogenic and less safe than their non-viral counterparts. Therefore, non-viral vectors of anywhere between 20-500nm are made, typically composed of materials that are biodegradable. For the delivery of nucleic acids, (ionizable) cationically charged materials are ideal, because they can complex with the negative charges on the RNAs. It appears that there is no further prerequisite to the kind of material to serve as RNA carrier in experimental nanomedicine, as long as it can be complexed in 'nano' particles. Lipid-based carrier materials are the oldest and most widely used ones (often referred to as lipoplexes) but also the field of biodegradable polymers has recently expanded rapidly into the direction of nanomedicine (often termed polyplexes). Such nanoparticles protect the RNA cargo from degradation in the bloodstream and should eventually help it to cross the plasma membrane of the target cell. This approach usually increases the circulation time of the RNA therapeutics, but the consequence is that the biodistribution is now also determined by the nanoparticle it is encapsulated in. A nanoparticle is typically >1000x larger than a siRNA molecule [12] which highly limits its penetration beyond the bloodstream. Nanoparticles can only extravasate in tissues with increased vascular permeability, such as diseased or inflamed tissue [16]. In healthy tissue, increased permeability is only seen in those organs that have the function of screening the blood for foreign substances and materials, resulting in rapid clearance of the nanoparticles by macrophages in the liver and spleen. To avoid rapid clearance, the particles are usually covered with a hydrophilic polymer, most often poly-ethylene glycol (PEG) that 'shields' the surface of the particles. The relatively large size of the particle also means that uptake into the target cell has to occur through a process called 'endocytosis', as direct diffusion through the cell membrane is even less likely than for 'naked' RNA. To facilitate endocytosis, delivery systems are often equipped with targeting ligands that bind to receptors or other surface molecules that are specific for the intended target cell and are then taken up by receptor-mediated endocytosis [11,13].

Endocytosed delivery systems accumulate in subcellular organelles called endosomes. Endosomes are sorting organelles that recognize foreign material and excrete it again, or degrade it by transferring it to lysosomes that have a highly acidic and hydrolytic environment. Biological drugs, like RNA therapeutics are extremely vulnerable to degradation in the endolysosomal pathway. Because of this, escape from the endosomes is an even more significant challenge to intracellular delivery than crossing the cell membrane, as will be discussed later.

To summarize thirty years of literature, delivery systems for RNA therapeutics typically consist of *at least one* of the following components: a cationic material, a hydrophilic polymer (often PEG) and a targeting moiety. For RNA therapeutics several types of delivery systems are currently tested in the clinic, ordered from low to high complexity and size: naked modified siRNA, siRNA-GalNAc conjugates, Dynamic PolyConjugates (DPCs) and lipid nanoparticles (LNPs). The naked siRNAs are listed here because the heavy backbone modifications certainly classify as delivery *technology*, but they are administered directly into the bloodstream, without any of the carrier components mentioned above. GalNAc-conjugates also consist of chemically modified siRNAs, that are resistant to degradation when administered naked but are covalently conjugated to a targeting ligand. Each conjugate consists of a single siRNA molecule that is coupled to a triantennary GalNAc, a well characterized galactoside ligand for the asialoglycoprotein receptor (ASGPR) expressed by hepatocytes [17]. (See Figure 1.3) This approach is therefore limited to liver indications. The high binding affinity to the receptor and the good perfusion of the liver result in high uptake of the conjugate and potent silencing of hepatocyte target genes [18]. Alnylam Pharmaceuticals currently has multiple drug candidates based on this conjugate in clinical trials. While treating diseases with the cause in other tissues than the liver is still a challenge, this hepatocyte delivery approach helps to build a pipeline and may generate some profits to fund the ongoing R&D to reach extra-hepatic targets. The simple structure of these conjugates allows solid phase synthesis that is cheap and reproducible, making this an attractive platform technology [19,20].

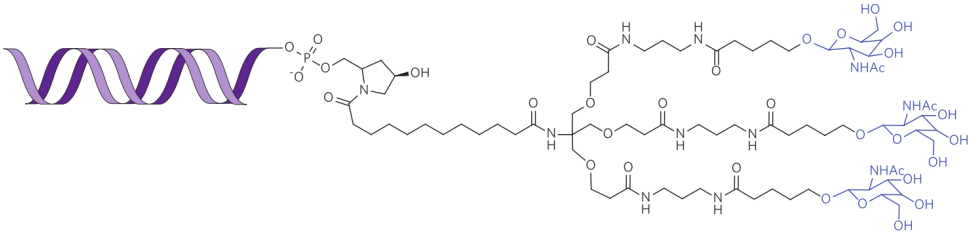

Figure 1.3 | GalNAc–siRNA conjugates
Structure of the triantennary GalNAc–siRNA conjugate used in several drug candidates. Modifications are made on the 3' end of the passenger strand, which will be degraded and not loaded into the RISC. Newer iterations of the conjugates have a linear structure that is easier to synthesize without losing the trivalent orientation of the ligands. Figure reproduced from REF. [11].

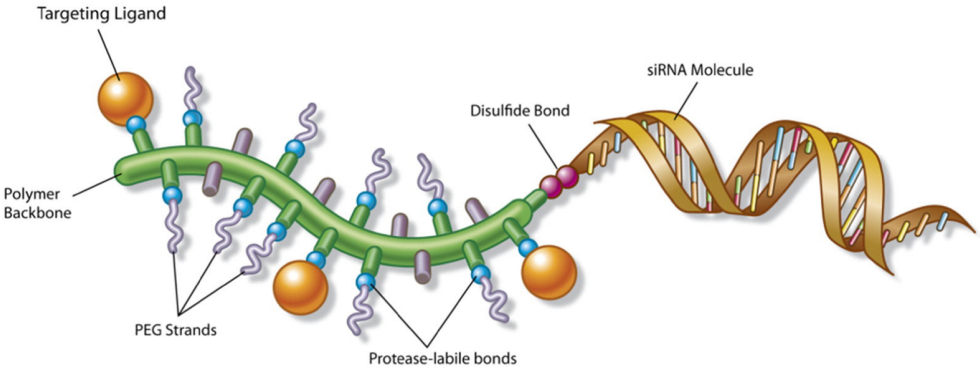

Figure 1.4 | Dynamic PolyConjugates. Schematic representation of a DPC
The endosomolytic polymer backbone is masked with PEG strands and targeting ligands, with bonds that are reversible in the endosomes; recent optimizations use protease-labile bonds that are specific to the endosome, while earlier generations use acid-labile maleamate bonds. The siRNA molecule is linked to the backbone with a disulfide bond, which should be cleaved when the construct reaches the cytosol. Figure reproduced from REF. [21].

Dynamic PolyConjugates (DPCs) are a different class of slightly more complex conjugates. Their application is not as widespread as the other described technologies, but they possess some interesting features that could also be applied to other delivery systems. DPCs are slightly larger than GalNAc-conjugates (20nm) but still structurally well-defined [21]. DPCs consist of a siRNA (reversibly) conjugated to a polymeric endosomolytic agent, the cationic polymer PBAVE (poly-butyl-amino-vinylether). The positive charges on the amines of the polymer are shielded with PEG and targeting ligands, using acid-labile maleamate linkages to unmask the endosomolytic properties once it reaches the acidic environment of the endosome [22,23]. These systems are currently also targeted to the liver with GalNAc ligands. The 'dynamic' chemistry allows functionalization with additional endosomolytic agents such as melittin, or other ligands targeting e.g. integrin α5β3 on endothelial cells, making DPCs a versatile technology that could potentially also reach extrahepatic targets. [24]. More recently, protease-sensitive unmasking of the membrane interactive polymer was described, that should increase the stability during storage and in the circulation [21]. See Figure 1.4. A DPC formulation called ARC-520 is currently tested in phase II trials for Hepatitis B (liver indication) sponsored by Arrowhead Research Corporation [25,26].

Lipid nanoparticles (LNPs) are amongst the earliest nanoparticles studied and were initially investigated for the delivery of plasmid DNA but have now been successfully adapted for the delivery of siRNAs [27]. **LNPs are the focus of this thesis** and their history of development is more elaborately described in **Chapter 2**. In brief, they are composed of mostly synthetic lipids that form spherical particles, encapsulating siRNA in their core. They contain PEG-conjugated lipids and ionizable cationic lipids with an optimized pKa [28]. (Figure 1.5) Depending on the PEG-lipid content, their sizes range from 25-100 nm [29]. Contrary to the conjugates, LNPs contain multiple RNA molecules per particle and deliver significantly more of the cargo once they reach their target site. This can be an advantage for difficult to reach targets. A disadvantage is their

large size compared to the conjugates, which may limit their penetration beyond the bloodstream to tissues with discontinuous endothelium, such as the liver [30]. Suitable alternative targets that are in reach of the circulating LNPs are circulating cells such as the immune cells in the bloodstream, opening up many immunomodulatory applications that could benefit from targeted gene silencing [31].

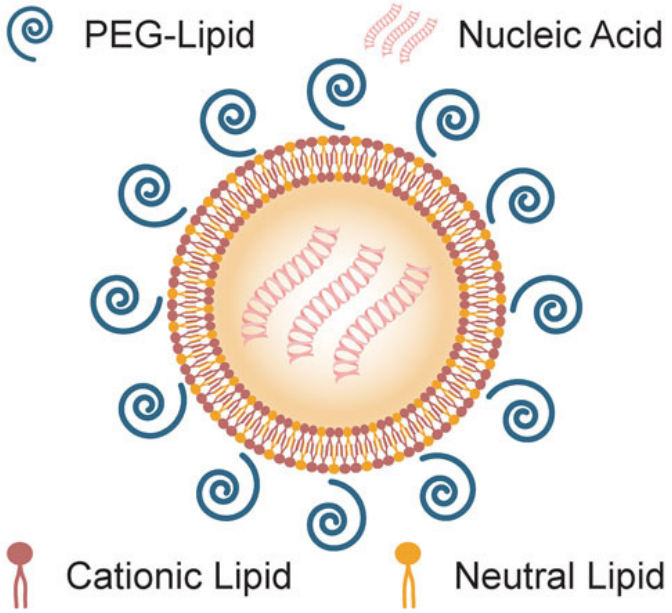

Figure 1.5 | Lipid nanoparticle for siRNA delivery
Schematic representation of a LNP for nucleic acid delivery. The core of the particle contains the negatively charged RNA, complexed with the cationic lipid. Cholesterol is distributed evenly throughout the whole particle. Hydrophilic PEG-lipids are mostly distributed on the surface of the particle. Figure reproduced from REF. [32].

Endosomal escape

As mentioned, RNA therapeutics need adequate delivery technology to get access to the target cell interior. All of the described types of delivery systems are taken up into the cell by endocytosis. Endocytosed molecules or particles are collected in the early endosome, which acts as a sorting and recycling organelle. Early endosomes containing foreign or unrecyclable material mature into late endosomes and fuse with lysosomes, in which the material is degraded by acidification and proteases and nucleases. For small molecule drugs this is not necessarily a problem, as they are often resistant to hydrolysis and enzymatic degradation. However, most macromolecular drugs are highly sensitive to degradation, so it is crucial that they 'escape' from the endosome intact and as early as possible. It is true that chemical modifications have significantly increased the stability of siRNAs and GalNAc-conjugates for instance, rely on the enzymatic resistance of the molecule to survive the endolysosomal environment and eventually reach the cytosol. Recent insights however, have shown that lysosomal degradation is not always the endpoint of endocytosis and that there may be more

reasons to escape the endosome as early as possible. Two separate studies followed the intracellular trafficking of lipid nanoparticles [33–35] and found that 70% of the internalized dose is readily exocytosed again by recycling pathways [34]. The second study puts a number on the fraction of the total dose that eventually reaches the cytosol, of only 1-2% [35]. This underlines the need for early endosomal escape, even if the drug molecules are resistant to degradation. Unfortunately neither of the studies were able to catch an 'endosomal escape' in the act, which indicates that such events are very rare and that the majority of the dose is either exocytosed or degraded even when a clinical effect is seen (It is estimated that less than 0.1% of the injected dose reaches the cytosol of the hepatocytes [33]). Some drug delivery systems are endowed with endosomal escape mechanisms that respond to the acidic environment of the endosome as a spatiotemporal trigger. Such mechanisms will also be explored in this thesis.

Aim and outline of the thesis

Although LNPs are the clinically most advanced siRNA delivery system, they still have some limitations. First of all, the process by which the siRNA is delivered into the cytosol is inefficient and poorly understood, leaving room for improvement. Secondly, current applications of LNP are limited to diseases with the genetic cause in the hepatocytes. Targeting LNPs beyond the liver still remains a challenge. Therefore, the aim of this thesis is to investigate strategies to improve cytosolic delivery and to adapt LNPs to enable targeting beyond the liver. The 'competing' technologies like DPCs and conjugates apply some interesting concepts that could also be applied to LNPs. This thesis reports several approaches to active targeting and the implementation of an endosomal escape mechanism, similar to that of DPCs.

Chapter 2 provides an overview of the development of LNPs for gene and RNA delivery and describes the role of each of the components. Experimental results demonstrate the importance of cationic lipids and PEG-lipid dissociation on transfection efficiency. If extrahepatic targets are to be reached, the circulation time of the LNP should be extended. Changing the PEG-lipid species and lipid composition can prolong the circulation time and this is the first step to reach other tissues than the liver.

In order to be taken up by specific cell types, the LNPs need to be functionalized with targeting ligands that recognize cell type specific surface molecules. In **Chapter 3**, copper-free "click" chemistry is explored as a means to functionalize liposomes with several azide-containing molecules. The kinetics of this type of chemistry are superior to the gold standard of maleimide-thiol coupling and the bio-orthogonal nature of the reaction allows for site-specific conjugation of ligands.

For accurate comparison of LNPs and RNA nanomedicine formulations in general, the encapsulation efficiency and cargo load have to be properly characterized. It has become clear from the literature that many labs do not measure the amount of RNA associated with the formulation and those labs that do, all have their own methods and protocols. In **Chapter 4** several commonly used quantification methods for siRNA are compared and evaluated.

In **Chapter 5** an artificial ligand-receptor pair is studied, that uses coiled-coil interactions between two short peptide sequences to specifically and avidly bind to each other. Lipid particles are functionalized with one of the peptides while the other peptide is grafted on the surface of the target cells. Interaction of the peptides leads to uptake of the particles and enables functional delivery of two types of model RNA therapeutics.

One approach to enhance endosomal escape is to couple endosomolytic peptides to the surface of LNPs. In **Chapter 6** a different type of click chemistry is used to couple the membranolytic peptide melittin to LNPs, as well as some other types of chemistries to exploit the acidic environment of the endosome as a trigger to release the peptide and facilitate endosomal escape.

As described in this introductory chapter, a lot of efforts have been made to translate the impact of RNA interference from the lab to the clinic but after nearly twenty years of research no products have made it to the market yet. In the meantime, the biomedical field has jumped on another gene editing system that has already made a huge impact in the lab and has equally high potential in the clinic. Many efforts are made to use the CRISPR-Cas9 gene editing system for therapeutic purposes, but to facilitate a smoother transition to the clinic, lessons should be taken from the development of RNA therapeutics. In **Chapter 7** the potential applications and delivery aspects of CRISPR-Cas9 constructs are reviewed, while drawing some parallels with the RNAi field.

In **Chapter 8** the results of this thesis are summarized and further improvements and remaining challenges are discussed.

References

[1] A. Fire, S. Xu, M.K. Montgomery, S.A. Kostas, S.E. Driver, C.C. Mello, Potent and specific genetic interference by double-stranded RNA in Caenorhabditis elegans., Nature. 391 (1998) 806–11. doi:10.1038/35888.

[2] S.M. Elbashir, J. Harborth, W. Lendeckel, A. Yalcin, K. Weber, T. Tuschl, Duplexes of 21 ± nucleotide RNAs mediate RNA interference in cultured mammalian cells., Nature. 411 (2001) 494–498. doi:10.1038/35078107.

[3] K.A. Whitehead, J.E. Dahlman, R.S. Langer, D.G. Anderson, Silencing or stimulation? siRNA delivery and the immune system., Annu. Rev. Chem. Biomol. Eng. 2 (2011) 77–96. doi:10.1146/annurev-chembioeng-061010-114133.

[4] W.F. Lima, T.P. Prakash, H.M. Murray, G.A. Kinberger, W. Li, A.E. Chappell, et al., Single-stranded siRNAs activate RNAi in animals., Cell. 150 (2012) 883–94. doi:10.1016/j.cell.2012.08.014.

[5] D. Yu, H. Pendergraff, J. Liu, H.B. Kordasiewicz, D.W. Cleveland, E.E. Swayze, et al., Single-stranded RNAs use RNAi to potently and allele-selectively inhibit mutant huntingtin expression., Cell. 150 (2012) 895–908. doi:10.1016/j.cell.2012.08.002.

[6] Z. Li, T.M. Rana, Therapeutic targeting of microRNAs: current status and future challenges., Nat. Rev. Drug Discov. 13 (2014) 622–638. doi:10.1038/nrd4359.

[7] S. Lin, R.I. Gregory, MicroRNA biogenesis pathways in cancer., Nat. Rev. Cancer. 15 (2015) 321–333. doi:10.1038/nrc3932.

[8] R. Kole, A.R. Krainer, S. Altman, RNA therapeutics: beyond RNA interference and antisense oligonucleotides., Nat. Rev. Drug Discov. 11 (2012). doi:10.1038/nrd3625.

[9] C.F. Bennett, E.E. Swayze, RNA targeting therapeutics: molecular mechanisms of antisense oligonucleotides as a therapeutic platform., Annu. Rev. Pharmacol. Toxicol. 50 (2010) 259–293. doi:10.1146/annurev.pharmtox.010909.105654.

[10] W. Shen, X.-H. Liang, H. Sun, S.T. Crooke, 2'-Fluoro-modified phosphorothioate oligonucleotide can cause rapid degradation of P54nrb and PSF., Nucleic Acids Res. (2015). doi:10.1093/nar/gkv298.

[11] R. Kanasty, J.R. Dorkin, A. Vegas, D. Anderson, Delivery materials for siRNA therapeutics., Nat. Mater. 12 (2013) 967–77. doi:10.1038/nmat3765.

[12] B.R. Meade, K. Gogoi, A.S. Hamil, C. Palm-Apergi, A. Van Den Berg, J.C. Hagopian, et al., Efficient delivery of RNAi prodrugs containing reversible charge-neutralizing phosphotriester backbone modifications., Nat. Biotechnol. 32 (2014). doi:10.1038/nbt.3078.

[13] H. Yin, R.L. Kanasty, A.A. Eltoukhy, A.J. Vegas, J.R. Dorkin, D.G. Anderson, Non-viral vectors for gene-based therapy., Nat. Rev. Genet. 15 (2014) 541–555. doi:10.1038/nrg3763.

[14] G.Y. Wu, C.H. Wu, Receptor-mediated in vitro gene transformation by a soluble DNA carrier system., J. Biol. Chem. 262 (1987) 4429–32. http://www.ncbi.nlm.nih.gov/pubmed/3558345.

[15] G.Y. Wu, C.H. Wu, Receptor-mediated gene delivery and expression in vivo., J. Biol. Chem. 263 (1988) 14621–14624. doi:10.1016/0014-2999(90)91416-9.

[16] J.W. Nichols, Y.H. Bae, EPR: Evidence and fallacy., J. Control. Release. 190 (2014) 451–64. doi:10.1016/j.jconrel.2014.03.057.

[17] J.U. Baenziger, D. Fiete, Galactose and N-acetylgalactosamine-specific endocytosis of glycopeptides by isolated rat hepatocytes., Cell. 22 (1980) 611–20. doi:10.1016/0092-8674(80)90371-2.

[18] J.K. Nair, J.L.S. Willoughby, A. Chan, K. Charisse, M.R. Alam, Q. Wang, et al., Multivalent N-Acetylgalactosamine-Conjugated siRNA Localizes in Hepatocytes and Elicits Robust RNAi-Mediated Gene Silencing., J. Am. Chem. Soc. 136 (2014) 16958–16961. doi:10.1021/ja505986a.

[19] K.G. Rajeev, J.K. Nair, M. Jayaraman, K. Charisse, N. Taneja, J. O'Shea, et al., Hepatocyte-Specific Delivery of siRNAs Conjugated to Novel Non-nucleosidic Trivalent N-Acetylgalactosamine Elicits Robust Gene Silencing in Vivo., ChemBioChem. 16 (2015) 903–908. doi:10.1002/cbic.201500023.

[20] S. Matsuda, K. Keiser, J.K. Nair, K. Charisse, R.M. Manoharan, P. Kretschmer, et al., siRNA Conjugates Carrying Sequentially Assembled Trivalent N- Acetylgalactosamine Linked Through Nucleosides Elicit Robust Gene Silencing In Vivo in Hepatocytes, ACS Chem. Biol. 10 (2015) 1181–1187. doi:10.1021/cb501028c.

[21] D.B. Rozema, A. V. Blokhin, D.H. Wakefield, J.D. Benson, J.C. Carlson, J.J. Klein, et al., Protease-triggered siRNA delivery vehicles., J. Control. Release. 209 (2015) 57–66. doi:10.1016/j.jconrel.2015.04.012.

[22] D.B. Rozema, K. Ekena, D.L. Lewis, A.G. Loomis, J.A. Wolff, Endosomolysis by masking of a membrane-active agent (EMMA) for cytoplasmic release of macromolecules., Bioconjug. Chem. 14 (2003) 51–57. doi:10.1021/bc0255945.

[23] D.B. Rozema, D.L. Lewis, D.H. Wakefield, S.C. Wong, J.J. Klein, P.L. Roesch, et al., Dynamic PolyConjugates for targeted in vivo delivery of siRNA to hepatocytes., Proc. Natl. Acad. Sci. U. S. A. 104 (2007) 12982–7. doi:10.1073/pnas.0703778104.

[24] C.I. Wooddell, D.B. Rozema, M. Hossbach, M. John, H.L. Hamilton, Q. Chu, et al., Hepatocyte-targeted RNAi therapeutics for the treatment of chronic hepatitis B virus infection., Mol. Ther. 21 (2013) 973–85. doi:10.1038/mt.2013.31.

[25] S.C. Wong, J.J. Klein, H.L. Hamilton, Q. Chu, C.L. Frey, V.S. Trubetskoy, et al., Co-injection of a targeted, reversibly masked endosomolytic polymer dramatically improves the efficacy of cholesterol-conjugated small interfering RNAs in vivo., Nucleic Acid Ther. 22 (2012) 380–90. doi:10.1089/nat.2012.0389.

[26] M.G. Sebestyén, S.C. Wong, V. Trubetskoy, D.L. Lewis, C.I. Wooddell, Targeted in vivo delivery of siRNA and an endosome-releasing agent to hepatocytes., Methods Mol. Biol. 1218 (2015) 163–86. doi:10.1007/978-1-4939-1538-5_10.

[27] C. Wan, T.M. Allen, P.R. Cullis, Lipid nanoparticle delivery systems for siRNA-based therapeutics, Drug Deliv. Transl. Res. 4 (2014) 74–83. doi:10.1007/s13346-013-0161-z.

[28] Y.Y.C. Tam, S. Chen, P.R. Cullis, Advances in lipid nanoparticles for siRNA delivery., Pharmaceutics. 5 (2013) 498–507. doi:10.3390/pharmaceutics5030498.

[29] N.M. Belliveau, J. Huft, P.J. Lin, S. Chen, A.K. Leung, T.J. Leaver, et al., Microfluidic Synthesis of Highly Potent Limit-size Lipid Nanoparticles for In Vivo Delivery of siRNA., Mol. Ther. Nucleic Acids. 1 (2012) e37. doi:10.1038/mtna.2012.28.

[30] E. Wisse, F. Jacobs, B. Topal, P. Frederik, B. De Geest, The size of endothelial fenestrae in human liver sinusoids: implications for hepatocyte-directed gene transfer., Gene Ther. 15 (2008) 1193–9. doi:10.1038/gt.2008.60.

[31] I. Hazan-Halevy, D. Landesman-Milo, D. Rosenblum, S. Mizrahy, B.D. Ng, D. Peer, Immunomodulation of hematological malignancies using oligonucleotides based-nanomedicines., J. Control. Release. (2016). doi:10.1016/j.jconrel.2016.07.052.

[32] K. Liszewski, Embattled RNAi Technology Tries New Tack, January 15. (2012). http://www.genengnews.com/gen-articles/embattled-rnai-technology-tries-new-tack/3977/?page=1.

[33] Y. Wang, L. Huang, A window onto siRNA delivery., Nat. Biotechnol. 31 (2013) 611–2. doi:10.1038/nbt.2634.

[34] G. Sahay, W. Querbes, C. Alabi, A. Eltoukhy, S. Sarkar, C. Zurenko, et al., Efficiency of siRNA delivery by lipid nanoparticles is limited by endocytic recycling., Nat. Biotechnol. 31 (2013) 653–8. doi:10.1038/nbt.2614.

[35] J. Gilleron, W. Querbes, A. Zeigerer, A. Borodovsky, G. Marsico, U. Schubert, et al., Image-based analysis of lipid nanoparticle-mediated siRNA delivery, intracellular trafficking and endosomal escape., Nat. Biotechnol. 31 (2013) 638–46. doi:10.1038/nbt.2612.

Chapter 2

Lipid nanoparticles and structural requirements for efficient transfections

Lipid nanoparticles and structural requirements for efficient transfection

RNA therapeutics have become the leading class of nucleic acid-based therapeutics, but already long before their discovery, many efforts have been made to deliver DNA-based drugs to target cells. Alongside polymeric vectors, lipid nanoparticles (LNPs) are the most-studied class of non-viral vectors for 'gene delivery' and they come in many forms and variations [1–3]. Alec Bangham already showed in the 1960s that phospholipids spontaneously form closed bilayer structures in an excess of water, which he called liposomes [4–6]. Soon after that, the potential use of liposomes as drug carriers was recognized [7] and a lot of progress was made to optimize them towards this new function. These optimizations included reducing their diameter to preferably <100nm and making them unilamellar (as opposed to them having multiple, concentric bilayers) [8–10] and prolonging their circulation time by including small percentages of 'PEGylated' lipids (lipids conjugated to a polyethylene glycol (PEG) polymer). Especially the PEGylation of liposomes has marked a turning point in the field of drug delivery, as it was shown that PEGylated lipids gave the liposomes 'stealth properties'. This avoided their rapid clearance by the mononuclear phagocyte system (MPS) in the liver and the spleen, allowing them to circulate long enough to accumulate in the tumor tissue as often observed in laboratory animals [11–13]. This discovery (together with the use of a pH gradient to load the drug) has led to the development and approval of the liposomal doxorubicin formulation Doxil® / Caelyx®, that is still considered the landmark formulation in nanomedicine [14].

Cationic lipids

The surface shielding of the liposomes may also have some unfavorable effects, as will be discussed later in this chapter. However, almost without exception, every intravenously administered drug delivery system of the current generation is PEGylated. Besides the PEGylated lipid, LNPs for nucleic acids always contain a cationic aminolipid for membrane interaction, a 'helper lipid' that increases transfection efficiency, and cholesterol which helps organize the membrane and keeps it in the 'liquid ordered' or 'gel state' [15,16]. Cationic lipids are of great interest for the delivery of nucleic acids because their charge can be used to form complexes with the negatively charged backbone of the nucleic acid cargo. This was first shown with plasmid DNA and these complexes were able to efficiently transfect cells in vitro, a process which was called 'Lipofection' [17,18]. The cationic lipids do not only interact with the nucleic acids, but also with the naturally occurring anionic lipids of the cell membrane and the endosomal membrane. It was shown that cationic lipids have a detergent-like effect and are able to destabilize biological membranes by the induction of a non-bilayer H_{II} phase which allows the entrance (or release) of macromolecules into the cytoplasm of the target cell [19–21]. The H_{II} phase describes the state in which lipids do not adopt a bilayer formation (lamellar phase), but a micellar phase, also called (inverse) hexagonal phase. See Figure 2.1d. This phase can be induced by lipids that have a more conical shape, which is determined by the balance between the hydrophilic headgroup and hydrophobic acyl chains, and by the saturation of the acyl chains. Lipids with a small headgroup have a relatively large hydrophobic part and therefore have a more conical shape. Furthermore, higher degrees of acyl chain unsaturation introduce

"kinks" in the acyl chains that makes the hydrophobic part occupy more space and again, give the lipid a more conical shape. The more pronounced the conical shape, the higher the lipids' affinity for the H_{II} phase. See Figure 2.1a-b. The most commonly used conical lipid in early generations of lipid nanoparticles for nucleic acid delivery was DOPE (dioleoylphosphatidylethanolamine) and it was shown that replacing it with its more cylindrical counterpart DOPC (dioleoylphosphatidylcholine), almost completely inhibits transfection efficiency [21–24]. In a pulse-chase experiment, cells were chased with formulations without nucleic acids of various compositions and it was found that chasing with an empty DOPE formulation could rescue the transfection activity of DOPC/DNA complexes. These empty formulations were called 'helper liposomes' and based on the results, DOPE a 'helper lipid' [22].

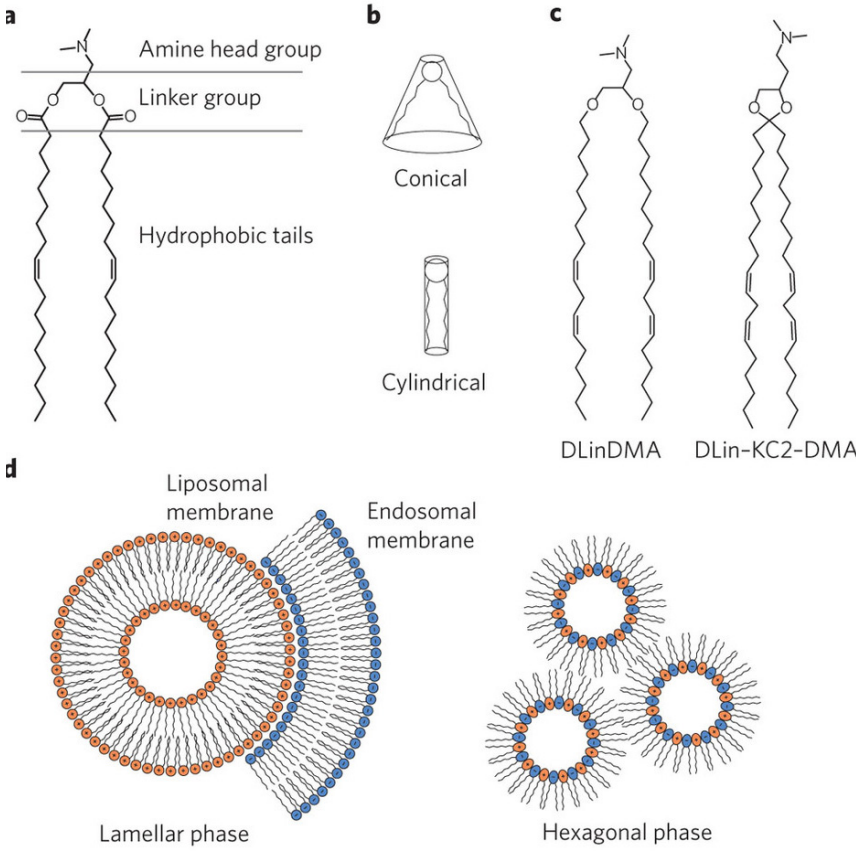

Figure 2.1 | Lipid structures and shapes
a) Ionizable lipids are composed of three sections: the amine head group, the linker group and the hydrophobic tails.
b) Lipids with a small head group and tails composed of unsaturated hydrocarbons tend to adopt a conical structure, whereas lipids with a large head group and saturated tails tend to adopt a cylindrical structure.
c) The structures of siRNA delivery lipids DLinDMA and DLin–KC2–DMA.
d) The mixing of cationic (orange) and anionic (blue) lipids promotes the transition from the more stable lamellar phase to the less stable hexagonal phase, thus aiding fusion of the liposomal and endosomal membranes. Figure reproduced from REF. [19].

Unfortunately, very few of the early generation lipid/nucleic acid complexes showed any effect in vivo, due to their rapid clearance and high toxicity, which can both be attributed to the (permanent) positive charge on the cationic lipid species. This led to the development of ionizable lipids, preferably with a pKa around 7 or lower and the first example of such a lipid was DODAP (dioleoyl-dimethylammoniumpropane), the ionizable variant of DOTAP (dioleoyl-trimethylammoniumpropane) [25,26]. When formulated at low pH (pH 4.0) these lipids are positively charged and can encapsulate the negatively charged nucleic acid, but at physiological pH (pH 7.4) the formed LNPs have a near neutral surface charge and therefore a lowered toxicity. When they are taken up by the target cells and accumulate in the acidic environment of the endosomes (pH 5.5-6.5), they return to their charged form and facilitate endosomal escape by interaction with the negative lipids in the endosomal membrane.

Combining the knowledge that chain saturation and headgroup pKa both influence the ability to adopt the H_{II} phase and thereby endosomal escape, a series of analogs to the ionizable lipid DODMA was synthesized that all had different acyl chain saturations. This led to the discovery of DlinDMA, the analog with two double bonds in each acyl chain, which had an excellent transfection efficiency and an apparent pKa of 6.7, which makes it charge neutral at physiological pH but charged in the endosome [27]. DlinDMA was the first type of "rationally designed" ionizable lipid and using this lipid, it was possible to demonstrate gene silencing by siRNA after systemic administration in non-human primates for the first time ever [28]. This milestone served as a benchmark for next generations of lipids with even greater transfection efficiencies. Lipid libraries where the amine headgroup, linker region and hydrophobic tails of the lipids were systematically varied in a high throughput manner, led to the discovery of the lipids DLin-KC2-DMA [29] and DLin-MC3-DMA [30]. See Figure 2.1c. Alternative synthesis routes and lipid designs have resulted in libraries of products also referred to as "lipidoids" because they hardly resemble the traditional phospholipids anymore, like 98N12-5 [31] and C12-200 [32]. The potency of the LNPs formulated with these new lipids is typically compared by the dose of siRNA required to silence the FVII gene in the hepatocytes of mice. When the *in vivo* activity of all the screened lipids was plotted versus their headgroup pKa, it was found that the optimal pKa value is 6.44 [30]. But although the importance of conical shape and chain unsaturation is now recognized and the optimal pKa can even be pinpointed, the structure of e.g. DLin-MC3-DMA could not be predicted beforehand nor can the next generation of aminolipids be designed. The most potent lipids are a result of combinatorial synthesis and high-through screening and not of rational design [29–34]. Nevertheless, this has proven to be a very effective approach and the dramatic improvements made over the years are shown in Figure 2.2.

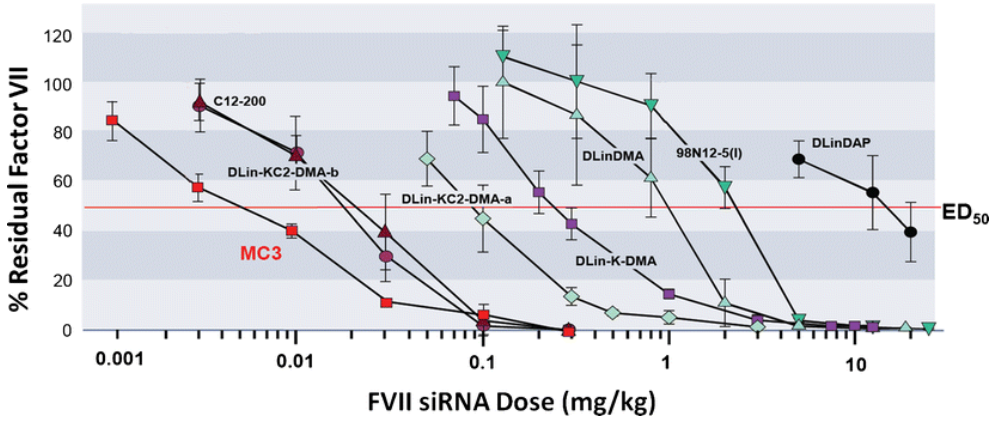

Figure 2.2 | Improved potency of LNPs containing ionizable cationic lipids
The early generation ionizable lipid DlinDAP required ~15 mg of siRNA/kg to reduce 50% of protein expression, while the most optimized form DLin-MC3-DMA required only 0.005 mg/kg. This is a reduction in required dose of 3000 times. Figure reproduced from REF. [3].

Now that doses as low as low as 0.005 mg siRNA/kg of body weight are sufficient to reduce 50% of gene activity in the liver of mice (DLin-MC3-DMA) [30], therapeutic gene silencing in humans also has become feasible. Because of the high costs of RNAi therapeutics, dosing human patients (~75 kg average body weight) at >10 mg/kg like with the early generation LNPs did not seem very realistic. Alnylam Pharmaceuticals (Cambridge, MA, USA) is currently running multiple clinical trials with siRNA LNPs containing different generations of ionizable lipids in many different liver indications. Results of the administration of siRNA LNPs for the treatment of transthyretin mediated amyloidosis (DLinDMA) have been published [35] as well as for familial hypercholesterolemia targeting the PCKS9 gene (lipidoid 98N12-5) [36].

PEG-lipids

These clinical achievements are promising, but so far, it seems that LNPs for siRNA primarily have applications in the liver. This is caused by the other critical component of LNPs, namely the PEG-lipid. When formulating nucleic acid lipid nanoparticles, it was found that the PEG-lipid plays an important role in preventing the formation of large aggregates of lipid and nucleic acid during formulation [26]. However, the surface shielding by the PEG-lipids also prevents interaction of the cationic lipids with the anionic lipids in the biological membranes and thus inhibits successful transfection [37]. To solve this, PEG-lipids with shorter acyl chains were developed [25,37]. The length of the acyl chain determines the hydrophobicity of the anchor and the rate at which the lipid dissociates from the surface of the LNP after intravenous administration. The circulation half-life of LNPs with Ceramide-PEG lipids ranges from 1 hour for Ceramide C14-PEG and 10 hours for Ceramide C20-PEG [25]. Once the PEG-lipids dissociate, serum proteins such as Apolipoprotein E (ApoE) can absorb to the surface of the LNPs which results in uptake into hepatocytes via the Low-Density Lipoprotein (LDL) receptor and scavenger receptors [38]. So paradoxically, the "breakthrough" discovery of surface PEGylation, which prevented uptake in the liver and initiated the success of long

circulating formulations such as Doxil® is now abolished by using sheddable PEGs. The difference however, is that conventional unPEGylated liposomes are primarily taken up in the macrophages in the liver while the 'endogenous targeting' with ApoE directs the LNPs to the hepatocytes, which contain a myriad of therapeutic targets. This effect is mainly attributed to the ionizable lipids that render the LNPs charge neutral because apolipoproteins absorb to neutral surfaces only, whereas the surface of cationic particles is immediately cluttered with all sorts of serum proteins and opsonins, causing rapid aggregation and clearance by the MPS. The favorable architecture of the liver (highly perfused and with fenestrated endothelium) and the exploitation of the endogenous retargeting make these LNPs extremely suitable for the silencing of genes in the liver [38]. But obviously, there is also a huge number of extrahepatic targets. Reaching these targets and tissues remains an important challenge for the coming years, as will be further discussed in **Chapter 8**. However, the combination of novel ionizable lipids and novel PEG-lipids has significantly advanced the field and applications in other relatively easy to reach cell types such as those of the immune systems are now also slowly emerging [39–42].

Experimental results

In this chapter, it is attempted to demonstrate the described structural features of LNP components and their effect on transfection efficiency. In summary, the degree of chain unsaturation influences the lipid's preference for the inverse hexagonal H_{II} phase and the headgroup pKa influences its ability to pull the anionic lipids of the endosomal membrane with it into this 'fusogenic' phase (Figure 2.1d). Combining these two features in novel lipid libraries has resulted in a number of lipids with highly increased potency that have greatly advanced the field and lowered the required doses for effective in vivo transfection. Unfortunately many of these advances are made in the pharmaceutical industry or by academic groups closely related to them. As a consequence, the potent next-generation lipids are not commercially available and although their synthesis routes are all published, in-house production is not possible in all labs. To still demonstrate the influence of (conical vs cylindrical) helper lipid and PEG-lipid dissociation on transfection efficiency of LNPs for RNA therapeutics, a series of formulations is tested that contain commercially available lipid species. These formulations are similar to the ones currently applied in clinics, but contain the ionizable cationic lipid DODAP in all formulations. The composition of the LNPs tested here was DODAP/Cholesterol/[helper lipid]/[PEG-lipid] in a ratio of 25/42.5/25/7.5. As helper lipids, DOPE (conical) and DSPC (cylindrical) were compared. Five types of PEG(2000)-lipids were used, with distearoylphosphatidylethanolamine (C18), Ceramide C16, Ceramide C8, distearoylglycerol (C18) and dimyristoylglycerol (C14) as anchors. Using a standard preparation method, ten formulations containing a splice correcting oligonucleotide (SCO) were made and tested in HeLa pLuc705 cells. This cell line contains a construct that expresses a truncated and dysfunctional form of luciferase, caused by the inclusion of an extra exon that contains a premature stop codon. When the splice correcting oligonucleotide '705' is successfully delivered to this cell line, the splicing is corrected (by blockage of the splicing site at position 705) and luciferase expression is restored [43]. See Figure 2.3.

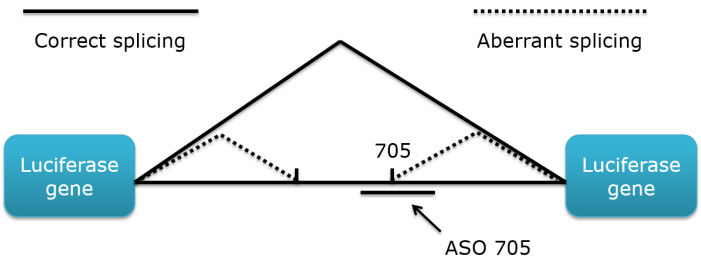

Figure 2.3 | Schematic representation of the splice correction in the luciferase reporter cell line
HeLa pLuc705 cells contain a variant of the luciferase gene that is aberrantly spliced, resulting in the insertion of a non-sense intron. This interruption introduces a premature stop codon, resulting in the expression of a truncated form of the luciferase protein. When the 705 anti-sense oligo is administered, the splicing site at position 705 is blocked, restoring natural splicing and the correct joining of the luciferase introns (depicted in blue) and expression of the intact luciferase protein. The splicing site at the 3' end could also be blocked to achieve the same result, but required much higher doses. This may be caused by the decreased accessibility of the 3' splice site which interacts with a large number of splicing factors [43].

The SCO is a single stranded anti-sense RNA 18mer and therefore a suitable model for small RNA therapeutics. The luciferase read-out allows for rapid screening of multiple formulations. Results of this screening are shown in Figure 2.4 below.

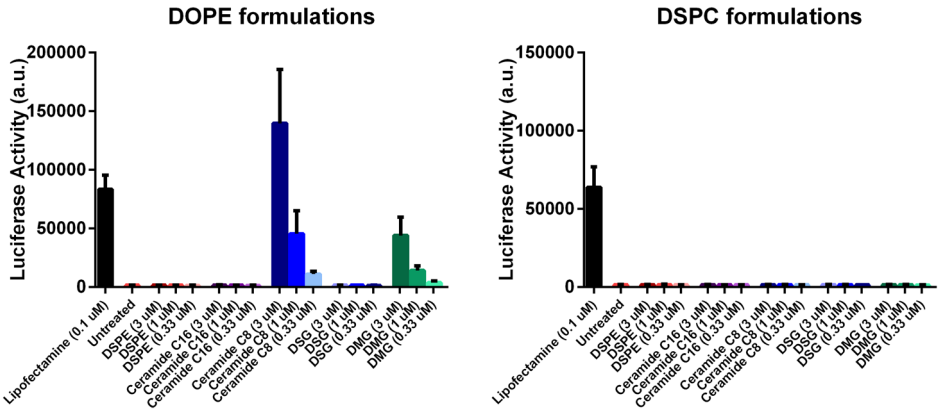

Figure 2.4 | Up-regulation of luciferase activity by transfection with a splice correcting oligonucleotide
Only the formulations that contain DOPE as the helper lipid exhibit transfection activity and only those with the shorter, more loosely anchored PEG lipids (Ceramide C8 and DMG C14). This demonstrates that the conically shaped lipid DOPE is required for successful transfection and that in these conditions, only Ceramide C8 and DMG anchored PEG-lipids sufficiently dissociate from the liposomal membrane to allow interaction with the cells.

Transfection efficiency

Using DODAP as the cationic lipid, none of the formulations containing DSPC as the helper lipid produced any increase in luciferase activity. LNP mediated transfection was seen in the formulations with DOPE as helper and with the more loosely anchored PEGs. Clearly, the conical shape of DOPE is required to induce endosomal escape, as the comparable formulations with the cylindrical helper lipid DSPC all fail to show any activity. Interestingly, all LNPs that are currently being used in clinics contain DSPC as helper lipid so in these formulations, the conical shape of the optimized cationic lipids is solely responsible for the induction of the H_{II} phase. In cell culture conditions, only the Ceramide C8 and the DMG (C14) anchors sufficiently shed from the bilayer to allow any interaction with the cells to initiate uptake. It is hypothesized that these lipids exchange with the cell membrane, secreted vesicles and excreted proteins. The C16 and C18 anchors (DSPE and DSG) appear to be too strongly anchored to dissociate from the LNP surface in these conditions, or at least in this timeframe (4 hours of incubation). The situation in the circulation is clearly different, because the lipid sink is much larger with all the lipoproteins and chylomicrons present in the bloodstream and clinically successful formulations may therefore also contain DSG-PEG [44]. The high activity in the highest concentration of the C16 Ceramide formulation should not be overestimated, as it contains a 30-fold higher concentration of the SCO than Lipofectamine. Of note, Lipofectamine/RNA complexes do not form stable complexes and aggregate so extensively that they sediment onto the cells that grow in monolayers in tissue culture plates. They are therefore neither applicable for intravenous administration, nor are they a good model for stable nucleic acid lipid particles, but merely a positive control for the luciferase assay. Still, the 3 μM concentration that was used in these experiments is not very likely to be reached in the target tissue, if this formulation were to be administered intravenously and this lack of potency is the reason that the LNP field went through the evolution described in this chapter..

Conclusion

The structural requirements for efficient transfection with lipid nanoparticles are demonstrated in a model cell line for splice correction by an antisense RNA oligonucleotide. It is clear that a conically shaped lipid is essential to show any effect and it is thought to be required to induce the inverse hexagonal (H_{II}) phase that allows endosomal escape of the RNA cargo. Interaction with the negatively charged membranes is only possible when the cationic surface of the LNP is sufficiently accessible. In these experimental conditions, it was shown that only the short Ceramide C8 and DMG (C14) anchors sufficiently dissociate from the LNP surface to allow such interactions. These results show that it certainly is possible to produce stable LNPs with commercially available lipids that are capable of –at least in vitro- transfection, but the required doses also demonstrate the need for further optimization. The ionizable cationic lipid used here is DODAP, which is the mono-unsaturated (18:1) variant of DlinDAP (di-unsaturated (18:2)), that is shown as the least potent aminolipid in Figure 2.2. Following the conclusion that chain-unsaturation improves the transfection efficiency of the lipid [27], DODAP is expected to have an even lower potency than DlinDAP. It is therefore not a surprise that the potency of the LNPs formulated here is somewhat

disappointing in terms of required doses. However, when limited to commercially available lipid components, it is clear that other strategies are required to improve transfection efficiency. These strategies include the enhancement of endosomal escape in a different way or the improvement of uptake by active targeting. In **Chapter 6** a strategy to enhance endosomal escape is presented and two different approaches to active targeting are described in **Chapter 3** and **Chapter 5**.

Materials and methods

Lipids

1,2-dioleoyl-3-dimethylammonium-propane (DODAP), N-palmitoyl-sphingosine-1-succinyl-[methoxy(polyethylene glycol)2000] (C16 Ceramide-PEG2000), N-octanoyl-sphingosine-1-succinyl-[methoxy(polyethylene glycol)2000] (C8 Ceramide-PEG2000), and 1,2-dioleoyl-sn-glycero-3-phospho-ethanolamine (DOPE) were from Avanti Polar Lipids (Alabaster, AL, USA). Cholesterol was from Sigma-Aldrich (St. Louis, MO, USA). 1,2-distearoyl-sn-glycero-3-[methoxy(polyethylene glycol-2000] (DSG-PEG2000) and 1,2-dimyristoyl-sn-glycero-3-[methoxy(polyethylene glycol-2000] (DMG-PEG2000) were from NOF Corporation (Frankfurt am Main, Germany). 1,2-distearoyl-sn-glycero-3-phosphocholine (DSPC) and 1,2-distearoyl-sn-glycero-3-phosphoethanolamine-N-[methoxy(polyethylene glycol)-2000] (DSPE-PEG(2000)) were a gift from Lipoid GmbH (Ludwigshafen, Germany).

LNP preparation

For all formulations, a lipid film was prepared by dissolving the lipids in chloroform and evaporating the organic solvent using a rotary evaporator. The formed dry lipid film was flushed with nitrogen to remove all traces of organic solvent. All lipid films consisted of DODAP:Cholesterol:[helper lipid]:[PEG-lipid] in a ratio of 25:42.5:25:7.5. As helper lipid, DSPC or DOPE was used. As PEG-lipid, DSPE-, Ceramide C16-, Ceramide C8-, DSG- and DMG- were used, all with a 2000 MW PEG-chain. The lipid film was hydrated in 70% 50 mM citrate buffer pH 4.0 and 30% ethanol absolute containing 705 splice correcting oligonucleotide to a final concentration of 250 ug/ml. The formulations were dialysed overnight in a 2K MWCO Slide-A-Lyzer G2 Dialysis Cassette (Thermo Fischer Scientific, Bleiswijk, Netherlands) at 4°C against PBS to remove ethanol and citrate. Unencapsulated nucleic acids were removed by three rounds of ultracentrifugation for 50 minutes at 55.000RPM in a Type 70.1 Ti rotor (Beckman Coulter B.V., Woerden, Netherlands) at 4°C. Encapsulation was measured as described in Chapter 4. In short, lipids and nucleic acids were separated by an extraction according to Bligh and Dyer [45]. The bottom phase containing the lipids was assayed for total phosphate, according to the method of Rouser et al.[46] with sodium biphosphate as a standard after destruction of the phospholipids with perchloric acid and heating at 180°C. The top phase was evaporated in a vacuum concentrator and reconstituted in MilliQ water to measure the concentration of nucleic acids using Nanodrop.

Cell culture and oligonucleotides

HeLa cells expressing the luciferase gene interrupted by mutated human β-globin intron 2 (IVS2-705) (HeLa pLuc705) [43] were cultured in Dulbecco's Modified Eagle's Medium with High Glucose supplemented with 10% (v/v) fetal bovine serum, Penicillin-Streptomycin-Amphotericin B and 200 ug/ml of Hygromycin B in a humidified atmosphere at 37°C containing 5% CO2. All medium and supplements were from Sigma-Aldrich. Antisense oligonucleotide Luc705 (5'-CCUCUUACCUCAGUUACA-3') consisting of all phosphorothioate bases and 2'-O-methyl modified at every nucleoside was provided by GlaxoSmithKline (Stevenage, United Kingdom) for use in the EU IMI COMPACT consortium. Cells were seeded in a 96 well plate at a density of 8.000 cells/well. Cells were incubated with the different formulations at the indicated concentrations in unsupplemented OptiMEM medium 4 hours at 37°C. Lipofectamine 2000 (Thermo Fischer Scientific) was used as a positive control according to the manufacturer's protocol. After incubation with the LNPs, medium was replaced with complete medium and incubated overnight at 37°C. The following day, cells were lysed with 100ul of Reporter Lysis Buffer (Promega, Leiden, Netherlands) and 50ul of lysate was mixed with 50µl of Luciferase Assay Reagent (Promega). Reagent was injected using a FLUOstar OPTIMA microplate reader (BMG Labtech, Ortenberg, Germany) equipped with an injection pump. 2 seconds after injection, luminescence was measured for 10 seconds according to supplier's recommendation.

References

[1] B. Ozpolat, A.K. Sood, G. Lopez-Berestein, Liposomal siRNA nanocarriers for cancer therapy, Adv. Drug Deliv. Rev. 66 (2014) 110–116. doi:10.1016/j.addr.2013.12.008.

[2] T.M. Allen, P.R. Cullis, Liposomal drug delivery systems: from concept to clinical applications., Adv. Drug Deliv. Rev. 65 (2013) 36–48. doi:10.1016/j.addr.2012.09.037.

[3] C. Wan, T.M. Allen, P.R. Cullis, Lipid nanoparticle delivery systems for siRNA-based therapeutics, Drug Deliv. Transl. Res. 4 (2014) 74–83. doi:10.1007/s13346-013-0161-z.

[4] A.D. Bangham, R.W. Horne, Negative staining of phospholipids and their structural modification by surface-active agents as observed in the electron microscope., J. Mol. Biol. 8 (1964) 660–8.

[5] A.D. Bangham, M.M. Standish, J.C. Watkins, Diffusion of univalent ions across the lamellae of swollen phospholipids., J. Mol. Biol. 13 (1965) 238–52.

[6] D.W. Deamer, From "banghasomes" to liposomes: a memoir of Alec Bangham, 1921-2010., FASEB J. 24 (2010) 1308–1310. doi:10.1096/fj.10-0503.

[7] G. Gregoriadis, B.E. Ryman, Liposomes as carriers of enzymes or drugs: a new approach to the treatment of storage diseases., Biochem. J. 124 (1971) 58P.

[8] F. Szoka, F. Olson, T. Heath, W. Vail, E. Mayhew, D. Papahadjopoulos, Preparation of unilamellar liposomes of intermediate size (0.1-0.2 mumol) by a combination of reverse phase evaporation and extrusion through polycarbonate membranes., Biochim. Biophys. Acta. 601 (1980) 559–71.

[9] M.J. Hope, M.B. Bally, G. Webb, P.R. Cullis, Production of large unilamellar vesicles by a rapid extrusion procedure: characterization of size distribution, trapped volume and ability to maintain a membrane potential., Biochim. Biophys. Acta. 812 (1985) 55–65.

[10] L.D. Mayer, M.J. Hope, P.R. Cullis, Vesicles of variable sizes produced by a rapid extrusion procedure., Biochim. Biophys. Acta. 858 (1986) 161–8.

[11] D. Papahadjopoulos, T.M. Allen, A. Gabizon, E. Mayhew, K. Matthay, S.K. Huang, et al., Sterically stabilized liposomes: improvements in pharmacokinetics and antitumor therapeutic efficacy., Proc. Natl. Acad. Sci. U. S. A. 88 (1991) 11460–4.

[12] T.M. Allen, C. Hansen, Pharmacokinetics of stealth versus conventional liposomes: effect of dose., Biochim Biophys Acta. 1068 (1991) 133–41.

[13] E.G. Mayhew, D. Lasic, S. Babbar, F.J. Martin, Pharmacokinetics and antitumor activity of epirubicin encapsulated in long-circulating liposomes incorporating a polyethylene glycol-derivatized phospholipid., Int. J. Cancer. 51 (1992) 302–9.

[14] Y.C. Barenholz, Doxil® - The first FDA-approved nano-drug: Lessons learned., J Control Release. 160 (2012) 117–34. doi:10.1016/j.jconrel.2012.03.020.

[15] O.G. Mouritsen, M.J. Zuckermann, What's so special about cholesterol?, Lipids. 39 (2004) 1101–13.

[16] A. Arora, H. Raghuraman, A. Chattopadhyay, Influence of cholesterol and ergosterol on membrane dynamics: a fluorescence approach, Biochem. Biophys. Res. Commun. 318 (2004) 920–926. doi:10.1016/j.bbrc.2004.04.118.

[17] P.L. Felgner, T.R. Gadek, M. Holm, R. Roman, H.W. Chan, M. Wenz, et al., Lipofection: a highly efficient, lipid-mediated DNA-transfection procedure., Proc. Natl. Acad. Sci. U. S. A. 84 (1987) 7413–7417. doi:10.1073/pnas.84.21.7413.

[18] P.L. Felgner, T.R. Gadek, M. Holm, R. Roman, H.W. Chan, M. Wenz, et al., Lipofection: a highly efficient, lipid-mediated DNA-transfection procedure., Proc. Natl. Acad. Sci. U. S. A. 84 (1987) 7413–7.

[19] R. Kanasty, J.R. Dorkin, A. Vegas, D. Anderson, Delivery materials for siRNA therapeutics., Nat. Mater. 12 (2013) 967–77. doi:10.1038/nmat3765.

[20] I.M. Hafez, N. Maurer, P.R. Cullis, On the mechanism whereby cationic lipids promote intracellular delivery of polynucleic acids., Gene Ther. 8 (2001) 1188–96. doi:10.1038/sj.gt.3301506.

[21] I.M. Hafez, P.R. Cullis, Roles of lipid polymorphism in intracellular delivery., Adv Drug Deliv Rev. 47 (2001) 139–48.

[22] H. Farhood, N. Serbina, L. Huang, The role of dioleoyl phosphatidylethanolamine in cationic liposome mediated gene transfer, BBA - Biomembr. 1235 (1995) 289–295. doi:10.1016/0005-2736(95)80016-9.

[23] S.W. Hui, M. Langner, Y.L. Zhao, P. Ross, E. Hurley, K. Chan, The role of helper lipids in cationic liposome-mediated gene transfer., Biophys. J. 71 (1996) 590–599. doi:10.1016/S0006-3495(96)79309-8.

[24] Y. Hattori, S. Suzuki, S. Kawakami, F. Yamashita, M. Hashida, The role of dioleoylphosphatidylethanolamine (DOPE) in targeted gene delivery with mannosylated cationic liposomes via intravenous route, J. Control. Release. 108 (2005) 484–495. doi:10.1016/j.jconrel.2005.08.012.

[25] S.C. Semple, S.K. Klimuk, T.O. Harasym, N. Dos Santos, S.M. Ansell, K.F. Wong, et al., Efficient encapsulation of antisense oligonucleotides in lipid vesicles using ionizable aminolipids: Formation of novel small multilamellar vesicle structures, Biochim. Biophys. Acta - Biomembr. 1510 (2001) 152–166. doi:10.1016/S0005-2736(00)00343-6.

[26] N. Maurer, K.F. Wong, H. Stark, L. Louie, D. McIntosh, T. Wong, et al., Spontaneous entrapment of polynucleotides upon electrostatic interaction with ethanol-destabilized cationic liposomes., Biophys. J. 80 (2001) 2310–2326. doi:10.1016/S0006-3495(01)76202-9.

[27] J. Heyes, L. Palmer, K. Bremner, I. MacLachlan, Cationic lipid saturation influences intracellular delivery of encapsulated nucleic acids, J. Control. Release. 107 (2005) 276–287. doi:10.1016/j.jconrel.2005.06.014.

[28] T.S. Zimmermann, A.C.H. Lee, A. Akinc, B. Bramlage, D. Bumcrot, M.N. Fedoruk, et al., RNAi-mediated gene silencing in non-human primates., Nature. 441 (2006) 111–4. doi:10.1038/nature04688.

[29] S.C. Semple, A. Akinc, J. Chen, A.P. Sandhu, B.L. Mui, C.K. Cho, et al., Rational design of cationic lipids for siRNA delivery., Nat. Biotechnol. 28 (2010) 172–6. doi:10.1038/nbt.1602.

[30] M. Jayaraman, S.M. Ansell, B.L. Mui, Y.K. Tam, J. Chen, X. Du, et al., Maximizing the potency of siRNA lipid nanoparticles for hepatic gene silencing in vivo., Angew. Chem. Int. Ed. Engl. 51 (2012) 8529–33. doi:10.1002/anie.201203263.

[31] A. Akinc, A. Zumbuehl, M. Goldberg, E.S. Leshchiner, V. Busini, N. Hossain, et al., A combinatorial library of lipid-like materials for delivery of RNAi therapeutics., Nat. Biotechnol. 26 (2008) 561–9. doi:10.1038/nbt1402.

[32] K.T. Love, K.P. Mahon, C.G. Levins, K.A. Whitehead, W. Querbes, J.R. Dorkin, et al., Lipid-like materials for low-dose, in vivo gene silencing., Proc. Natl. Acad. Sci. U. S. A. 107 (2010) 1864–9. doi:10.1073/pnas.0910603106.

[33] S. Sun, M. Wang, S. a Knupp, Y. Soto-Feliciano, X. Hu, D.L. Kaplan, et al., Combinatorial library of lipidoids for in vitro DNA delivery., Bioconjug. Chem. 23 (2012) 135–40. doi:10.1021/bc200572w.

[34] L. Li, F. Wang, Y. Wu, G. Davidson, P.A. Levkin, Combinatorial synthesis and high-throughput screening of alkyl amines for nonviral gene delivery., Bioconjug. Chem. 24 (2013) 1543–51. doi:10.1021/bc400158w.

[35] T. Coelho, D. Adams, A. Silva, P. Lozeron, P.N. Hawkins, T. Mant, et al., Safety and efficacy of RNAi therapy for transthyretin amyloidosis., N. Engl. J. Med. 369 (2013) 819–29. doi:10.1056/NEJMoa1208760.

[36] K. Fitzgerald, M. Frank-Kamenetsky, S. Shulga-Morskaya, A. Liebow, B.R. Bettencourt, J.E. Sutherland, et al., Effect of an RNA interference drug on the synthesis of proprotein convertase subtilisin/kexin type 9 (PCSK9) and the concentration of serum LDL cholesterol in healthy volunteers: a randomised, single-blind, placebo-controlled, phase 1 trial., Lancet. 383 (2014) 60–8. doi:10.1016/S0140-6736(13)61914-5.

[37] J.J. Wheeler, L. Palmer, M. Ossanlou, I. MacLachlan, R.W. Graham, Y.P. Zhang, et al., Stabilized plasmid-lipid particles: construction and characterization, Gene Ther. 6 (1999) 271–281. doi:10.1038/sj.gt.3300821.

[38] A. Akinc, W. Querbes, S. De, J. Qin, M. Frank-Kamenetsky, K.N. Jayaprakash, et al., Targeted delivery of RNAi therapeutics with endogenous and exogenous ligand-based mechanisms., Mol. Ther. 18 (2010) 1357–1364. doi:10.1038/mt.2010.85.

[39] P.J.C. Lin, Y.Y.C. Tam, I. Hafez, A. Sandhu, S. Chen, M.A. Ciufolini, et al., Influence of cationic lipid composition on uptake and intracellular processing of lipid nanoparticle formulations of siRNA, Nanomedicine Nanotechnology, Biol. Med. 9 (2013) 233–246. doi:10.1016/j.nano.2012.05.019.

[40] S. Ramishetti, R. Kedmi, M. Goldsmith, F. Leonard, A.G. Sprague, B. Godin, et al., Systemic Gene Silencing in Primary T Lymphocytes Using Targeted Lipid Nanoparticles, (2015) 6706–6716.

[41] S. Weinstein, I.A. Toker, R. Emmanuel, S. Ramishetti, I. Hazan-Halevy, D. Rosenblum, et al., Harnessing RNAi-based nanomedicines for therapeutic gene silencing in B-cell malignancies, Proc. Natl. Acad. Sci. (2015) 201519273. doi:10.1073/pnas.1519273113.

[42] G. Basha, T.I. Novobrantseva, N. Rosin, Y.Y.C. Tam, I.M. Hafez, M.K. Wong, et al., Influence of cationic lipid composition on gene silencing properties of lipid nanoparticle formulations of siRNA in antigen-presenting cells., Mol. Ther. 19 (2011) 2186–2200. doi:10.1038/mt.2011.190.

[43] S.H. Kang, M.J. Cho, R. Kole, Up-regulation of luciferase gene expression with antisense oligonucleotides: implications and applications in functional assay development., Biochemistry. 37 (1998) 6235–6239. doi:10.1021/bi980300h.

[44] B.L. Mui, Y.K. Tam, M. Jayaraman, S.M. Ansell, X. Du, Y.Y.C. Tam, et al., Influence of polyethylene glycol lipid desorption rates on pharmacokinetics and pharmacodynamics of siRNA lipid nanoparticles., Mol. Ther. Nucleic Acids. 2 (2013) e139. doi:10.1038/mtna.2013.66.

[45] E.G. Bligh, W. Dyer, A rapid method of total lipid extraction and purification, Can. J. Biochem. Physiol. 37 (1959) 911–917.

[46] G. Rouser, S. Fleischer, A. Yamamoto, Two dimensional thin layer chromatographic separation of polar lipids and determination of phospholipids by phosphorus analysis of spots, Lipids. 5 (1970) 494–496. doi:10.1007/BF02531316.

Chapter 3

Liposome functionalization with copper-free "click chemistry"

Erik Oude Blenke[1]
Gruson Klaasse[2]
Hannes Merten[3]
Andreas Plückthun[3]
Enrico Mastrobattista[1]
Nathaniel I. Martin[2]

[1]Department of Pharmaceutics, Utrecht Institute of Pharmaceutical Sciences (UIPS), Faculty of Science, Utrecht University, Universiteitsweg 99, 3584 CG Utrecht, The Netherlands

[2]Department of Chemical Biology and Drug Discovery, Utrecht Institute of Pharmaceutical Sciences (UIPS), Faculty of Science, Utrecht University, Universiteitsweg 99, 3584 CG Utrecht, The Netherlands

[3]Department of Biochemistry, University of Zürich, Winterthurerstrasse 190, 8057 Zürich, Switzerland

Journal of Controlled Release. 202 (2015) 14–20
doi: 10.1016/j.jconrel.2015.01.027

Abstract

The modification of liposomal surfaces is of interest for many different applications and a variety of chemistries are available that makes this possible. A major disadvantage of commonly used coupling chemistries (e.g. maleimide-thiol coupling) is the limited control over the site of conjugation in cases where multiple reactive functionalities are present, leading to heterogeneous products and in some cases dysfunctional conjugates. Bioorthogonal coupling approaches such as the well-established copper-catalyzed azide-alkyne cycloaddition (CuAAC) "click" reaction are attractive alternatives as the reaction kinetics are favorable and azide-containing reagents are widely available. In the work described here, we prepared lipids containing a reactive cyclooctyne group and, after incorporation into liposomes, demonstrated successful conjugation of both a small molecule dye (5'-TAMRA-azide) as well as a larger azide-containing model protein based upon a designed ankyrin repeat protein (azido-DARPin). By applying the strain-promoted azido-alkyne cycloaddition (SPAAC) the use of Cu(I) as a catalyst is avoided, an important advantage considering the known deleterious effects associated with copper in cell and protein studies.

We demonstrate complete control over the number of ligands coupled per liposome when using a small molecule azide with conjugation occurring at a reasonable reaction rate. By comparison, the conjugation of a larger azide-modified protein occurs more slowly, however the number of protein ligands coupled was found to be sufficient for liposome targeting to cells. Importantly, these results provide a strong proof of concept for the site-specific conjugation of protein ligands to liposomal surfaces via SPAAC. Unlike conventional approaches, this strategy provides for the homogeneous coupling of proteins bearing a single site-specific azide modification and eliminates the chance of forming dysfunctional ligands on the liposome. Furthermore, the absence of copper in the reaction process should also make this approach much more compatible with cell-based and *in vivo* applications.

Graphical Abstract

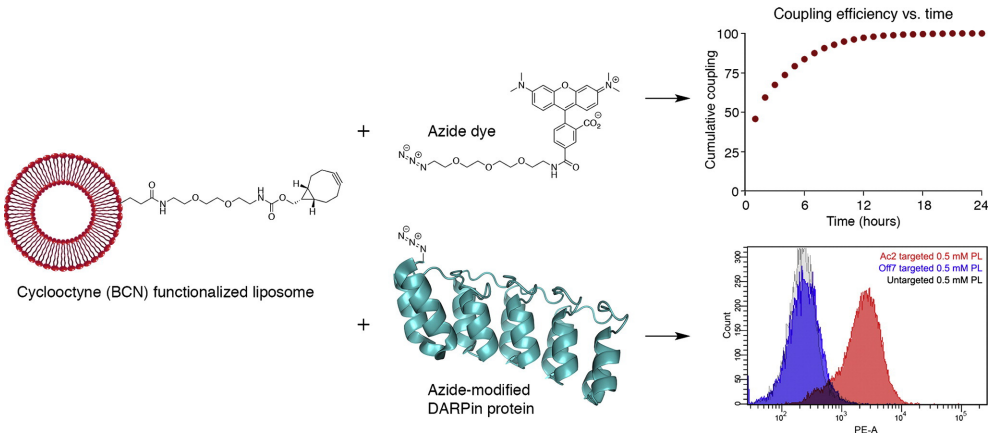

1. Introduction

Liposomes (phospholipid vesicles of 60-200 nm in size) have been widely used as model systems to mimic cell membranes, as nanocompartments to contain complex chemical or enzymatic reactions, and as drug delivery systems for the controlled and targeted delivery of drugs in the human body. Many of these applications require surface modification of the liposomes, i.e. the covalent attachment of functional molecules such as targeting ligands to preformed liposomes. The common strategy is to synthesize a new lipid that contains a reactive group that can react with a complementary reactive group on the ligand. Many different chemistries have been explored for surface modification [1]. Ideally, these reactions should be fast and specific and reaction conditions should be mild enough not to cause damage to the lipid membrane or to the ligand. In cases where the ligand to be coupled is a protein it is crucial that the coupling reaction does not negatively impact the structure and associated activity of the protein. In this regard, the most widely used coupling method is based upon maleimide-thiol coupling, where the liposomes are functionalized with a maleimide group that in turn reacts with a thiol-containing ligand to form a thioether bond. In the case of proteins, both naturally occurring thiol groups (e.g. found on cysteine residues) or introduced by a chemical reaction (e.g. by thiolation of lysines) can be used for coupling [2]. When using peptide or protein ligands, a common disadvantage of using naturally occurring reactive groups can be that the reaction is not site-specific. Thiols, amines, and carboxylic acid groups become more abundant with increasing protein size, and as such generate more possible conjugation sites. This can result in heterogeneous coupling where ligands might be conjugated at different or multiple sites, leading to the need for complicated separation schemes to obtain homogenous products. Even more problematic is the chance that binding affinity might be compromised if the reacting group is too close to the binding site of the protein to be immobilized.

Site-specific conjugation can be achieved by employing bio-orthogonal coupling reactions such as "click-chemistry" approaches. In this regard the Cu(I)-catalyzed reaction between an azide and an alkyne is fast and efficient and allows homogeneous and site-specific conjugation because the reactive groups can be introduced at a site of choice. The Cu(I)-catalyzed azide–alkyne [3 + 2] cycloaddition (CuAAC) was first applied in the context of liposomes by the group of Schuber who employed an alkyne-modified lipid to couple an azido-modified mannose ligand [3]. The use of the required copper catalyst however, is a limitation as it is known to be toxic to cells and can interfere with protein activity [4]. An alternative is the Staudinger ligation, in which a phosphine group reacts with the azide to form an amide bond [5]. This was also used for liposome functionalization [6] but the kinetics of this reaction are slow and the phosphine group is prone to oxidation [7]. As an alternative meant to address these limitations, the strain-promoted azido-alkyne cycloaddition (SPAAC) has been developed. In SPAAC ligations a ring-strained alkyne is reactive enough to lead to spontaneous addition with an azide, a process that eliminates the need for a toxic metal catalyst and with faster reaction kinetics [8]. Importantly, the *in vivo* compatibility and bio-orthogonality of copper-free SPAAC ligations have also been successfully demonstrated inside living organisms [9,10].

In the present work we describe the preparation of two different lipids that contain a reactive bicyclo[6.1.0]nonyne (BCN) cyclooctyne group [11] capable of "clicking" with a variety of azide-containing ligands (Figure 3.1). Both small and large (bio) molecules containing azides are readily available and methods to introduce the azide functionality into peptides or proteins are numerous [12]. Azide incorporation can be performed after protein expression using standard labeling approaches [13]. Alternatively, azide-containing amino acids can be specifically introduced during protein biosynthesis, allowing for complete control over the location of the azide [14–17]. We here demonstrate incorporation of our new BCN-lipids into the bilayer of liposomes followed by the successful coupling of both azide-containing small molecule ligands and recombinantly expressed proteins at the liposomal surface.

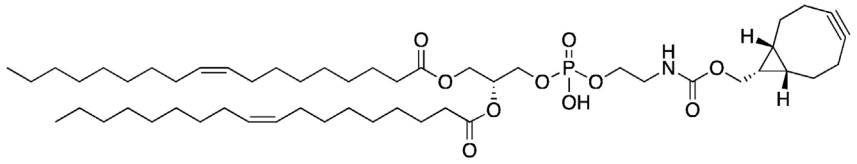

1

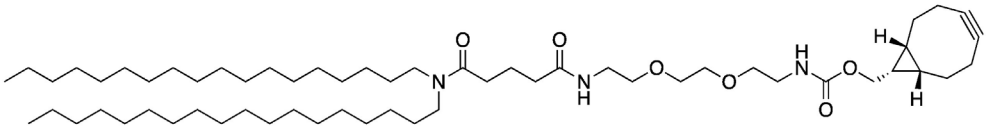

2

Figure 3.1 | Structures of BCN-lipid conjugates 1 and 2 prepared for incorporation into liposomes allowing for modification with azides via SPAAC

2. Materials and methods

2.1 Chemicals

Dioleoylphosphatidylcholine (DOPC), Dioleoylphosphatidylethanolamine (DOPE), L-α-phosphatidylethanolamine-N-(lissamine rhodamine B sulfonyl) (Rho-PE) were from Avanti Polar Lipids (Alabaster, AL, USA). (1R,8S,9s)-bicyclo[6.1.0]non-4-yn-9-ylmethyl succinimidyl carbonate was from SynAffix BV, Oss, The Netherlands) Dioctadecylamine, Cholesterol, calcein and Triton X-100 were from Sigma-Aldrich (St. Louis, MO, USA). 5-Carboxytetramethylrhodamine-PEG3-Azide (5'-TAMRA-PEG3-Azide) was from Baseclick GmbH (Tutzing, Germany).

2.2 Synthesis of lipid-BCN conjugates 1 and 2

DOPE-BCN conjugate (1): (2R)-3-(((2-(((((1R,8S,9s)-bicyclo[6.1.0]non-4-yn-9-yl)methoxy) carbonyl)amino)ethoxy)(hydroxy)phosphoryl)oxy)propane-1,2-diyl dioleate.
(1R,8S,9s)-bicyclo[6.1.0]non-4-yn-9-ylmethyl succinimidyl carbonate (50 mg, 0.17 mmol) was dissolved in 6 ml dry CH_2Cl_2 which was then added to a solution of 1,2-dioleoyl-sn-glycero-3-phosphoethanolamine (DOPE) (127 mg, 0.17 mmol) in 4 ml dry CH_2Cl_2. NEt_3 (78 µL, 0.55 mmol) was added and the solution was left stirring overnight. The product was

purified directly by column chromatography (95:5 CH_2Cl_2/MeOH) to yield the product as a colorless oil (114 mg, 73%).
Analytical data: ^{1}H NMR (400 MHz, $CDCl_3$) δ 9.35 (bs, 2H), 5.82 (s, 1H), 5.31 (m, 3H), 5.18 (m, 1H), 4.36 (dd, 2H), 4.11 (m, 3H), 3.92 (m, 4H), 3.57 (m, 1H), 3.38 (d, 2H), 3.07 (q, 6H), 2.62 (s, 4H), 2.23 (m, 8H), 1.97 (q, 6H), 1.26 (m, 38H, should be 40H), 0.84 (m, 6H); ^{13}C NMR (75 MHz, $CDCl_3$) δ 173.57, 130.00, 129.62, 129.59, 98.74, 62.68, 34.19, 34.01, 31.89, 29.75, 29.53, 29.31, 29.24, 29.22, 29.18, 29.15, 27.22, 24.90, 24.83, 22.67, 21.41, 20.15, 14.11; HRMS (ESI) calcd for $C_{52}H_{89}NO_{10}P$ $[M-H]^-$ 918.6224 found 918.6198.

Dioctadecylamine-BCN conjugate (2): ((1R,8S,9s)-bicyclo[6.1.0]non-4-yn-9-yl)methyl (15-octadecyl-10,14-dioxo-3,6-dioxa-9,15-diazatritriacontyl)carbamate.
BCN-POE_3-NH-C(O)$CH_2CH_2CH_2$C(O)OSu (100mg, 0.186 mmol) was dissolved in 6 ml dry CH_2Cl_2 which was then added to a suspension of dioctadecylamine (100 mg, 0.192 mmol) in 4 ml dry CH_2Cl_2. Et_3N (78 µL, 0.55 mmol) was added and over 2 hours the solution became homogenous. The solution was left to stir after which the product was purified directly by column chromatography (95:5 EtOAc:MeOH) resulted in a colorless oil (152 mg, 87%).
Analytical data: R_f 0.25 (95:5 EtOAc/MeOH); ^{1}H NMR (300 MHz, $CDCl_3$) δ 6.38 (s, 1H), 5.40 (s, 1H), 4.16 (d, 2H), 3.61 (bs, 4H), 3.56 (q, 5H), 3.41 (m, 5H), 3.27 (t, 2H), 3.19 (t, 2H) 2.37 (t,2H), 2.25 (m, 8H), 1.95 (t, 2H), 1.26 (bs, 80H, should be 72), 0.88 (m, 8H); ^{13}C NMR (75 MHz, D_2O) δ 170.27, 169.30, 154.24, 96.18, 67.62, 67.52, 67.30, 60.09, 45.39, 43.36, 38.17, 36.53, 33.18, 29.32, 27.10, 27.06, 26.98, 26.86, 26.79, 26.76, 26.54, 26.46, 25.23, 24.50, 24.33, 20.09, 20.05, 19.00, 18.82, 17.52, 15.20, 11.51; HRMS (ESI) calcd for $C_{58}H_{108}N_3O_6$ $[M+H]^+$ 942.8232 found 942.8257.

2.3 Liposome preparation

Lipid stock solutions were prepared in ethanol and combined in a round bottom flask in a DOPC/DOPE/cholesterol/BCN-lipid ratio of 49/25/25/1. Labeled liposomes for flow cytometry were made by adding 0.2 mol% of Rho-PE. After removal of organic solvent with a rotary vacuum pump the resulting lipid film was flushed with nitrogen. Liposomes were formed by hydration of the lipid film with Hepes buffered saline (HBS; 10 mM Hepes, 145 mM NaCl, pH 7.4)) to a final concentration of 50 mM total lipid (TL). The size of the liposomes was reduced by extruding at least 20 times using a Lipex™ Extruder (Northern Lipids, Burnaby, BC, Canada) through polycarbonate membranes with a final pore size of 100 nm (Nuclepore, Pleasanton, CA, USA). Liposomes were then incubated with 5'-TAMRA-PEG3-Azide (Baseclick, Tutzing, Germany) in methanol in a 10:1 ratio of BCN-lipid:azide unless stated otherwise (this 10:1 ratio is corrected for the amount of BCN-lipid facing the inside of the liposome and as such is not available for coupling). The final methanol concentrations added to the liposomes were less than 0.25% (v/v).

2.4 Azido-DARPin conjugation to liposomes

To serve as an azide-containing model protein, a designed ankyrin repeat protein (azido-DARPin) was employed. EpCAM targeting DARPin 'Ac2' and Maltose Binding Protein (MBP) targeting control DARPin 'Off7' were expressed as previously described [18,19] where azido-homoalanine was incorporated at the N-terminus instead of the

initiator methionine and no cysteine functionality was introduced.
After preparation, liposomes were incubated overnight with azido-DARPin solutions in PBS, in BCN-lipid:azide ratios ranging from 100:1 to 5:1. After incubation, liposomes were ultracentrifuged at 55.000 RPM and resuspended three times, to wash away unconjugated protein. The total amount of phosphate in the resuspended samples was compared to an uncentrifuged sample to calculate the dilution and loss of sample between runs.

2.5 Liposome characterization

The total phosphate content of the liposome formulations was determined according to the method of Rouser et al. [20] with sodium biphosphate as a standard after destruction of the phospholipids with perchloric acid (PCA) and heating at 180°C. The mean particle size and the polydispersity index were measured by dynamic light scattering, using a Malvern CGS-3 multiangle goniometer with He-Ne laser source (λ=632.8 nm, 22 mW output power) under an angle of 90° (Malvern Instruments, Malvern, UK). The zeta-potential of the liposomes was measured using laser Doppler electrophoresis on a Zetasizer Nano-Z (Malvern Instruments) with samples dispersed in 10 mM Hepes buffer pH 7.4 (no added salts).

2.6 Coupling quantification by UPLC

Quantification of the coupling was done with a Waters Acquity UPLC system (Waters Corporation, Milford, MA, USA) with PDA and FLR detectors on a BEH300 C18 1.7 µm column. The gradient mobile phase at a flow rate of 0.25 ml/min was changed from 100% solvent A (Acetonitrile:H_2O 5:95 with 0.1% PCA) to 100% solvent B (Acetonitrile with 0.1% PCA) in 5 minutes and ran on solvent B for 2 additional minutes. UV detection with the PDA detector was done on 210 nm and the FLR detector was used at 545/575 for the 5'-TAMRA containing samples. Free ligand had a retention time of 2-3 minutes whereas conjugated ligand eluted at the end of the chromatogram with the liposomes. Peaks in the FLR channel were integrated and AUCs were used to calculate the ratio of coupled/uncoupled.

2.7 SDS-PAGE and Western Blotting

All liposome samples were diluted to a concentration of 2 mM phospholipids as this was found to be the highest amount of lipid that could be loaded without interfering with the electrophoresis of the protein on SDS-PAGE. The DARPin stock solution was diluted to concentrations equaling 100%, 75%, 50%, 40%, 30%, 20% and 10% of the total added amounts of protein in each of the liposome samples (20:1 ratio, 10:1 ratio, 5:1 ratio). Samples were mixed with reducing loading buffer and run on Bolt® 4-12% Bis-Tris gels (Life Technologies, Carlsbad, CA, USA) and then electrotransferred to a nitrocellulose membrane using the iBlot Dry Blotting system (Life Technologies). The membrane was blocked with 5% BSA in TBS-0.1% Tween 20 (TBS-T) for 1 hour at RT and then stained overnight at 4°C with a mouse anti-polyhistidine tag monoclonal antibody (CLANT227, Cedar Lane Technologies, Burlington, Ontario, Canada) diluted 1:1000 in 5% BSA in TBS-T. After washing with TBS-T the membrane was incubated with goat

anti-mouse IgG (H+L) with HRP conjugate (#31430 Pierce Antibodies) diluted 1:2000 in 5% BSA in TBS-T. After washing, protein bands were visualized with SuperSignal West Femto Chemiluminescent Substrate (Thermo Scientific) and detected using a Gel Doc Imaging system equipped with a XRS camera and Quantity One analysis software (Bio-Rad). Coupling efficiency was determined based on band intensity, as quantified with ImageJ software (v1.48 for Windows PC).

2.8 Flow cytometry

HT29 cells cells were cultured in Dulbecco's Modified Eagle's Medium with High Glucose (Sigma-Aldrich) containing 4.5 g/L D-dextrose and 4 mM L-glutamine supplemented with 10% (v/v) fetal bovine serum (Sigma-Aldrich) at 37°C in a humidified atmosphere containing 5% CO_2. Cells were regularly tested negative for mycoplasma.
Cells were harvested and seeded at 50.000 cells/well in a round-bottom 96-well plate. Rho-labeled liposomes with and without EpCAM targeting DARPin (Ac2) or with MBP-targeting control DARPin (Off7) were added to the wells in triplicate in a final concentration of 7.8125 µM – 1 mM total lipid and incubated in the dark at 4°C. For the experiment varying the ligand density, Rho-labeled liposomes with targeting DARPin (Ac2) densities of 0.01% - 0.2% were added to the wells in triplicate at a fixed final concentration of 0.5 µM or 0.25 µM total lipid and incubated in the dark at 4°C.
After incubation cells were washed three times with 0.3% BSA in PBS and fixed with a final concentration of 2.5% formalin (from a 10% Neutral Buffered Formalin Solution, Sigma-Aldrich). The mean rhodamine fluorescence intensity was measured with a BD FACSCanto II (Becton & Dickinson, Mountain View, CA, USA) and 10.000 events per well were acquired. Data was analyzed with BD FACSDiva™ software. Histogram overlays were made manually in Photoshop CS6 (Adobe) using the Diva-Fit method[21].

2.9 Calcein leakage

To show that incorporation of the anchor or that the conditions of the click reaction itself do not damage or cause leakage of the membrane, the leakage of calcein from the liposomes was measured. Liposomes were loaded with 75 mM calcein, which is quenched in this concentration, creating a low baseline signal. When calcein leaks out, it is diluted over the large exterior volume. A further dilution step assures that leaked calcein concentration are in the linear range. Leakage was monitored in presence and absence of the 5'-TAMRA-azide in 10:1 ratio (BCN-lipid:azide). Liposomes with and without the anchor were also compared, as well as the influence of incubation at 4°C or at room temperature. Samples were taken at t=0, t=1, t=2, t=4, t=8, t=12 and t=24 hours and calcein fluorescence was measured at 485/520 nm.
Leakage was expressed as percentages using the formula

$$Leakage\ (\%) = \frac{signal(t) - signal\ (0)}{signal(max) - signal(0)}$$

where the maximum signal was obtained by solubilization of the liposomes using 0.5% final concentration of Triton X-100. Samples were diluted before measuring to a concentration where Triton X-100 did not interfere with the fluorescence detection.

3. Results and Discussion

3.1 Liposome characterization

Several liposome formulations bearing different surface modifications were examined. Preliminary comparison of the two BCN-lipid conjugates revealed little difference in the ease of incorporation into liposomes. We did, however, observe slightly better azide coupling efficiency with compound 2 and for this reason employed this BCN-lipid in all subsequent experiments. The optimal liposome composition was found to consist of a mixture of DOPC/DOPE/cholesterol in a ratio of 50/25/25 with and without 1% of BCN-lipid 2. Extrusion through 0.1 µm membranes typically produced vesicles of 0.12 µm in diameter and a polydispersity of <0.1. While incorporation of 1% of the BCN-lipid did not change the characteristics of the vesicles, incorporation of 5% of the synthetic lipid did increase the size and polydispersity slightly (data not shown). Measurements of the zeta-potential showed that the liposomes are neutral when unfunctionalized and acquire a negative charge when the DARPins are conjugated. This change was expected as the liposome surfaces here used are not PEGylated and protein conjugation thus has a significant influence on charge. See Table 3.1.

Table 3.1 | Size and charge characteristics of the different formulations

Formulation	Size (µm)	PDI	Zeta Potential (mV)
No anchor	0.12 ±0.03	0.09	-3.5 ±0.2
Unfunctionalized	0.12 ±0.03	0.08	-3.1 ±0.1
10:1 TAMRA-dye (0.1%)	0.12 ±0.03	0.09	-4.4 ±0.2
Ac2 DARPin	0.12 ±0.04	0.10	-16.6 ±0.6
Off7 DARPin	0.12 ±0.03	0.09	-17.0 ±0.4

3.2 Coupling efficiency of small molecule azide-dye

To investigate the coupling efficiency of the SPAAC ligation a commercially available 5'-TAMRA-azide dye was coupled the liposomes. Using fluorescence detection, this dye could be readily detected with high accuracy without interference from any of the other components. As expected, the retention time of the TAMRA dye–lipid conjugate increased relative to the azide dye starting material as evidenced by a shifting of the peak to the later end of the UPLC chromatogram. Integration of the peak areas for signals corresponding to the conjugated and unconjugated species were used to calculate the conjugated/unconjugated ratio.

The synthetic BCN-lipids 1 and 2 were compared in a low liposome concentration (5 mM total lipid) to investigate the reaction kinetics of each when coupling to the 5'-TAMRA-azide at 10:1 BCN-lipid:azide ratio. At these concentrations, the conjugation was not complete after 24 hours, but the reaction rate when using lipid 2 was significantly faster than for lipid 1 (see Figure 3.2A). The difference in reaction rate may be due to a difference in the length of the spacer unit. In BCN-lipid 1, the reactive cyclooctyne unit is conjugated directly to the phosphate headgroup, whereas lipid 2 contains has a longer spacer making the reactive group more mobile and less prone to steric hindrance at the liposomal membrane surface.

Because of the favorable coupling kinetics we chose to continue exclusively with BCN-lipid 2 for further characterization. When the total lipid concentration was increased to 50 mM total lipid, reaction kinetics dramatically increased to ~75% conversion after 4 hours and conjugation was essentially complete after overnight incubation (Figure 3.2B).

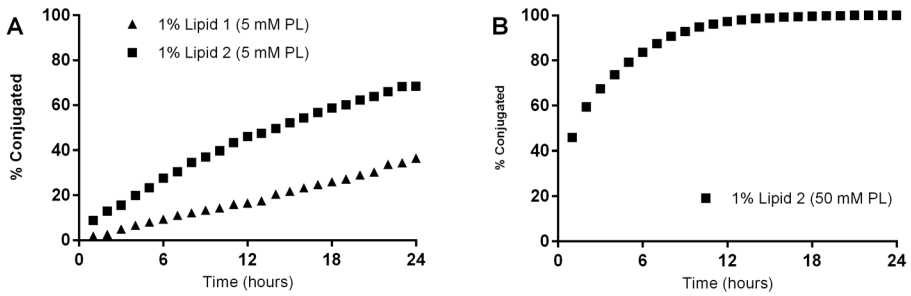

Figure 3.2 | Reaction kinetics of 5'-TAMRA-azide to the liposomes
A: Initial comparison of both anchors, 1% functional lipid incorporated in 5 mM total phospholipids.
B: 1% of Lipid 2 incorporated in 50 mM total phospholipids.

Next, the conjugation efficiency of different BCN-lipid:azide ratios was investigated. At the same lipid concentration, ratios from 100:1 to 1:1 were incubated as well as with a twofold excess of azide (see Table 3.2). Coupling of all ratios down to 5:1 was complete after overnight incubation. At the ratio of 2.5:1 coupling was more than 95% but in the 1:1 ratio only 50% of the dye molecules were conjugated. This is not explained by the fact that half of the reactive BCN moieties are on the inside of the liposomes, as the ratios mentioned are corrected for this (ratios are relative to the amount of BCN on the outside of the liposomal surface, which is assumed to be 50%). Interestingly, the level of conjugation measured for the sample that was incubated with a 1:2 ratio of BCN:azide, was only 25%. The observation that when working with substoichiometric levels of the BCN-lipid the amount surface conjugated dye cannot be increased by simply adding more of the azide-dye may indicate that a fraction of the BCN groups are not reactive or available for binding. A possible explanation is that part of the liposomes is not unilamellar, although that is generally assumed when membrane extrusion is used. If a liposome has more than one bilayer, the BCN groups in the inner layers are not available for reaction and total available fraction is less than 50%. Another possible reason for incomplete availability of the BCN moiety may be due to its relative hydrophobicity, causing it to fold back into the bilayer as has been previously described in polymer vesicles [22]. A final explanation for the incomplete coupling when using equimolar ratio is that the surface of the liposome becomes occupied at a certain point after which no additional dye molecules can be conjugated. This may explain why conjugation of the 1:1 sample did not go to completion while half of the BCN groups remain unreacted.

Working with the assumption that a liposome consists of 100.000 lipid molecules [23], this results in the theoretical number of molecules per liposome as shown in Table 3.2. Between ratios of 1:5 and 1:100 conjugation of small molecule azide is complete, so the exact number of conjugated molecules can be controlled by the feed concentration. It obviously depends on the application which density of surface modification is desired, but in the case of targeting ligands our data (section 3.4) as well as previous reports show that numbers well below 100 are sufficient to achieve cell association [24].

Table 3.2 | BCN-lipid:azide ratios used for conjugation to the small molecule azide-dye
Corresponding numbers of ligand per liposome are listed in the third row. Numbers in parentheses are theoretical, as conjugation was not complete in these ratios.

Azide:BCN ratio	0.01	0.02	0.04	0.10	0.20	0.40	1.00	2.00
% Azide conjugated	100%	100%	100%	100%	100%	>95%	50%	25%
Ligands conjugated per liposome	5	10	20	50	100	(200)	(500)	(500)

3.3 Conjugation of an azide-containing DARPin to liposomal surfaces

The site-specific introduction of azido-amino acids into recombinant proteins allows for full control over the position of the conjugation site. As previously described, azido-homoalanine was introduced at the N-terminus of an anti-EpCAM DARPin, where it replaces the initiator methionine, providing a single, orthogonal conjugation site that does not interfere with the binding domain of the DARPin [19]. Liposomes containing BCN-lipid 2 were incubated with the azido-DARPin at ratios of 20:1, 10:1, 5:1 BCN-lipid:azide. For optimal electrophoresis the samples were diluted and protein was detected using a polyhistidine antibody after Western blotting, alongside free protein dilutions as a calibration standard. A liposome sample without the BCN-lipid was included to show that there is no non-specific binding to the liposomes and that the washing steps are sufficient to wash away all unconjugated protein. Free DARPin samples were loaded in concentrations corresponding to 50% of the amount that was added to the samples for conjugation. Band intensities in Figure 3.3 already indicate that conjugation is less than that amount.

For more accurate quantification, the three samples mentioned above were loaded together with protein dilutions equaling 100%, 75%, 50%, 40%, 30%, 20% and 10% of total added protein. Bands were quantified and conjugation ratios were calculated as shown in Table 3.3. (Quantitative blots included in Supplementary Materials Figures S3.1-3)

Table 3.3 | BCN-lipid:azide ratios used for conjugation to the azido-DARPins

Azide:BCN ratio	0.05	0.10	0.20
% Azide conjugated	23.4%	17.5%	11.4%
Ligands conjugated per liposome	6	9	12

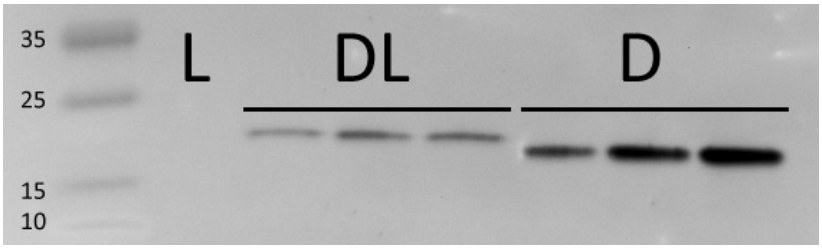

Figure 3.3 | Western Blot of DARPins and conjugated-DARPin liposome samples
(L) Liposomes without BCN-lipid (DL) DARPin-conjugated liposomes in 20:1, 10:1, 5:1 BCN-lipid:azide ratios (D) unconjugated DARPin samples corresponding to 50% of the amount added to each of the conjugated samples.

Compared with coupling of the small molecule dye, coupling of the protein was less efficient (based on molar quantities) and did not reach completion, even though BCN is always in molar excess, and the reaction time was sufficient to reach a plateau. This may be due to the large size of the protein leading to possible steric hindrance. Higher levels of protein conjugation are achievable by increasing the amount of azido-protein added, but the efficiency of the process (percentage of total protein coupled) is then lowered. By increasing the feed ratio of azide, more protein could be coupled, but the amount coupled relative to the amount that was added is much lower, resulting in the low conjugation percentages.

3.4 Cell association of DARPin functionalized liposomes

To show the functionality of the DARPin modified liposomes, binding studies were undertaken using EpCAM expressing HT-29 cells. Using the SPAAC approach the liposomes were functionalized with DARPin 'Ac2' which is known to bind EpCAM with low nanomolar affinity [18] or with DARPin 'Off7', which binds Maltose Binding Protein (used as off-target control). Non-functionalized liposomes were also used as secondary control. Experiments were carried out at 4°C to block internalization mechanisms so any cell association is considered surface binding and not internalization.

When lipid concentrations were varied, i.e. more liposomes were added, increased cell binding was seen with increasing amounts of those liposomes functionalized with 'Ac2'. The liposomes that were functionalized with the off-targeting DARPin did not show any cell association and neither did the unfunctionalized liposomes, indicating that the cell association was DARPin specific. See Figure 3.4A
In a second experiment, liposome concentrations were kept constant, while the density of surface modification was varied. BCN-lipid:azide ratios from 100:1 to 5:1 were used (keeping the azide concentration constant), corresponding to a theoretical maximal conjugation of 5 to 100 ligands per liposome (ligand densities from 0.01% to 0.2% BCN-lipid to total lipid). Cell association was found to be independent of ligand density, suggesting that the lower ligand loading is sufficient to achieve cell binding in vitro. The number of total liposomes did have an effect, showing more total cell association in the higher liposome concentration, but again showing no influence of the degree of surface modification (see Figure 3.4B).

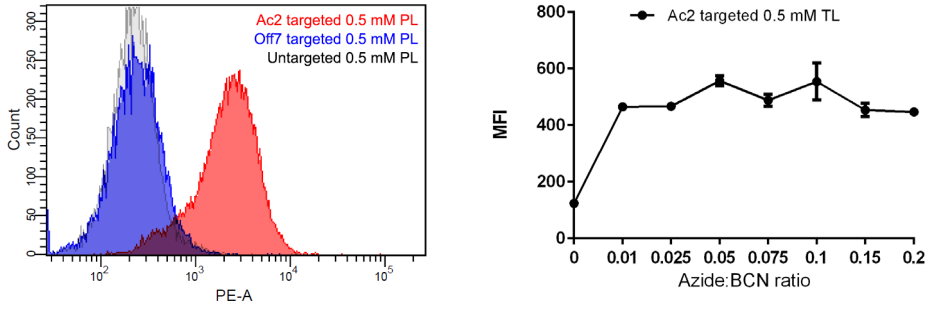

Figure 3.4 | Binding of Rho-PE labeled DARPin-modified liposomes to HT-29 cells
A: 'Ac2' targeted liposomes bind to the EpCAM expressing HT-29 cells whereas 'Off7' targeted and untargeted liposomes do not.
B: When the number of ligands is varied, no increased binding is seen.

It has been previously demonstrated that for cell targeting, there is no need for extremely high degrees of surface modification[24] and certainly not when the binding affinity of the ligand is as high as that of the DARPin. On the contrary, increasing ligand density on a liposomal surface can result in an avidity effect, wherein the discriminative capacity for cells expressing high levels of target versus low expressing cells is lost [24]. It was recently shown that increasing the avidity of a nanoparticulate system led to nanomolar affinities, also for cell types that were considered 'low expressers' of the target antigen [25]. The receptor density-avidity relationship is a nonlinear one and most probably is also very much influenced by receptor and ligand type. In the experiments we here describe all the conditions explored were found to result in strong cell association in vitro.

3.5 Leakage assay

To assess the effect of the coupling reaction on the stability of the liposomes, a calcein leakage assay was performed. While no effect on size or polydispersity was observed after incubation and conjugation of the ligands (see Table 3.1), the leakage assay was performed to show that there is no (temporary) destabilization or rupture of the liposomal membrane during conjugation. The liposome composition used here is inherently leaky due to the use of unsaturated lipids. Despite the presence of cholesterol a quick release was observed in the first hours after removal of the calcein from the exterior volume. Figure 3.5A shows the leakage rates of azide-treated liposomes with and without BCN-lipid 2 and Figure 3.5B shows the leakage of liposomes containing the BCN-lipid that were incubated with or without the azide. No increased leakage was seen after incorporation of the BCN-lipid or during the click reaction. Leakage rates were expressed relative to the maximum leakage that was measured after solubilization of the liposomes with Triton X-100. Leakage reached a plateau of approximately 30% and could not be decreased by incubation at 4°C as compared to RT (see Supplementary Materials Figure S3.4).

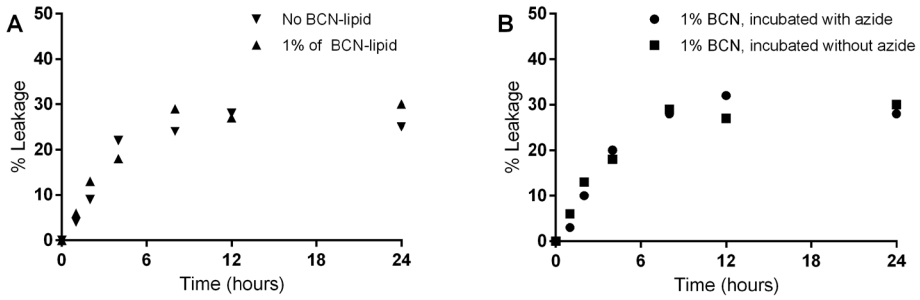

Figure 3.5 | Leakage of calcein from liposomes under coupling conditions
A: Liposomes with and without 1% of BCN-lipid show similar leakage profiles.
B: Liposomes with 1% of BCN-lipid, incubated with and without azide. The click reaction did not have an influence on the amount of leaked calcein.

4. Conclusion

To date, modification of liposomes via "click chemistry" has relied upon either the Staudinger ligation [6] or the copper (I) catalyzed alkyne/azide cycloaddition (CuAAC) [26,27]. We here described what is, to our knowledge, the first demonstration of liposome functionalization by using a strain-promoted alkyne/azide cycloaddition (SPAAC) wherein the cyclooctyne moiety is incorporated into the liposomal membrane. The inverse approach, employing azide-modified lipids in the liposome has been previously reported, however, this then requires modification of the ligand to introduce a cyclooctyne group [28]. The SPAAC approach eliminates the need of the copper catalyst, which can be toxic in many liposome applications. When a small molecule azide is used as the 'ligand' reasonable reaction rates are achieved and the degree of surface modification can be fully controlled. A growing number of azide-modified compounds are commercially available and methods to incorporate azides in peptides and proteins are also increasing. In this work we show the application of site-specific conjugation by conjugating an azide-modified DARPin to a liposome and the feasibility of this approach for cell targeting. Site-specific conjugation is an advantage over other conjugation methods and SPAAC is an attractive alternative for copper-catalyzed CuAAC.

Acknowledgements

The research leading to these results has received support from the Innovative Medicines Initiative Joint Undertaking under grant agreement n° 115363 resources of which are composed of financial contribution from the European Union's Seventh Framework Programme (FP7/2007-2013) and EFPIA companies' in kind contribution. Financial support also provided by Utrecht University and the Netherlands Organization for Scientific Research (VIDI grant to NIM).

References

[1] R.I. Jølck, L.N. Feldborg, S. Andersen, S.M. Moghimi, T.L. Andresen, Engineering liposomes and nanoparticles for biological targeting., Adv. Biochem. Eng. Biotechnol. 125 (2011) 251–80. doi:10.1007/10_2010_92.

[2] M. Fleiner, P. Benzinger, T. Fichert, U. Massing, Studies on Protein–Liposome Coupling Using Novel Thiol-Reactive Coupling Lipids: Influence of Spacer Length and Polarity, Bioconjug. Chem. 12 (2001) 470–475. doi:10.1021/bc000101m.

[3] F. Said Hassane, B. Frisch, F. Schuber, Targeted liposomes: convenient coupling of ligands to preformed vesicles using "click chemistry"., Bioconjug. Chem. 17 (2006) 849–54. doi:10.1021/bc050308l.

[4] B.C. Bundy, J.R. Swartz, Site-specific incorporation of p-propargyloxyphenylalanine in a cell-free environment for direct protein-protein click conjugation., Bioconjug. Chem. 21 (2010) 255–63. doi:10.1021/bc9002844.

[5] E. Saxon, Cell Surface Engineering by a Modified Staudinger Reaction, Science (80-.). 287 (2000) 2007–2010. doi:10.1126/science.287.5460.2007.

[6] H. Zhang, Y. Ma, X.-L. Sun, Chemically-selective surface glyco-functionalization of liposomes through Staudinger ligation., Chem. Commun. (Camb). (2009) 3032–4. doi:10.1039/b822420j.

[7] F.L. Lin, H.M. Hoyt, H. van Halbeek, R.G. Bergman, C.R. Bertozzi, Mechanistic investigation of the staudinger ligation., J. Am. Chem. Soc. 127 (2005) 2686–95. doi:10.1021/ja044461m.

[8] N.J. Agard, J.A. Prescher, C.R. Bertozzi, A strain-promoted [3 + 2] azide-alkyne cycloaddition for covalent modification of biomolecules in living systems., J. Am. Chem. Soc. 126 (2004) 15046–7. doi:10.1021/ja044996f.

[9] P.V Chang, J.A. Prescher, E.M. Sletten, J.M. Baskin, I.A. Miller, N.J. Agard, et al., Copper-free click chemistry in living animals., Proc. Natl. Acad. Sci. U. S. A. 107 (2010) 1821–6. doi:10.1073/pnas.0911116107.

[10] S.T. Laughlin, C.R. Bertozzi, In vivo imaging of Caenorhabditis elegans glycans., ACS Chem. Biol. 4 (2009) 1068–72. doi:10.1021/cb900254y.

[11] J. Dommerholt, S. Schmidt, R. Temming, L.J.A. Hendriks, F.P.J.T. Rutjes, J.C.M. Van Hest, et al., Readily accessible bicyclononynes for bioorthogonal labeling and three-dimensional imaging of living cells, Angew. Chemie - Int. Ed. 49 (2010) 9422–9425. doi:10.1002/anie.201003761.

[12] A.J. de Graaf, M. Kooijman, W.E. Hennink, E. Mastrobattista, Nonnatural amino acids for site-specific protein conjugation., Bioconjug. Chem. 20 (2009) 1281–95. doi:10.1021/bc800294a.

[13] S.F.M. van Dongen, R.L.M. Teeuwen, M. Nallani, S.S. van Berkel, J.J.L.M. Cornelissen, R.J.M. Nolte, et al., Single-step azide introduction in proteins via an aqueous diazo transfer., Bioconjug. Chem. 20 (2009) 20–3. doi:10.1021/bc8004304.

[14] Y. Ryu, P.G. Schultz, Efficient incorporation of unnatural amino acids into proteins in Escherichia coli, 3 (2006) 263–265. doi:10.1038/NMETH864.

[15] A. Deiters, T.A. Cropp, D. Summerer, M. Mukherji, P.G. Schultz, Site-specific PEGylation of proteins containing unnatural amino acids., Bioorg. Med. Chem. Lett. 14 (2004) 5743–5. doi:10.1016/j.bmcl.2004.09.059.

[16] M. Fernández-Suárez, H. Baruah, L. Martínez-Hernández, K.T. Xie, J.M. Baskin, C.R. Bertozzi, et al., Redirecting lipoic acid ligase for cell surface protein labeling with small-molecule probes., Nat. Biotechnol. 25 (2007) 1483–7. doi:10.1038/nbt1355.

[17] K.L. Kiick, E. Saxon, D.A. Tirrell, C.R. Bertozzi, Incorporation of azides into recombinant proteins for chemoselective modification by the Staudinger ligation., Proc. Natl. Acad. Sci. U. S. A. 99 (2002) 19–24. doi:10.1073/pnas.012583299.

[18] N. Stefan, P. Martin-Killias, S. Wyss-Stoeckle, A. Honegger, U. Zangemeister-Wittke, A. Plückthun, DARPins recognizing the tumor-associated antigen EpCAM selected by phage and ribosome display and engineered for multivalency., J. Mol. Biol. 413 (2011) 826–43. doi:10.1016/j.jmb.2011.09.016.

[19] M. Simon, U. Zangemeister-Wittke, A. Plückthun, Facile double-functionalization of designed ankyrin repeat proteins using click and thiol chemistries., Bioconjug. Chem. 23 (2012) 279–86. doi:10.1021/bc200591x.

[20] G. Rouser, S. Fleischer, A. Yamamoto, Two dimensional thin layer chromatographic separation of polar lipids and determination of phospholipids by phosphorus analysis of spots, Lipids. 5 (1970) 494–496. doi:10.1007/BF02531316.

[21] K. Weber, B. Fehse, Diva-Fit: a step-by-step manual for generating high-resolution graphs and histogram overlays of flow cytometry data obtained with FACSDiva software, CTT. 1 (2009) 1–4. doi:10.3205/ctt-2009-en-000045.01.

[22] S. A. Meeuwissen, M.F. Debets, J.C.M. van Hest, Copper-free click chemistry on polymersomes: pre- vs. post-self-assembly functionalisation, Polym. Chem. 3 (2012) 1783. doi:10.1039/c2py00466f.

[23] D.A. Marsh, CRC Handbook of Lipid Bilayers, CRC Press, Boca Raton, FL, 1990.

[24] D. Kirpotin, J.W. Park, K. Hong, S. Zalipsky, W.L. Li, P. Carter, et al., Sterically stabilized anti-HER2 immunoliposomes: design and targeting to human breast cancer cells in vitro., Biochemistry. 36 (1997) 66–75. doi:10.1021/bi962148u.

[25] J.E. Silpe, M. Sumit, T.P. Thomas, B. Huang, A. Kotlyar, M.A. van Dongen, et al., Avidity modulation of folate-targeted multivalent dendrimers for evaluating biophysical models of cancer targeting nanoparticles., ACS Chem. Biol. 8 (2013) 2063–71. doi:10.1021/cb400258d.

[26] R. Tarallo, A. Accardo, A. Falanga, D. Guarnieri, G. Vitiello, P. Netti, et al., Clickable functionalization of liposomes with the gH625 peptide from Herpes simplex virus type I for intracellular drug delivery., Chemistry. 17 (2011) 12659–68. doi:10.1002/chem.201101425.

[27] S. Cavalli, A.R. Tipton, M. Overhand, A. Kros, The chemical modification of liposome surfaces via a copper-mediated [3 + 2] azide-alkyne cycloaddition monitored by a colorimetric assay., Chem. Commun. (Camb). (2006) 3193–5. doi:10.1039/b606930d.

[28] H.E. Bostic, M.D. Smith, A.A. Poloukhtine, V.V Popik, M.D. Best, Membrane labeling and immobilization via copper-free click chemistry., Chem. Commun. (Camb). 48 (2012) 1431–3. doi:10.1039/c1cc14415d.

Supplementary Materials

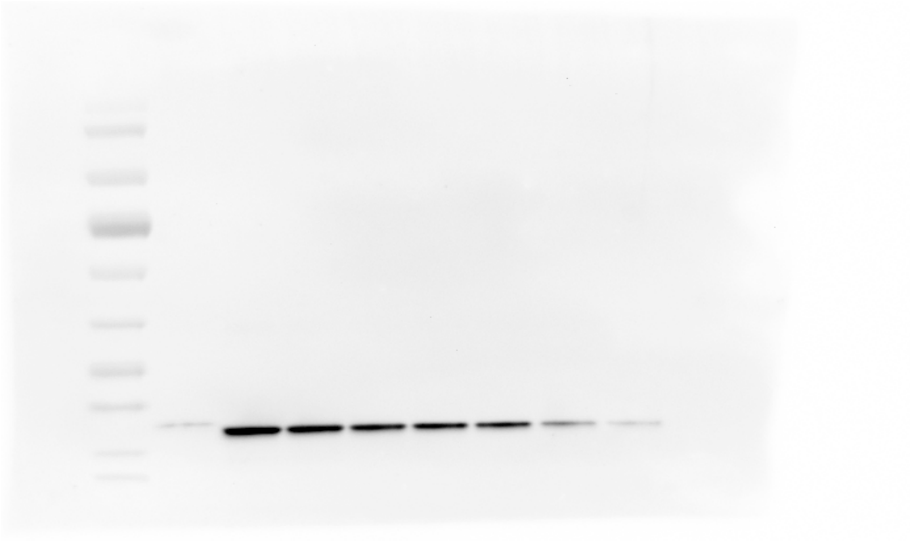

Figure S3.1 | Liposomes incubated with azido-DARPin in BCN lipid:azide ratio of 1:5
Western Blot used for quantification of coupled protein. Lane 2: liposome sample in 2mM PL. Lane 3-10, DARPin protein samples corresponding to 100%, 75%, 50%, 40%, 30%, 20%, 10% of the total amount of protein added.

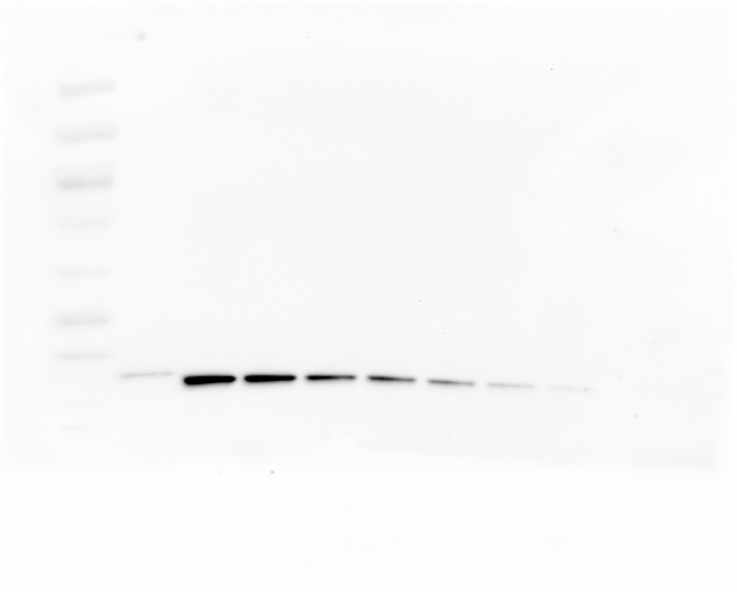

Figure S3.2 | Liposomes incubated with azido-DARPin in BCN lipid:azide ratio of 1:10
Western Blot used for quantification of coupled protein. Lane 2: liposome sample in 2mM PL. Lane 3-10, DARPin protein samples corresponding to 100%, 75%, 50%, 40%, 30%, 20%, 10% of the total amount of protein added.

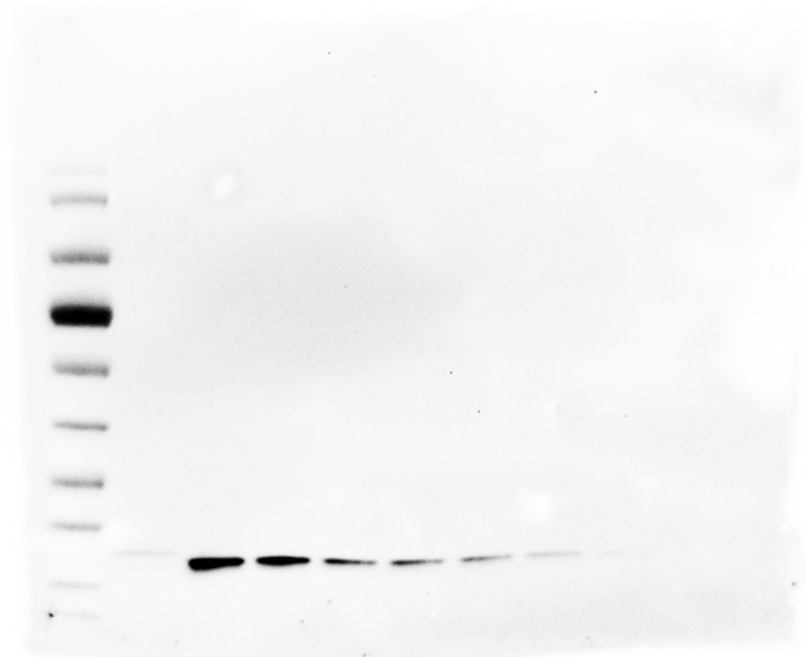

Figure S3.3 | Liposomes incubated with azido-DARPin in BCN lipid:azide ratio of 1:20
Western Blot used for quantification of coupled protein. Lane 2: liposome sample in 2mM PL. Lane 3-10, DARPin protein samples corresponding to 100%, 75%, 50%, 40%, 30%, 20%, 10% of the total amount of protein added.

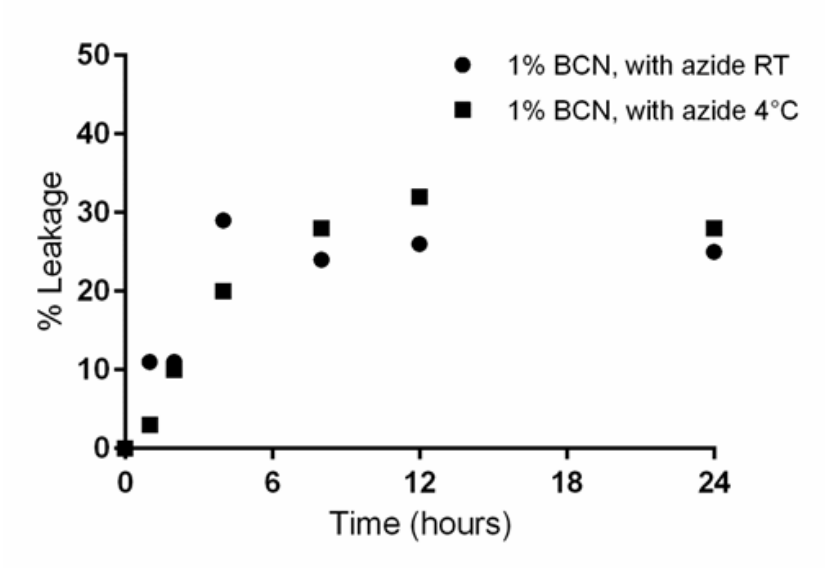

Figure S3.4 | Leakage of calcein from liposomes under coupling conditions
Leakage from the liposomes could not be prevented by incubation at 4°C. The leakage profile is similar to that of the samples incubated at room temperature.

Chapter 4

A critical evaluation of quantification methods for oligonucleotides formulated in lipid nanoparticles

Erik Oude Blenke[1]
Martijn J. W. Evers[1]
Volker Baumann[2]
Johannes Winkler[2]
Gert Storm[1]
Enrico Mastrobattista[1]

[1]Department of Pharmaceutics, Utrecht Institute of Pharmaceutical Sciences (UIPS), Faculty of Science, Utrecht University, Universiteitsweg 99, 3584 CG Utrecht, The Netherlands

[2]University of Vienna, Department of Pharmaceutical Chemistry, Althanstraße 14, Vienna, Austria

Submitted for publication

Abstract

There is a very large variety in the types of nanoparticulate lipid formulations for oligonucleotides, and remarkably, also a very large heterogeneity in the methods for analyzing oligonucleotide load, encapsulation efficiency and oligonucleotide release. Furthermore, a literature survey showed that the extent to which these procedures are reported in scientific literature varies greatly, with some of them not even reporting any quantification at all. This greatly hampers the reproducibility of nanoparticle preparation between different researchers and between different laboratories, which slows down the clinical translation of such nanomedicines. In this work, a standardized extraction method is proposed, in which potential contaminants from the carrier are removed by a simple extraction of the oligonucleotides. These extracts were then analyzed with seven commonly used methods for oligonucleotide quantification, including several absorbance based methods and the most commonly applied dye binding assay. Strikingly, differences in absolute values up to fourfold were found when the same sample was analyzed using different methods which should be taken into consideration when reports using different methods are compared. Furthermore, these results indicate that the most commonly applied method, the dye binding assay, may not be suitable for short oligonucleotides like siRNAs. The procedure described here allowed for the comparison of loading efficiency and capacity of three different formulations. Additionally, by means of an advanced UPLC technique, the structural integrity of the oligonucleotide cargo in the formulations could be assessed. The found differences in quantification methods as described here underscore the need for proper documentation of methods to correctly interpret published results, which –with regard to oligonucleotide analysis- is currently lacking in many reports.

Graphical Abstract

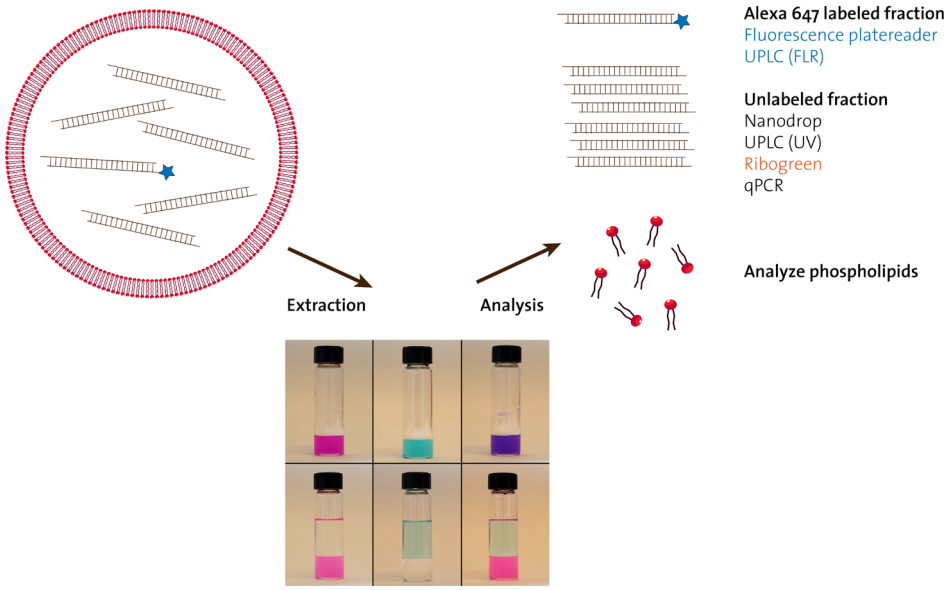

1. Introduction

Lipid nanoparticles (LNP) are amongst the most advanced nucleic acid delivery systems currently in clinical trials [1,2]. But also in pre-clinical and academic settings a lot of efforts are put in further improving and developing such systems [3]. Despite an explosion in the number of papers and groups working on nanomedicine, clinical translation has lagged behind. An increasing number of voices from within the field is now arguing that instead of making even more and more advanced delivery systems, the focus should be on a more rational evaluation and better characterization of the 'simple' types [4–8]. When taking LNPs as example, a head-to-head comparison of published lipid systems is hampered by the wide variety in encapsulation efficiency, load per particle and nucleic acid to lipid ratio in different systems. When nucleic acids are not encapsulated in the carrier but are merely complexed to them, it has been reported that the association of nucleic acids is incomplete and reversible [9]. However, many researchers appear to assume that the whole load of nucleic acids that is added is associated (complexed) with the carrier system and strikingly, in a literature survey of recent publications about lipid systems for nucleic acids, one third of all papers (13/36) did not quantify the total load of nucleic acids and encapsulation efficiency (See Supplementary Table S4.1). The most widely used method of characterization is with a gel-retardation assay (10/36), where the optimal ratio between carrier and cargo is determined, but this is rarely applied in a quantitative way. The second most-applied method is the Ribogreen® dye-binding assay (6/36) but some limitations to the two most commonly used methods have been reported [9]. More worrisome is the finding that many of the surveyed reports proceed to in vivo studies without reporting any quantification at all (7/13 non-quantified preparations are used in vivo). Each method will have its benefits and limitations under certain conditions and there is probably no gold standard, but the high heterogeneity in quantification protocols or the total lack thereof contributes to the low reproducibility of current scientific literature and the lack of clinical translation [8,10].

In this work, the degree of loading and the encapsulation efficiency of three nucleic acid lipid formulations is compared by using a selection of commonly used quantification methods for nucleic acids. To get an impression of the robustness of the various analytical assays, their interchangeability and their accuracy, we have made a head-to-head comparison of the most frequently used analytical techniques for nucleic acid quantifications in pharmaceutical formulations. These results should guide the formulation scientists in deciding which assay would work best for their application.

Many of these analytical methods rely on fluorescence or absorbance detection, but particulate systems (or excipients thereof, like lipids or detergents) interfere with such methods. Therefore, we propose a simple extraction method for lipid-based formulations to remove most compounds that may interfere with the tested analytical assays. The extraction method has been validated for two types of small ribonucleic acids (an siRNA and a single stranded antisense oligonucleotide) and the quantification methods have been evaluated for three types of LNP formulation methods, with varying nucleic acid loads. Quantification of the nucleic acid load can be done spectroscopically, measuring the absorbance of the nucleobases, or with an intercalating reagent that

produces a fluorescent signal (dye binding, Ribogreen® assay). For some purposes, formulations are loaded with (a fraction of) fluorophore labeled cargo, for example to study the stability in complex fluids [9] or cellular uptake [11]. The fluorescent fraction of the cargo can also be used to determine the concentrations in the formulations. Finally, two methods of quantitative PCR (originally designed for measuring intact siRNA in the target cell) are compared and employed to quantify the nucleic acid load of the LNPs in a highly sensitive and sequence based manner.

2. Materials and Methods

2.1 Materials

Nucleic acids

All nucleic acids used here are provided by GlaxoSmithKline (Stevenage, UK) for use in the EU IMI COMPACT consortium. Sequences are as follows:

Luciferase siRNA	Sense 5'-CUUACGCUGAGUACUUCGAdTdT-3'
	Antisense 5'-UCGAAGUACUCAGCGUAAGdTdT-3'
Negative Control siRNA (LV2)	Sense 5'-AUCGUACGUACCGUCGUAUdTdT-3'
	Antisense 5'-AUACGACGGUACGUACGAUdTdT-3'
GAPDH siRNA	Sense 5'-GGUCAUCCAUGACAACUUUdTdT-3'
	Antisense 5'-AAAGUUGUCAUGGAUGACCdTdT-3'
Luciferase ASO	5'-CCUCUUACCUCAGUUACA-3' (All PS)
Negative Control ASO	5'-CCTGUUAUACCACUUACA-3' (All PS)

Underlined bases indicate a 2'O-methyl modification. dT indicates a deoxyribonucleic acid base, all of which have phosphorothioate (PS) bonds. Antisense oligonucleotides consist completely out of PS bonds.

Labeled siRNA and ASO have the respective negative control sequences and are labeled with Alexa 647 on a C6 linker. All labeling was done on the 3' end and in case of siRNA, on the sense strand.

Lipids

1,2-dioleoyl-3-trimethylammonium-propane (DOTAP), 1,2-dioleoyl-3-dimethylammonium-propane (DODAP), N-palmitoyl-sphingosine-1-succinyl[methoxy(polyethylene glycol)2000] (C16 Ceramide-PEG2000), L-α-phosphatidylethanolamine-N-(lissamine rhodamine B sulfonyl) (Rho-PE) were from Avanti Polar Lipids (Alabaster, AL, USA). Cholesterol was from Sigma-Aldrich (St. Louis, MO, USA). 1,2-dipalmitoyl-sn-glycero-3-phosphocholine (DPPC), 1,2-dipalmitoyl-sn-glycero-3-phospho-(1'-rac-glycerol) (DPPG), 1,2-distearoyl-sn-glycero-3-phosphocholine (DSPC) and 1,2-distearoyl-sn-glycero-3-phosphoethanolamine-N-[methoxy(polyethylene glycol)-2000] (DSPE-PEG(2000)) were a gift of Lipoid GmbH (Ludwigshafen, Germany).

2.2 Liposome preparation

For all formulations, a lipid film was made first by dissolving the lipids in chloroform and evaporating the organic solvent using a rotary evaporator and a 25 ml round bottom flask. The formed dry lipid film was flushed with nitrogen until all residual chloroform was removed. For nucleic acid formulations, all lipid films consisted of DSPC:DODAP:Cholesterol:CeramideC16-PEG2000 at a ratio of 25:25:40:10. For the 'preformed vesicle method', the lipid film was hydrated in 70% 50 mM citrate buffer pH 4.0 and 30% ethanol absolute to a final concentration of 8 mM total lipid. The formed vesicles were then extruded at least 10 times using a Lipex™ Extruder (Northern Lipids, Burnaby, BC, Canada) through Track etch polycarbonate membranes with a final pore size of 100 nm (Nuclepore, Pleasanton, CA, USA). A solution of 90% GAPDH siRNA and 10% Alexa 647 labeled LV2 Control siRNA or 90% Luciferase ASO and 10% Alexa 647 labeled Negative Control ASO in 70% 50 mM citrate buffer pH 4.0 and 30% ethanol absolute was then added dropwise to the empty vesicles under heavy stirring after both the vesicles and the nucleic acid solution were preheated to 45°C. The vesicles were then incubated at 45°C for 90 minutes to allow reorganization of the vesicles. Ethanol was removed and buffer was replaced by overnight dialysis in a 2K MWCO Slide-A-Lyzer G2 Dialysis Cassette (Life Technologies) at 4°C against PBS. The other lipid films are hydrated with the same amount of nucleic acids, either in 70% 50 mM citrate buffer pH 4.0 and 30% ethanol absolute or in 100% 50 mM citrate buffer 4.0 and then extruded as above. The final NA/lipid ratio of all formulations was 0.06 (wt/wt). These formulations were also dialysed as above and after dialysis, unencapsulated nucleic acids were removed by three rounds of ultracentrifugation in a Type 70.1 Ti rotor for 50 minutes at 55.000RPM at 4°C. The pictures in Figure 1. were made with formulations containing 0.5 mol% Rhodamine-PE and 50:50% of the labeled:unlabeled siRNA. For the extraction validation, liposomes consisting of 10 mol% DOTAP, DPPG or DSPE-PEG2000 and 60:30 mol% of DPPC:Cholesterol were hydrated in Hepes Buffered Saline (10 mM HEPES, 145 mM NaCl) pH 7.4 to a final concentration of 10 mM total lipid. The hydrodynamic diameter and the polydispersity index of the liposomes were measured by dynamic light scattering, using a Malvern CGS-3 multiangle goniometer with He-Ne laser source (λ=632.8 nm, 22 mW output power) under an angle of 90° (Malvern Instruments, Malvern, UK). The zeta-potential was measured using laser Doppler electrophoresis in a Zetasizer Nano-Z (Malvern Instruments) with samples dispersed in 10 mM Hepes buffer pH 7.4 (no additional salts). The encapsulation efficiency was calculated using the following formula:

$$Encapsulation\ efficiency\ (\%) = \frac{\frac{[nucleic\ acids]}{[phospholipids]}\,after\ ultracentrifugation}{\frac{[nucleic\ acids]}{[phospholipids]}\,after\ dialysis} * 100$$

2.3 Extraction of lipids and nucleic acids

Lipids and nucleic acids were separated by an extraction according to Bligh and Dyer[13]. For every 100 µl of liposome sample in aqueous buffer, 375 µl of chloroform:methanol in 1:2 ratio was added. This forms one single phase in which both lipids and nucleic acids are dissolved. 125 µl of chloroform was then added and vortexed. 125 µl of MilliQ water was then added and vortexed. Tubes were then centrifuged at 1500xg for 90 seconds.

The top phase contains the water (including the salts in the initial sample) and methanol. This phase was transferred to a separate tube and the bottom phase consisting of chloroform could be assayed for total phosphate, according to the method of Rouser et al.[21] with sodium biphosphate as a standard after destruction of the phospholipids with perchloric acid and heating at 180°C. The top phase was evaporated in a vacuum concentrator and reconstituted in MilliQ water to measure the concentration of nucleic acids.

2.4 Extraction validation

To calculate the recovery of lipids in the organic phase and nucleic acids in the aqueous phase, liposomes consisting of DPPC:Cholesterol:X in 6:3:1, with X being (cationic) DOTAP, (anionic) DPPG, (neutral) DSPE-PEG2000 were spiked with nucleic acids. The nucleic acid solution contained 90% GAPDH siRNA and 10% Alexa 647 labeled Negative Control siRNA and was mixed in a 1:1 ratio with the three liposomes samples, with a final phospholipid concentration of 1 mM and a nucleic acid concentration of 1 uM. This mixture was extracted as described above and the organic phase was assayed for phosphate. As a 100% value an unextracted sample and unspiked sample of the same concentration was used. The top phase was evaporated as described and after reconstitution measured by UPLC as described below. As controls, siRNA samples were also mixed 1:1 with MilliQ. These were extracted and of half of the samples the top phase was collected. The other half were evaporated (including the organic phase) until completely dry and then reconstituted in MilliQ (there was no possible loss of sample in this tube and it was therefore used as the 100% value).

2.5 UPLC analysis

Nucleic acid quantification by UPLC was done using a Waters Acquity UPLC system (Waters Corporation, Milford, MA, USA) with PDA and FLR detectors on an Acquity UPLC Oligonucleotide BEH C18, 130A, 1.7uM, 2.1x100mm column (Waters Corporation). Gradient mobile phase at a flow rate of 0.2 ml/min was changed from 95% solvent A (10/90% Methanol/HFIP 400mM and 15mM TEA in water) to 40% solvent B (Methanol) in 5 minutes. Column operating temperature was 60°C as recommended by the manufacturer. UV detection with the PDA detector was done on 260nm and the FLR detector was used at 650/665 for detection of the Alexa 647 conjugated nucleic acids. Peaks were integrated and AUCs were compared to standard curves of the corresponding sequence to calculate concentrations. Whenever possible, quantification in the FLR channel was preferred over the PDA channel. For forced degradation, a 10 µM solution of LV2 Control siRNA was incubated with 100 µg/ml RNAse A (Thermo Fischer Scientific, Waltham, MA, USA) for 48 hours at room temperature and then injected in concentrations 1, 2.5, 5 and 10 µM.

2.6 Nanodrop

Nucleic acid concentrations were determined spectrophotometrically using a NanoDrop ND-1000 (Thermo Fischer Scientific). Absorbance at 260nm and a nucleic acid conversion factor was used to calculate concentrations.

2.7 Fluorescence detection

The concentration of Alexa 647 labeled nucleic acids was measured using a Jasco FP8300 Spectrofluorometer with micro-well plate reader. (JASCO Benelux BV., De Meern, Netherlands) Wavelengths used were 650/665 and a calibration curve was used to calculate concentrations.

2.8 Ribogreen® Assay

The commercially available Quant-iT™ RiboGreen® RNA Assay Kit (Thermo Fischer Scientific) was used according to the manufacturer's instructions. It was found that the 'low range assay' (1 ng/mL to 50 ng/mL) was not sensitive enough to detect the single stranded SCO so for these formulation the 'high range assay' (20 ng/mL to 1 µg/mL) was used. The corresponding sequences were used as a calibration curve. Measurement was done at 485/520 nm.

2.9 qPCR

Sample processing for cDNA synthesis and qPCR
The reference GAPDH siRNA duplex was diluted from a 1 µM solution to 1 nM as described in E. M. Kroh et al. [18] This stock solution was further diluted stepwise 295,520 fold to receive a 3.38 pM solution. For ensuring quantitative reverse transcription, a dilution array was prepared by diluting the 3.38 pM solution four times eight fold. The 3.38 pM solution contains 32,768 copies/µl. Four µl of this solution were used for cDNA synthesis (RevertAid First Strand cDNA Synthesis Kit, Thermo FisherScientific) and diluted six-fold before use as template in qPCR reactions. The samples were diluted and analyzed in the same way as the standard.

cDNA synthesis
cDNA synthesis was performed with the Thermo Scientific RevertAid First Strand cDNA Synthesis Kit in 40 µl reaction volumes. A GAPDH siRNA specific stem-loop RT primer was designed as described [14,16]. Three µl of a 1 µM GAPDH specific stem-loop RT primer were added to a PCR tube, followed by 3 µl of standard or sample solution, and filled up with 19 µl nuclease free water. Content was mixed by flipping and reunited by a short spin at ~200g for 5 sec. The RNA-RT primer solution was heated to 65°C for 5 min, 22°C for 30 sec and 20°C for 30 sec and directly on ice for > 2 min to enable specific binding of RNA to the added stem-loop RT primer. The cDNA reaction was completed by adding 15 µl mastermix, mixed by flipping followed by a short spin at ~200g. To improve sensitivity, reverse transcription was performed with a pulsed program (30 min at 16°C, 60 cycles at 30°C for 30 sec, 42 C for 30 sec and 50°C for 1 sec). The reaction was stopped by heating to 85°C for 5 min. A reverse transcriptase minus (RT-) sample was included as a control.

qPCR
qPCR analysis was performed with a Roche LightCycler® 96 System by using either Roche Probe or SYBR Green I master mix in a 20 µl reaction volume. GAPDH specific forward primer and universal stem-loop reverse primer (both Microsynth, Balgach, Switzerland) were added to a final concentration of 250 nM. The probe based assay was prepared

by diluting the ZEN probe (Integrated DNA Technologies, Coralville, IA, USA) to a final concentration of 300 nM. Fluorescence of SYBR Green I was measured in FAM channel and Yakima Yellow of the ZEN probe in the VIC channel. Each cDNA sample was analyzed in triplicate and the qPCR efficiency was determined by performing in run cDNA dilution arrays for both probe and dye based assay (Supplementary information).

3. Results

3.1 LNP preparation methods and physicochemical properties

Table 4.1 | Hydrodynamic diameter and zeta potential of the siRNA and SCO formulations

siRNA formulations	Size (nm)	PDI	Zeta Potential (mV)
1. Preformed vesicles	109.8 ± 0.7	0.05 ± 0.00	-6.45 ± 0.36
2. Film hydrated (with 30% ethanol)	117.1 ± 1.8	0.07 ± 0.01	-6.42 ± 0.12
3. Film hydrated (without ethanol)	134.1 ± 1.3	0.04 ± 0.03	-6.75 ± 0.30
SCO formulations			
1. Preformed vesicles	104.2 ± 0.8	0.04 ± 0.03	-9.06 ± 0.19
2. Film hydrated (with 30% ethanol)	121.5 ± 0.4	0.06 ± 0.00	-7.13 ± 0.17
3. Film hydrated (without ethanol)	152.8 ± 0.1	0.20 ± 0.01	-8.39 ± 0.47

The formulations used to compare the different quantification methods were prepared with different techniques. All of them consisted of the same lipid composition, namely DSPC:DODAP:Cholesterol:Ceramide-C16-PEG2000 at a ratio of 25:25:40:10. The first formulation was made using the 'preformed vesicle method', in which preformed empty vesicles are destabilized with ethanol to make them more permeable for the large nucleic acids. Because formulation is done at pH 4.0, the cationic lipids are charged so they can complex the nucleic acids which makes the vesicles coalesce, entrapping the nucleic acids in between the bilayers of the formed multi-lamellar vesicles [12]. The ethanol in the formulation putatively diminishes the charge interaction of the cationic lipids and anionic nucleic acids, thereby avoiding aggregation. Therefore it was also attempted to use the 'conventional' film hydration method in presence of ethanol and at pH 4.0 followed by high pressure extrusion. As a comparison, the third formulation was made using the same method but without ethanol. All three methods were used to make a formulation encapsulating double stranded siRNA and a single stranded RNA splice correcting oligonucleotide (SCO) in a lipid:NA weight ratio of approximately 15:1. No strong differences regarding size distribution and zeta potential were observed between formulating siRNA and the SCO. The most obvious difference between formulation methods was that the extrusion of the vesicles without ethanol required significantly more pressure and time than when extruding them with 30% ethanol. This could indicate aggregation but if this occurred it was only partially reflected in the size distribution and polydispersity index (PDI) of the final formulation, see Table 4.1.

Formulations extruded in ethanol had a diameter closer to that of the membrane they are extruded through (100nm) but only the SCO formulation that was hydrated and extruded without ethanol had a markedly increased size and PDI. Formulation methods differed more significantly in encapsulation efficiency as will be discussed later.

3.2 Interference of intact particles on RNA quantification by dye binding assay

The most widely applied quantitative method for determining the siRNA loading in LNPs is the Ribogreen® dye binding assay. When applying this to the formulations described above, it was found that only a fraction of the formulated siRNA was accessible for dye binding in the intact LNPs. Two alternatives were explored, namely solubilization of the LNPs with 0.5% Triton X-100 as suggested in one of the found protocols and a complete extraction of the nucleic acids from the formulation according to Bligh and Dyer.

Both methods allowed for complete recovery of the nucleic acid load as compared to only 35% that was accessible for dye binding in the intact LNPs (determined from the stock solution of free siRNA that was added to the formulations as a reference), see Figure 4.1. The added detergent did disturb the fluorescent signal, which would result in a strong underestimation (~80%) of the nucleic acid amount but in this case, that could be compensated for by using a standard curve that also contained 0.5% Triton X-100. The medium in which a calibration curve is made are a typical example of details that are lacking in the reports, but clearly also of a detail that can significantly alter the outcome of the measurements.

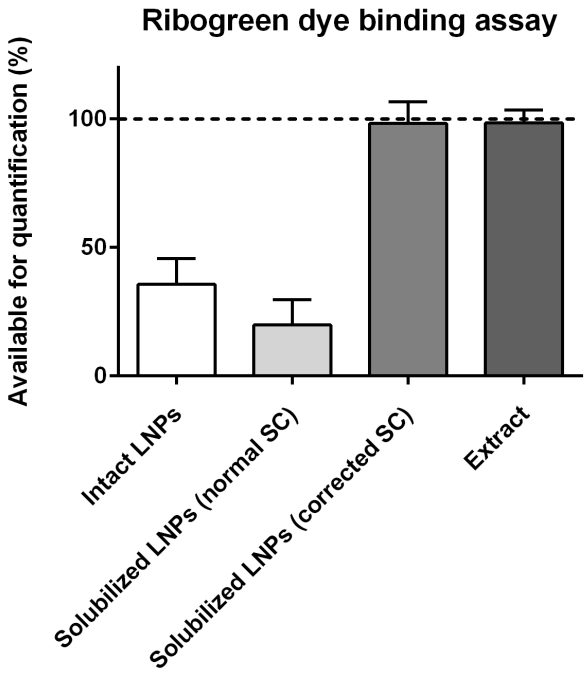

Figure 4.1 | Accessibility of the nucleic acids formulated in LNPs for the Ribogreen® dye binding assay. Only 35% of the siRNA cargo was quantified when intact LNPs were used, most likely because the nucleic acids inside the particles are not completely accessible for the dye. Solubilization of the LNPs with 0.5% Triton X-100 released all nucleic acids but the detergent strongly influenced the fluorescence signal, resulting in very low values when the normal standard curve (SC) was used. This had to be corrected for by using an additional standard curve that contained the same amount of detergent. Alternatively, extraction of the nucleic acids allowed complete access of the dye to the cargo. The 100% value was determined from the stock solution with which the lipid film was hydrated during formulation.

Other quantification methods may not be compatible with either the detergent or the LNP excipients and for these methods the extraction could be used. For example, spectrophotometric detection with Nanodrop is heavily influenced by the presence of detergent and lipids and the injection of intact LNPs in the UPLC column resulted in irreversible damage to the column. Therefore, to directly compare all quantification methods, the LNP samples were extracted first and quantification was done on the extracts.

3.3 Bligh & Dyer extraction validation

Because intact lipid particles can interfere with nucleic acid detection methods and because the nucleic acids are inside the particle and may thus not be detected by several methods, lipids and nucleic acids were separated before measurement. This was done using a Bligh and Dyer extraction that first solubilizes the particles in a miscible mixture of organic solvent and aqueous buffer. After addition of more chloroform and water, phases separate and lipids are extracted to the bottom phase, while nucleic acids are in the top phase [13]. This was visualized by using a formulation labeled 'red' (with lipid conjugated Rhodamine) containing a nucleic acid labeled 'blue' (with Alexa 647). See Figure 4.2.

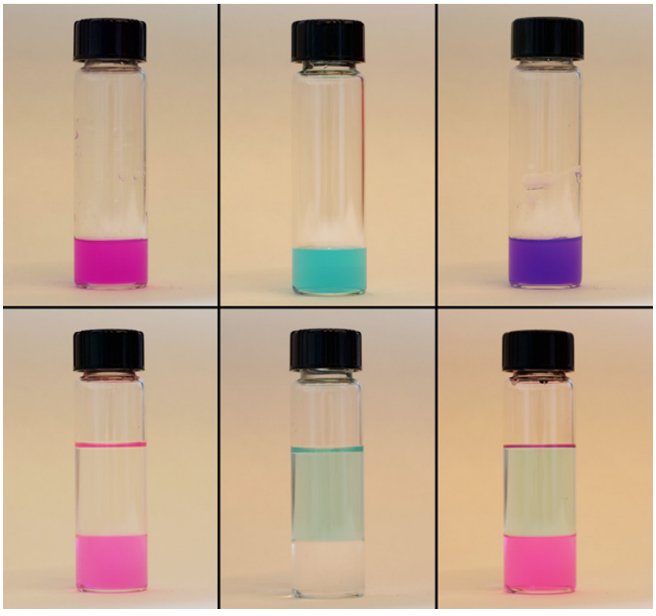

Figure 4.2 | Bligh & Dyer extraction of lipid formulations encapsulating oligonucleotides
op row, from left to right: Rhodamine-PE labeled liposomes, unlabeled liposomes loaded with Alexa 647 labeled siRNA and labeled liposomes loaded with labeled siRNA. Bottom row: same samples as top row, but extracted using the Bligh and Dyer technique. Two clearly separated phases are seen. The labeled phospholipids partition in the bottom organic phase (consisting mostly of chloroform) and the labeled siRNA is extracted to the aqueous phase on the top.

To more accurately quantify the extraction recovery of lipids, a known concentration of (labeled) siRNA was spiked into liposomes with a positive, negative or neutral (PEGylated) surface. To quantify the amount of phospholipids in the organic phase, the total phosphate concentration was measured and compared to unextracted samples that were used as a 100% value. The extraction recovery of nucleic acids from the liposome samples and a dilution in MilliQ to the aqueous phase was determined using UPLC, measuring both the labeled and the unlabeled fraction. (See Figure 4.3.)

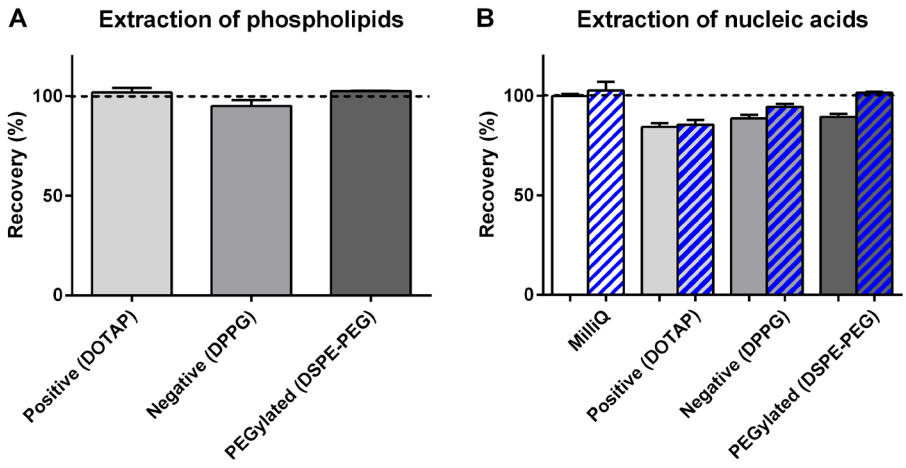

Figure 4.3 | Recovery of phospholipids and nucleic acids after extraction
A: Recovery of phospholipids in the organic phase .
B: Recovery of the nucleic acids in the aqueous phase.
Positive, negative and PEGylated liposomes consisted of DPPC:Chol:X in ratio of 6:3:1, with X being DOTAP, DPPG and DSPE-PEG2000 respectively. Unextracted samples were used as 100% values and to calculate recovery percentages. The blue bars represent recovery of the labeled fraction and the grey bars represent the unlabeled GAPDH fraction.

Recovery of phosphate was almost complete, varying from 97-102% and no difference was seen between formulations. This indicates that also the more hydrophilic PEG-lipid is completely extracted to the organic phase. The nucleic acid recovery in the aqueous phase was measured by UPLC and was found to be approximately 100% when extracted from MilliQ water. This shows that none of the nucleic acids participate in the organic phase, as to be expected from their molecular structure. The samples that were spiked with liposomes have a less complete recovery than extraction from MilliQ, indicating that the lipids may pull part of the nucleic acids to the organic phase. This effect is more pronounced when cationic lipids are used, but the recovery is still well above 80%.

3.4 Quantification of nucleic acids

In order to remove the nucleic acids that were not encapsulated in the LNPs, all formulations were subjected to three rounds of ultracentrifugation to spin down the particles and resuspended in PBS. Samples 'before' and 'after' separation of unencapsulated nucleic acids were taken from each of the three formulation methods

and quantified with seven different quantification/detection methods after extraction. The absolute values are plotted in Figure 4.4 to show the differences between the different methods (different symbols) and between triplicates of the same method (error bars, showing standard deviation).

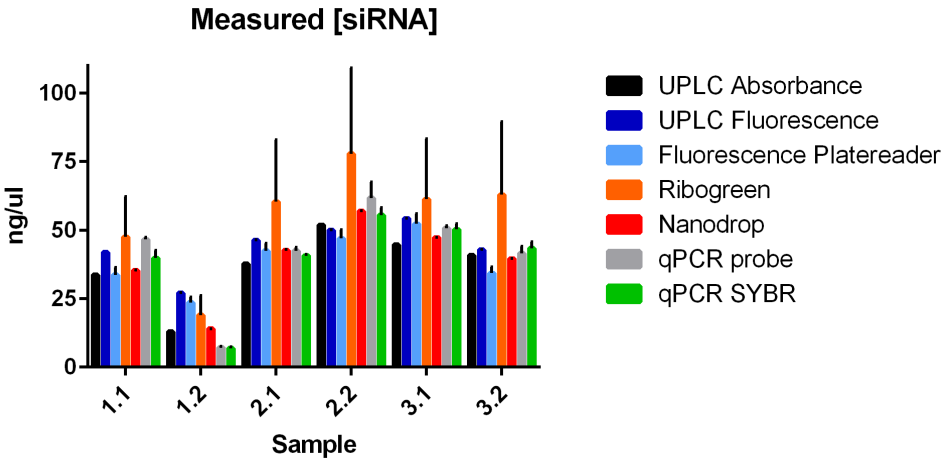

Figure 4.4 | Absolute values from the six siRNA samples, as obtained by different quantification methods
Samples 'before' ultracentrifugation were numbered x.1 and 'after' x.2. The first number represents the three formulation methods. Samples were diluted or concentrated during processing as is also seen in phospholipid measurements and absolute values have to be corrected accordingly. None of the methods seem to consistently over- or underestimate the value, but Ribogreen® values are the highest in five out of six samples and have a very high standard deviation, suggesting that for this application the dye binding assay may not be the most suitable. (Values as mean±SD)

Several conclusions can be drawn from the graph. First, absolute values in some cases vary almost 100% between methods. For example, in sample 1.2 the UPLC measurement on the fluorescent fraction gives a value almost twice as high as the measurements on the non-fluorescent fraction by UPLC and Nanodrop. This obviously has a huge consequence when either of the methods is used to dose the amount of oligonucleotides in follow-up experiments. Secondly, apart from the Ribogreen® assay, triplicate measurements using the same method are very accurate, as seen from the small standard deviation. This indicates that the assays themselves may find a reproducible value, but that the obtained values heavily depend on which method is used. The Ribogreen® assay found values that are deviating more from the values of the other methods and also has a very high standard deviation between repeated measurements. These two findings may be related, but in our hands, the Ribogreen® assay failed to produce reproducible results and is clearly the outlier in this study. Although the other values are closer to each other, there is not one method that always produces the highest or lowest values. This suggests that there is some variation between the methods, but there are no interfering factors that consistently over- or underestimate the siRNA content in either of the methods.

3.5 Encapsulation efficiency

The variation in the absolute values is caused by differences in the formulation method and varying dilution factors during the processing and purification. To determine the encapsulation efficiency of the three employed formulation methods, the absolute values were corrected for the amount of phospholipids and then values before and after separation of unencapsulated oligonucleotides were compared. The encapsulation values obtained with seven different methods are shown in Table 4.2.

Table 4.2 | Encapsulation efficiencies of siRNA in the three different formulation methods as measured with the seven different quantification methods.

	Nanodrop	Ribogreen®	UPLC (UV)	UPLC (FLR)	Platereader	qPCR (probe)	qPCR (SYBR green)
1. Preformed vesicles	29%	26%	28%	47%	50%	11%	13%
2. Film hydrated (with 30% ethanol)	95%	95%	97%	76%	80%	103%	97%
3. Film hydrated (without ethanol)	93%	98%	101%	88%	73%	91%	96%

The 'preformed vesicle method', or formulation #1 clearly has a much lower encapsulation efficiency than the other two formulations that were made with film hydration methods. However, the efficiencies obtained with the two methods that detect the fluorescent Alexa 647 cargo are much higher than the other efficiencies, while in formulation #2 and #3 the fluorescence based methods follow the trend of the other methods. All oligonucleotides are covalently labeled with a single fluorophore, so a wide distribution in the number of labels per molecule cannot be of influence on these measurements. A clear explanation for this discrepancy cannot be given, but it does show that it is not recommended to extrapolate the total encapsulated fraction from measuring the fluorescently-labeled fraction. From these results, it appears that the fluorescence based methods are less reliable, at least when only a small fraction of the total cargo is labeled. Apart from some small differences in absolute values, all other absorbance based methods produce very similar values of encapsulation efficiency. This again shows that the variations within methods are not that high, but that incorrect conclusions are more likely to be drawn when different methods are compared. The qPCR quantifications produced values much in line with the other methods, except for sample two, where the results are much lower. This could be caused by a contamination in the sample that inhibited amplification of the target strand. Because the values of the 'after' sample from the first formulation method (1.2) were underestimated by the qPCR methods, the calculated encapsulation efficiency is much lower. Although the goal of this work was not primarily to compare the three formulation methods, the preformed vesicle method is clearly less favorable than the other two methods, in terms of encapsulation efficiency.

The process of encapsulation, purification, extraction and quantification was repeated using the same preparation methods and lipid composition, but with a short, single stranded RNA splice correcting oligonucleotide (SCO). Except for the qPCR measurements, all methods could be adapted to the different cargo and no significant

differences were observed on the outcome. For the Ribogreen® assay, the working range had to be adjusted to 10 times higher concentrations of nucleic acids. This was still in the low nanomolar range (which is more sensitive than the other assays, except qPCR) but it also required 10 times higher concentrations of the Ribogreen® dye, making this assay 10 times more expensive for the SCO than for siRNA.

3.6 UPLC analysis to determine nucleic acid integrity

The quantification methods described above cannot say anything about the sequence and structural integrity of the NA. We have therefore also included a UPLC method with a commercially available column which employs a combination of reversed phase and ion-pairing and is able to separate oligonucleotides based on length and sequence. The high operating temperature and pressure separate the sense and anti-sense strands of siRNAs that can then be detected at different retention times. However, separation is more challenging when oligonucleotides have backbone modifications such as phosphorothioate bonds or 2'O-methyl modifications and the nucleic acids used here have both. It was attempted to optimize the analysis method towards complete baseline separation of the sense and the anti-sense strands of the siRNAs but that was not completely successful for all the used sequences.

Nevertheless, enough structural information could be gathered from the chromatograms to distinguish between different sequences. Moreover, it was possible to identify degradation products and to assess whether the measured samples were still intact. A small fraction of LV2 control siRNA was enzymatically degraded using RNAse A and then injected. A multitude of smaller peaks was detected after digestion and the original peak had completely disappeared (See Figure 4.5). All peaks had lower retention times, as all degradation products are obviously shorter than the original product. The peak at 1.15 min is the injection peak, which may contain individual nucleotides that have no retention on the column. An increasing number of peaks was seen when higher concentrations were injected, showing that less abundant degradation products require higher initial concentrations to be detected. Admittedly, not all degradation products could be detected at feed concentrations that are typical in liposomal formulations, but UPLC analysis remains a powerful method to determine structural integrity of the measured samples. A 'complete' peak of the full length product (that is, identical in triplicate samples) together with the absence of degradation products, can ensure that the sample is completely intact. No degradation products were detected in any of the samples used here.

3.7 Quantitative PCR

qPCR based detections were performed essentially as described for small RNAs [14–16]. Since the qPCR amplification is sequence dependent, only the GAPDH strands, but not the labelled controls were detected. For the enzymatic reactions, the siRNA solutions needed to be diluted strongly in a stepwise manner. A GAPDH siRNA solution with an initial concentration of 1 μM was used as a standard and diluted and analyzed in parallel to the samples. Two different reverse transcription methods, using either stem-loop primers [14] or the S-Poly(T)method [17], were tested. The S-Poly(T) gave poor results in the subsequent qPCR, which was attributed to the chemical modification

of the siRNA. In particular, the phosphorothioate bond in the 3'-dT overhang seems to impede efficient polyadenylation, a major step for one of two routinely used methods for generating cDNA. Thus, we resorted to use a stem-loop primer method which efficiently amplified the siRNA (Supplementary Information). The samples were subsequently analyzed with both a probe and a dye based qPCR assay. Both analysis methods showed only negligible differences between the two, apart from generally higher values for the dye based detection, which is a known characteristic. (Figure 4.4) This was taken into account through the use of a standard solution for calibration which served as the basis for determining the copy number per and the concentrations of the analyte solutions [18].

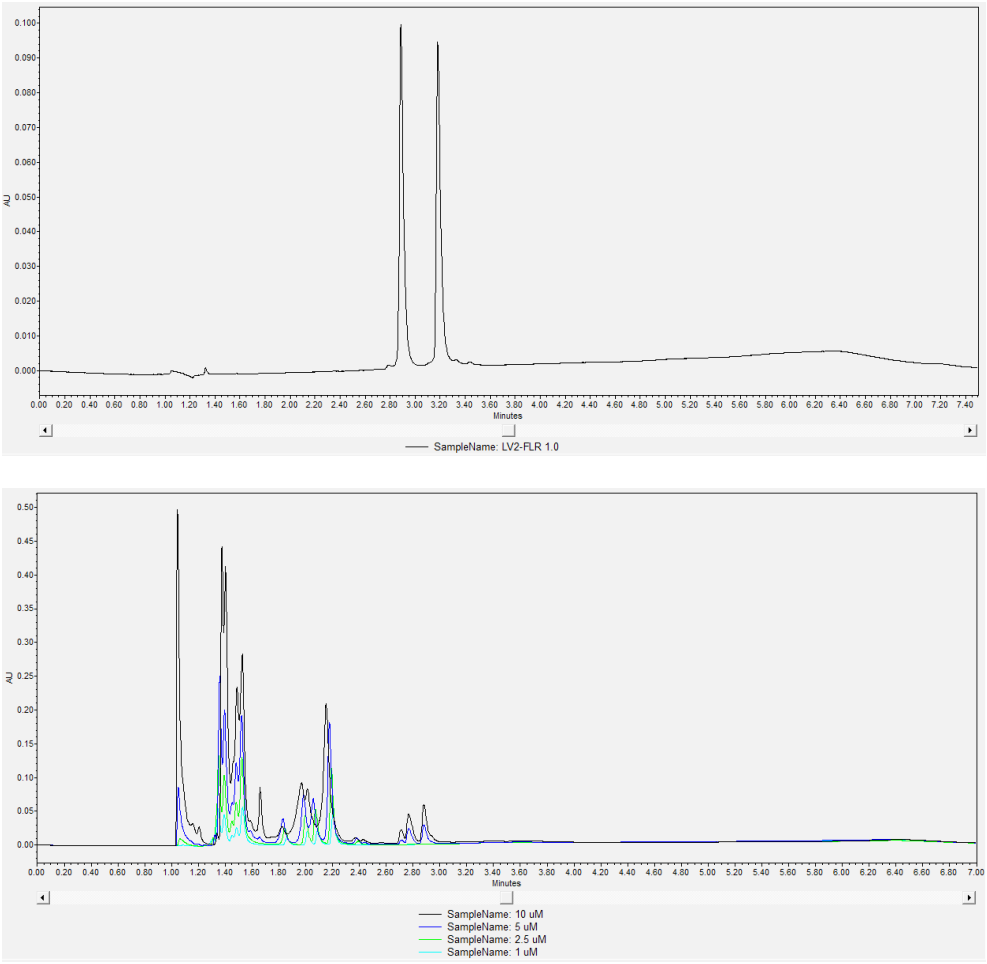

Figure 4.5 | Strand separation of siRNAs for identification and analysis of degradation products
Top: Complete strand separation of the sense and anti-sense strands gives a unique pattern for each sequence and helps identifying sequences and whether they are intact.
Bottom: Peak distribution of RNAse A degraded LV2 siRNA. Shorter fragments have shorter retention times and are more abundant than the longer fragments. Less abundant degradation products are only detected when higher initial concentrations of siRNA were used.

3. Discussion and conclusion

In the work presented here, seven different methods for quantification of short oligonucleotides that are commonly used in the field of drug delivery were systematically evaluated. Three different formulation methods were compared, by producing lipid nanoparticles with identical lipid composition, containing siRNA or a splice correcting oligonucleotide. The formulation methods used were the 'preformed vesicles method' [12] and two variations of the lipid film hydration method. All formulations were purified by dialysis and unencapsulated oligonucleotides were removed by ultracentrifugation and washing. Particulate systems can cause scattering in spectroscopic methods and the encapsulation of the oligonucleotides inside the particles can hamper detection (because of fluorescence quenching, or the unavailability to reagents such as the Ribogreen® reagent, see references [9,19,20] and our results in Figure 4.1. Therefore, the oligonucleotides were separated from the particles first, by a validated extraction method, to liberate the cargo from the carrier and remove interfering substances. All samples were treated exactly the same and the extracts were assayed for oligonucleotide concentration using seven different methods. These methods were spectroscopic detection using a Nanodrop spectrophotometer, fluorescent detection of the Alexa 647 labeled fraction of the cargo (10% of total), the commercial Ribogreen® Assay, UPLC analysis using UV detection (260nm) and fluorescence detection (Alexa 647) and two methods of qPCR. Most of these methods are readily available to most labs and routinely used in publications to quantify siRNA and characterize formulations (See Supplementary Table S4.1).

Remarkably, when measuring the same sample using different quantification methods, significant differences in absolute values were found, in the most extreme cases up to four times higher than other methods measuring the same sample. Replicates using the same quantification method were found to be consistent in most cases, which means that differences are predominantly caused by differences between analytical methods. This makes the comparison between for example, formulation methods, encapsulation efficiency and transfection efficiency (based on measured doses) impossible if different measurement methods are used, even more so when inter-lab variation also plays a role. This is worrisome as different labs all use their own methods and protocols while there appears to be a clear need for standardization. Findings like these can partially explain the reported low reproducibility of scientific literature and more within-lab validation and external-lab validation could definitely improve this reproducibility issue [10].

Although comparing formulation methods was not the primary goal of this work, by using the standardized method described here, we were able to unambiguously demonstrate differences in encapsulation efficiencies. Method #2 was found to be the most ideal in these conditions, as it has a high encapsulation efficiency and a proper size distribution and polydispersity. The mean size and polydispersity of method #3 was higher than that of the other two, possibly because aggregation of the anionic oligonucleotides and cationic lipids occurred to a higher extent in the absence of ethanol. The encapsulation efficiency of method #1 was clearly lower than that of the other two methods and also much lower than was originally reported [12]. The original

publication also reports the influence of lipid composition and ethanol concentrations, so if the preformed vesicle method is preferred, it can most likely be optimized by changing those parameters. Here, method #2 was the most efficient and convenient formulation method.

Despite the remarkable differences in absolute values between methods, it is not possible to say which one of them is the most accurate, although it could be said that in this case the Ribogreen® assay gives the biggest variations and is far away from the other values. Possibly, the Ribogreen® reagent is sensitive to 'environmental influences', such as temperature, light, time of incubation. This makes it suitable for determining encapsulation efficiencies (when samples are measured in the same assay) but less suitable for comparing samples from different experiments or on different dates. The high variations may also be caused by the short length of the oligonucleotides used here, while the assay was developed to quantify isolated mRNA (and the dye is known to intercalate between the bases, which could be obstructed by backbone modifications). The finding that higher concentrations of dye are necessary to quantify the SCO than for the siRNA indicates that the assay is less sensitive for single-stranded oligonucleotides and may be influenced by the sequence and chemical modifications (the SCO has a full phosphorothioate backbone), and that therefore the Ribogreen® dye may be better suited for long transcripts or for determining total mRNA in cell extracts.

The two quantification methods based on the fluorescence detection of the conjugated Alexa 647 label, produced similar results, but those were quite far away from the values obtained with other methods. This is possibly caused by the fact that only 10% of the cargo used here was labeled and that extrapolation of the recovery of the labelled sequence with altered biophysical properties does not produce reliable results for encapsulation efficiency. These methods may be more suitable when bigger fractions of labeled cargo are used. The reported problem that larger quantities of fluorophores are quenched inside liposomal carrier systems [9,19,20] can be avoided by solubilizing the LNPs with Triton X-100 or by the proposed extraction method.

Quantitative PCR is the most complicated method used herein. Its main virtue is the possibility to detect nucleic acids in a sequence-specific manner, even within mixtures of many different sequences, and its low detection limit. In addition, it is suitable for detection after extraction from cells and tissues. For quantification of the samples and the calculation of encapsulation efficiency, the samples needed to be strongly diluted, making several individual diluting steps necessary. In the context of determining encapsulation efficiency, this method may be too complicated, but it can be useful in settings in which low detection limits, high sequence specificity are needed, or within biological settings.

Other factors that could play a role in determining the 'preferred' method, are summarized in the table below (Table 4.3). The ease of use, price and accessibility of a method could play a role if high throughput analysis of the experiments is desired. To make the table less subjective, some considerations for assay validation are also taken into account, such as specificity, accuracy, precision and detection limit.

If sample concentrations are low, some options may be unsuitable and obviously, when only unlabeled oligonucleotides are used, the fluorescence based methods are not an option. On the other hand, a fluorescent plate reader is probably available to every lab so this may be the most accessible and cheapest option of all.

Table 4.3 | Advantages and disadvantages of the employed analysis methods

Method	Ease of use/ accessibility	Working range	Advantages	Disadvantages
Nanodrop	+++	10-100ng/µl*	-Low sample volume (1µl) -Easiest and fastest method	-Sensitive to impurities -High detection limit -Detection based on average extinction coefficient, not standard curve*
Ribogreen®	++	0-5 nM (siRNA) 0-50 nM (ASO)	-Cheap and commercially available kit -Only requires fluorescence platereader -Very low detection limit	-Very sensitive to 'environmental influences' (high variability) -High working range consumes a lot of reagent (limits use to 20 plates per assay kit) -Low accuracy compared to other methods
UPLC	+	0-4 µM	-Structural information (double strands and degradation products) -High specificity -Detection of backbone (UV260) and fluorescent fraction	-Requires expensive system and dedicated 'OST' column
Platereader	+++	0-1 µM	-Cheapest method described, only requires fluorescence platereader	-Measures fluorescently labeled fraction only
qPCR	+	0-10 pM	-Detects only intact sample (high specificity) -Lowest detection limit of all methods (several copies/µl)	-Most laborious method

*Nanodrop calculates concentrations based on spectroscopy and an average extinction coefficient for RNA or DNA and does not make use of a standard curve of the actual sequence that is analyzed.

In our experimental setup, the UPLC method is the most preferred method. It does require a UPLC system which may not be available to every lab, but HPLC alternatives also exist (although this increases runtime and decreases throughput). Analysis may take some time as each sample and standard has to be run consecutively rather than in parallel but the system is automated and therefore has a high throughput. Of all the methods tested, UPLC analysis has the highest precision and specificity together with qPCR, but is quicker and easier to use. It can detect the backbone and fluorescent label in parallel and separation of strands and potential degradation products gives structural information that cannot be obtained by any other method.

In summary, we give an example of how lipid nanocarrier systems could be compared in a more systematic way. Using a standardized method for separating the oligonucleotides from the lipids, we were able to indicate a clear preference for one of the three tested formulation methods to prepare nucleic acid lipid nanoparticles. More importantly, we demonstrate that there are substantial differences between routinely used detection methods for oligonucleotides, which makes comparison very difficult. Of course, the research laboratories should make their own decision as to which method to use, and these decisions may even be based on practical issues such as price and availability. However, this work illustrates the importance of method validation and brings to light one of the possible causes of the low reproducibility of, and the discrepancies between reports from different labs. It is probably unrealistic to expect that the field could find one method that would be agreed upon to be used as the standard method, given the huge number of laboratories working on nanoformulations for oligonucleotides. Nevertheless, the field would benefit if labs would approach this problem in a more standardized way or at least report their quantification methods in more detail. We would like to give the US. National Cancer Institute's 'Nanotechnology Characterization Laboratory' (http://nanolab.cancer.gov/) as an example of how standardization of characterization techniques might contribute to better therapies and a protocol for quantification of oligonucleotides could be added to their list of standard procedures. We advise to pay more attention to procedures such as the separation of the unencapsulated material, dissociation from the carrier and quantification methods, both when interpreting, as well as reporting results. Neglecting to describe or even perform such procedures could be the cause of the reproducibility issues that hold back the progress of the field.

Acknowledgements
The research leading to these results has received support from the Innovative Medicines Initiative Joint Undertaking under grant agreement n° 115363 resources of which are composed of financial contribution from the European Union's Seventh Framework Programme (FP7/2007-2013) and EFPIA companies' in kind contribution. We gratefully acknowledge Martin Hofer and Ralf Steinborn (Genomics Core Facility, VetCore of VetMedUni Vienna) for support and assistance by designing and performing the used absolute RT-qPCR assay. We would also like to thank Lipoid GmbH for supporting our research by generously supplying us with phospholipids.

Bibliography

[1] A. Wittrup, J. Lieberman, Knocking down disease: a progress report on siRNA therapeutics, Nat. Rev. Genet. 16 (2015) 543–552. doi:10.1038/nrg3978.

[2] H. Yin, R.L. Kanasty, A.A. Eltoukhy, A.J. Vegas, J.R. Dorkin, D.G. Anderson, Non-viral vectors for gene-based therapy., Nat. Rev. Genet. 15 (2014) 541–555. doi:10.1038/nrg3763.

[3] C. Wan, T.M. Allen, P.R. Cullis, Lipid nanoparticle delivery systems for siRNA-based therapeutics, Drug Deliv. Transl. Res. 4 (2014) 74–83. doi:10.1007/s13346-013-0161-z.

[4] D.J.A. Crommelin, A.T. Florence, Towards more effective advanced drug delivery systems, Int. J. Pharm. 454 (2013) 496–511. doi:10.1016/j.ijpharm.2013.02.020.

[5] T. Lammers, SMART drug delivery systems: Back to the future vs. clinical reality, Int. J. Pharm. 454 (2013) 527–529. doi:10.1016/j.ijpharm.2013.02.046.

[6] R. Kirsh, S. Hood, C. Brook, A. Gilmartin, P. Dell'orco, T. Meek, Will nanomedicine deliver on its promise of changing therapeutics or remain an interesting and important research tool in cell biology and physiology?, Int. J. Pharm. 454 (2013) 530–531. doi:10.1016/j.ijpharm.2013.06.042.

[7] Y. Wang, D.W. Grainger, Barriers to advancing nanotechnology to better improve and translate nanomedicines, Front. Chem. Sci. Eng. 8 (2014) 265–275. doi:10.1007/s11705-014-1442-x.

[8] H.-D. Volk, M.M. Stevens, D.J. Mooney, D.W. Grainger, G.N. Duda, Key elements for nourishing the translational research environment, Sci. Transl. Med. 7 (2015) 282cm2–282cm2. doi:10.1126/scitranslmed.aaa2049.

[9] K. Buyens, B. Lucas, K. Raemdonck, K. Braeckmans, J. Vercammen, J. Hendrix, et al., A fast and sensitive method for measuring the integrity of siRNA-carrier complexes in full human serum, J. Control. Release. 126 (2008) 67–76. doi:10.1016/j.jconrel.2007.10.024.

[10] M. Baker, 1,500 scientists lift the lid on reproducibility, Nature. 533 (2016) 452–454. doi:10.1038/533452a.

[11] D. Vercauteren, R.E. Vandenbroucke, A.T. Jones, J. Rejman, J. Demeester, S.C. De Smedt, et al., The use of inhibitors to study endocytic pathways of gene carriers: optimization and pitfalls., Mol. Ther. 18 (2010) 561–569. doi:10.1038/mt.2009.281.

[12] N. Maurer, K.F. Wong, H. Stark, L. Louie, D. McIntosh, T. Wong, et al., Spontaneous entrapment of polynucleotides upon electrostatic interaction with ethanol-destabilized cationic liposomes., Biophys. J. 80 (2001) 2310–2326. doi:10.1016/S0006-3495(01)76202-9.

[13] E.G. Bligh, W. Dyer, A rapid method of total lipid extraction and purification, Can. J. Biochem. Physiol. 37 (1959) 911–917.

[14] C. Chen, D. a Ridzon, A.J. Broomer, Z. Zhou, D.H. Lee, J.T. Nguyen, et al., Real-time quantification of microRNAs by stem-loop RT-PCR., Nucleic Acids Res. 33 (2005) e179. doi:10.1093/nar/gni178.

[15] F. Tang, P. Hajkova, S.C. Barton, K. Lao, M.A. Surani, MicroRNA expression profiling of single whole embryonic stem cells., Nucleic Acids Res. 34 (2006) e9. doi:10.1093/nar/gnj009.

[16] E. Varkonyi-Gasic, R. Wu, M. Wood, E.F. Walton, R.P. Hellens, Protocol: a highly sensitive RT-PCR method for detection and quantification of microRNAs., Plant Methods. 3 (2007) 12. doi:10.1186/1746-4811-3-12.

[17] K. Kang, X. Zhang, H. Liu, Z. Wang, J. Zhong, Z. Huang, et al., A novel real-time PCR assay of microRNAs using S-Poly(T), a specific oligo(dT) reverse transcription primer with excellent sensitivity and specificity., PLoS One. 7 (2012) e48536. doi:10.1371/journal.pone.0048536.

[18] E.M. Kroh, R.K. Parkin, P.S. Mitchell, M. Tewari, Analysis of circulating microRNA biomarkers in plasma and serum using quantitative reverse transcription-PCR (qRT-PCR), Methods. 50 (2010) 298–301. doi:10.1016/j.ymeth.2010.01.032.

[19] P. Vader, L.J. van der Aa, J.F.J. Engbersen, G. Storm, R.M. Schiffelers, A method for quantifying cellular uptake of fluorescently labeled siRNA, J. Control. Release. 148 (2010) 106–109. doi:10.1016/j.jconrel.2010.06.019.

[20] B. Lucas, K. Remaut, N.N. Sanders, K. Braeckmans, S.C. De Smedt, J. Demeester, Towards a better understanding of the dissociation behavior of liposome-oligonucleotide complexes in the cytosol of cells, J. Control. Release. 103 (2005) 435–450. doi:10.1016/j.jconrel.2004.12.017.

[21] G. Rouser, S. Fleischer, A. Yamamoto, Two dimensional thin layer chromatographic separation of polar lipids and determination of phospholipids by phosphorus analysis of spots, Lipids. 5 (1970) 494–496. doi:10.1007/BF02531316.

Supplementary information

Literature screening for analysis methods

Ref.	Method	Applications
[1]	Gel retardation to find which N/P ratio fully complexes siRNA	cell culture
[2]	No quantification at all (complexes)	cell culture/in vivo mice
[3]	No quantification at all (complexes)	cell culture/in vivo mice
[4]	EE% by Ribogreen with and without Triton-X100 Total content by absorbance (not specified)	cell culture/in vivo mice
[5]	No quantification at all (complexes)	cell culture
[6]	No quantification at all (complexes)	cell culture
[7]	Gel retardation on supernatant and pellet after centrifugation	in vivo shrimp
[8]	No quantification	cell culture/in vivo mice
[9]	Gel retardation (+/-) RNAse and (+/-) heparin	cell culture
[10]	Fluorescence detection of labeled RNA (platereader)	cell culture/in vivo mice
[11]	No quantification at all (complexes)	cell culture/in vivo mice
[12]	Gel retardation (+/-) serum HPLC-MS (Absorbance and mass spectrometry)	cell culture/in vivo mice
[13]	No quantification at all (complexes)	cell culture/ex vivo human skin
[14]	Ribogreen with Triton X-100 on final sample/total added	cell culture
[15]	Gel retardation and gel quantification software	cell culture
[16]	Fluorescence fluctuation spectroscopy	cell culture
[17]	Ribogreen with heparin/OBG on final sample/total added	cell culture
[18]	No quantification at all (complexes)	cell culture
[19]	Absorbance (platereader)	protocol
[20]	HPLC (absorbance)	cell culture/in vivo mice
[21]	Ribogreen with and without Triton	protocol description
[22]	Fluorescence correlation spectroscopy	cell culture

[23]	Qualitative scoring on confocal microscopy (labeled RNA)	cell culture
[24]	Quantification of radioactively labeled siRNA	SPR with recombinant receptor
[25]	Gel retardation with and without Triton X-100	Release fom mucoadhesive sponges
[26]	Gel retardation	cell culture/in vivo mice
[27]	Gel retardation	cell culture/in vivo mice
[28]	Ribogreen assay	cell culture/in vivo mice
[29]	Gel retardation	ex vivo human skin
[30]	Ribogreen assay	cell culture/ex vivo
[31]	No quantification at all	cell culture/in vivo mice
[32]	No quantification at all	cell culture/in vivo mice
[33]	No quantification at all	cell culture
[34]	No quantification at all	cell culture
[35]	Gel retardation	cell culture
[36]	No quantification at all	cell culture/in vivo mice (eye)

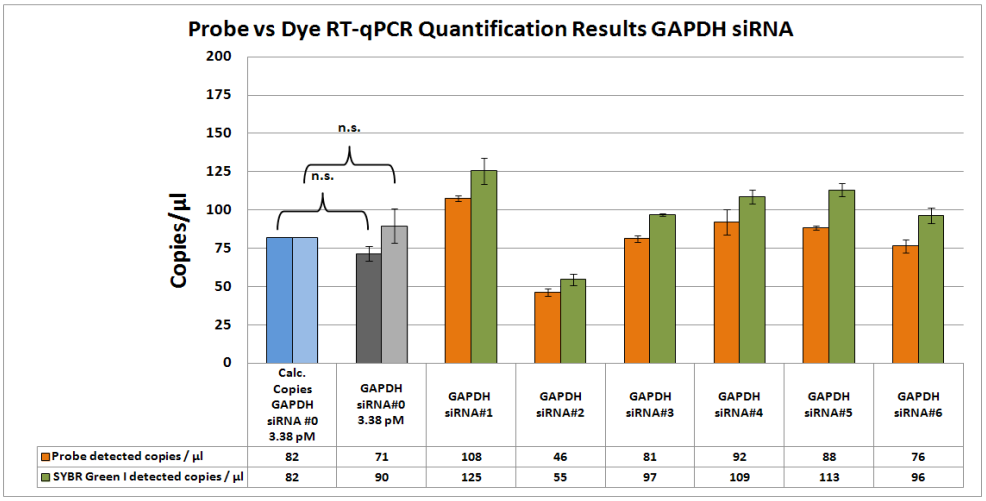

	Calc. Copies GAPDH siRNA #0 3.38 pM	GAPDH siRNA#0 3.38 pM	GAPDH siRNA#1	GAPDH siRNA#2	GAPDH siRNA#3	GAPDH siRNA#4	GAPDH siRNA#5	GAPDH siRNA#6
Probe detected copies / µl	82	71	108	46	81	92	88	76
SYBR Green I detected copies / µl	82	90	125	55	97	109	113	96

Figure S4.1 | Absolute quantification of GAPDH siRNA copies extracted form liposomes.
The analyzed reference sample GAPDH#0 adjusted to 3.38 pM [37] provided for both assays, probe and dye, no significant deviation to the calculated copy number per µl. In general the dye based assay detects in 50% of analyzed samples more copies/µl as compared to the probe based result, which is a well known characteristic of dye qPCR assays. Each bar represents three technical replicates. Students t-test for one sample was used for statistics but no significant result was received (parameter for calculation: two sided with three technical replicates of each side, t value table for (f=2, 0.975) =4.303, calculated value 3.665 - not significant n.s.). Deviation of analyzed GAPDH siRNA samples #0-6 between probe and dye assay determined copies/µl provided a significant difference for sample #3, 5, 6 (parameter for calculation: Students t-test, paired samples, two-sided two sided with three technical replicates in each group; p-value limit 0.05, p-values 0.1387, 0.2844, 0.0517, 0.006, 0.1735, 0.0111, 0.0389 representing samples GAPDH#0-6 respectively).

References

[1] D. Yang, Y. Li, Y. Qi, Y. Chen, X. Yang, Y. Li, et al., Delivery of siRNA Using Cationic Liposomes Incorporating Stearic Acid-modified Octa-Arginine., Anticancer Res. 36 (2016) 3271–6.

[2] Y. Yang, X. Xie, X. Xu, X. Xia, H. Wang, L. Li, et al., Thermal and magnetic dual-responsive liposomes with a cell-penetrating peptide-siRNA conjugate for enhanced and targeted cancer therapy, Colloids Surfaces B Biointerfaces. 146 (2016) 607–615. doi:10.1016/j.colsurfb.2016.07.002.

[3] Y. Hattori, Y. Machida, M. Honda, N. Takeuchi, Y. Yoshiike, H. Ohno, et al., Small interfering RNA delivery into the liver by cationic cholesterol derivative-based liposomes., J. Liposome Res. (2016) 1–10. doi:10.1080/08982104.2016.1205599.

[4] S. Chen, Y.Y. Tam, P.J. Lin, M.M. Sung, Y.K. Tam, P.R. Cullis, Influence of particle Size on the in vivo potency of lipid nanoparticle formulations of siRNA, J Control Release. 235 (2016) 236–244. doi:10.1016/j.jconrel.2016.05.059.

[5] R.N. Majzoub, E. Wonder, K.K. Ewert, V.R. Kotamraju, T. Teesalu, C.R. Safinya, Rab11 and Lysotracker Markers Reveal Correlation between Endosomal Pathways and Transfection Efficiency of Surface-Functionalized Cationic Liposome-DNA Nanoparticles., J. Phys. Chem. B. (2016). doi:10.1021/acs.jpcb.6b04441.

[6] X. Wang, Y. Xiong, C. Zhang, J. Zhou, J. Yang, K. Wang, et al., Experimental study on inhibition of the growth of human adenoid cystic cancer cells by RNA interference targeting against survivingene, 8 (2016) 375–383.

[7] P. Sanitt, N. Apiratikul, N. Niyomtham, B. Yingyongnarongkul, W. Assavalapsakul, S. Panyim, et al., Cholesterol-based cationic liposome increases dsRNA protection of yellow head virus infection in Penaeus vannamei, J. Biotechnol. 228 (2016) 95–102. doi:10.1016/j.jbiotec.2016.04.049.

[8] L. Duan, Y. Yan, J. Liu, B. Wang, P. Li, Q. Hu, et al., Target delivery of small interfering RNAs with vitamin E-coupled nanoparticles for treating hepatitis C, Sci. Rep. 6 (2016) 24867. doi:10.1038/srep24867.

[9] Z. Chen, T. Zhang, B. Wu, X. Zhang, Insights into the therapeutic potential of hypoxia-inducible factor-1 α small interfering RNA in malignant melanoma delivered via folate-decorated cationic liposomes, Int. J. Nanomedicine. 11 (2016) 991–1002. doi:10.2147/IJN.S101872.

[10] X. Xie, W. Lin, M. Li, Y. Yang, J. Deng, H. Liu, et al., Efficient siRNA Delivery Using Novel Cell-Penetrating Peptide-siRNA Conjugate-Loaded Nanobubbles and Ultrasound, Ultrasound Med. Biol. 42 (2016) 1362–1374. doi:10.1016/j.ultrasmedbio.2016.01.017.

[11] T.O. Kabilova, A. V. Sen'kova, V.P. Nikolin, N.A. Popova, M.A. Zenkova, V. V. Vlassov, et al., Antitumor and Antimetastatic Effect of Small Immunostimulatory RNA against B16 Melanoma in Mice, PLoS One. 11 (2016) e0150751. doi:10.1371/journal.pone.0150751.

[12] H. Koide, A. Okamoto, H. Tsuchida, H. Ando, S. Ariizumi, C. Kiyokawa, et al., One-step encapsulation of siRNA between lipid-layers of multi-layer polycation liposomes by lipoplex freeze-thawing, J. Control. Release. 228 (2016) 1–8. doi:10.1016/j.jconrel.2016.01.032.

[13] E. Desmet, S. Bracke, K. Forier, L. Taevernier, M.C.A. Stuart, B. De Spiegeleer, et al., An elastic liposomal formulation for RNAi-based topical treatment of skin disorders: Proof-of-concept in the treatment of psoriasis, Int. J. Pharm. 500 (2016) 268–274. doi:10.1016/j.ijpharm.2016.01.042.

[14] P. Guo, J. Yang, D. Jia, M.A. Moses, D.T. Auguste, ICAM-1-Targeted, Lcn2 siRNA-Encapsulating Liposomes are Potent Anti-angiogenic Agents for Triple Negative Breast Cancer., Theranostics. 6 (2016) 1–13. doi:10.7150/thno.12167.

[15] D. Belletti, G. Tosi, F. Forni, I. Lagreca, P. Barozzi, F. Pederzoli, et al., PEGylated siRNA lipoplexes for silencing of BLIMP-1 in Primary Effusion Lymphoma: In vitro evidences of antitumoral activity, Eur. J. Pharm. Biopharm. 99 (2016) 7–17. doi:10.1016/j.ejpb.2015.11.007.

[16] L. Wayteck, H. Dewitte, L. De Backer, K. Breckpot, J. Demeester, S.C. De Smedt, et al., Hitchhiking nanoparticles: Reversible coupling of lipid-based nanoparticles to cytotoxic T-lymphocytes, Biomaterials. 77 (2016) 243–254. doi:10.1016/j.biomaterials.2015.11.016.

[17] X. Zeng, A.M. de Groot, A.J.A.M. Sijts, F. Broere, E. Oude Blenke, S. Colombo, et al., Surface coating of siRNA–peptidomimetic nano-self-assemblies with anionic lipid bilayers: enhanced gene silencing and reduced adverse effects in vitro, Nanoscale. 7 (2015) 19687–19698. doi:10.1039/C5NR04807A.

[18] X. Jing, C. Foged, B. Martin-Bertelsen, A. Yaghmur, K.M. Knapp, M. Malmsten, et al., Delivery of siRNA Complexed with Palmitoylated α-Peptide/β-Peptoid Cell-Penetrating Peptidomimetics: Membrane Interaction and Structural Characterization of a Lipid-Based Nanocarrier System., Mol. Pharm. 13 (2016) 1739–49. doi:10.1021/acs.molpharmaceut.5b00309.

[19] Y. Endo-Takahashi, Y. Negishi, R. Suzuki, K. Maruyama, Y. Aramaki, MicroRNA Imaging in Combination with Diagnostic Ultrasound and Bubble Liposomes for MicroRNA Delivery., Methods Mol. Biol. 1372 (2016) 209–13. doi:10.1007/978-1-4939-3148-4_16.

[20] Y. Yao, Z. Su, Y. Liang, N. Zhang, pH-Sensitive carboxymethyl chitosan-modified cationic liposomes for sorafenib and siRNA co-delivery., Int. J. Nanomedicine. 10 (2015) 6185–97. doi:10.2147/IJN.S90524.

[21] Y. Sakurai, T. Hada, H. Harashima, Preparation of a Cyclic RGD: Modified Liposomal SiRNA Formulation for Use in Active Targeting to Tumor and Tumor Endothelial Cells., Methods Mol. Biol. 1364 (2016) 63–9. doi:10.1007/978-1-4939-3112-5_6.

[22] G.R. Dakwar, K. Braeckmans, J. Demeester, W. Ceelen, S.C. De Smedt, K. Remaut, Disregarded Effect of Biological Fluids in siRNA Delivery: Human Ascites Fluid Severely Restricts Cellular Uptake of Nanoparticles, ACS Appl. Mater. Interfaces. 7 (2015) 24322–24329. doi:10.1021/acsami.5b08805.

[23] H. Kim, C. Leal, Cuboplexes: Topologically Active siRNA Delivery, ACS Nano. 9 (2015) 10214–10226. doi:10.1021/acsnano.5b03902.

[24] T.L. Nascimento, H. Hillaireau, M. Noiray, C. Bourgaux, S. Arpicco, G. Pehau-Arnaudet, et al., Supramolecular Organization and siRNA Binding of Hyaluronic Acid-Coated Lipoplexes for Targeted Delivery to the CD44 Receptor, Langmuir. 31 (2015) 11186–11194. doi:10.1021/acs.langmuir.5b01979.

[25] T. Furst, G.R. Dakwar, E. Zagato, A. Lechanteur, K. Remaut, B. Evrard, et al., Freeze-dried mucoadhesive polymeric system containing pegylated lipoplexes: Towards a vaginal sustained released system for siRNA, J. Control. Release. 236 (2016) 68–78. doi:10.1016/j.jconrel.2016.06.028.

[26] X.-F. Ma, J. Sun, C. Qiu, Y.-F. Wu, Y. Zheng, M.-Z. Yu, et al., The role of disulfide-bridge on the activities of H-shape gemini-like cationic lipid based siRNA delivery, J. Control. Release. 235 (2016) 99–111. doi:10.1016/j.jconrel.2016.05.051.

[27] V. Rengaswamy, D. Zimmer, R. Süss, J. Rössler, RGD liposome-protamine-siRNA (LPR) nanoparticles targeting PAX3-FOXO1 for alveolar rhabdomyosarcoma therapy, J. Control. Release. 235 (2016) 319–327. doi:10.1016/j.jconrel.2016.05.063.

[28] Y. Sato, Y. Note, M. Maeki, N. Kaji, Y. Baba, M. Tokeshi, et al., Elucidation of the physicochemical properties and potency of siRNA-loaded small-sized lipid nanoparticles for siRNA delivery, J. Control. Release. 229 (2016) 48–57. doi:10.1016/j.jconrel.2016.03.019.

[29] M. Dorrani, O.B. Garbuzenko, T. Minko, B. Michniak-Kohn, Development of edge-activated liposomes for siRNA delivery to human basal epidermis for melanoma therapy, J. Control. Release. 228 (2016) 150–158. doi:10.1016/j.jconrel.2016.03.010.

[30] S. Warashina, T. Nakamura, Y. Sato, Y. Fujiwara, M. Hyodo, H. Hatakeyama, et al., A lipid nanoparticle for the efficient delivery of siRNA to dendritic cells, J. Control. Release. 225 (2016) 183–191. doi:10.1016/j.jconrel.2016.01.042.

[31] C. Luo, L. Miao, Y. Zhao, S. Musetti, Y. Wang, K. Shi, et al., A novel cationic lipid with intrinsic antitumor activity to facilitate gene therapy of TRAIL DNA, Biomaterials. 102 (2016) 239–248. doi:10.1016/j.biomaterials.2016.06.030.

[32] A. Ewe, O. Panchal, S.R. Pinnapireddy, U. Bakowsky, S. Przybylski, A. Temme, et al., Liposome-polyethylenimine complexes (DPPC-PEI lipopolyplexes) for therapeutic siRNA delivery in vivo., Nanomedicine. (2016). doi:10.1016/j.nano.2016.08.005.

[33] M. Martínez-Negro, K. Kumar, A.L. Barrán-Berdón, S. Datta, P. Kondaiah, E. Junquera, et al., Efficient Cellular Knockdown Mediated by siRNA Nanovectors of Gemini Cationic Lipids Having Delocalizable Headgroups and Oligo-Oxyethylene Spacers, ACS Appl. Mater. Interfaces. 8 (2016) 22113–22126. doi:10.1021/acsami.6b08823.

[34] D.C. Arruda, A. Schlegel, P. Bigey, V. Escriou, Lipoplexes Strengthened by Anionic Polymers: Easy Preparation of Highly Effective siRNA Vectors Based on Cationic Lipids and Anionic Polymers., Methods Mol. Biol. 1445 (2016) 137–48. doi:10.1007/978-1-4939-3718-9_8.

[35] E. Jubeli, W.P.D. Goldring, M.D. Pungente, Cationic Lipid-Based Nucleic Acid Vectors., Methods Mol. Biol. 1445 (2016) 19–32. doi:10.1007/978-1-4939-3718-9_2.

[36] Y. Taketani, T. Usui, T. Toyono, N. Shima, S. Yokoo, M. Kimakura, et al., Topical Use of Angiopoietin-like Protein 2 RNAi-loaded Lipid Nanoparticles Suppresses Corneal Neovascularization, Mol. Ther. Acids. 5 (2016) e292. doi:10.1038/mtna.2016.1.

[37] E.M. Kroh, R.K. Parkin, P.S. Mitchell, M. Tewari, Analysis of circulating microRNA biomarkers in plasma and serum using quantitative reverse transcription-PCR (qRT-PCR), Methods. 50 (2010) 298–301. doi:10.1016/j.ymeth.2010.01.032.

Chapter 5

Coiled coil interactions for the targeting of liposomes for nucleic acid delivery

Erik Oude Blenke[1]
Joep van den Dikkenberg[1]
Bartjan van Kolck[2]
Alexander Kros[2]
Enrico Mastrobattista[1]

[1]Department of Pharmaceutics, Utrecht Institute of Pharmaceutical Sciences (UIPS), Faculty of Science, Utrecht University, Universiteitsweg 99, 3584 CG Utrecht, The Netherlands

[2]Supramolecular and Biomaterials Chemistry, Leiden Institute of Chemistry, Leiden University, Einsteinweg 55, 2333 CC Leiden, The Netherlands

Nanoscale. 2016 (16) 8955-65
doi: 10.1039/c6nr00711b

Abstract

Coiled coil interactions are strong protein-protein interactions that are involved in many biological processes, including intracellular trafficking and membrane fusion. A synthetic heterodimeric coiled-coil forming peptide pair, known as E3 $(EIAALEK)_3$ and K3 $(KIAALKE)_3$ was used to functionalize liposomes encapsulating a splice correcting oligonucleotide or siRNA. These peptide-functionalized vesicles are highly stable in solution but start to cluster when vesicles modified with complementary peptides are mixed together, demonstrating that the peptides are quickly coiling and crosslinking the vesicles. When one of the peptides was anchored to the cell membrane using a hydrophobic cholesterol anchor, vesicles functionalized with the complementary peptide could be docked to these cells, whereas non-functionalized cells did not show any vesicle tethering. Although the anchored peptides do not have a downstream signaling pathway, microscopy pictures revealed that after four hours, the majority of the docked vesicles were internalized by endocytosis. Finally, for the first time, it was shown that coiled coil assembly at the interface between the vesicles and the cell membrane induces active uptake and leads to cytosolic delivery of the nucleic acid cargo. Both the siRNA and the splice correcting oligonucleotide were functionally delivered, resulting respectively in the silencing or recovery of luciferase expression in the appropriate cell lines. These results demonstrate that the docking to the cell by coiled coil interaction can induce active uptake and achieve successful intracellular delivery of otherwise membrane impermeable nucleic acids in a highly specific manner.

Graphical Abstract

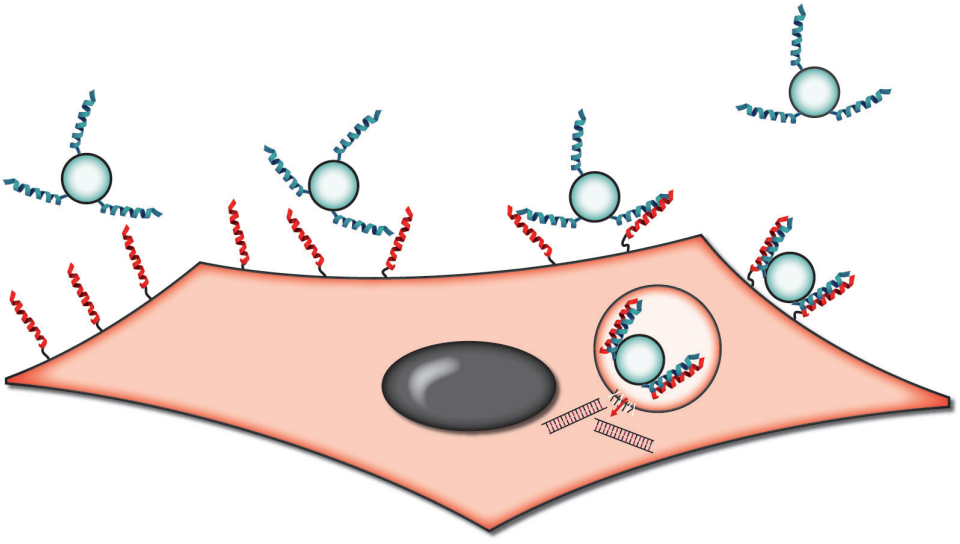

1. Introduction

Coiled coil domains are structural motifs found in proteins of 2-7 α-helical strands that are coiled around each other [1–4]. The primary structure is typically composed of multiple heptad repeat amino acid sequences (denoted as *abcdefg*) in which the *a* and *d* residues are non-polar and create the hydrophobic core of the coil. The *e* and *g* positions are charged residues that introduce electrostatic interaction and specificity between opposing coils [5]. Coiled coil interactions are involved in many biological processes, including intracellular trafficking and membrane fusion, mainly mediated by SNARE proteins (soluble N-ethylmaleimide-sensitive factor attachment protein receptor) [6,7].

In nanomaterial research, synthetic coiled coil motifs have been used to create a tunable system for the controlled display of ligands on nanoparticles[8–10], defined architectures [11,12], and for the self-assembly of polymer-peptide hybrid systems [13–17]. The group of Kopeĉek used coiled coil peptides on a HPMA polymer scaffold as a means to induce highly specific antigen crosslinking on malignant B cells both *in vitro* and *in vivo* [18–21]. These examples demonstrate the versatile application of coiled-coils as surface modifications for molecular recognition and their potential as signaling molecules on complex surfaces such as the cell membrane.

In this study, the aim is to investigate the potential of synthetic coiled coil peptides for liposomal drug delivery purposes. To this end, two synthetic, parallel coiled coil forming peptide sequences are used that are referred to as K3 $(KIAALKE)_3$ and E3 $(EIAALEK)_3$ (three repeats of lysine-rich and glutamic acid-rich heptads). Originally they have been designed as affinity tags for recombinant protein purification [22,23]. Inspired by their natural role in membrane fusion, coiled coil sequences have been previously used to mimic a system where liposomal membranes fuse upon coiling of the two complementary peptides [24–26]. Recent work showed that the peptide could be incorporated into a cellular membrane by conjugating it to a hydrophobic moiety. Subsequently, liposomes that were functionalized with the opposing coil could be targeted to these cells, as was demonstrated for several cell lines and zebra-fish embryos [27–29]. In the present work we use the K3/E3 combination to specifically dock stable nucleic acid lipid particles to the target cell and achieve intracellular delivery. Nucleic acid drugs, like siRNA or splice correcting antisense oligonucleotides (SCO) have the potential to modulate disease pathways on the transcriptional level, but due to their large size and negatively charged backbone they cannot reach their intracellular site of action. Therefore they require a delivery vehicle such as the liposomes used here. Liposomes are lipid vesicles that protect the oligonucleotides from degradation and can help to deliver them to their intracellular target site, but they do require further surface modification to get access to the target cell. In the work presented here, the lipid vesicles were functionalized with either K3 or E3 coil peptides and the cell surface was modified by insertion of the complementary peptide using a hydrophobic anchor. Assembly of the K3/E3 coiled coils at the cell surface was shown to initiate endocytosis and to eventually achieve functional delivery of two types of membrane impenetrable oligonucleotides. This poses a novel alternative to viral carriers or lipid/polymer based transfection reagents that are either associated with toxicity/immunogenicity, or are

highly unspecific. Live cell confocal imaging was used to monitor peptide-specific docking over time and revealed this to happen in a very short timeframe and with a very high distinctive character, demonstrating the high affinity and specificity of the used peptide pair.

2. Experimental section

2.1 Materials

Dioleoylphosphatidylethanolamine (DOPE), 1,2-dioleoyl-3-dimethylammonium-propane (DODAP), N-palmitoyl-sphingosine-1-succinyl[methoxy(polyethylene glycol)2000] (C16 Ceramide-PEG2000), 1,2-distearoyl-sn-glycero-3-phosphoethanol-amine-N-[maleimide(polyethylene glycol)-2000] (DSPE-PEG2000-Maleimide), L-α-phosphatidylethanolamine-N-(lissamine rhodamine B sulfonyl) (Rho-PE) were from Avanti Polar Lipids (Alabaster, AL, USA). Cholesterol was from Sigma-Aldrich (St. Louis, MO, USA). siRNA sequences directed against Luciferase are as follows Sense 5'-CUUACGCUGAGUACUUCGAdTdT-3'Antisense5'-UCGAAGUACUCAGCGUAAGdTdT-3'. Antisense oligonucleotide Luc705 is made of all phosphorothioate bases 5'-CCUCUUACCUCAGUUACA-3' (underlined bases are 2'-O-methyl modified).
All oligonucleotides were provided by GlaxoSmithKline (Stevenage, UK) for use within the EU IMI COMPACT consortium. Cysteine modified K3 and E3 peptides (Ac-CKIAALKEKIAALKEKIAALKE-NH_2 and Ac-CEIAALEKEIAALEKEIAALEK-NH_2) were ordered in >90% purity from Genscript Corp. (Piscataway, NJ, USA). Lipidated peptides Cholesterol-PEG_{12}-K3 and Cholesterol-PEG_{12}-E3 (CPK and CPE) were synthesized as described before [25].

2.2 Liposome preparation

Stable nucleic acid-lipid particles are prepared using the preformed vesicle method of Maurer et al. [30] using a lipid composition of DODAP/DOPE/Cholesterol/C16 Ceramide-PEG2000 at a ratio of 26/22/46/6.
For labeled vesicles, 0.5% Lissamine Rhodamine-PE was included. Using a rotary evaporator, a dry lipid film of 40 µmol total lipid was created in a round bottom flask. After flushing with nitrogen, the lipid film was hydrated in 70% citrate buffer 50 mM pH 4.0 and 30% ethanol to a lipid concentration of 8 mM. The hydrated lipids were extruded through 100 nm pore-sized filters (Nuclepore, Pleasanton, CA, USA) using a Lipex™ Extruder (Northern Lipids, Burnaby, BC, Canada) for 10-12 times. Nucleic acids (NA) (splice correcting oligo or siRNA) were dissolved in 70% citrate buffer 50 mM pH 4.0 and 30% ethanol. Both the vesicles and the NA solution were preheated to 37°C and then mixed together under continuous heavy stirring in a final NA/lipid ratio of 0.06 (wt/wt). The mixture was then incubated for 1 hour at 37°C to allow reorganization of the vesicles. Ethanol was removed and buffer was replaced by overnight dialysis in a 10K MWCO Slide-A-Lyzer G2 Dialysis Cassette (Life Technologies) at 4°C against PBS. Unloaded vesicles were dialyzed directly after extrusion. After dialysis, loaded vesicles were subjected to three rounds of ultracentrifugation in a Type 70.1 Ti rotor for 50 minutes at 55.000RPM at 4°C to wash away unencapsulated NA.

2.3 Insertion of K3- and E3-peptides into the formulated vesicles

To reduce the C-terminal cysteine thiol groups, K3 and E3 peptides were incubated with Immobilized TCEP Disulfide Reducing Gel (Pierce #77712) for 1 hour at room temperature and then separated from TCEP Gel slurry by centrifugation in paper filter spin cups (Pierce #69700). Immediately afterwards they are added to DSPE-PEG2000-Maleimide micelles, dispersed in PBS pH 7.4, in a 1:1 molar ratio of thiol:maleimide and incubated overnight at 4°C. For insertion of the peptide micelles into the vesicles [31], the vesicles and the micelles are preheated to 45°C. The K3 or E3 micelles were then added to the vesicles at 1:100 molar ratio and incubated overnight at 45°C (extrapolated from the total amount of phospholipids, measured as described below). To remove uninserted micelles, the resulting vesicles were subjected to three rounds of ultracentrifugation in a Type 70.1 Ti rotor for 50 minutes at 55.000RPM at 4°C.

2.4 Characterization of vesicles

To separate the lipids from the NA, samples are extracted according to Bligh and Dyer [32]. The top phase of the extraction was collected and evaporated using a centrifugal concentrator. When completely dry, the samples were reconstituted in MilliQ water and the amount of nucleic acid was measured by UV/VIS spectrophotometry at 260nm using a NanoDrop 1000 spectrophotometer (Thermo Scientific). The lipid fraction in chloroform was assayed for total phosphate amount according to the method of Rouser using sodium biphosphate as a standard [33]. Total lipid amount was then extrapolated from the amount of phospholipid (DOPE) present in the formulation. The encapsulation efficiency was calculated using the formula

$$Encapsulation\ efficiency\ (\%) = \frac{\frac{[oligonucleotides]}{[phospholipids]}after\ ultracentrifugation}{\frac{[oligonucleotides]}{[phospholipids]}before\ dialysis} * 100$$

The hydrodynamic diameter and the polydispersity index were measured by dynamic light scattering, using a Malvern CGS-3 multiangle goniometer with He-Ne laser source (λ=632.8 nm, 22 mW output power) under an angle of 90° (Malvern Instruments, Malvern, UK). The zeta-potential of the liposomes was measured using laser Doppler electrophoresis on a Zetasizer Nano-Z (Malvern Instruments) with samples dispersed in 10 mM Hepes buffer pH 7.4 (no additional salts).

2.5 Aggregation assay

To demonstrate that the peptides are freely accessible on the distal end of the inserted PEG-lipids, the peptide mediated aggregation of the vesicles is measured by dynamic light scattering as described above. The vesicles were diluted to 25 nM phospholipid in PBS and hydrodynamic diameter was measured every minute for a total of 25 minutes. K3- and E3-functionalized vesicles were mixed together and immediately afterwards the measurement was started. K3- and E3-functionalized vesicles were mixed with unfunctionalized vesicles as controls.

2.6 Cell culture

For antisense oligo delivery, HeLa cells expressing the luciferase gene interrupted by mutated human β-globin intron 2 (IVS2-705) (HeLa pLuc705) were used [34]. For siRNA delivery HeLa cells stably transfected with a EGFPLuciferase gene under the PGK-promotor were used (construct described here [35]). All cells were cultured in Dulbecco's Modified Eagle's Medium with High Glucose supplemented with 10% (v/v) fetal bovine serum and Penicillin-Streptomycin-Amphotericin B at 37°C in a humidified atmosphere containing 5% CO_2. Medium for the HeLa pLuc705 cell line also contained 200 ug/ml of Hygromycin B. All medium and supplements were from Sigma-Aldrich. Cells were regularly tested for mycoplasma and all cell lines used were found to be negative.

2.7 Microscopy

10.000 HeLa pLuc705 cells were seeded per channel of an Ibidi µ-Slide VI$^{0.4}$ (Ibidi GmbH, Munich, Germany) one day prior to the addition of the vesicles. At the day of the experiment, cells were washed with PBS once and incubated with 5 µM CPE or CPK in OptiMEM medium without phenol red (Life Technologies) for 5 minutes at 37°C. As control OptiMEM medium without the peptides was used. Cells were washed with PBS and incubated with Rhodamine labeled vesicles (125 µM phospholipid) in OptiMEM for 10 minutes at 37°C. Cells were washed with PBS and incubated in OptiMEM containing 1 ug/ml Hoechst 33342 (Life Technologies, Bleiswijk, Netherlands) and incubated for 15 minutes at 37°C. Cells were washed with PBS and immediately imaged in OptiMEM on a Keyence BZ-9000 fluorescence microscope (Keyence, Düsseldorf, Germany) using a Nikon CFI Plan APO VC 60x oil immersion lens (NA 1.4 WD 0.13). Overlay pictures were made in BZ-II Analyzer software (Keyence). For uptake studies, cells were incubated on separate slides at 37°C for an additional 1 or 4 hours and then washed and imaged. No nuclear staining was applied in these studies.

To test the distinctive character of the peptide pair, 10.000 HeLa pLuc705 cells were seeded in a µView clear-bottom 96 well plate (Greiner Bio-One B.V. Alphen aan de Rijn, Netherlands). Next day, nuclei were stained as described above and after aspiration of the medium, the middle of the well was blocked with a piece of Teflon (PTFE) tube, with an outer diameter of 3mm. The area outside the tube was incubated with CPE as above and after washing, the ring barrier was removed and the whole well was incubated with Rhodamine labeled K-functionalized vesicles (125 µM phospholipid). After washing, the cells were incubated in OptiMEM and imaged in a Yokogawa Cell Voyager 7000 (Yokogawa, Tokyo, Japan). (See inset in Figure 5.5 for a schematic view).

A similar experiment was performed with cells in suspension. For this cells were stained with Hoechst as described above and then split in separate vials. These were incubated separately with CPE or OptiMEM with 250 nM of Calcein-AM (Life Technologies) for 5 minutes at 37°C. In between incubation steps cells were washed with PBS using centrifugation at 250xg for 3 minutes. After this the two vials were combined and 10.000 cells were then transferred to a µView clear-bottom 96 well plate and imaged while still in suspension in the Cell Voyager. An equal volume of K3-functionalized

rhodamine-labeled vesicles (final concentration of 125 µM total lipid) was injected 30 seconds after onset of the live cell imaging using the built-in dispenser. A picture was taken every 30 seconds over a time period of 15 minutes. These pictures were converted into a time-lapse movie with 5 frames/second. See Supplementary Video 1 and 2.

2.8 Transfection studies

Transfection studies were done in 24 well plates, with HeLa pLuc705 cells seeded at a density of 45.000 cells/well and HeLa PGK-EGFPLuciferase cells at a density of 35.000 cells/well 24h before before transfections. At the day of the experiment, cells were washed once with PBS and half of the wells were incubated with 5 uM CPE or CPK in OptiMEM and the other half with plain OptiMEM for 5 minutes at 37°C. Cells were washed with PBS and incubated with SCO or siRNA loaded vesicles (1 uM oligonucleotides) in OptiMEM for 4 hours at 37°C. Afterwards, transfection mixes were replaced by complete medium and plates are incubated for 24 hours at 37°C. As a positive control for nucleic acid delivery, Lipofectamine 2000 (Life Technologies) was used according to manufacturer's protocol. Each condition was measured in triplo. The following day, cells were washed once with PBS and lysed with 250ul of lysis buffer (Tris 25 mM, EDTA 2mM, 1% Triton X-100, 10% glycerol) on a shaking board at 37°C for 10 minutes. For each well, 50ul of lysate was mixed with 50µl of Luciferase Assay Reagent (Promega, Leiden, Netherlands) in triplo. Reagent was injected using a FLUOstar OPTIMA microplate reader (BMG Labtech, Ortenberg, Germany) equipped with an injection pump. 2 seconds after injection, luminescence was measured for 10 seconds according to supplier's recommendation. Results are plotted as mean plus standard deviation in GraphPad Prism 6. Statistical analysis was performed using multiple paired t-tests. Statistical significance is denoted as *** with $p < 0.001$.

3. Results

3.1 Formulation of stable nucleic acid vesicles with high loading

The stable nucleic acid lipid particles used here were prepared by the preformed vesicle method [30]. In this procedure, ethanol is used to destabilize preformed empty unilamellar vesicles which enables entrapment of the nucleic acids. The vesicles used here consist of DOPE/DODAP/Cholesterol/C16 Ceramide-PEG2000 at a molar ratio of 22/26/46/6. DODAP is a lipid with a positive charge at pH of formulation which is necessary for interaction with the nucleic acids and with the predominantly negatively charged cell membrane [30,36]. DOPE is a so called 'helper lipid', that prefers to adopt the inverted hexagonal (H_{II}) phase which favors intracellular delivery [36]. A PEG-lipid with the Ceramide C16 anchor was used, because it is known to dissociate from the bilayer [37]. The diameter of unfunctionalized vesicles is ~80 nm and their zeta potential is almost neutral due to the PEG-lipids (See Table 5.1).

Table 5.1 | Basic characteristics of the unloaded vesicles (averages and standard deviation of three measurements)

Sample	Size	PDI	Zeta Potential
Unfunctionalized vesicles	83.6 ± 0.6	0.06	-3.4 ± 0.3
E3-functionalized vesicles	97.4 ± 1.3	0.08	-7.7 ± 0.6
K3-functionalized vesicles	96.6 ± 0.7	0.07	-7.2 ± 0.7

Two types of nucleic acids were encapsulated in two separate batches of liposomes, a double stranded siRNA against luciferase and a single stranded splice correcting oligonucleotide (SCO) that corrects the splicing of luciferase pre-mRNA in the HeLa pLuc705 cell line [34]. The nucleic acids that were not encapsulated were removed from the vesicles by ultracentrifugation and the encapsulation efficiency was calculated, corrected for the total amount of phospholipids. The encapsulation efficiencies for both types of nucleic acids are generally high, with values around 90% encapsulation on average which is typical for this preparation method [30] (Table 5.2).

Table 5.2 | Encapsulation efficiencies for the different types of nucleic acids (averages and standard deviation of three different formulations)

Nucleic acid	Encapsulation efficiency
siRNA	92.4% ± 4.2%
SCO	87.1% ± 5.4%

3.2 Insertion of the coiled coil forming peptides into the lipid vesicles

The formulated liposomes were functionalized with the coiled coil forming peptides K3 $C(KIAALKE)_3$ and E3 $C(EIAALEK)_3$. The peptides are covalently coupled to a DSPE-PEG2000-maleimide lipid via a thioether bond, on the N-terminal cysteine (See Figure 5.1). The formed peptide micelles are then inserted into the vesicles using the 'post-insertion method' [31]. These vesicles are functionalized with 1% of the total lipids in the outer layer being coupled to a peptide. The insertion of the peptides is reflected by an increase in hydrodynamic diameter to ~100nm and a small change in zeta potential (Table 5.1).

3.3 Rapid clustering and aggregation of complementary functionalized vesicles

To demonstrate that the conjugated peptides are functional and accessible, the size increase and aggregation were monitored when the two populations of vesicles were mixed together. The two individual populations were stable when stored, but when mixed together, they quickly agglomerated to bigger clusters. An increase in turbidity was observed by eye. Dynamic light scattering measurements over time showed a gradual increase in particle size (Figure 5.2A). Immediately after mixing particle size increased, which is in line with the high association constant of the coiled coil pair. The increase in size appeared to be bigger over time, which is explained by the exponential effect of larger particles clustering together. No size increase was seen when either of the populations were mixed together with unfunctionalized vesicles, excluding the possibility that clustering is caused by one of the peptides inserting into the

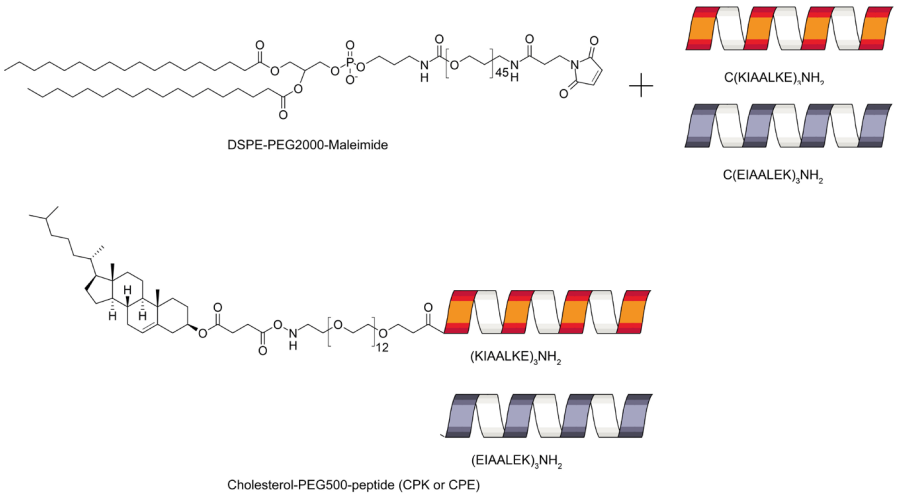

Figure 5.1 | Peptide sequences and anchors used
Peptides were coupled via maleimide-thiol linkage to a lipid (top) or were directly conjugated to the cholesterol anchor (bottom). The lipid anchored peptides were inserted into the liposomes and the cholesterol anchored peptides were used to functionalize cell membranes.

membrane of other vesicles (Figure 5.2B). The degree of size increase is concentration dependent with lower concentrations showing less or no size increase at all, while higher concentrations are more problematic to measure due to obscuration of the laser (data not shown). This is in line with previous experiments where full length SNARE-driven vesicle fusion was studied showing that docking of the complementary SNAREs (and not fusion) is the rate-limiting step [38]. In other words, the collision and docking of two vesicles is the bottleneck in the process, which directly correlates with vesicle concentration [26]. This also explains why the fusion or aggregation rate of these artificial systems is much slower (timeframes of minutes or hours, rather than (milli)seconds) than that of physiological fusion where tethering proteins facilitate the earliest vesicle contact [6,7].

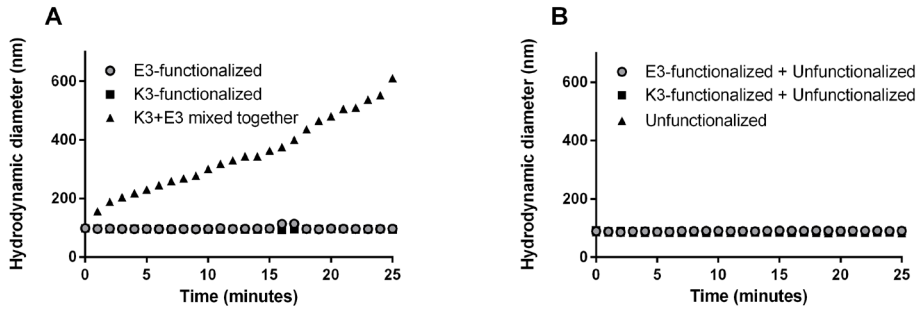

Figure 5.2 | Increase in hydrodynamic diameter of the mixed vesicles over time
Individual populations were stable in size but when the E3- and K3-functionalized vesicles were mixed together, a quick increase in size was observed.

3.4 Docking of the functionalized vesicles to the cell membrane

Next, it was tested whether the vesicles could also be docked to live cells using the K3/E3 coiled coil interaction. In earlier work, it was shown that using a hydrophobic anchor, both peptides could be inserted into existing membranes, either liposomal [25] or the membranes of living cells [27]. In the present work, the membranes of live HeLa pLuc705 cells were functionalized with a cholesterol anchored peptide on a short PEG spacer (Cholesterol-PEG_{12}-peptide, abbreviated as CPK and CPE, see Figure 5.1). After washing, the cells were incubated with liposomes labeled with 0.5 mol% rhodamine-PE, functionalized with either the K3 or E3 peptide and then imaged using an epifluorescence microscope. Strikingly, it was found that K3-functionalized liposomes docked to E3-functionalized cells, but not the other way around (Figure 5.3).

This is in contrast with previous work that showed that both the CPE and the CPK lipopeptide could be inserted into the cellular membrane when CHO cells were used [27]. It should be noted that it is experimentally difficult to study whether the lipopeptide has indeed inserted into the membrane via its hydrophobic anchor. However, the absence of fluorescent signal when untreated cells are incubated with the K3-functionalized vesicles strongly indicates that the signal is dependent on the CPE peptide. Additionally, when CPE-incubated cells were incubated with E3-functionalized vesicles no fluorescence was observed, showing that the signal is dependent on heterodimeric coiled-coil formation between the K3 and E3 peptides (Figure 5.3D).

Similar to our results, Yano et al. found that when the K3 and E3 peptides were recombinantly fused to a membrane protein, only when the E3 variant was expressed, it could be fluorescently tagged by the complementary K4 peptide [39]. It is known that these peptides interact differently with membranes and it is likely that these interactions are also cell type dependent. The interactions of the lipidated K3 and E3 peptides with a model membrane were previously studied using surface sensitive infrared reflection absorption spectroscopy (IRRAS) and circular dichroism (CD) spectroscopy. These studies showed that peptide E3 has no interaction with the membrane whereas the K3 peptide has a much higher binding affinity for the membrane amphiphiles [40,41]. This is explained by the so-called snorkeling effect of K3 similar to class A peptide amphiphiles. Also, the net charge of the E3 and K3 peptides, which is -3 and +3 respectively, while the cellular membrane has a net negative charge plays a role. Applying this knowledge to our findings, it is expected that the CPE lipopeptide is not hindered by charge interaction with the membrane, allowing it to insert into it with its hydrophobic anchor. The CPK lipopeptide is more likely to stick to the negatively charged glycolipids on the surface of the cell membrane, preventing insertion of the cholesterol anchor with the proper orientation. The peptide is then either washed away or the membrane interactions prevent it from dimerization with the complementary peptide. The microscope images show that the interaction of the K3-functionalized vesicles with the untreated cell membrane is not strong enough to bind the liposomes to the cell membrane after the washing steps, as evidenced by the lack of a fluorescent signal (See Figure 5.3B and C). Only the coiled coil interaction of the CPE and K3-functionalized vesicles is strong enough to unequivocally label the membrane, again exemplifying the strong interaction between the peptide pair.

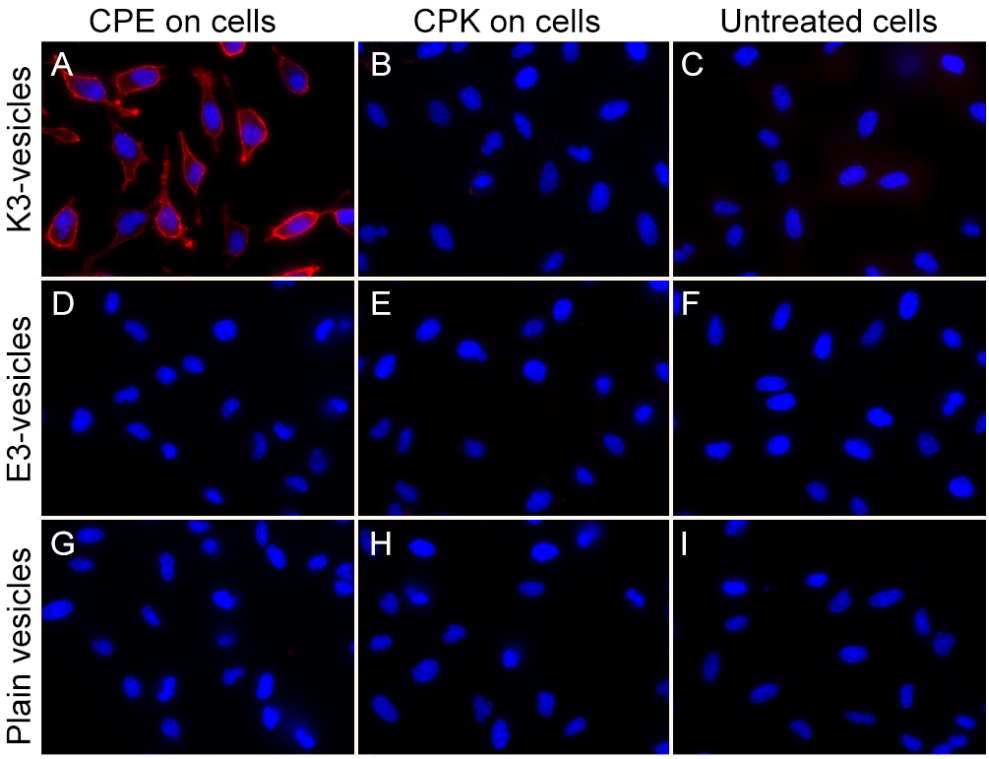

Figure 5.3 (A-I) | Microscopy pictures of HeLa pLuc705 cells incubated with rhodamine labeled vesicles
Overlay of red and blue channel is shown for all combinations but only when CPE functionalized cells were incubated with K3-functionalized vesicles, cell binding was seen in the red channel. Nuclei were stained with Hoechst 33342 dye in the blue channel.

Because there may be more diffusion and cross-over in solution, a complementary experiment was performed with cells in suspension. HeLa pLuc705 cells were counted and then split, after which half of them was incubated with CPE and the other half with control medium containing Calcein-AM to distinguish between the two populations, also before incubation with the vesicles. After washing, the cells were pooled in a one to one ratio and incubated with K3-functionalized vesicles. After another washing step, the cells were imaged under the microscope in suspension (Figure 5.5).

Also in suspension, two different populations could be distinguished. The green labeled unfunctionalized cells did not show any interaction with the vesicles whereas the functionalized cells were clearly labeled red. The red labeled cells cluster more than the unfunctionalized cells, which could indicate that there is some homo-coiling of the CPE peptides in the functionalized cells, or that the K3-functionalized vesicles are crosslinking the cells, similar to as was seen in the aggregation assay with K3- and E3-functionalized vesicles (Figure 5.2). When monitoring over a timeframe of 15 minutes, it was seen that membrane labeling starts immediately after addition of the labeled liposomes. A video of the increasing red fluorescence over time is available in the Supplementary Materials (Video S1 and S2).

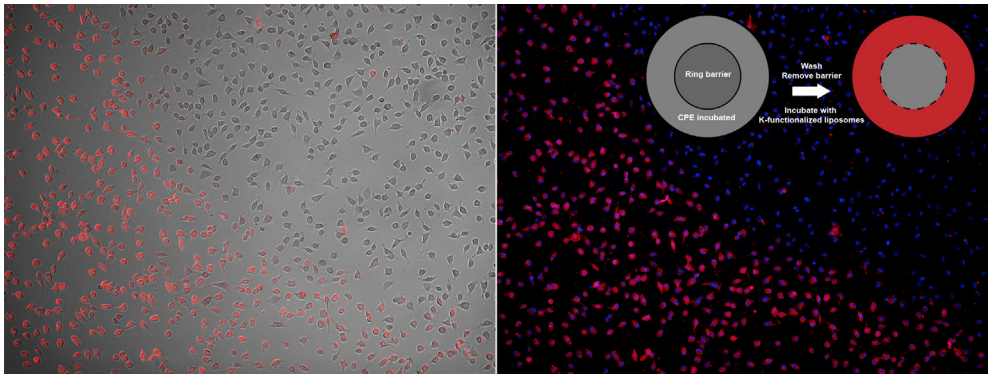

Figure 5.4 | Adherent CPE-functionalized and unfunctionalized HeLa pLuc705 cells incubated with rhodamine-labeled K3-functionalized vesicles
After seeding, part of the well (96 well plate) was blocked using a Teflon ring. Outside this barrier, cells were incubated with CPE. After washing, the barrier was removed and the entire well was incubated with rhodamine-labeled K3-functionalized vesicles (inset). Overlays with the brightfield picture (left) and with the Hoechst nuclear staining (right) show that the CPE-functionalized cells were labeled red and the outer rim of where the barrier was positioned was clearly visible.

The cells in these experiments had the exact same background and thus membrane proteins and receptors, with the CPE peptide as the only difference. The ability to distinguish between these two cell populations both in adherent cells and in suspension demonstrates the high specificity of the peptide pair. This allows for new possibilities to selectively target cells in the same vessel, regardless of any existing cell surface properties.

5

3.5 Functional delivery of nucleic acid payloads after docking

When docking was successfully demonstrated, it was tested whether these vesicles and the coiled coil interaction could be used to functionally deliver model nucleic acid payloads. For delivery of the single stranded oligonucleotide (SCO), the HeLa pLuc705 cell line was used. This cell line is stably transfected with a luciferase gene that is interrupted by a mutated human β-globin intron 2 (IVS2-705), described by Kang et al. [34]. Under normal conditions, this results in the encounter of a premature stop codon and the expression of a truncated, non-functional luciferase protein. When the 705 exon skipping SCO is successfully delivered, the splicing site (at position 705) is masked and the unnatural exon is spliced out, resulting in restoration of luciferase expression [34]. For the delivery of conventional siRNA, a HeLa cell line, stably expressing a luciferase construct was used [35]. Similar as in the microscopy experiments, the cells were incubated with the CPE or CPK lipopeptide but now followed by incubation with SCO or siRNA loaded liposomes, functionalized with K3, E3 or unfunctionalized. After the transfection experiments, cells were lysed and luciferase expression was measured.

Successful transfection and restoration of luciferase expression was demonstrated when the HeLa pLuc705 cells were modified with CPE and the SCO loaded vesicles were functionalized with the K3-peptide. K3-functionalized vesicles did not transfect the unfunctionalized cells. When compared to the positive control Lipofectamine 2000, the

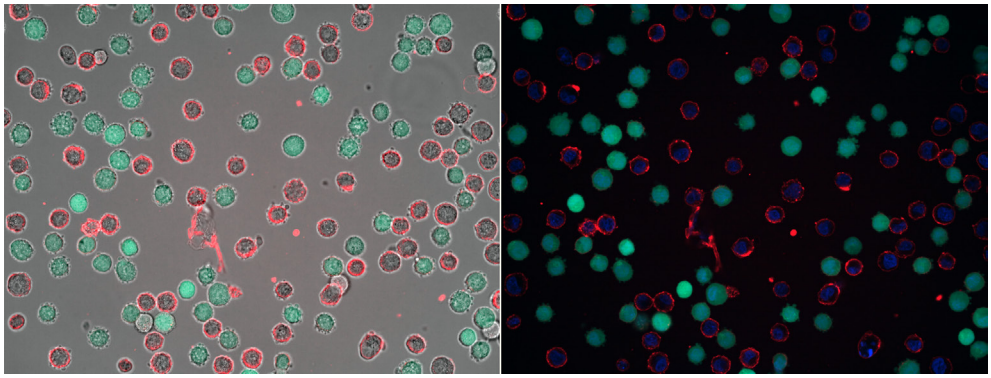

Figure 5.5 | Mixed population of CPE-functionalized and unfunctionalized HeLa pLuc705 cells incubated with rhodamine-labeled K3-functionalized vesicles in suspension
Unfunctionalized cells were incubated with Calcein-AM to distinguish between the two populations. Overlays with the brightfield picture (left) and with the Hoechst nuclear staining (right) show that the CPE-functionalized cells were clearly labeled red while the other population that was not functionalized had no detectable interaction with the vesicles at all.

efficiency of exon-skipping is approximately 60%. Unfunctionalized vesicles did not deliver the nucleic acid cargo and neither did the E3-functionalized vesicles to the CPK modified cells (Figure 5.6). This was also seen in the docking experiment and this again shows that the effect is dependent on coiled coil formation of the complementary peptides. The same peptide dependency is seen when siRNA is delivered to the HeLa PGK-Luciferase cells, however, the silencing effect when compared to Lipofectamine was only 25% (Figure 5.7).

What is of more importance, is the mechanism by which these vesicles deliver the nucleic acids. Clearly, the docking of the peptides is important, since unfunctionalized vesicles do not transfect. A logical explanation would be that docking of vesicles at the cell membrane triggers a direct fusion mechanism with the cell membrane, thereby delivering the splice correcting oligonucleotide. The fusion of natural membranes is initiated by SNARE proteins that pull the opposing membranes in juxtaposition [6,7]. That could also be the mechanism of delivery for the vesicles in the present work, but herein, the peptides are on the distal end of a PEG polymer (MW ~2000, PEG_{45}) so the two membranes are in fact not that close. In the work of Pähler et al., the effect of parallel versus anti-parallel docking of the E3/K3 pair on synthetic vesicles was investigated [42]. Half of the peptides were synthesized in reverse order, such that when the peptides assembled, the N- and C-termini were together (anti-parallel docking) as opposed to the two N-termini in the normal situation (parallel docking). It was found that anti-parallel coil assembly only resulted in docking while the parallel orientation also led to fusion (defined as the exchange of lipids and aqueous content between the different vesicle populations) [42].

This was explained by the increased distance between the bilayers when the peptides dock anti-parallel and in that work, the peptides were conjugated directly to the bilayer, without any additional PEG spacer like in our work. Therefore, with our PEGylated vesicles, it is not likely that the membranes are brought in direct contact immediately after docking.

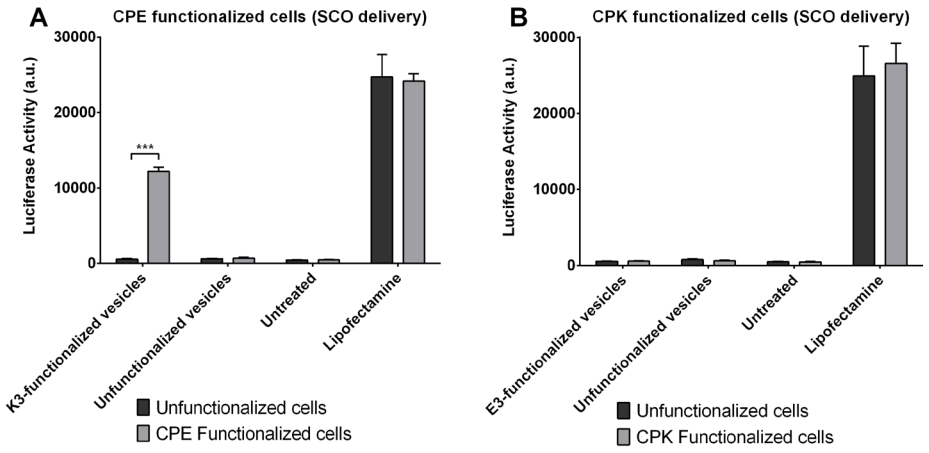

Figure 5.6 | Luciferase expression in HeLa pLuc705 cells after transfections with SCO loaded vesicles
Baseline expression was low and was restored after successful transfection. Grey bars represent CPE modified cells (left) and CPK modified cells (right). Black bars represent unfunctionalized cells (*** denotes $p < 0.001$).

To investigate the delivery mechanism, microscopy images of the labeled vesicles, docked to the cells were taken over time to monitor cellular uptake. When the cells are imaged directly after incubation, a very clear, homogeneously distributed membrane labeling is seen (Figure 5.8).

After one hour, the membrane labeling is less clear and bright red spots are appearing, indicating that the vesicles are in fact taken up in endosomal compartments. After four hours of incubation, which corresponds with the incubation time in transfection studies, the membrane labeling has become much less intense, while the endosomal spots have become much more prominent and numerous. These pictures show that despite the absence of a downstream signaling cascade, the vesicles are actively taken up, possibly by non-specific uptake mechanisms such as macropinocytosis or membrane recycling mechanisms.

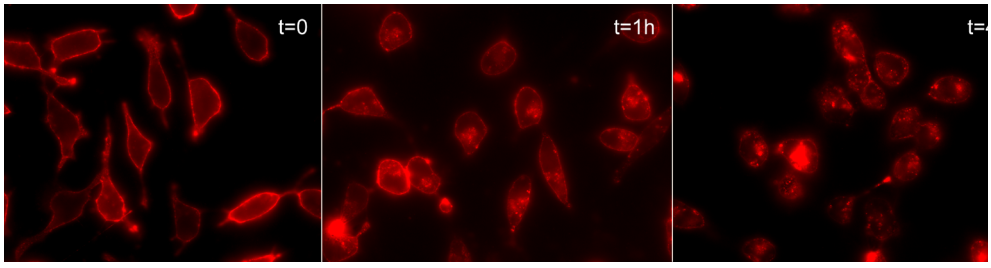

Figure 5.8 | Microscopy pictures of CPE-functionalized HeLa pluc705 cells incubated with K3-functionalized rhodamine-labeled vesicles over time
Directly after adding the vesicles, the cell membrane is clearly and homogeneously labeled. After one hour of incubation, brightly colored compartments are starting to appear. After four hours, the membrane labeling has almost disappeared and more numerous and brighter compartments are now visible, indicating active uptake of the vesicles over time.

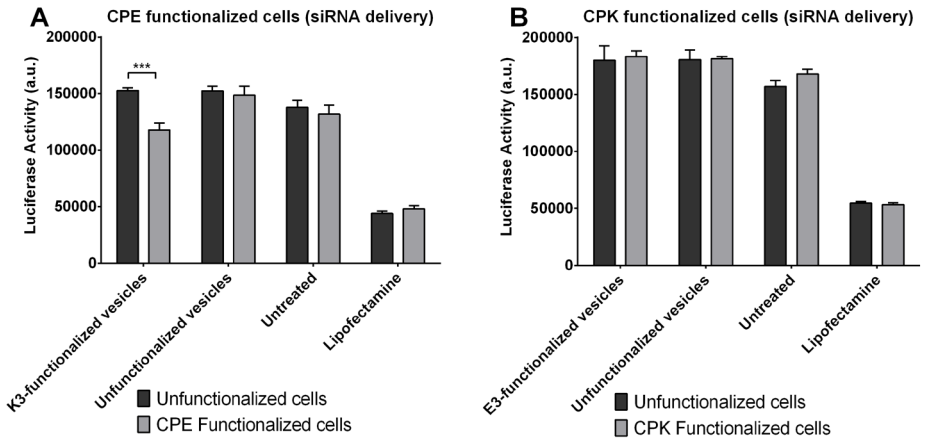

Figure 5.7 | Luciferase silencing in HeLa PGK-Luciferase cells after transfections with siRNA loaded vesicles Baseline expression is high and is silenced after successful transfection. Grey bars represent CPE modified cells (left) and CPK modified cells (right). Black bars represent unfunctionalized cells (*** denotes $p < 0.001$).

4. Discussion and conclusion

The results presented here show that the highly distinctive interaction between the K3- and E3-peptides and more specifically, the interaction between K3-functionalized vesicles and CPE-functionalized cells, can lead to functional delivery of two types of small oligonucleotides that normally do not cross the cellular membrane. It was demonstrated that merely the docking to the cell membrane and the coiling of the peptide pair at the cell surface, leads to uptake in endocytic vesicles and eventually to cytosolic delivery. Furthermore, this interaction is specific enough to distinguish between cells of identical background in the same vial that were or were not functionalized with the complementary peptide. This discrimination is independent of any existing surface protein expression and allows for highly specific cell binding and recognition.

Alternative to our approach of inserting of the CPE lipopeptide into the cell membrane, the peptide could be recombinantly expressed to tag specific cell subsets and to obtain highly targeted docking of liposomes to their cell membranes required as a first step towards targeted delivery of nucleic acids [39]. For an *in-vivo* application however, this would require another transfection with another targeted vector in order to get this artificial construct expressed on the target cell first. A more viable two-step approach was described by the group of Kopeĉek, where one of the coil forming peptides was fused to a Fab' fragment and in this way docked on the target cells *in vitro* and *in vivo*. A polymer functionalized with the complementary peptide could then interact with its target cell through assembly of the peptides[18,19]. This approach was also shown to be feasible *in vivo* and could be combined with imaging applications [20,21]. Another *in-vivo* application is inspired by the very interesting work by Raemdonck et al. in which "hitchhiking nanoparticles" are described [43]. In that work, lipid nanoparticles were reversibly coupled to isolated cytotoxic T-lymphocytes that are known to migrate to the tumor upon re-administration

to the body. This way, the concentration of nanoparticles in the tumor is increased. The cholesterol lipopeptide could be an alternative way to functionalize the lymphocytes ex-vivo and the very high affinity and specificity of the peptide pair that was demonstrated in the present work, could aid the nanoparticles in hitchhiking to the tumor area.

Expanding on this, there are many other applications where cells are manipulated *ex-vivo* that could benefit from a highly specific non-viral gene delivery system to modify the cells of interest. For example, T-cells can be re-directed by transferring T-cell receptor genes, or by transducing them with chimeric antigen receptors [44]. Another important example is the gene editing system CRISPR/Cas9 which at this point also appears to have more *ex-vivo* applications than *in vivo* use due to the current high off-target mutagenesis [45]. So far it was used to inactivate latent HIV-infections in primary T-cells [46] and to correct the dystrophin gene in Duchenne's Muscular Dystrophy patient-derived induced pluripotent stem cells [47,48].

To summarize, there is a growing interest in the ex-vivo manipulation of cells, both on the cell surface as well as the genomic level, to use them as a targeted delivery system. These applications can benefit from a highly selective, non-viral delivery system that is capable of functionally delivering nucleic acid cargos. This work shows the proof of concept that such molecules can be delivered using an artificial coiled coil forming targeting system that is independent of any existing cell surface properties or genetic background.

Electronic Supplementary Information

Two videos of the experiment shown in Figure 5.5, demonstrating the distinctive character of the peptide pair in a mixed population of cells are available online via http://pubs.rsc.org/en/content/articlelanding/2016/nr/c6nr00711b
Video S5.1 shows the experiment in the Brightfield channel including the green channel (Calcein-AM stained unfunctionalized cells) and orange channel (Rhodamine labeled liposomes). Video S5.2 shows the exact same frames but combining the fluorescent channels only, including the blue channel for Hoechst nuclear staining. Both videos consist of 31 frames at a frame rate of 5 fps. The labeled liposomes are injected after frame 1. The videos span a total timeframe of 15 minutes.

Acknowledgements

The research leading to these results has received support from the Innovative Medicines Initiative Joint Undertaking under grant agreement n° 115363 (IMI-COMPACT), resources of which are composed of financial contribution from the European Union's Seventh Framework Programme (FP7/2007-2013) and EFPIA companies' in kind contribution. A.K. acknowledges the financial support of the Netherlands Organization of Scientific Research (NWO) via a VICI grant.

References

[1] A.L. Boyle, D.N. Woolfson, De novo designed peptides for biological applications., Chem. Soc. Rev. 40 (2011) 4295–306. doi:10.1039/c0cs00152j.

[2] B. Apostolovic, M. Danial, H.-A. Klok, Coiled coils: attractive protein folding motifs for the fabrication of self-assembled, responsive and bioactive materials., Chem. Soc. Rev. 39 (2010) 3541–75. doi:10.1039/b914339b.

[3] S. Cavalli, F. Albericio, A. Kros, Amphiphilic peptides and their cross-disciplinary role as building blocks for nanoscience., Chem. Soc. Rev. 39 (2010) 241–63. doi:10.1039/b906701a.

[4] H. Robson Marsden, A. Kros, Self-assembly of coiled coils in synthetic biology: inspiration and progress., Angew. Chem. Int. Ed. Engl. 49 (2010) 2988–3005. doi:10.1002/anie.200904943.

[5] J.M. Mason, K.M. Arndt, Coiled coil domains: Stability, specificity, and biological implications, ChemBioChem. 5 (2004) 170–176. doi:10.1002/cbic.200300781.

[6] R. Jahn, R.H. Scheller, SNAREs--engines for membrane fusion., Nat. Rev. Mol. Cell Biol. 7 (2006) 631–43. doi:10.1038/nrm2002.

[7] F. Li, F. Pincet, E. Perez, W.S. Eng, T.J. Melia, J.E. Rothman, et al., Energetics and dynamics of SNAREpin folding across lipid bilayers., Nat. Struct. Mol. Biol. 14 (2007) 890–6. doi:10.1038/nsmb1310.

[8] C. Fortier, G. De Crescenzo, Y. Durocher, A versatile coiled-coil tethering system for the oriented display of ligands on nanocarriers for targeted gene delivery, Biomaterials. 34 (2013) 1344–1353. doi:10.1016/j.biomaterials.2012.10.047.

[9] E. Zacco, J. Hütter, J.L. Heier, J. Mortier, P.H. Seeberger, B. Lepenies, et al., Tailored Presentation of Carbohydrates on a Coiled Coil-Based Scaffold for Asialoglycoprotein Receptor Targeting, ACS Chem. Biol. 10 (2015) 2065–2072. doi:10.1021/acschembio.5b00435.

[10] Y. Assal, Y. Mizuguchi, M. Mie, E. Kobatake, Growth Factor Tethering to Protein Nanoparticles via Coiled-Coil Formation for Targeted Drug Delivery, Bioconjug. Chem. 26 (2015) 1672–1677. doi:10.1021/acs.bioconjchem.5b00266.

[11] J.M. Fletcher, R.L. Harniman, F.R.H. Barnes, A.L. Boyle, A. Collins, J. Mantell, et al., Self-assembling cages from coiled-coil peptide modules., Science. 340 (2013) 595–9. doi:10.1126/science.1233936.

[12] H. Gradišar, S. Božič, T. Doles, D. Vengust, I. Hafner-Bratkovič, A. Mertelj, et al., Design of a single-chain polypeptide tetrahedron assembled from coiled-coil segments., Nat. Chem. Biol. 9 (2013) 362–6. doi:10.1038/nchembio.1248.

[13] M. Pechar, R. Pola, R. Laga, A. Braunová, S.K. Filippov, A. Bogomolova, et al., Coiled coil peptides and polymer-peptide conjugates: Synthesis, self-assembly, characterization and potential in drug delivery systems, Biomacromolecules. 15 (2014) 2590–2599. doi:10.1021/bm500436p.

[14] U.I.M. Gerling-Driessen, N. Mujkic-Ninnemann, D. Ponader, D. Schöne, L. Hartmann, B. Koksch, et al., Exploiting Oligo(amido amine) Backbones for the Multivalent Presentation of Coiled-Coil Peptides, Biomacromolecules. 16 (2015) 2394–2402. doi:10.1021/acs.biomac.5b00634.

[15] E. Zacco, C. Anish, C.E. Martin, H.V. Berlepsch, E. Brandenburg, P.H. Seeberger, et al., A Self-Assembling Peptide Scaffold for the Multivalent Presentation of Antigens, Biomacromolecules. 16 (2015) 2188–2197. doi:10.1021/acs.biomac.5b00572.

[16] T.A. P.F. Doll, T. Neef, N. Duong, D.E. Lanar, P. Ringler, S.A. Müller, et al., Optimizing the design of protein nanoparticles as carriers for vaccine applications, Nanomedicine Nanotechnology, Biol. Med. (2015) 1–10. doi:10.1016/j.nano.2015.05.003.

[17] W. Shen, K. Zhang, J.A. Kornfield, D.A. Tirrell, Tuning the erosion rate of artificial protein hydrogels through control of network topology, Nat. Mater. 5 (2006) 153–158. doi:10.1038/nmat1573.

[18] K. Wu, J. Liu, R.N. Johnson, J. Yang, J. Kopeček, Drug-free macromolecular therapeutics: Induction of apoptosis by coiled-coil-mediated cross-linking of antigens on the cell surface, Angew. Chemie - Int. Ed. 49 (2010) 1451–1455. doi:10.1002/anie.200906232.

[19] T.-W. Chu, J. Yang, J. Kopeček, Anti-CD20 multivalent HPMA copolymer-Fab' conjugates for the direct induction of apoptosis., Biomaterials. 33 (2012) 7174–7181. doi:10.1016/j.biomaterials.2012.06.024.

[20] K. Wu, J. Yang, J. Liu, J. Kopeček, Coiled-coil based drug-free macromolecular therapeutics: In vivo efficacy, J. Control. Release. 157 (2012) 126–131. doi:10.1016/j.jconrel.2011.08.002.

[21] R. Zhang, J. Yang, T.-W. Chu, J.M. Hartley, J. Kopeček, Multimodality Imaging of Coiled-Coil Mediated Self-Assembly in a "Drug-Free" Therapeutic System, Adv. Healthc. Mater. 4 (2015) 1054–1065. doi:10.1002/adhm.201400679.

[22] B. Tripet, L. Yu, D.L. Bautista, W.Y. Wong, R.T. Irvin, R.S. Hodges, Engineering a de novo-designed coiled-coil heterodimerization domain off the rapid detection, purification and characterization of recombinantly expressed peptides and proteins., Protein Eng. 9 (1996) 1029–1042. doi:10.1093/protein/9.11.1029.

[23] H. Chao, D.L. Bautista, J. Litowski, R.T. Irvin, R.S. Hodges, Use of a heterodimeric coiled-coil system for biosensor application and affinity purification, J. Chromatogr. B Biomed. Appl. 715 (1998) 307–329. doi:10.1016/S0378-4347(98)00172-8.

[24] H. Robson Marsden, N.A. Elbers, P.H.H. Bomans, N.A.J.M. Sommerdijk, A. Kros, A reduced SNARE model for membrane fusion., Angew. Chem. Int. Ed. Engl. 48 (2009) 2330–2333. doi:10.1002/anie.200804493.

[25] F. Versluis, J. Voskuhl, B. Van Kolck, H. Zope, M. Bremmer, T. Albregtse, et al., In situ modification of plain liposomes with lipidated coiled coil forming peptides induces membrane fusion, J. Am. Chem. Soc. 135 (2013) 8057–8062. doi:10.1021/ja4031227.

[26] H. Robson Marsden, A. V. Korobko, T. Zheng, J. Voskuhl, A. Kros, Controlled liposome fusion mediated by SNARE protein mimics, Biomater. Sci. 1 (2013) 1046. doi:10.1039/c3bm60040h.

[27] H.R. Zope, F. Versluis, A. Ordas, J. Voskuhl, H.P. Spaink, A. Kros, In vitro and in vivo supramolecular modification of biomembranes using a lipidated coiled-coil motif, Angew. Chemie - Int. Ed. 52 (2013) 14247–14251. doi:10.1002/anie.201306033.

[28] L. Kong, S.H.C. Askes, S. Bonnet, A. Kros, F. Campbell, Temporal Control of Membrane Fusion through Photolabile PEGylation of Liposome Membranes, Angew. Chemie Int. Ed. 55 (2016) 1396–1400. doi:10.1002/anie.201509673.

[29] N.L. Mora, A. Bahreman, H. Valkenier, H. Li, T.H. Sharp, D.N. Sheppard, et al., Targeted anion transporter delivery by coiled-coil driven membrane fusion, Chem. Sci. 7 (2016) 1768–1772. doi:10.1039/C5SC04282H.

[30] N. Maurer, K.F. Wong, H. Stark, L. Louie, D. McIntosh, T. Wong, et al., Spontaneous entrapment of polynucleotides upon electrostatic interaction with ethanol-destabilized cationic liposomes., Biophys. J. 80 (2001) 2310–2326. doi:10.1016/S0006-3495(01)76202-9.

[31] J.N. Moreira, T. Ishida, R. Gaspar, T.M. Allen, Use of the post-insertion technique to insert peptide ligands into pre-formed stealth liposomes with retention of binding activity and cytotoxicity, Pharm. Res. 19 (2002) 265–269. doi:10.1023/A:1014434732752.

[32] E.G. Bligh, W. Dyer, A rapid method of total lipid extraction and purification, Can. J. Biochem. Physiol. 37 (1959) 911–917.

[33] G. Rouser, S. Fleischer, A. Yamamoto, Two dimensional thin layer chromatographic separation of polar lipids and determination of phospholipids by phosphorus analysis of spots, Lipids. 5 (1970) 494–496. doi:10.1007/BF02531316.

[34] S.H. Kang, M.J. Cho, R. Kole, Up-regulation of luciferase gene expression with antisense oligonucleotides: implications and applications in functional assay development., Biochemistry. 37 (1998) 6235–6239. doi:10.1021/bi980300h.

[35] B. Su, A. Cengizeroglu, K. Farkasova, J.R. Viola, M. Anton, J.W. Ellwart, et al., Systemic TNFα gene therapy synergizes with liposomal doxorubicine in the treatment of metastatic cancer., Mol. Ther. 21 (2013) 300–8. doi:10.1038/mt.2012.229.

[36] I.M. Hafez, N. Maurer, P.R. Cullis, On the mechanism whereby cationic lipids promote intracellular delivery of polynucleic acids., Gene Ther. 8 (2001) 1188–96. doi:10.1038/sj.gt.3301506.

[37] K.W.C. Mok, A.M.I. Lam, P.R. Cullis, Stabilized plasmid-lipid particles: Factors influencing plasmid entrapment and transfection properties, Biochim. Biophys. Acta - Biomembr. 1419 (1999) 137–150. doi:10.1016/S0005-2736(99)00059-0.

[38] E.A. Smith, J.C. Weisshaar, Docking, not fusion, as the rate-limiting step in a SNARE-driven vesicle fusion assay., Biophys. J. 100 (2011) 2141–50. doi:10.1016/j.bpj.2011.03.015.

[39] Y. Yano, A. Yano, S. Oishi, Y. Sugimoto, G. Tsujimoto, N. Fujii, et al., Coiled-coil tag - Probe system for quick labeling of membrane receptors in living cells, ACS Chem. Biol. 3 (2008) 341–345. doi:10.1021/cb8000556.

[40] M. Rabe, C. Schwieger, H.R. Zope, F. Versluis, A. Kros, Membrane interactions of fusogenic coiled-coil peptides: Implications for lipopeptide mediated vesicle fusion, Langmuir. 30 (2014) 7724–7735. doi:10.1021/la500987c.

[41] M. Rabe, H.R. Zope, A. Kros, Interplay between Lipid Interaction and Homo-coiling of Membrane-Tethered Coiled-Coil Peptides., Langmuir. 31 (2015) 9953–64. doi:10.1021/acs.langmuir.5b02094.

[42] G. Pähler, C. Panse, U. Diederichsen, A. Janshoff, Coiled-coil formation on lipid bilayers--implications for docking and fusion efficiency., Biophys. J. 103 (2012) 2295–303. doi:10.1016/j.bpj.2012.08.053.

[43] L. Wayteck, H. Dewitte, L. De Backer, K. Breckpot, J. Demeester, S.C. De Smedt, et al., Hitchhiking nanoparticles: Reversible coupling of lipid-based nanoparticles to cytotoxic T lymphocytes, Biomaterials. 77 (2016) 243–254. doi:10.1016/j.biomaterials.2015.11.016.

[44] W.J. Urba, D.L. Longo, Redirecting T Cells, N. Engl. J. Med. 365 (2011) 754–757. doi:10.1056/NEJMe1106965.

[45] N. Savič, G. Schwank, Advances in therapeutic CRISPR/Cas9 genome editing., Transl. Res. 168 (2016) 15–21. doi:10.1016/j.trsl.2015.09.008.

[46] H.-K. Liao, Y. Gu, A. Diaz, J. Marlett, Y. Takahashi, M. Li, et al., Use of the CRISPR/Cas9 system as an intracellular defense against HIV-1 infection in human cells., Nat. Commun. 6 (2015) 6413. doi:10.1038/ncomms7413.

[47] D.G. Ousterout, A.M. Kabadi, P.I. Thakore, W.H. Majoros, T.E. Reddy, C. a. Gersbach, Multiplex CRISPR/Cas9-based genome editing for correction of dystrophin mutations that cause Duchenne muscular dystrophy., Nat. Commun. 6 (2015) 6244. doi:10.1038/ncomms7244.

[48] H.L. Li, N. Fujimoto, N. Sasakawa, S. Shirai, T. Ohkame, T. Sakuma, et al., Precise correction of the dystrophin gene in duchenne muscular dystrophy patient induced pluripotent stem cells by TALEN and CRISPR-Cas9, Stem Cell Reports. 4 (2015) 143–154. doi:10.1016/j.stemcr.2014.10.013.

Chapter 6

Strategies for the activation and release of the membranolytic peptide melittin from liposomes using endosomal pH as a trigger

Erik Oude Blenke[1]
Malgorzata Sleszynska[1,2]
Martijn J.W. Evers[1]
Gert Storm[1]
Nathaniel I. Martin[2]
Enrico Mastrobattista[1]

[1]Department of Pharmaceutics, Utrecht Institute of Pharmaceutical Sciences (UIPS), Faculty of Science, Utrecht University, Universiteitsweg 99, 3584 CG Utrecht, The Netherlands

[2]Department of Chemical Biology and Drug Discovery, Utrecht Institute for Pharmaceutical Sciences (UIPS), Faculty of Science, Utrecht University, Universiteitsweg 99, 3584CG Utrecht, The Netherlands

Submitted for publication

Abstract

Endosomolytic peptides are often coupled to drug delivery systems to enhance endosomal escape, which is crucial for the delivery of macromolecular drugs that are vulnerable to degradation in the endolysosomal pathway. Melittin is a 26 amino acid peptide derived from bee venom that has a very high membranolytic activity. However, such lytic peptides also impose a significant safety risk when applied in vivo as they often have similar activity against red blood cells and other non-target cell membranes. Our aim is to control the membrane-disrupting capacity of these peptides in time and space by physically constraining them to a nanocarrier surface in such a way that they only become activated when delivered inside acidic endosomes. To this end, a variety of chemical approaches for the coupling of lytic peptides to liposomes via functionalized PEG-lipids were explored, including maleimide-thiol chemistry, click-chemistry and aldehyde-hydrazide chemistry. The latter enables reversible conjugation via a hydrazone bond, allowing for release of the peptide under endosomal conditions. By carefully choosing the conjugation site and by using a pH activated analog of the melittin peptide, lytic activity towards a model membrane is completely inhibited at physiological pH. At endosomal pH the activity is restored by hydrolysis of the acid-labile hydrazone bond, releasing the peptide in its most active, free form. Furthermore, using an analogue containing a non-hydrolyzable bond as a control, it was shown that the activity observed can be completely attributed to release of the peptide, validating dynamic covalent conjugation as a suitable strategy to maintain safety during circulation.

Graphical Abstract

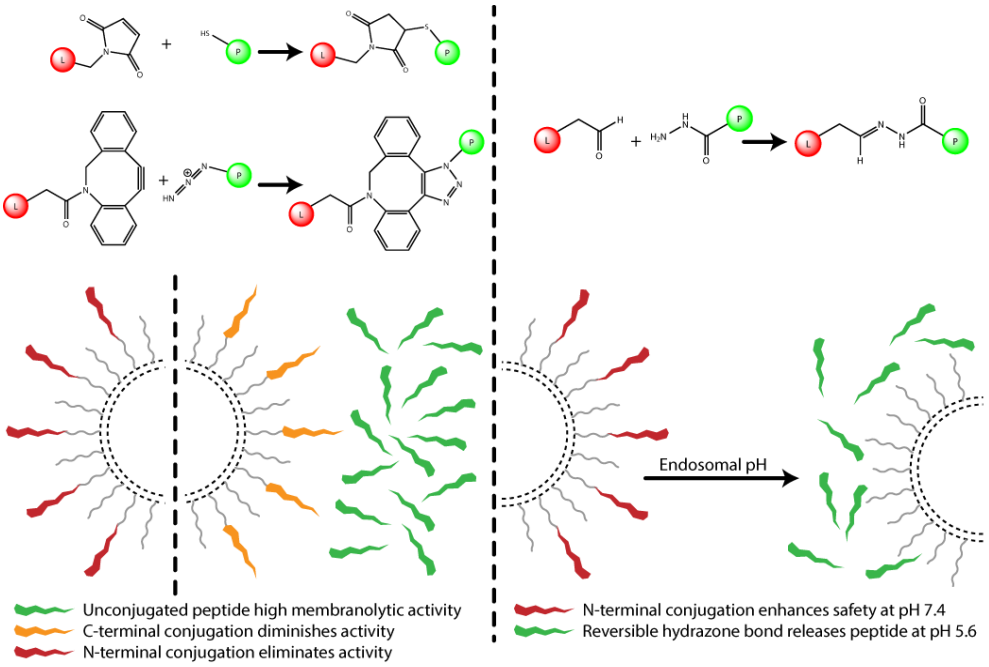

1. Introduction

The major bottleneck of intracellular delivery of therapeutic biomacromolecules using nanoparticulate systems is entrapment in the endosome. It is crucial that the cargo is released into the cytosol before it is degraded in the endolysosomal compartment, a highly acidic and proteolytic environment. A common strategy to enhance endosomal escape is to decorate the nanocarrier with endosomolytic or cell penetrating peptides (CPPs) [1–3]. A recurring problem with this approach is that none of these peptides are specific for the endosomal membrane, but interact with all biological membranes including those of red blood cells. In fact, the activity of membrane active peptides is often measured by hemolysis of red blood cells [4] and therefore imposes a significant safety risk if nanocarriers functionalized with such peptides are to be administered into the bloodstream. The application of endosomolytic peptides is therefore something of a double-edged sword, where more potent peptides are also often associated with increased toxicity. Several strategies have been proposed to mask or inactivate the lytic peptide until it has reached the target membrane. For example, Hansen et al. conjugated the cell penetrating peptide TAT to liposomes and constrained the other terminus of the peptide with a UV-cleavable bond, which allowed the construct to be photoactivated [5]. However, UV-radiation may not be the most suitable trigger, as it has limited penetration depth in the human body [6]. Many groups have used the endosomal environment as a trigger, reporting peptides with side-chain modifications that are removed by aminopeptidase and dipeptidyl peptidase [7] or phosphatases [8]. Another attractive strategy is to exploit the difference in pH between the bloodstream (physiological pH, 7.4) and the endosome (5.5-6.5). Using acid-labile chemistry, such as maleic anhydride to mask the lysines in the peptide, the endosomolytic activity is inhibited, but restored when it reaches the acidic environment of the endosome [9–12]. The common goal of these approaches is to maximize the potency of the endosomolytic agent in the endosome, but minimize its activity and thereby toxicity in the bloodstream.

In the work presented here, liposomes were functionalized with melittin, a 26 amino acid peptide derived from bee venom known for its high affinity for lipid membranes and potent lytic activity (Table 6.1) [3]. Melittin has previously been used to functionalize cationic polymers for gene delivery [10–14] and has also been used in the clinically evaluated Dynamic PolyConjugate (DPC) formulation for siRNA delivery [15,16]. In light of these previous reports we were also interested in developing approaches for coupling lytic peptides like melittin to liposomal surfaces. Our group recently described the use of copper-free "click" chemistry for conjugating other peptides to liposomes [17]. Our preliminary investigations with mellitin indicated that while introduction of an N-terminal azide group did not affect activity, upon conjugation to the liposomal surface a significant reduction in lytic activity was observed. Furthermore, we found that the activity of melittin is also diminished as pH is decreased, an effect which has also been previously reported [18]. We therefore opted to explore strategies wherein the melittin peptide is physically constrained by conjugation to liposomes via acid sensitive linkers so as to facilitate release at the lower pH of the endosome. As a second control mechanism we also selected a variant of the melittin peptide known to exhibit lower lytic activity at physiological pH but an optimal activity at endosomal pH (referred to as acid-melittin, Table 6.1) [19].

Several different chemical approaches were explored for the *in situ* coupling of melittin peptides to preformed liposomes and the efficiency of coupling investigated. PEGylated lipids functionalized with cyclooctyne, maleimide, or aldehyde moieties were used for coupling to peptides modified to contain azide, cysteine, or hydrazide groups respectively. The membrane activity of the different constructs was tested in a calcein leakage assay, a model for membrane perturbation and endosomal escape. The results of these investigations demonstrate that the conjugation of an aldehyde-modified lipid to a hydrazide-functionalized acid-melittin peptide via an acid sensitive hydrazine linkage leads to a system wherein lytic activity is abolished at pH 7.4 but restored at pH values below 5.6.

2. Results and discussion

2.1 Peptide synthesis

The five peptides used in this study (see Table 6.1) were synthesized following standard Fmoc-based solid-phase peptide synthesis procedures. The introduction of the azido group at the N-terminus in derivatives **2** and **4** was accomplished by coupling commercially available 2-azidoacetic acid in the final step of the synthesis. Similarly, a triply-protected hydrazide building block, prepared according to a slightly modified literature procedure [20], was attached to the N-termini of resin-bound acid-melittin-cysteine to give the analogue **5**. Following cleavage from the resin with subsequent removal of all protecting groups the peptides were purified to homogeneity by RP-HPLC. HPLC-MS analysis confirmed the identity and high purity of the desired products.

Table 6.1 | Melittin peptides prepared in present study

Peptide	#	Sequence and Structural Modifications
Melittin	**1**	GIGAVLKVLTTGLPALISWIKRKRQQ
Azido-Melittin	**2**	
Acid-Melittin [19]	**3**	GIGAVLEVLTTGLPALISWIEEEEQQC
Azido-acid-Melittin	**4**	
Hydrazide-Acid-Melittin	**5**	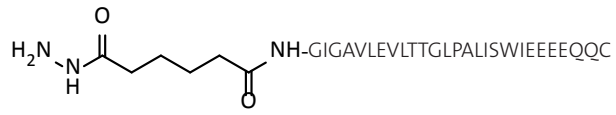

2.2 Surface modification of liposomes with melittin using click chemistry

In earlier work, we reported the surface modification of liposomes using copper-free click chemistry employing a novel lipid containing a bicyclononyne (BCN) cyclooctyne group on a short PEG spacer [17]. This approach allows for the site-specific and bio-orthogonal conjugation of azide-containing ligands. To apply a similar approach in the present study we employed the commercially available DSPE-PEG(2000)-dibenzocyclooctyne (DBCO) lipid containing a much longer spacer and the DBCO click moiety instead of the BCN group [21]. A drawback of the DBCO group is that it is more hydrophobic, which limits the maximum amount of functionalized lipid that can be incorporated. In the liposomes used here, 6% of all phospholipids were PEGylated, but when the DBCO-PEG lipid was used, only 2% of functionalized PEG lipid could be incorporated (with the other 4% unfunctionalized DSPE-PEG). When incorporation of higher percentages of the DBCO-PEG lipid was attempted, the liposomes tended to aggregate likely because the hydrophobic DBCO group folds back into the bilayer. (Resulting in higher average diameters and high polydispersity. See Table S6.1) However, when conjugating the azido(N)-melittin peptide (compound **4**) to these liposomes, coupling was very efficient, reaching complete turnover in almost all cases, as verified by UPLC. Owing to the tryptophan residue present in the melittin sequence, the peptide could be detected with high sensitivity and successful conjugation resulted in a shift of the lipidated peptide to the end of the spectrum. Size and PDI remained the same after conjugation, indicating that the melittin peptide does not interact with the membrane of the liposome itself, when the surface is PEGylated.

The endosomolytic activity of azido-melittin and its conjugates was tested using an established fluorescence-based assay employing liposomes loaded with calcein as model membranes [22]. The concentration of calcein inside the target liposomes is high and quenches the fluorescent signal but when the membrane is punctured calcein leaks out which can then result in a fluorescent signal. The target liposomes are not PEGylated and are therefore vulnerable to puncture or rupture by endosomolytic peptides, unlike the carrier liposomes used in this experiment, whose surface is protected by PEG-lipids. Calcein release from the target liposomes induced by different concentrations of the peptides examined is plotted as a percentage of maximum leakage, induced by complete lysis with Triton X-100 (Figure 6.1). The free azido-melittin peptide (**2**) is extremely potent, inducing complete leakage already at the lowest concentration tested (5 μM). The other conditions tested are melittin conjugated to carrier liposomes and to the DSPE-PEG-DBCO lipids alone, which will form micelles in solution. The high potency of the free melittin peptide demonstrates the importance of verifying complete coupling by UPLC. 5 μM of free peptide already induced maximum leakage, so if conjugation to the lipids were incomplete, the results with the micelles or liposomes could be compromised by the unconjugated fraction.

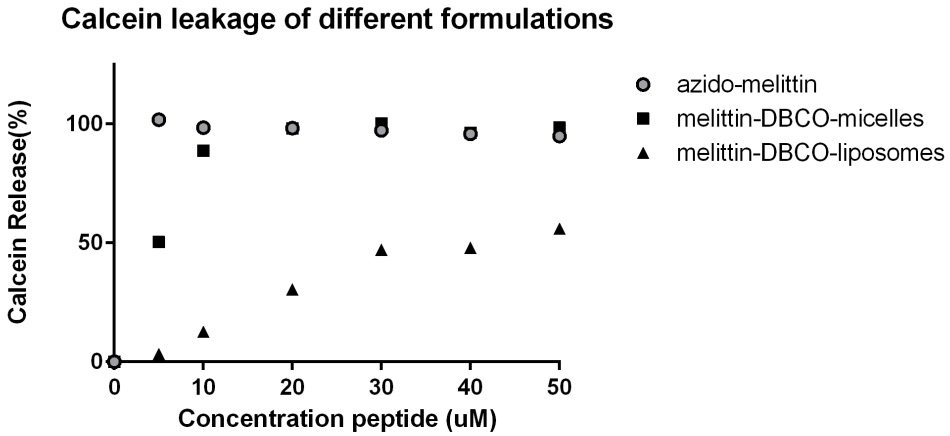

Figure 6.1 | Membrane activity of free azido-melittin and conjugates in the calcein leakage assay
Membrane activity of peptide **2** in free form, conjugated to DSPE-PEG-DBCO as micelles and on the surface of carrier liposomes. Calcein release from target liposomes with self-quenched concentrations of entrapped calcein, was measured after 1 hour at pH 7.4. Results are plotted relative to 100% leakage, induced by addition of 0.5% Triton X-100 to the calcein liposomes.

2.3 Activity of melittin click conjugates in calcein leakage assay

When conjugated to DSPE-PEG micelles, the potency of the peptide is slightly decreased, but maximum leakage is still reached at almost all concentrations. When the peptide is conjugated to the carrier liposome, activity is decreased much more. Even at the highest concentrations of melittin conjugated to the liposome, only ~50% of the maximum leakage is reached. An explanation for these findings could relate to the orientation in which the peptide inserts itself into the target membrane. If the peptide punctures the membrane by insertion of its free N- or C-terminus, conjugation at that terminus would likely interfere with membrane lysis. When using the click chemistry approach, the peptide used here is conjugated at the N-terminus but the results with the micelles indicate that blocking of this terminus does not hamper the activity. However, when these micelles are anchored to the carrier liposome membrane, the peptide is limited in its movement, which could inhibit the membrane activity, especially if this is dependent on local concentration of the peptide. If that is the case, conjugating more peptides to a liposome may increase the potency, but as was shown before, the amount of DBCO lipid that can be incorporated in the liposomes is limited.

To increase the peptide-per-liposome number and achieve higher densities of surface modification with the lytic peptide, maleimide-thiol chemistry was next evaluated. When using the DSPE-PEG-maleimide lipid there is no limit to the amount of PEG-lipid that can be substituted with functionalized PEG-lipid. Liposomes with up to 6% of DSPE-PEG-maleimide were stable in size and monodisperse (PDI <0.1). These liposomes were used to investigate the effect of incorporating higher densities of the cysteine functionalized melittin peptide **3** on the liposomal surface.

2.4 Membrane activity of melittin peptides at different pHs

Formulation and storage of the liposomes are typically done at physiological pH and the calcein leakage assay described above was also performed at pH 7.4. However, the pH in the endosome is around 5.5-6.0, low enough to cause conformational changes in the peptide and alter its activity. The calcein leakage assay with free peptide (**1**) was repeated at four different pH values between 5.6 and 7.4 and it was found that despite its high potency at pH 7.4, the activity of melittin is much lower at endosomal pH (Figure 6.2). This presents a possible drawback, as the melittin peptide could cause toxicity (hemolysis) in the circulation, but also be less potent under endosomal conditions where it is supposed to be active. To tackle both problems, a pH sensitive analog of melittin was used, that has optimized activity at endosomal pH (compound **3**). In this so-called 'acid-melittin' analogue all basic residues are replaced with glutamic acid, to make the peptide pH responsive[19]. When concentration ranges of free peptides **1**, **3** and **5** were tested at pH 5.6, 6.2, 6.8 and 7.4 the potencies dramatically changed. At pH 5.6 melittin reached only ~75% of maximum leakage in the highest concentration, while acid-melittin (**3**) was almost as potent as the normal melittin (**1**) was at 7.4. The activity of the pH sensitive variant is only ~25% at physiological pH, also addressing the safety issue in part.

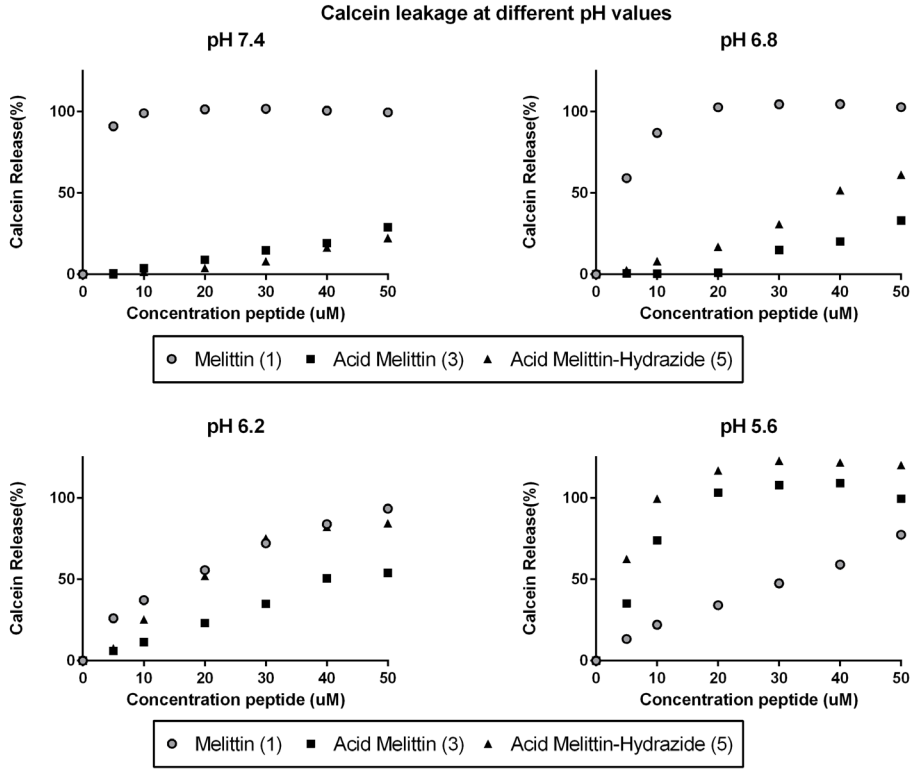

Figure 6.2 | Membrane activity of free peptides in the calcein leakage assay at different pH values
Membrane activity of free peptides in the calcein leakage assay at different pH values ranging from physiological pH (7.4) to endosomal pH (5.6). Activity of melittin decreases when pH is lowered while the acid-optimized analog acid-melittin increases in potency at endosomal pH.

For the final design of the conjugate, hydrazide-aldehyde coupling was employed. Therefore compound **5**, with an N-terminal hydrazide moiety was synthesized. This analog behaved similar to compound **3** at different pH values and even performed slightly better, indicating that modification of the N-terminus influences the lytic activity of the peptide, in this case, in a positive way (Figure 6.2).

2.5 Click chemistry vs maleimide-thiol chemistry and effect of different densities

Next, the density of peptides on the surface of the carrier liposomes was investigated. For this, acid-melittin was used (compounds **3** and **4**) because of its favorable behavior at different pHs relative to wild-type melittin. Because only 2% of DBCO functionalized lipid could be incorporated in the liposomes, DSPE-PEG(2000)-maleimide lipid was used, to conjugate to a C-terminal cysteine in the acid-melittin peptide. Because the whole fraction of PEGylated lipid could be replaced with PEG-maleimide lipid, densities of 2%, 4% and 6% were investigated. The total amount of conjugated peptide and of functionalized lipid was kept the same, so complete conjugation resulted in more peptides per liposome when higher densities were used. For conjugation with click-chemistry, compound **4** was used, conjugated at the N-terminus. For conjugation with maleimide-thiol chemistry, compound **3** was used, with a C-terminal cysteine. Therefore, the results of the 2% click chemistry and 2% maleimide-thiol conjugation could be used to compare the influence of N- versus C-terminal conjugation on the endosomolytic effect (Figure 6.3).

Strikingly, the conjugation of azido acid mellitin **4** to liposomes via the N-terminus completely abolished its effect in the calcein leakage assay, also at pH 5.6. This again demonstrates that the N-terminus is important for the lytic activity. By comparison, conjugation via the cysteine modified C-terminus of acid melittin analogue **3** did result in leakage of ~40% but the density of peptides on the surface of the liposome did not have a very big effect. The observation that C-terminal conjugation to a carrier system results in higher activity is in line with the report of Boeckle et al. where melittin was coupled to polymeric PEI nanoparticles. Also there, it was reported that conjugation of the peptide decreases the activity, regardless of the terminus used for conjugation [13]. It is likely that the mechanism of membrane penetration is different when the peptide is free or conjugated. For example, it has been hypothesized that melittin peptides form multimers that create pores, which is less likely to happen when they are anchored to a liposome. Alternatively, they insert one of their termini in the hydrophobic core of the membrane, which can be prevented by conjugation to that terminus. Finally, it is speculated that these mechanism are concentration dependent and therefore also influenced by the mobility of the peptides that is obviously lower when anchored [3,13,23–26]. The finding that at physiological pH there is no membrane activity in any of the formulations is advantageous given the fact that the peptides are also lytic towards erythrocyte membranes in circulation. However, the lytic activity at endosomal pH is also significantly lower than that of the free peptide. For optimal performance and safety, the difference in lytic activity between pH 5.6 and 7.4 should be as big as possible. Considering the results of the calcein leakage assay after conjugation and at different pH values, we surmised that such a goal could be reached by a system having the acid-melittin peptide conjugated at pH 7.4 but free in solution at the endosomal pH of 5.6. To achieve this, an acid-labile bond was used for conjugation.

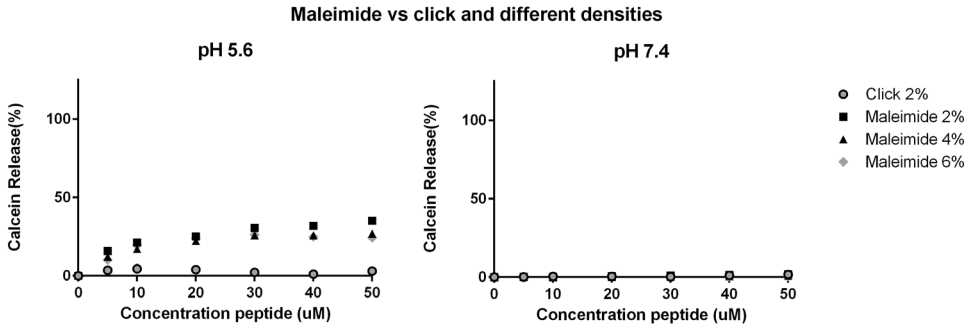

Figure 6.3 | Liposome formulations with acid-melittin coupled with click chemistry or maleimide-thiol chemistry at different densities
When coupling **4** with click chemistry, activity in the calcein leakage assay is completely abolished. C-terminal conjugation of **3** to the carrier liposomes preserves membrane activity but does only reach a maximum of ~40%. The density of the peptide on the surface of the carrier liposomes does not drastically alter the outcome.

2.6 Conjugation of acid-melittin to liposomes via an acid-labile hydrazone bond

To conjugate the peptide via a bond that is released at endosomal pH, a hydrazide was introduced at the N-terminus of acid melittin resulting in analogue **5**. For conjugation of peptide **5** to the liposomes, a fourth type of PEG lipid was used, DSPE-PEG(2000)-aldehyde. The conjugation of a hydrazide to an aldehyde results in the formation of an acid-labile hydrazone bond. Alternatively, the hydrazone bond can be reduced with hydride, resulting in an irreversible, stable hydrazine bond. The hydrazine conjugation was therefore used as a control, to distinguish between the contribution of pH on the activity of the peptide at different pHs and of the effect of covalent conjugation. In other words, any effect between different pHs with the stable conjugate is caused by peptide conformation, whereas the difference between the stable and acid sensitive conjugates as a function of pH is due to hydrolysis of the hydrazone linkage.

Interestingly, conjugation of peptide **5** to preformed liposomes, as done in the previous experiments, was not possible with this type of chemistry. Possibly, the conjugation efficiency was too low, or the product was rapidly hydrolyzed, due to an equilibrium that is formed between the hydrazone form and free aldehyde [27]. Furthermore, when the conjugation reaction was attempted in the presence of hydride (to immediately reduce the hydrazone bond) no conjugates could be detected by UPLC, indicating that the bond is not formed to a significant extent, when working with the relatively low concentrations used here. Therefore the hydrazone-forming, peptide-lipid conjugation reaction was first performed in DMSO and the formed micelles subsequently inserted into the membrane of the PEGylated carrier liposomes as described before [28]. The small percentages of DMSO present in the final sample did not interfere with the calcein leakage assay (See Supplementary results).

The resulting formulations of liposomes were tested in the calcein leakage assay as shown in Figure 6.4. Under both pH conditions, the hydride reduced stable hydrazine bond containing conjugate exhibited a complete loss of lytic activity. This is in line

with the other stable N-terminal conjugates prepared with click chemistry as shown in Figure 6.3. In contrast, the acid-labile hydrazone bond was found to be largely hydrolyzed after 1 hour at pH 5.6 leading to release of peptide **5** and calcein leakage of up to 80%. The effect of concentration appears to be bi-phasic, indicating that a certain threshold of free peptide must be reached to catalyze efficient membrane puncture. This suggests that there is indeed a concentration dependent mechanism of action, as discussed above. The finding that the calcein release at pH 5.6 is not quite complete when the acid labile hydrazone conjugate is used, suggests that not all the bonds are hydrolyzed in the timeframe of 1 hour. Furthermore, the fact that the hydrazone formulation is not completely inactive in the highest concentration of peptide at pH 7.4 indicates that the bond is not completely stable at physiological pH and that some hydrolysis may still occur.

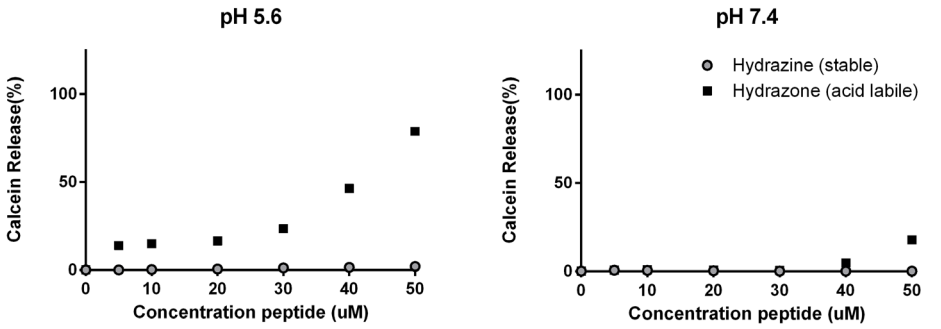

Figure 6.4 | Liposome formulations with hydrazide-acid-melittin coupled via a stable or acid labile bond Stable conjugation of the hydrazide-acid-melittin **5** to the carrier liposomes does not result in any leakage at all, neither at pH 5.6 where the peptide is most active, demonstrating again that conjugation to the N-terminus completely inactivates the peptide. The acid labile hydrazone bond is hydrolyzed at pH 5.6, releasing the peptide in its free form, inducing leakage at endosomal pH.

3. Discussion and conclusion

In the work presented here, three types of chemistry were explored to conjugate peptides to preformed liposomes. Traditionally, the gold standard for such conjugation is maleimide-thiol chemistry, where maleimide-functionalized PEG lipids are used to couple with cysteine residues in peptides. The main disadvantages of this approach are that cysteines may form disulfide bridges in solution (and already before conjugation) and that maleimides are not stable in aqueous solution, which prohibits storage of the liposomes for longer times until coupling. Furthermore, in more complex ligands like small proteins or antibodies the numerous cysteine residues often present make it difficult to control the site of conjugation. Furthermore, cysteine residues in proteins often have a specific function or are used in disulfide bridges, and may not available for coupling.

As an alternative, copper-free click chemistry was also investigated, with a DBCO-functionalized PEG lipid and a variant of the melittin peptide bearing an N-terminal azide group. This approach worked very efficiently and much faster than with the BCN-

lipid previously described by our group, demonstrating again that this is an attractive option, especially if bioorthogonal conjugation is required [17]. However, in the case of melittin, it turned out that the activity in the calcein leakage assay decreased when the peptide was conjugated, in particular to the N-terminus. If desired, an azide could also be incorporated at the C-terminus (or anywhere else in the peptide) with a different technique, for example by introducing an unnatural amino-acid such as azido-homoalanine during synthesis [29]. Instead, this finding was used to our advantage as a means to inactivate the peptide when circulating in the bloodstream, simply by conjugating it to the liposomal surface. As a second safety mechanism against hemolysis and interaction with non-target cells, the acid sensitive melittin analogue **5** was developed and after conjugation this resulted in complete elimination of the lytic activity at physiological pH.

To take full advantage of the maximized activity of acid-melittin at *endosomal pH*, the coupling strategy was changed to release the peptide in its free form at low pH. For this, a PEG-aldehyde lipid was used and to conjugate to a hydrazone moiety introduced at the N-terminus of the peptide to generate an acid-labile hydrazone bond. Due to the competing hydrolysis of the hydrazone bond, yields of such reactions were found to be very low when attempting direct conjugation of aldehyde modified liposomal surfaces. To solve this, the hydrazone forming reaction step was performed in organic solvent and the resulting DSPE-PEG-peptide micelles were inserted into preformed liposomes according to a previously published procedure known as 'post-insertion' [28]. As a control, the hydrazone bond could also be reduced with sodium borohydride to form a stable hydrazine bond that is not reversible in acidic environment. Liposomes functionalized with hydrazine coupled peptides did not induce any leakage at all in the calcein assay, including at the pH of 5.6 where acid-melittin has the maximum activity. For the formulation in which the peptide is reversibly conjugated, the lytic activity is restored at endosomal pH. This finding along with the observed absence of any effect in the irreversible conjugate indicates that the leakage is caused by the release of the free lytic peptide. However, the sub-maximal leakage induced even at the highest concentration of peptide indicates that not all of the peptides are released, as free hydrazide-acid-melittin (**5**) already induced complete leakage at concentrations of 10-20 uM. Complete release may be achieved at lower pH or after longer incubation times at pH 5.6 but the residence time in the endosome is likely not longer than the one hour timeframe that was used here [30,31].

The work here described clearly demonstrates that the lytic activity of the melittin peptide can be effectively "switched off" by conjugation to the N-terminus and that it can be restored by releasing the peptide in its free form using endosomal pH as a spatiotemporal trigger. The effect of N- versus C-terminal conjugation was also demonstrated when comparing click-chemistry designed analogues **2** and **4** with the maleimide-thiol chemistry compatible variants **3** and **5**. Because the peptide is more active in its free form, also when compared to the C-terminus conjugated form, we employed the strategy to completely release it in the endosome and used N-terminal conjugation for safety in the bloodstream. The effect of conjugation site of melittin was previously reported by Boeckle et al. [13] and it was explained by the hypothesis that the N-terminus of the peptide is inserted into the membrane to exert its function [24,25].

To summarize, this work shows the proof-of-concept that an endosomolytic peptide can be reversibly conjugated to a carrier liposome, using endosomal pH as the trigger for release. Calcein leakage from model liposomes was used as read-out both for toxicity (safety) and endosomolytic activity. As a second safety mechanism to avoid hemolysis and activity towards non-target membranes, the pH-sensitive variant of melittin was used, resulting in an inactive formulation at physiological pH. Triggered by a conformational change of the acid-melittin at pH 5.6 and hydrolysis of the hydrazone bond, activity was restored. This effect can be completely attributed to release of the peptide, as the formulation with a non-cleavable bond did not show any activity, even at pH 5.6.

Drug delivery systems equipped with an endosomal escape mechanism as described here are typically used for the delivery of biomacromolecules, such as peptides/proteins and nucleic acids. This may require a liposome with slightly different composition (for example, containing some cationic lipid to complex nucleic acid cargo) but both the in-situ coupling of peptides to preformed liposomes as well as the post-insertion of peptide-micelles in a preformed liposome can be applied to any lipid composition [28]. Additionally, before reaching the endosome, the liposomes need to be internalized via endocytosis, which could be achieved by active targeting with a targeting ligand. The coupling chemistries described here could all be used to couple targeting ligands as well, so to maintain specificity, one technique could be used to couple the endosomolytic peptide and another could conveniently be used to couple the targeting peptide. It is important to note that peptides conjugated to the outside of a liposome are susceptible to enzymatic degradation and do not remain intact very long in the bloodstream. This problem is usually not addressed in scientific literature because it is not a technical challenge to e.g. make the peptides out of (D) amino acids instead of (L). But interestingly, apart from C- versus N-terminal conjugation Boeckle et al. also reported an increase in membrane activity of the peptide when it was composed of all (D) amino acids. It is not clear whether this influences the conformation of the peptide which makes it more potent or that it is a result of increased stability, but it is another opportune effect [13]. Alternatively, drug delivery systems can be functionalized with peptoids or peptidomimetics to enhance enzymatic resistance [32].

Taken together, this work demonstrates the feasibility of using a two-pronged safety mechanism to render a membrane active peptide inactive while circulating in the blood but at the same time maximizing the potency of the peptide within the acidic environment of the endo-lysosomal pathway.

Acknowledgements

The research leading to these results has received support from the Innovative Medicines Initiative Joint Undertaking under grant agreement n° 115363 resources of which are composed of financial contribution from the European Union's Seventh Framework Programme (FP7/2007-2013) and EFPIA companies' in kind contribution. Financial support also provided by Utrecht Institute for Pharmaceutical Sciences (UIPS) with a Seed Grant to MS, NIM and EM. The authors thank Lipoid GmbH for the supplying of lipids and thank Lies Fliervoet and Carl Schuurmans for the structures in the graphical abstract.

Experimental section

Materials

1,2-dipalmitoyl-sn-glycero-3-phosphatidylcholine (DPPC), Egg-phosphatidylcholine (EPC) and 1,2-distearoyl-sn-glycero-3-phosphoethanolamine-N-[methoxy(polyethylene glycol)-2000] (DSPE-PEG2000) were a gift from Lipoid GmbH (Ludwigshafen, Germany). 1,2-distearoyl-sn-glycero-3-phosphoethanolamine-N-[maleimide(polyethylene glycol)-2000] (DSPE-PEG2000-maleimide) and 1,2-distearoyl-sn-glycero-3-phosphoethanolamine-N-[dibenzocyclooctyl(polyethylene glycol)-2000] (DSPE-PEG2000-DBCO) were from Avanti Polar Lipids (Alabaster, AL, USA). 1,2-distearoyl-sn-glycero-3-phosphoethanolamine-N-[aldehyde(polyethylene glycol)-2000] (DSPE-PEG2000-aldehyde) was from Nanocs (Bio-Connect Services BV, Huissen, Netherlands). Calcein, cholesterol and Triton X-100 were from Sigma-Aldrich (St. Louis, MO, USA).

All the amino acid derivatives were purchased from GL Biochem (Shanghai) Ltd. 2-azidoacetic acid was provided by Sigma-Aldrich (St. Louis, MO, USA). Hydrazide building block was synthesized following the procedure described previously [20], with slight modifications.

HPLC was carried out on Shimadzu (analytical) and Applied Biosystems (preparative) chromatographs equipped with a UV detector (λ = 214 nm). The following solvent system was used: (A) acetonitrile in 0.1% aqueous TFA (5:95, v/v) and (B) acetonitrile in 0.1% aqueous TFA (95:5, v/v). Preparative HPLC was carried out using Dr. Maisch C18 column (10 µm, 22 × 250 mm) in a linear gradient from 40 to 70% of (B) for 60 min, except for analogue **4**, where the applied gradient was from 50 to 80% of (B) for 60 min. All purifications were performed at a flow rate of 12 mL/min. The chromatograms of the pure peptides and mass spectra were recorded on an HPLC-MS system (Shimadzu - Finnigan LCQ Deca XP Max) using Dr. Maisch C_{18} column (5 µm, 4.6 × 250 mm).

Peptide synthesis

All peptides were prepared using standard Fmoc solid-phase synthesis and performed on a Symphony Multiple Peptide Synthesizer (Protein Technologies Inc., USA), i.e. by stepwise coupling of Fmoc-amino acids to the growing peptide chain on rink amide resin (TentaGel S RAM, Rapp Polymere GmbH, capacity 0.22 mmol/g). The amino acid side chain protecting groups were: Trt for Cys and Gln, OtBu for Glu, Boc for Lys and Trp, Pbf for Arg, and tBu for Ser and Thr. The standard procedures used for SPPS [28] involved (i) deprotection steps using 20% solution of piperidine in DMF, 5 and 15 min and (ii) couplings in DMF using HBTU, HOBt in the presence of DIPEA. The amino acids were coupled twice at a threefold excess. After the second coupling any remaining free amino groups were capped by treatment with 0.5 M acetic anhydride solution in DMF. N-terminal azide or hydrazide building block (analogues **2, 4, 5**) were attached manually in the final coupling step using the same procedure as for activation and coupling of Fmoc-amino acids. After completion of the synthesis the protected peptidyl resins were treated with cleavage cocktail, TFA:H_2O:EDT:TIPS, and stirred under N_2 for 2 h or in case of analogues 1 and 2 - for 3 h. Then the peptides were precipitated with cold diethyl ether

and centrifuged to afford crude products. The resulting materials were dissolved, frozen and lyophilized. The crude peptides were purified by RP-HPLC as described before. HPLC-MS was used to confirm the identity of the compounds and their purity.

Abbreviations
Boc, tert-butyloxycarbonyl group; DIPEA, N,N-diisopropylethylamine; DMF, dimethylformamide; EDT, 1,2-ethanedithiol; HBTU, N,N,N',N'-tetramethyl-O-(1H-benzotriazol-1-yl)uronium hexafluorophosphate; HOBt, 1-hydroxybenzotriazole; HPLC, High Pressure Liquid Chromatography; MS, mass spectrometry; OtBu, tert-butyl ester group; Pbf, 2,2,4,6,7-pentamethyldihydrobenzofuran-5-sulfonyl group; tBu, tert-butyl group; TFA, trifluoroacetic acid; TIPS, triisopropylsilane; Trt, trityl group

Liposome preparation

All carrier liposomes used in this work were composed of DPPC:Cholesterol:DSPE-PEG2000 in a ratio of 1.88:1:0.12 (equaling six percent of surface PEGylation). For conjugation of peptides, a fraction or the total amount of the DSPE-PEG2000 was replaced with DBCO-, or maleimide- functionalized PEG-lipid. For post-insertion of the peptide-**5** micelles, liposomes of DPPC:Cholesterol:DSPE-PEG2000 in a ratio of 1.92:1:0.08 were used. For all preparations, lipids were added to a round-bottom flask and dissolved in chloroform. The organic solvent was then evaporated using a rotary evaporator until a dry lipid film was formed. This lipid film was further flushed with a stream of nitrogen to remove all residual chloroform. The lipid film was hydrated in PBS 7.4 (B. Braun Melsungen AG, Melsungen, Germany) and the formed liposome dispersion was extruded through 100 nm pore-sized filters (Nuclepore, Pleasanton, CA, USA) using a Lipex™ Extruder (Northern Lipids, Burnaby, BC, Canada) for 10-12 times. The liposomes for the calcein leakage assay were composed of EPC:Cholesterol in a ratio of 2:1 and the lipid film was hydrated with a solution of 75 mM calcein and extruded as described above. After extrusion, calcein liposomes were transferred to a 10K MWCO Slide-A-Lyzer G2 Dialysis Cassette (Life Technologies) and dialyzed against a ~300 fold volume of HEPES (10 mM) buffered saline (HBS) at 4°C. After intervals of 8 hours or more, dialysis fluid was replaced with fresh HBS until no calcein could be detected in it fluorometrically (see below). The hydrodynamic diameter and polydispersity index of all liposomes were measured by dynamic light scattering, using a Malvern CGS-3 multiangle goniometer with He-Ne laser source (λ=632.8 nm, 22 mW output power) under an angle of 90° (Malvern Instruments, Malvern, UK).

Peptide conjugation

For coupling of **2**, the peptide was dissolved in PBS to a concentration of 500 μM and added to the liposomes with a total DPPC concentration of 20 mM and containing 1%, 2% or 3% PEG-DBCO lipid, in the ratios as noted in Table S6.1. These samples where then incubated overnight on a roller bench. The liposomes used in the leakage assay of Figure 6.1 had a concentration of 100 mM DPPC and contained 2% PEG-DBCO. **2** was added to those liposomes to a final concentration of 500 μM. To make micelles of DSPE-PEG-DBCO and **2**, both were dissolved in PBS and added together in a ratio of 2:1 with a final peptide concentration of 500 μM.

For coupling of **3** and **4**, stock solutions of peptide were made in DMSO in a concentration of 2.5 mM. These were added to liposomes containing PEG-DBCO or PEG-maleimide in a ratio of 4:1 (peptide to functionalized PEG). Considering that half of the functionalized PEG lipids is facing to the inside of the liposome, this results in an effective concentration of 2:1. The ratio was kept the same, so different densities of coupled peptide required different concentrations of liposomes. Liposomes containing 2% of PEG-DBCO or PEG-maleimide lipid were hydrated to a final concentration of 60 mM DPPC. Liposomes containing 4% and 6% of PEG-maleimide were hydrated to 30 mM and 20 mM DPPC respectively. The final concentration of DMSO in the liposomes was 10% and the final concentration of acid-melittin was 250 μM. Coupling efficiency was measured with UPLC (see below) and DLS measurements were done again after conjugation. No aggregation of the liposomes was seen, unless otherwise stated (see Table S6.1).
Coupling of **5** to preformed liposomes containing 6% of PEG-aldehyde was attempted in aqueous solution but this did not lead to any measurable conjugation (neither in presence of 20 mM sodium borohydride (Sigma-Aldrich)). Therefore, micelles were made in DMSO in an approximate ratio of 3:1 peptide to aldehyde in a concentration of 1.25 mM peptide. After overnight incubation, the sample was split and to one sodium borohydride was added to a final concentration of 20 mM and to the other 20 mM of TCEP (Sigma-Aldrich) to reduce the C-terminal cysteine. Two batches of liposomes containing 4% DSPE-PEG were made, hydrated in PBS pH 7.4 and PBS set to pH 5.6 with a total concentration of DPPC of 50 mM. These batches were split and 20 mM sodium borohydride and 20 mM TCEP were added to each of them (four samples total). The micelles with hydride and TCEP were added to the corresponding liposome samples and incubated at 40°C for 30 minutes. The final concentration of DMSO in the liposomes was 20% and the final concentration of acid-melittin was 250 μM.

Coupling quantification by UPLC

Coupling of the peptides was verified on a Waters Acquity UPLC system (Waters Corporation, Milford, MA, USA) with PDA and FLR detectors on a BEH300 C18 1.7 μm column. The mobile phase was changed in a gradient from 100% solvent A (Acetonitrile:water 5:95 with 0.1% TFA) to 100% solvent B (Acetonitrile with 0.1% TFA) in 5 minutes and ran on solvent B for 2 additional minutes at a flow rate of 0.25 ml/min. UV detection with the PDA detector was done on 210 nm and 280 nm and the FLR detector was used at 295/350 to detect the tryptophan residue in the peptides. Free peptides had a retention time around 3-4 minutes whereas the lipid conjugated peptide eluted at the end of the chromatogram. Conjugation was confirmed by the complete disappearance of the free peptide peak. The lowest amount that was injected was 0.301625 μM of peptide and this was still detectable. With the typical concentration of 250 μM of peptide that was added, the absence of the free peptide peak means less than 0.01 % of free peptide was present.

Calcein leakage assay

Membrane activity of free peptides and the peptides conjugated to liposomes was measured in a calcein leakage assay. EPC liposomes containing 75 mM of calcein were used as model membranes that could be punctured or lysed by the peptides/

liposomes. Leakage causes dilution of the self-quenched calcein to the external volume of the liposomes, increasing the fluorescent signal which was measured using a Jasco FP8300 plate reader (Jasco, Tokyo, Japan) at 495/520 excitation/emission wavelengths. Leakage was expressed as a percentage of the maximum release (max), induced by lysis of the target liposomes with Triton X-100 (0.5% final concentration). To determine 0% leakage, calcein liposomes were incubated in buffer and release was calculated using the following formula:

$$Calcein\ Release(\%) = \frac{Fluorescence(Sample) - Fluorescence(0)}{Fluorescence(\max) - Fluorescence(0)} * 100$$

For free peptide samples and for all melittin samples the ratio of sample to target liposomes was 1:9 and therefore dilutions at 10x the assay concentration were made in PBS pH 7.4 (Braun) or set to pH 6.8, 6.2 or 5.6 with hydrochloric acid. For acid-melittin samples, the ratio of sample to target liposomes was 1:4 and therefore dilutions at 5x the assay concentration were made in the appropriate buffers. Samples were incubated at room temperature for 1 hour and then measured in the platereader.

References

[1] A.K. Varkouhi, M. Scholte, G. Storm, H.J. Haisma, Endosomal escape pathways for delivery of biologicals, J. Control. Release. 151 (2011) 220–228. doi:10.1016/j.jconrel.2010.11.004.

[2] A. Erazo-Oliveras, N. Muthukrishnan, R. Baker, T.-Y. Wang, J.-P. Pellois, Improving the Endosomal Escape of Cell-Penetrating Peptides and Their Cargos: Strategies and Challenges, Pharmaceuticals. 5 (2012) 1177–1209. doi:10.3390/ph5111177.

[3] K.K. Hou, H. Pan, P.H. Schlesinger, S.A. Wickline, A role for peptides in overcoming endosomal entrapment in siRNA delivery — A focus on melittin, Biotechnol. Adv. (2015). doi:10.1016/j.biotechadv.2015.05.005.

[4] B.C. Evans, C.E. Nelson, S.S. Yu, K.R. Beavers, A.J. Kim, H. Li, et al., Ex Vivo Red Blood Cell Hemolysis Assay for the Evaluation of pH-responsive Endosomolytic Agents for Cytosolic Delivery of Biomacromolecular Drugs, J. Vis. Exp. (2013). doi:10.3791/50166.

[5] M.B. Hansen, E. Van Gaal, I. Minten, G. Storm, J.C.M. Van Hest, D.W.P.M. Löwik, Constrained and UV-activatable cell-penetrating peptides for intracellular delivery of liposomes, J. Control. Release. 164 (2012) 87–94. doi:10.1016/j.jconrel.2012.10.008.

[6] E. Oude Blenke, E. Mastrobattista, R.M. Schiffelers, Strategies for triggered drug release from tumor targeted liposomes., Expert Opin. Drug Deliv. 10 (2013) 1399–410. doi:10.1517/17425247.2013.805742.

[7] S.A. Bode, M.B. Hansen, R. Oerlemans, J.C.M. van Hest, D.W.P.M. Lowik, Enzyme-Activatable Cell-Penetrating Peptides through a Minimal Side Chain Modification, Bioconjug. Chem. (2015) 150427115856009. doi:10.1021/acs.bioconjchem.5b00066.

[8] J.P.M. Motion, J. Nguyen, F.C. Szoka, Phosphatase-triggered fusogenic liposomes for cytoplasmic delivery of cell-impermeable compounds, Angew. Chemie - Int. Ed. 51 (2012) 9047–9051. doi:10.1002/anie.201204198.

[9] D.B. Rozema, K. Ekena, D.L. Lewis, A.G. Loomis, J.A. Wolff, Endosomolysis by masking of a membrane-active agent (EMMA) for cytoplasmic release of macromolecules, Bioconjug. Chem. 14 (2003) 51–57. doi:10.1021/bc0255945.

[10] M. Meyer, A. Zintchenko, M. Ogris, E. Wagner, A dimethylmaleic acid–melittin-polylysine conjugate with reduced toxicity, pH-triggered endosomolytic activity and enhanced gene transfer potential, J. Gene Med. 9 (2007) 797–805. doi:10.1002/jgm.1075.

[11] M. Meyer, A. Philipp, R. Oskuee, C. Schmidt, E. Wagner, Breathing life into polycations: Functionalization with pH-responsive endosomolytic peptides and polyethylene glycol enables siRNA delivery, J. Am. Chem. Soc. 130 (2008) 3272–3273. doi:10.1021/ja710344v.

[12] M. Meyer, C. Dohmen, A. Philipp, D. Kiener, G. Maiwald, C. Scheu, et al., Synthesis and Biological Evaluation of a Bioresponsive and Endosomolytic siRNA–Polymer Conjugate, Mol. Pharm. 6 (2009) 752–762. doi:10.1021/mp9000124.

[13] S. Boeckle, E. Wagner, M. Ogris, C- versus N-terminally linked melittin-polyethylenimine conjugates: The site of linkage strongly influences activity of DNA polyplexes, J. Gene Med. 7 (2005) 1335–1347. doi:10.1002/jgm.783.

[14] S. Boeckle, J. Fahrmeir, W. Roedl, M. Ogris, E. Wagner, Melittin analogs with high lytic activity at endosomal pH enhance transfection with purified targeted PEI polyplexes, J. Control. Release. 112 (2006) 240–248. doi:10.1016/j.jconrel.2006.02.002.

[15] C.I. Wooddell, D.B. Rozema, M. Hossbach, M. John, H.L. Hamilton, Q. Chu, et al., Hepatocyte-targeted RNAi therapeutics for the treatment of chronic hepatitis B virus infection., Mol. Ther. 21 (2013) 973–85. doi:10.1038/mt.2013.31.

[16] M.G. Sebestyén, S.C. Wong, V. Trubetskoy, D.L. Lewis, C.I. Wooddell, Targeted in vivo delivery of siRNA and an endosome-releasing agent to hepatocytes., Methods Mol. Biol. 1218 (2015) 163–86. doi:10.1007/978-1-4939-1538-5_10.

[17] E. Oude Blenke, G. Klaasse, H. Merten, A. Plückthun, E. Mastrobattista, N.I. Martin, Liposome functionalization with copper-free "click chemistry," J. Control. Release. 202 (2015) 14–20. doi:10.1016/j.jconrel.2015.01.027.

[18] Y.-X. Tan, C. Chen, Y.-L. Wang, S. Lin, Y. Wang, S.-B. Li, et al., Truncated peptides from melittin and its analog with high lytic activity at endosomal pH enhance branched polyethylenimine-mediated gene transfection, J. Gene Med. 14 (2012) 241–250. doi:10.1002/jgm.2609.

[19] A. Ahmad, S. Ranjan, W. Zhang, J. Zou, I. Pyykkö, P.K.J. Kinnunen, Novel endosomolytic peptides for enhancing gene delivery in nanoparticles, Biochim. Biophys. Acta - Biomembr. 1848 (2015) 544–553. doi:10.1016/j.bbamem.2014.11.008.

[20] J.B. Matson, S.I. Stupp, Drug release from hydrazone-containing peptide amphiphiles, Chem. Commun. 47 (2011) 7962. doi:10.1039/c1cc12570b.

[21] M.F. Debets, S.S. van Berkel, S. Schoffelen, F.P.J.T. Rutjes, J.C.M. van Hest, F.L. van Delft, Aza-dibenzocyclooctynes for fast and efficient enzyme PEGylation via copper-free (3+2) cycloaddition., Chem. Commun. (Camb). 46 (2010) 97–99. doi:10.1039/b917797c.

[22] E. Mastrobattista, G.A. Koning, L. van Bloois, A.C.S. Filipe, W. Jiskoot, G. Storm, Functional characterization of an endosome-disruptive peptide and its application in cytosolic delivery of immunoliposome-entrapped proteins., J. Biol. Chem. 277 (2002) 27135–43. doi:10.1074/jbc.M200429200.

[23] E. Fattal, S. Nir, R.A. Parente, F.C. Szoka, Pore-forming peptides induce rapid phospholipid flip-flop in membranes., Biochemistry. 33 (1994) 6721–31.

[24] R. Smith, F. Separovic, T.J. Milne, A. Whittaker, F.M. Bennett, B.A. Cornell, et al., Structure and orientation of the pore-forming peptide, melittin, in lipid bilayers., J. Mol. Biol. 241 (1994) 456–66. doi:10.1006/jmbi.1994.1520.

[25] M. Bachar, O.M. Becker, Protein-induced membrane disorder: a molecular dynamics study of melittin in a dipalmitoylphosphatidylcholine bilayer., Biophys. J. 78 (2000) 1359–75. doi:10.1016/S0006-3495(00)76690-2.

[26] A.S. Ladokhin, S.H. White, "Detergent-like" permeabilization of anionic lipid vesicles by melittin, Biochim. Biophys. Acta - Biomembr. 1514 (2001) 253–260. doi:10.1016/S0005-2736(01)00382-0.

[27] J. Kalia, R.T. Raines, Hydrolytic stability of hydrazones and oximes, Angew. Chemie - Int. Ed. 47 (2008) 7523–7526. doi:10.1002/anie.200802651.

[28] J.N. Moreira, T. Ishida, R. Gaspar, T.M. Allen, Use of the post-insertion technique to insert peptide ligands into pre-formed stealth liposomes with retention of binding activity and cytotoxicity, Pharm. Res. 19 (2002) 265–269. doi:10.1023/A:1014434732752.

[29] A.J. de Graaf, M. Kooijman, W.E. Hennink, E. Mastrobattista, Nonnatural amino acids for site-specific protein conjugation., Bioconjug. Chem. 20 (2009) 1281–95. doi:10.1021/bc800294a.

[30] G. Sahay, W. Querbes, C. Alabi, A. Eltoukhy, S. Sarkar, C. Zurenko, et al., Efficiency of siRNA delivery by lipid nanoparticles is limited by endocytic recycling., Nat. Biotechnol. 31 (2013) 653–8. doi:10.1038/nbt.2614.

[31] J. Gilleron, W. Querbes, A. Zeigerer, A. Borodovsky, G. Marsico, U. Schubert, et al., Image-based analysis of lipid nanoparticle-mediated siRNA delivery, intracellular trafficking and endosomal escape., Nat. Biotechnol. 31 (2013) 638–46. doi:10.1038/nbt.2612.

[32] X. Zeng, A.M. de Groot, A.J.A.M. Sijts, F. Broere, E. Oude Blenke, S. Colombo, et al., Surface coating of siRNA–peptidomimetic nano-self-assemblies with anionic lipid bilayers: enhanced gene silencing and reduced adverse effects in vitro, Nanoscale. 7 (2015) 19687–19698. doi:10.1039/C5NR04807A.

Table S6.1 | Conjugation efficiency and size measurements of liposomes conjugated with click chemistry

DBCO content	DBCO:azide ratio	Size	PDI	Coupling efficiency
0%	-	151.4±2.3	0.08±0.05	-
1%	-	152.8±1.5	0.13±0.02	-
1%	4:1	152.1±0.5	0.12±0.01	>99.9%
1%	2:1	155.3±3.0	0.09±0.05	>99.9%
1%	1:1	**343.7±23.1**	**0.86±0.07**	**>95.0%**
2%	-	165.2±1.9	0.15±0.01	-
2%	8:1	162.4±2.3	0.14±0.01	>99.9%
2%	4:1	165.2±0.8	0.12±0.01	>99.9%
2%	2:1	164.7±0.4	0.13±0.04	>99.9%
3%	-	**234.0±11.4**	**0.52±0.06**	-
3%	12:1	**222.2±9.6**	**0.44±0.04**	>99.9%
3%	6:1	**222.0±4.5**	**0.45±0.05**	>99.9%
3%	3:1	**231.8±5.1**	**0.45±0.01**	>99.9%

Incorporation of more than 2% DSPE-PEG(2000)-DBCO lipid caused aggregation of the liposomes, also when no peptide is conjugated at all. With lower percentages of DBCO lipid, formulations are stable in size, also when peptide is conjugated. Coupling efficiency is measured by UPLC and no free peptide could be detected in all but the 1:1 sample. The detection limit was >0.01% of the lowest amount added. All liposomes contained 6% of PEG lipids.

Table S6.2 | Physicochemical properties of peptides

Peptide		HPLC T_R (min)	Molecular Weight	
			Calculated	Found $[M]^{2+}$
Melittin	**1**	14.09[a]	2846.52	1422.34
Azido-Melittin	**2**	18.90[a]	2929.55	1464.44
Acid-Melittin-cysteine	**3**	18.42[a]	2898.34	1449.46
Azido-Acid-Melittin	**4**	19.57[b]	2878.24	1438.71
Hydrazide-Acid-Melittin-Cysteine	**5**	23.21[a]	3040.50	1520.20

[a] Linear gradient from 40 to 70% of (B) for 30 min at a flow rate 1 mL/min, Dr. Maisch C_{18} column

[b] Linear gradient from 50 to 80% of (B) for 30 min at a flow rate 1 mL/min, Dr. Maisch C_{18} column

The following solvent system was used: (A) acetonitrile in 0.1% aqueous TFA (5:95, v/v) and (B) acetonitrile in 0.1% aqueous TFA (95:5, v/v).

Table S6.3 | Calcein Leakage measurements with DMSO (RAW DATA)

pH 7.4	pH 6.8	pH 6.2	pH 5.6	
149,2937	148,0347	145,9575	115,0819	0.5% Triton
149,9865	149,2962	145,9884	116,8047	0.5% Triton
149,5735	149,3956	145,32	107,4901	0.5% Triton
10,1344	9,6981	9,9809	9,8657	2%DMSO
10,1373	9,8895	10,0158	9,9043	2%DMSO
10,1193	9,9806	9,8925	9,8261	2%DMSO
10,0848	9,8243	9,9757	9,8877	2%DMSO
9,8163	9,4492	9,6059	9,4855	no DMSO
9,7979	9,6174	9,5789	9,4699	no DMSO
9,8081	9,6103	9,6509	9,3782	no DMSO
9,5069	9,5829	9,525	9,4588	no DMSO

Chapter 7

CRISPR-Cas9 gene editing: delivery aspects and therapeutic potential

Erik Oude Blenke[1]
Martijn J. W. Evers[1]
Enrico Mastrobattista[1]
John van der Oost[2]

[1]Department of Pharmaceutics, Utrecht Institute of Pharmaceutical Sciences (UIPS), Faculty of Science, Utrecht University, Universiteitsweg 99, 3584 CG Utrecht, The Netherlands

[2]Laboratory of Microbiology, Wagening University, Stippeneng 4, 6708 WE Wageningen, The Netherlands

Journal of Controlled Release. 2016 (in press)
doi: 10.1016/j.jconrel.2016.08.002

Abstract

The CRISPR-Cas9 gene editing system is considered the biotechnological breakthrough of the century, initiating rumors about future Nobel Prizes and heating up a fierce patent war, but also making significant scientific impact. The Clustered Regularly Interspaced Short Palindromic Repeats (CRISPR), together with CRISPR-associated proteins (Cas) are a part of the prokaryotic adaptive immune system and have successfully been repurposed for genome editing in mammalian cells. The CRISPR-Cas9 system has been used to correct genetic mutations and for replacing entire genes, opening up a world of possibilities for the treatment of genetic diseases. In addition, recently some new CRISPR-Cas systems have been discovered with interesting mechanistic variations. Despite these promising developments, many challenges have to be overcome before the system can be applied therapeutically in human patients and enabling delivery technology is one of the key challenges. Furthermore, the relatively high off-target effect of the system in its current form prevents it from being safely applied directly in the human body. In this review, the transformation of the CRISPR-Cas gene editing systems into a therapeutic modality will be discussed and the currently most realistic in vivo applications will be highlighted.

Graphical Abstract

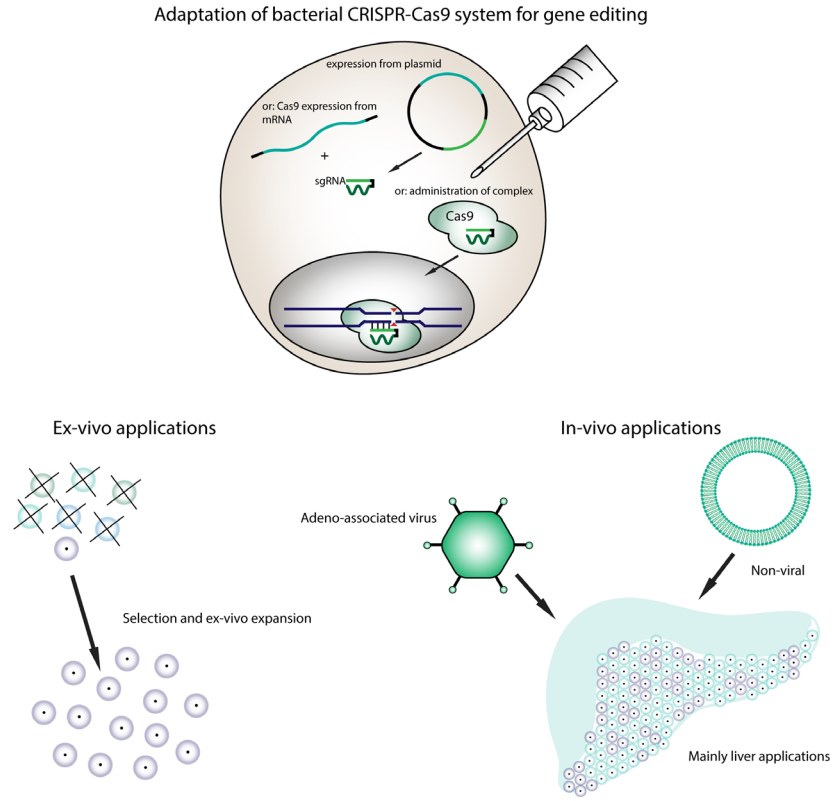

1. Introduction

The CRISPR-Cas9 gene editing system has received a tremendous amount of attention ever since the discovery of relevant mechanistic features [1–4] in 2010-2011 and the first application in eukaryotes in 2012 [1]. Applications appear to be nearly endless, ranging from improving crop resistance [5] to overcoming HIV infections [6] and the controversial human embryo editing [7]. The most captivating application is the prospect of being able to correct genetic defects in diseased tissues and cells [8], although this may currently still be out of reach [9].
However, the system being named the Science Magazine's Breakthrough of the Year 2015 [10] makes it undisputed that CRISPR-Cas9 is here to stay and it is already speculated that its inventors may receive a Nobel Prize within the coming decade [7].
Similar to RNA interference, where a eukaryotic defense system against viral infections is exploited to modulate gene expression [11], this new genome editing system makes use of an adaptive immune system found in prokaryotes. There is a multitude of such systems and CRISPR-Cas9 is certainly not the first one to be described [12,13], but its simplicity and ease of use have sparked the interest of researchers in diverse fields and initiated a run to clinical applications, again very similar to the early days of RNAi [14,15].
To exploit this potential, development of carrier systems capable of delivering the CRISPR-Cas9 system to human cells is of utmost importance, taking lessons from the RNAi field where possible. In this review, the basic mechanism of CRISPR-Cas9 genome editing is explained and current and potential therapeutic applications are highlighted. A special focus will be on the delivery aspects of the system, discussing the requirements for delivery vehicles to allow safe and effective ex vivo and in vivo manipulation for therapy in human patients.

2. CRISPR-Cas9 genome editing mechanism

Clustered Regularly Interspaced Short Palindromic Repeats (CRISPR), together with CRISPR-associated proteins (Cas) are a part of the adaptive immune system found in bacteria and archaea. This adaptive immune system can detect and destroy Mobile Genetic Elements (MGEs) such as unwanted viral and plasmid DNA in a highly specific manner. As mentioned before, there are other bacteria-derived targeted nucleases, like Meganucleases, TALEN or ZFN, that are already being translated into clinical application [16–19].
The CRISPR-Cas system is a family of proteins, subdivided in Class 1 (Types I, III and IV) and Class 2 (Types II, V, VI) [12], all consisting of specific endonuclease proteins (Cas) and a guide RNA molecule [20–23]. The guide RNA molecule guides the Cas protein to a very specific MGE related DNA target (Figure 7.1). This bacterial molecular machinery can be adapted for use in higher organisms, in particular for gene-editing. To this end, the endonuclease and the guide RNA have to be heterologously expressed.
For this purpose, a specific subtype of CRISPR-Cas is preferred: Class 2. The Class 2 CRISPR-Cas systems generally consists of a single multi-domain protein, such as the Type II nuclease: Cas9 [21–23]. The relatively simple architecture of Class 2 nucleases (Cas9) makes them so easy to apply, as compared to the large, multi-subunit protein Class 1 complexes.

2.1 CRISPR-Cas nucleases and guide RNAs

CRISPR-Cas based immunity in bacteria proceeds in three distinct stages. The three stages are acquisition, expression and interference [13,24]. *Acquisition:* As an adaptive defense system, bacteria and archaea collect sequences of foreign (plasmid or virus) DNA of 30-45 nucleotides long and integrate them as new spacers in the repetitive CRISPR arrays. To allow self/non-self discrimination, foreign target sequences (protospacers) are selected on the basis of a flanking motif, the protospacer-adjacent motif. *Expression:* During the expression stage, the CRISPR array is transcribed in one large pre-crRNA and is subsequently processed into smaller CRISPR RNAs (crRNAs). Each crRNA corresponds to one acquired foreign DNA sequence, so expression will result in a pool of crRNAs that all recognize a particular genetic element. The enzymes involved in this step vary between the different CRISPR-Cas subtypes. In the Cas9 system, the repeats of the pre-crRNA first hybridizes with a second, conserved RNA, called the transactivating CRISPR RNA (tracrRNA), after which the dsRNA is specifically cleaved by a non-Cas ribonuclease (RNaseIII). In the system adapted for gene editing (Figure 7.1B), these two RNAs are fused and expressed together as a single guide RNA (sgRNA) [1]. *Interference:* In this stage, the Cas nucleases are guided by the mature crRNAs to target and (in the presence of an adjacent PAM motif) cleave the corresponding protospacer sequences in invading MGEs when present. Hybridization of the tracrRNA:crRNA/Cas9 complex -or the sgRNA/Cas9 complex to the corresponding protospacer sequence results in double stranded breaks and thereby inactivation of the invading DNA [21,22,24].

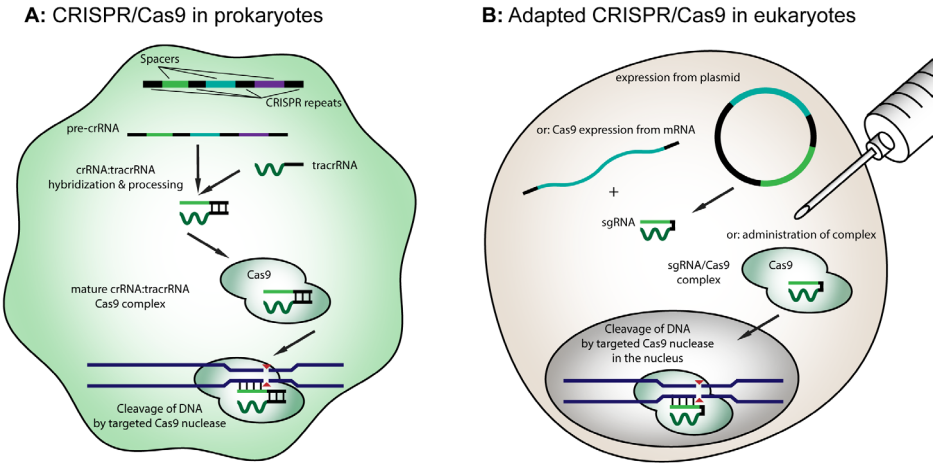

Figure 7.1 | Mechanism of CRISPR-Cas9 in prokaryotes and the adapted mechanism in eukaryotes
A: In prokaryotes, the protospacer sequences acquired from invading pathogens are stored as spacers in the CRISPR-loci, flanked by CRISPR repeats. These are transcribed into a precursor (pre-crRNA) after which the repeats hybridize with anti-repeat sequences within the tracrRNA. This dsRNA is recognized and cleaved by a housekeeping ribonuclease (RNaseIII), resulting in a mature crRNA/tracrRNA hybrid that forms a stable complex with Cas9. Upon a viral invasion, it guides the nuclease to the target sequence in the DNA for cleavage. B: In eukaryotes, a sgRNA is used that combines the function of the crRNA and tracrRNA. This can be expressed from a plasmid or from mRNA, alongside the Cas9 enzyme which is not naturally present in eukaryotes. Alternatively, the sgRNA/Cas9 complex can be administered as a whole. After translocation across the nuclear membrane (due to an engineered Nuclear Localization Signal; NLS) the heterologous complex cleaves the target sequence in the chromosomal DNA.

Expression of multiple sgRNAs from the same construct is called multiplexing, and can be used to target multiple genes or to enhance the knock-out by targeting multiple sites in the same gene [8].

2.2 PAM sequences

It should be noted that after integration of the invading DNA in the CRISPR locus, the 'foreign' sequence is also present in the bacterial genome. To avoid cleavage of the DNA in the CRISPR locus, a safety mechanism is built into the crRNA-sequence. The PAM-sequence is part of the MGE DNA, but is not copied into the CRISPR locus. Cas9- mediated cleavage of the target DNA only occurs when the PAM-sequence is present at the 3' end. When there is base-pair complementarity but no PAM-sequence, it indicates that the crRNA is bound to the CRISPR locus itself and the sequence is then not degraded [25]. PAM sequences vary per bacterial species [26]. The most widely used Cas9 nuclease is derived from *Streptococcus pyogenes* (*SpyCas9*) and has GG as its PAM-sequence, meaning that every target protospacer sequence is located adjacent to two guanine bases (protospacer-NGG) [1]. In the unlikely case that this sequence is not present in the intended target DNA, another Cas9 species could be used that binds to a different PAM sequence.

2.3 Non-homologous end joining (NHEJ) and homology-directed repair (HDR)

Cleavage by the targeted nuclease results in a double stranded break (DSB) at a desired sequence-specific location in the target DNA. In eukaryotes, this DSB can be repaired by two distinct mechanisms: Non-homologous end joining (NHEJ) or homology directed repair (HDR). NHEJ generates small insertions or deletions (indels) which can inactivate the target sequence by inducing a frame-shift or introducing a pre-mature stop codon. This method is applied for the rapid generation of knock-out cell lines or animal models [27], functional genomic screens [28] and other applications of transcriptional modulation/gene silencing [29]. Alternatively, HDR repairs the DNA strands based on structural homology. In the naturally occurring situation, this could be homology to a nearby located (and structurally related) gene or in therapeutic gene editing, a co-expressed or co-delivered repair template. When two DSBs are created this can result in complete excisions of a target gene and even a provided donor DNA template sequence could be precisely inserted into a specific target site [30–32] (Figure 7.2).

To summarize, the Cas9 system is the most flexible and easiest system to adapt, because it uses only a single enzyme that mediates both the crRNA processing as well as the DNA cleavage. The specificity of the targeted nuclease can be simply altered by replacing the guide RNA, unlike ZFNs and TALENs that require protein engineering for every new target. With CRISPR-Cas9, any 22 nucleotides long DNA sequence can be targeted as long as it is flanked by the NGG motif (when SpyCas9 is used). In the simplest and most widely used application of this system, where a genetic knock-out is made, only two components need to be expressed in the host cell to cleave the target gene: the Cas9 nuclease and the sgRNA. Guide RNAs can be expressed from the same plasmid as the Cas9 protein, which is (human) codon optimized and contains a nuclear

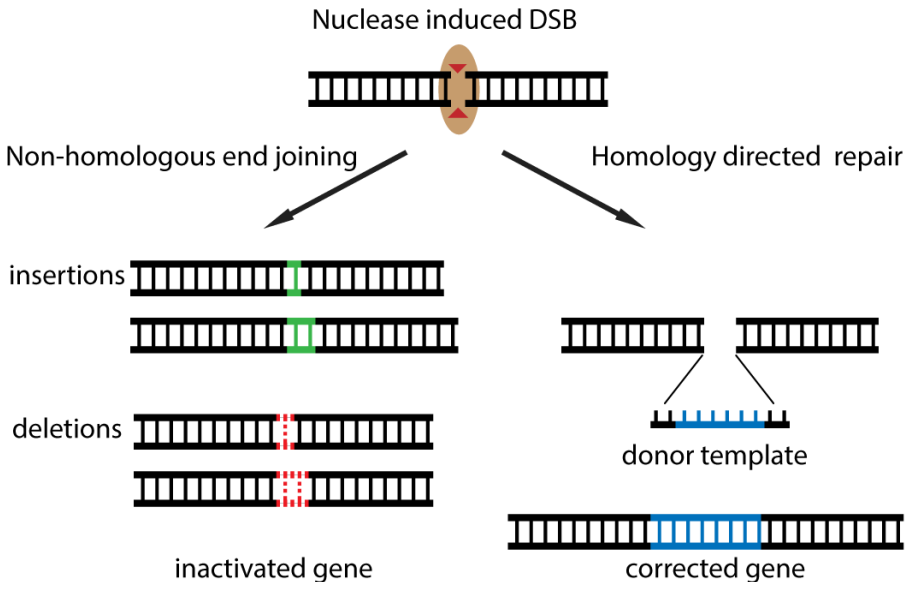

Figure 7.2 | Two different repair mechanisms of a double stranded break
After the targeted nuclease has created a double stranded break, there are two possible repair pathways. The first is the error-prone non-homologous end joining (NHEJ) which results in insertions or deletions (indels) in the gene, often creating a frameshift and thereby inactivating the gene. The second pathway is homology directed repair (HDR) which only takes place in the presence of a homologue part of DNA. When such a donor or repair template is co-administered, this can be used to replace or correct the gene.

localization sequence (NLS) when applied in eukaryotes. Alternatively, the enzyme can be expressed from an mRNA for more transient expression. In the more complex situation where a gene is replaced, a DNA template has to be co-delivered to replace the excised gene. Examples of these therapeutic applications will be discussed in the following paragraphs.

3. Biomedical applications of the CRISPR-Cas9 system

There is a huge number of applications in a wide variety of research fields and various organisms. This review will be limited to applications in mammals/mammalian cells that could be of use in the biomedical field. The large majority of publications utilizes a NHEJ strategy to induce knock-outs of the target gene or gain-of-function mutations in the target gene. However, the number of reports of successfully replaced genes with HDR is also growing.
Since the first report of the prokaryotic CRISPR-Cas9 system being programmable to cut isolated DNA at a desired location [1] it has literally been a race to adapt the system for use in human cells with publications from four independent groups coming out almost back-to-back [8,33–35]. Jennifer Doudna and Emmanuelle Charpentier (University of California, Berkeley and that time at Umeå University, respectively) [1] and Feng Zhang from the Broad Institute and Massachusetts Institute of Technology, Cambridge are generally regarded as the front-runners of adapting this technology [36].

Unfortunately, there is an on-going dispute about the intellectual property, which is unusual as academic institutions normally come to an agreement to share the rights to the invention in such cases. This demonstrates that all players realize how big the impact of CRISPR-Cas9 applications could be and frankly, how much money could be made off of those [37]. In the mean-time however, the Zhang lab has reported on another Type II CRISPR effector called Cpf1 [38] which could cause the patent battle to settle down, now that it has become clear that there can be alternative systems to achieve the same goal. The Cpf1 system may even have some slight advantages over the Cas9 system when it comes to gene replacement, as will be discussed briefly in the section on improvements to the system later.

3.1 Genetic knock-out animals

The first biomedical application of the CRISPR-Cas9 system was the generation of genetic knock-out mice and rats by co-injecting Cas9 mRNA and sgRNAs in one-cell stage embryos, again published by different groups very shortly after each other [27,39,40]. Conditional knock-outs could also be generated in mice and rats by integrating a donor template containing a Cre/lox recombination site as well as by a knock-in of an 11kb template, showing that the HDR pathway could also be used for embryo engineering [41–43]. Genetic knock-outs of rabbits [44] and cynomolgous monkeys [45] were also generated by injecting one-cell stage embryos, demonstrating that this approach is feasible in the full range of preclinical animal models.

3.2 Quick genome screening and drug target identification and validation

The emergence of CRISPR-Cas9 has made the generation of knock-out animals for drug screening and target validation a routine procedure. Before, RNA interference has made an important addition to this, but gene silencing using short-hairpin RNAs (shRNAs) has several drawbacks. First of all, gene silencing based on mRNA degradation is transient. In addition, it often results in only a partial knock-down of the intended target [46]. Apart from that, it turned out there is significant off-target effect due to extensive modulation of micro-RNAs [47], although admittedly, CRISPR-Cas9 in its original form is not completely free of off-target effects either. However, the ease of applicability and low costs of the CRISPR-Cas9 has removed many of the barriers to high-throughput knock-out screens for gene function [46]. Targeted endonucleases can now be expressed by lentiviruses encoding Cas9 and a genome wide array of sgRNAs [48,49]. This approach was validated by screening for resistance to lethal doses of the nucleotide analog 6-thioguanine and etoposide, and the sgRNA screen correctly identified all known genes resulting in resistance. Furthermore, through a negative selection screening, other gene sets involved in fundamental processes could be identified [48]. A similar screening against BRAF inhibitor vemurafenib led to the correct identification of all known genes involved in resistance mechanisms to that drug as well as some novel hits [49]. This Cas9-based screen was repeated with a comparable library of shRNAs and interestingly, only a fraction of the shRNAs appeared to hit the Cas9 targets, demonstrating the superiority of the CRISPR-based screening approach [49]. For a more complete overview on genome-scale knock-out screening using CRISPR-Cas9, see reviews [28,46,50].

3.3 Human embryo editing and high off-target effects

A logical follow-up to the animal embryo knock-out experiments was the editing of genes in human embryos, but ethical issues prohibit the use of normal embryos for such studies. Alternatively, tripronuclear (3PN) zygotes were used, that contain one oocyte nucleus and two sperm nuclei. These polyspermic zygotes are common byproducts of in vitro fertilization and are normally discarded in clinics because they are nonviable in vivo but do form blastocysts in vitro. In these zygotes, the β-subunit of the human β-globin (HBB) gene that is mutated in **β**-thalassemia, was cut by the CRISPR-Cas9 enzyme and a sgRNA. A replacing donor template was successfully integrated in approximately 15% of all cases, but also Homology Directed Repair with a very similar and closely located gene, HBD (delta-subunit of β-globin) was seen in 25% of the cases. Apart from that, there was a high degree of off-target cleavage and the authors concluded that the CRISPR-Cas9 system has to be improved significantly before embryo editing can be applied in a clinical setting [51]. It may have to do with the controversy around this subject [52], but it is striking how critical the authors are on these results, while such high off-target cleavage and low HDR efficiency are also seen in other studies and are a well-known limitation of the current system [53,54].

Initial reports found that a single mismatch between the sgRNA and the target DNA abolished nuclease mediated cleavage [8]. This indicated that the system is highly specific and that one mismatch would lead to inactivation of the nuclease but this turned out to be highly dependent on the position in the sgRNA and on the target sequence. A more systematic investigation revealed that multiple mismatches are tolerated, at different positions depending on the sequence, the number, position and distribution [54]. Mismatches are better tolerated when they are located at the 5' end of the sgRNA (that is, further away from the PAM sequence at the 3', where hybridization with the target DNA is initiated). Off-target sites with as many as five mismatches were identified that were mutagenized to a comparable extent as the intended target site [53,54]. Apart from that, indel frequency at the target site is not 100% and therefore not even every cut at the intended site leads to a gene inactivating frameshift by NHEJ. This was also seen in all the experiments with the embryos. In a later stage, the embryos were 'mosaiced', indicating that cleavage in the multi-cell stages occurred with varying frequencies and efficiencies in daughter cells. Of course, in the case of the knock-out animals, several rounds of selection and crossbreeding will follow [43] but the need to select successfully engineered cells hampers the direct application of the CRISPR-Cas9 system in human patients (Figure 7.3). It is impossible to say right now what an acceptable off-target cleavage rate is, because it is not known to which degree the specificity can be further optimized. Significant progress has already been made, but one could argue that it has to be 0% if it ever is to be safely applied in humans[7]. Therefore, many of the current therapeutic applications aim to engineer the target cells ex-vivo, thereby also avoiding the recurring delivery problem.

3.4 Ex-vivo modifications of T-cells

A cell type that is particularly suitable for ex-vivo engineering is the T-lymphocyte, because it can be easily harvested from the patient's blood, modified and expanded

outside the body and then re-administered without any immunogenicity (Figure 7.3B). This could give the immune system a boost in conditions where the body's defense mechanism is compromised such as in HIV-infection or cancer [55].

A recombinant Cas9 enzyme was pre-incubated with a sgRNA targeting CXCR4, a co-receptor for HIV entry and then electroporated into isolated human CD4+ T-cells. This resulted in knock-out of CXCR4 in ~40% of the cells, which could be sorted and enriched based on CXCR4 expression [56]. Other studies confirmed that editing of CCR5 (another HIV co-receptor) with a Zinc Finger Nuclease is safe and reduces viral DNA in HIV-infected patients [57]. In the same CRISPR-Cas study, the cell surface receptor PD-1 (PDCD1 gene) was also targeted. PD-1 is a so-called "immune check-point" that inhibits the cancer cell killing signaling in exhausted or chronically activated T-cells, and blocking the PD-1 protein has made a dramatic improvement in cancer immunotherapy. It was shown that by electroporating Cas9/PD-1 sgRNA and a HDR repair template into CD4+ cells, a gene replacement was induced in ~20% of the cells. Note, in this study a defective repair template was used to inactivate the PD-1 gene. This is not necessary as it was shown in the same study (and another [58]) that a knock-out could be generated by NHEJ as well, but this shows that ex-vivo gene replacement is also possible using the CRISPR-Cas9 system which could have potential benefit in other applications.

For example, another approach of cancer immunotherapy is endowing T-cells with a chimeric antigen receptor (CAR), usually consisting of the single-chain variable fragment (scFv) from a monoclonal antibody and a co-stimulatory signaling domain. This has the theoretical advantage that a broad repertoire of receptors with high affinity can be used, that these are applicable in every patient, and that there is minimal risk of graft-to-host immunity because the patient's own cells are used [59]. CAR T-cells are currently being evaluated in the clinic [60] and an "off-the-shelf" approach for T-cell receptor engineering was recently described using TALEN nucleases [61]. For many gene editing applications, the way has been paved by other programmable nucleases like ZFN and TALEN and it is likely that because of the low costs and tailorability, also CRISPR-Cas based applications will emerge.

3.5 In vivo applications

In vivo application of CRISPR-Cas9 is conceivable for indications where the current low efficacy of gene editing is sufficient to show a phenotypic- and most importantly- a clinical effect. One such example is the knock-out of Proprotein convertase subtilisin/kexin type 9 (PCSK9), involved in the Low Density Lipoprotein (LDL) clearance pathway. It was found that rare individuals that have an inactivating mutation in the PCSK9 gene not only have extremely low plasma LDL levels, but also appear to be protected against cardiovascular heart disease. Surprisingly, this knock-out did not lead to any apparent other symptoms or adverse events, making it an attractive drug target [62]. Clinical trials with PCSK9 targeting siRNA lipid nanoparticles are currently ongoing, as the protein is predominantly expressed in the liver, making it a suitable target for treatment with nanoparticles [63]. PCSK9 knock-out by adeno-associated virus-delivered CRISPR-Cas was demonstrated in mice, showing mutagenesis in ~50% of hepatocytes which resulted in decreased plasma PCSK9 levels, increased LDL receptor

levels, and a 35-40% decrease in plasma cholesterol levels [64]. This study demonstrates that for certain indications, it is not essential to reach all cells, nor effectively edit all of them to show an effect, making the current incomplete targeting not necessarily an obstacle (Figure 7.3C).

In fact, much lower editing efficiency was shown to still be clinically relevant. In a mouse model of hereditary tyrosinemia type I (HTI), the underlying Fah gene was corrected in the liver by hydrodynamic injection of CRISPR-Cas plasmid and a HDR repair template. This resulted in the initial expression of the wild-type Fah protein in ~1/250 cells (0.4%) but this was enough to rescue the bodyweight-loss phenotype [30]. In this particular disease, it was shown that correction of 1/10.000 hepatocytes could already reverse the disease progression, suggesting that there could be many other indications that could benefit from even such low gene editing frequencies [65]. Furthermore, it appeared that there is positive selection for the edited cells, as after 30 days, ~33% of all hepatocytes in the treated mice were expressing the corrected protein [30]. This is explained by the fact that hepatocytes that are deficient for the Fah gene are poisoned by toxic metabolites, allowing selective outgrowth of the corrected, resistant, cells.

A similar phenomenon was seen in the muscle cells of mice in a Duchenne's muscular dystrophy (DMD) model in which the defective dystrophin gene was corrected. Previously, correction of the dystrophin gene by HDR in mouse embryos was shown [66]. But as germline editing in humans is currently not feasible [52] and the homology directed repair pathway is not active in postmitotic tissues such as heart and skeletal muscle a NHEJ strategy had to be applied in adult mice. In two back-to-back papers, an AAV-CRISPR-Cas mediated excision of the defective dystrophin exon 23 was reported, which skips the premature stop-codon and restores the reading frame. (Indeed, this results in a shorter version of the dystrophin protein, but one that is more active than the one expressed in DMD patients). The approach described here is similar to the one currently being evaluated with "exon-skipping" anti-sense oligonucleotides. The advantage of this approach is that a similar construct could be designed for any other mutation underlying DMD, which also holds true for the sgRNA used in CRISPR-Cas studies [67]. Also in these studies, outgrow of successfully modified cells was seen, indicating that positive selection may occur on the healthier cells [68,69].
However, although the low efficiency of gene editing is not necessarily a problem, the in vivo delivery remains a challenge. In the following paragraph, the delivery methods of the current successes are described and suggestions for future applications are made.

4. Towards delivery systems for in vivo applications

In principle, utilization of the CRISPR-Cas system is as simple –or difficult- as delivering one plasmid. This plasmid should then encode the (codon optimized and NLS-tagged) Cas9 enzyme and one or more sgRNA(s). When the aim is to replace a gene, a repair template also has to be delivered or co-expressed, but this does not complicate the delivery strategy very much. What does complicate the delivery is when the gene editing is supposed to happen in vivo. In this regard, CRISPR-Cas is very similar to RNAi and more sophisticated delivery systems are required to translate achievements in the

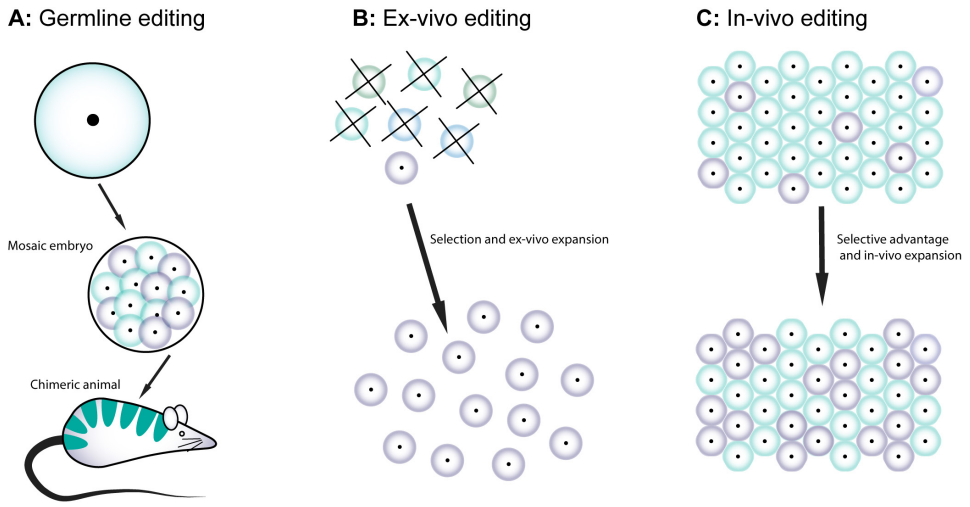

Figure 7.3 | Applications of CRISPR-Cas9 and effects of incomplete gene editing
A: CRISPR-Cas9 is injected into embryos in the one-cell stage, editing occurs after multiple rounds of cell division. Because not every cell is edited, this results in a mosaic embryo. The resulting pups can be selected and crossbred until a full transgenic animal is obtained.
B: When cells are edited ex-vivo, this also results in a heterogeneous population of cells, but here the successfully edited cells can be selected and expanded before being re-administered to the patient.
C: Until the editing efficiency is improved, in-vivo application of CRISPR-Cas9 will also result in only a partially modified population of cells. In indications where edited cells are fitter than the diseased cells, the edited cells can outgrow the diseased cells, creating 'islands' of healthy cells.

lab to the clinic. Granted, the development of RNAi therapeutics is in a much more mature stage now, but at the same time it illustrates what a lengthy process clinical translation can be if the delivery technology is missing [70].

4.1 Ex-vivo delivery technology

Early development of the CRISPR-Cas system and most of the current applications use established methods for gene delivery, including lipofection [31], microinjection [43,71] and electroporation [72,73]. However, plasmids have to be delivered to the nucleus, which is known to be a challenge in non-dividing cells. Another potential drawback of plasmid delivery is the random integration of (part of) the plasmid in the genome causing stable expression and potentially (unwanted) mutagenesis. Furthermore, prolonged expression of a targeted nuclease (in this case a ZFN) was shown to result in more off-target effects [74]. Therefore, more recent studies aim for a fine-tuned, more transient expression by administering mRNA instead of a plasmid or by administering the Cas9/sgRNA complex directly. (See Figure 7.1B) When an in vitro transcribed sgRNA was combined with a purified Cas9 and then electroporated into the cell, the intended genome editing occurred quickly after delivery while the nuclease was already largely degraded after 12 hours [75]. Apart from minimizing off-target effects, delivery of the nuclease or mRNA instead of a plasmid also avoids the nuclear barrier.

Two innovative strategies for ex-vivo delivery without polymers or lipids are iTOP and mechanical cell deformation. The iTOP method, short for induced transduction by osmocytosis and propanebetaine, uses a buffer composition that combines NaCl hypertonicity-induced macropinocytosis and a small-molecule transduction compound (propanebetaine) to transduce extracellular macromolecules into cells. Using this method, the Cas9 enzyme and a sgRNA were successfully delivered to a variety of cell types, with a higher indel frequency and less toxicity than cationic lipids [76]. The other method uses microfluidic devices with a diameter slightly smaller than the cells that temporarily deform the membrane and create transient membrane disruptions that facilitate passive diffusion of material into the cytosol. With this method, small single stranded DNAs, siRNAs, and plasmids encoding CRISPR-Cas9 and a sgRNA could be delivered to a wide variety of cell-types [77]. Unfortunately, as yet neither of these delivery techniques are suitable for in vivo delivery so more advanced delivery systems need to be developed. When designing delivery systems for CRISPR-Cas, many of the "old" challenges need to be faced again. The questions of using viral or non-viral vectors, the ideal surface charge, how to overcome the nuclear barrier and how to reach the desired target tissue are still very relevant for CRISPR-Cas delivery. In the paragraphs below, some more advanced delivery systems are discussed that could potentially also be applied in vivo.

4.2 In-vivo delivery systems

A study by Ramakrishna et al. demonstrated that the Cas9 nuclease and the sgRNA could also be delivered using cell penetrating peptides (CPPs) [78]. In this work, a nona-arginine based (R9) CPP was conjugated to Cas9 on a C-terminally introduced cysteine after expression and the sgRNA was complexed with a similar CPP. The sgRNA/CPP complex resulted in 300-400nm particles with a net positive charge. When the Cas9-CPP and sgRNA-CPP were administered simultaneously, gene editing could be observed at the target site, albeit with low frequency (<15% after three rounds of treatment). Because the sgRNA is loaded into the Cas9 enzyme, it was tested whether the sgRNA/Cas9-CPP complex could facilitate cellular entry to both, but this was not the case. Possibly, the negatively charged sgRNA neutralizes the positive charge of the CPP, which also blocks the entry of the enzyme into the cell [78]. This makes the application of this system in vivo less likely, because the individual components need to be delivered to the same cell simultaneously, which is a significant challenge. Furthermore, the relatively large and highly cationic sgRNA/CPP complexes will probably not have very favorable circulation kinetics or biodistribution.

Another innovative approach that does deliver the enzyme and the sgRNA together, is the use of DNA nanoclews[79]. DNA nanoclews are nanoparticles based on a cage of DNA that is made by rolling circle amplification. By using structural homology to the sgRNA, the complex of the Cas enzyme and the sgRNA could in turn be complexed to the DNA cage. This was then coated with PEI to give the particle a positive charge for uptake and to enhance endosomal escape [79]. Consequently, this makes it less likely that this particle will be adaptable for delivery in vivo given the high toxicity of unmodified PEI.

Therefore, despite the widespread search for non-viral delivery systems, so far almost all in vivo success with CRISPR-Cas was achieved using viral vectors. The most widely applied vectors are Adeno Associated Vectors (AAV) because of their broad range of serotype specificity and low immunogenicity. Given the large number of targets in the liver that have already been validated for RNAi therapy, AAV8 seems to be a suitable vector for in vivo applications of CRISPR-Cas at this moment [65]. Looking at other RNAi indications, there also seems to be a large interest in targeting the dystrophin gene in DMD. Dystrophin correction by CRISPR-Cas was already shown to be feasible and for this indication, AAV9 is a suitable vector as it provides robust expression in the major tissues affected in DMD, such as skeletal muscle, heart, and brain [66,68,69]. However, the low packaging capacity of AAV (~4.5 kb) is hardly sufficient for the packaging of the commonly used *Streptococcus pyogenes* Cas9 (SpyCas9) and a sgRNA (together ~4.2 kb) leaving no room for a DNA repair template or additional sgRNAs [80]. This can be solved by incorporating the Cas9 gene and the sgRNA in separate vectors [81] but this still requires the delivery of both viruses to the same target cell which may be challenging in vivo. Similarly, a split-intein Cas9 was developed that could be divided over two AAV cassettes and naturally joined after each part of the protein was expressed in the cell. This provides additional space for regulatory elements like tissue-specific promoters and multiple sgRNAs in each of the vectors but unfortunately at the cost of splicing efficiency (<35% compared to wildtype SpyCas9) [82]. A rationally designed truncated version of SpyCas9 also lost ~50% activity compared to wild-type [83]. As an alternative, the group of Feng Zhang identified different orthologs of Cas9 and found a ~1 kb shorter, but equally active Cas9 in *Staphylococcus aureus*. They packaged this SaCas9 into the hepatocyte-tropic AAV serotype 8 vector and successfully demonstrated 40% knock-down of ApoB and PCSK9 in the liver (enough to show clinically relevant effect) [80].

Promising as this improvement is, it still does not leave enough room for a DNA repair template if the therapeutic indication requires gene replacement. Furthermore, off-target mutagenesis caused by prolonged expression of the nuclease is still a risk when adenoviruses are used. To tackle both problems, a non-viral second vector was used for the delivery of Cas9 mRNA alongside a viral vector expressing the sgRNA and a HDR repair template [84]. Mice were first treated with a single dose of AAV8, which resulted in sgRNA expression after 3 days, but tenfold higher expression after 7 and 14 days. This pronounced sustained expression really demonstrates why expression of the nuclease from such a vector could cause a potential risk of mutagenesis. To maximize co-expression, a single dose of mRNA formulated in a lipid nanoparticle (LNP) containing the lipid-like material C12-200 was administered intravenously at day 7. This delivery vehicle was previously used for siRNA delivery and just like the AAV8 vector, this type of LNP is known to predominantly target hepatocytes [85]. Initial gene correction was >6%, far more than the previously achieved 0.4% after hydrodynamic injection by the same group [30]. As a result, treatment completely rescued disease symptoms and successful homology directed repair was confirmed by deep sequencing [84].

Seeing that CRISPR-Cas therapeutics are more or less following the same path as RNAi therapeutics, it is expected that in short order, CRISPR-Cas will also completely transit to non-viral delivery systems. The demonstration that the LNPs that are in clinical

evaluation for siRNA delivery are also capable of delivering CRISPR-Cas constructs is a clear indication that this transition is feasible in the near future. The fact that many metabolic diseases could be clinically reversed by restoring roughly 5% of protein expression in hepatocytes shows that the low efficiency of gene editing does not restrain therapeutic use [9].

5. Improvements on the system

Throughout this review, it has been mentioned a couple of times that not the low editing efficiency, but rather the high off-target effect of the CRISPR-Cas system could limit its application in patients. This has so far not been discussed because many improvements have already been made and it is the general opinion of the community that this will not be an issue in the long term [52]. In this section, some of these improvements will be highlighted.

The earliest attempt to minimize off-target cleavage was the use of double nickases. Already in the first applications of CRISPR-Cas9 in eukaryotes, it was described that the nuclease could be converted into a targeted nickase [1]. By making a small mutation in one of the two catalytic domains (HNH and RuvC), Cas9 would cleave only one of the two strands (Cas9n, for 'Cas9 nickase'). Two almost simultaneous reports described the use of two of such targeted nickases by expressing Cas9n and two sgRNAs each targeting the same target site, but on opposite strands. This way, only a double stranded break is created when both nickases cut on-target. Off-target single nicks are not repaired by the NHEJ-pathway but by base excision repair pathways where no insertions or deletions are formed. This paired nicking approach reduced off-target activity by 50- to 1,500-fold without sacrificing on-target cleavage efficiency [86,87].

However, this approach could become technically challenging in multiplex or genome-wide library based applications. By carefully looking at the 'design rules' of sgRNAs, it was found that by shortening the sgRNAs from 20 nucleotides to 17-19 nucleotides, on-target efficiency could be significantly improved whilst minimizing off-target cleavage. This may sound counterintuitive, but it was found that the 5' end of sgRNAs was less important for target recognition and that mismatches at that side were tolerated to a much larger extent [53]. Possibly, the nucleotides furthest away from the PAM sequence at the 3' side compensate for mismatches elsewhere in the sequence, which would mean that shorter sgRNAs are more sensitive to mismatches and thus more specific. To test this hypothesis, a series of sgRNAs targeting the same site was designed, containing 15, 17, 19 or 20 complementary nucleotides. The 15 nucleotide sgRNA was found to be too short to induce cleavage, but the 17 and 19 nucleotide sgRNAs induced similar target site cleavage as the full length sgRNA but with more than 5000 times reduced off-target effects. These truncated sgRNAs (tru-gRNAs) could also be combined with the paired nickase approach to even further reduce off-target cleavage [88].

When crystal structures of the SpyCas9-sgRNA complex became available, it was hypothesized that it possesses more energy than is needed to recognize its target DNA strand. Several residues in the SpyCas9 were identified that interact aspecifically with

the target DNA. These were systematically substituted to study their contribution to off-target effects. The groups of Feng Zhang and Keith Joung each produced a couple of mutants, coined eSpCas9 ("enhanced specificity") and SpCas9-HF1 ("high fidelity") respectively, that had a significant reduction in off-target effects, without abolishing on target efficacy [89,90]. Structure-based engineering of the Cas9 enzyme has led to spectacular improvements in on-target efficiency but notably, the SpCas9-HF1 and eSpCas9 each contain different mutations. So in theory, these could potentially be combined for even further improvement.

The aforementioned examples illustrate how easily the CRISPR-Cas9 system can be tailored and adapted and there is little doubt that the specificity and efficiency will be further improved. Another "improvement" however, is the transition to another enzyme than Cas9, called Cpf1, by the groups of Feng Zhang, Koonin and Van der Oost. This class 2 CRISPR-associated enzyme was recently discovered in multiple strains of *Prevotella* and *Francisella* (hence the name, CRISPR from *Prevotella* and *Francisella* 1), and out of 16 Cpf1 orthologs, two enzymes with efficient genome-editing activity in human cells were identified. Cpf1 differs from Cas9 in three ways. First, it utilizes a T-rich protospacer adjacent motif preceding the target gene, instead of a G-rich PAM following the target DNA; since such motifs are equally abundant, this is not really an advantage over the other system. Secondly, rather than using a tracrRNA and an RNaseIII-like ribonuclease to process the precursor crRNA to a mature guide, Cpf1 protein itself includes the RNA cleavage site [91,92]. This has practical advantage that multiplex targeting can be done by a synthetic CRISPR array controlled by a single promoter [92]. The third difference is that Cpf1 cleaves the DNA via a staggered double stranded break, creating overhangs that potentially make gene replacement more efficient. The CRISPR-Cpf1 system is still in the development stage, but now that more therapeutic Cas9 gene-knockdown applications are emerging, this could accelerate the development of the elusive gene-replacement applications as well. Moreover, more class 2 CRISPR-associated nucleases are being discovered [93,13].

6. Conclusion

In a timeframe of only 3 years, CRISPR-Cas9, -originally a bacterial defense system that recognizes foreign DNA sequences and selectively cleaves them- has been repurposed to a targeted nuclease that can inactivate diseased genes or potentially even restore them. What sets CRISPR-based systems (Cas9, Cpf1, and others (reviewed by Mohanraju et al. [92])) apart from other targeted nucleases such as ZFN, TALEN and Meganucleases is the ease of application and tailorability, as only the Cas9/Cpf1 enzyme has to be expressed, that can be retargeted by simply changing the guide RNA sequence. There are many similarities between CRISPR-Cas and RNA interference. To start with, the ability to knock-out a gene, but then on the genomic DNA level rather than to knock it down at transcript RNA level. Furthermore, CRISPR-Cas9 has already found many applications as a biotechnological tool, and the development of therapeutic applications is already well under way. In doing so, companies should take caution not to fall into the same traps as with RNAi therapeutics development. Although the potential is huge, overcoming the delivery barrier remains crucial to achieve clinical success. Here, many lessons can be learned from the RNAi field, as it was already

shown that the same delivery tech could also deliver CRISPR-Cas9 constructs [84]. With regard to applications, it has been questioned whether RNAi and CRISPR-Cas could co-exist, as CRISPR-Cas offers a permanent solution to problems that RNAi can only address transiently. However, with regard to delivery, the RNAi field is years ahead of CRISPR-Cas and application of CRISPR-Cas in human subjects seems more challenging. Therefore, for applications like targeting the PCSK9 gene to lower plasma cholesterol levels, it is not unthinkable that RNAi therapeutics make it to the market first and are then gradually phased out when CRISPR-Cas therapeutics become a reality [70].

Until then, work has to be done on further improving the specificity and reducing the off-target effects of CRISPR-Cas systems. At this point, gene editing in cells ex-vivo seems most feasible, because it overcomes both the delivery hurdle as well as the imperfect specificity (because successfully edited cells can be selected). Furthermore, complete gene replacement via the homology directed repair pathway has not been very efficient so far and seems further away from clinical application than gene knock-out, especially in vivo. But with the number of labs working on this technology, the amount of money that has been raised by companies wishing to bring this to the clinic, and the vast amount of therapeutic applications that lie on the horizon, it seems just a matter of time before these challenges are overcome. With existing knowledge and a focus on delivery technology, CRISPR-Cas based therapeutics could be developed faster than their RNAi counterparts, allowing safe and efficient gene editing in human patients in the near future.

References

[1] M. Jinek, K. Chylinski, I. Fonfara, M. Hauer, J.A. Doudna, E. Charpentier, A Programmable Dual-RNA – Guided, Science. 337 (2012) 816–822. doi:10.1126/science.1225829.

[2] J.E. Garneau, M.-È. Dupuis, M. Villion, D. a Romero, R. Barrangou, P. Boyaval, et al., The CRISPR/Cas bacterial immune system cleaves bacteriophage and plasmid DNA., Nature. 468 (2010) 67–71. doi:10.1038/nature09523.

[3] J.S. Modica-Napolitano, J.R. Aprille, Delocalized lipophilic cations selectively target the mitochondria of carcinoma cells, Adv. Drug Deliv. Rev. 49 (2001) 63–70. doi:10.1016/S0169-409X(01)00125-9.

[4] E. Deltcheva, K. Chylinski, C.M. Sharma, K. Gonzales, Y. Chao, Z.A. Pirzada, et al., CRISPR RNA maturation by trans-encoded small RNA and host factor RNase III, Nature. 471 (2011) 602–607. doi:10.1038/nature09886.

[5] A. Chaparro-Garcia, S. Kamoun, V. Nekrasov, Boosting plant immunity with CRISPR/Cas., Genome Biol. 16 (2015) 254. doi:10.1186/s13059-015-0829-4.

[6] R. Kaminski, Y. Chen, T. Fischer, E. Tedaldi, A. Napoli, Y. Zhang, et al., Elimination of HIV-1 Genomes from Human T-lymphoid Cells by CRISPR/Cas9 Gene Editing, Sci. Rep. 6 (2016) 22555. doi:10.1038/srep22555.

[7] B.J. Travis, Germline Editing Dominates DNA Summit, Science (80-.). 350 (2015) 1299–1300. doi:10.1126/science.350.6266.1299.

[8] L. Cong, F.A. Ran, D. Cox, S. Lin, R. Barretto, N. Habib, et al., Multiplex Genome Engineering Using CRISPR/Cas Systems, Science (80-.). 339 (2013) 819–823. doi:10.1126/science.1231143.

[9] D.B.T. Cox, R.J. Platt, F. Zhang, Therapeutic genome editing: prospects and challenges, Nat. Med. 21 (2015) 121–131. doi:10.1038/nm.3793.

[10] J. Travis, Making the cut, Science (80-.). 350 (2015) 1456–1457. doi:10.1126/science.350.6267.1456.

[11] A. Fire, S. Xu, M.K. Montgomery, S.A. Kostas, S.E. Driver, C.C. Mello, Potent and specific genetic interference by double-stranded RNA in Caenorhabditis elegans., Nature. 391 (1998) 806–11. doi:10.1038/35888.

[12] K.S. Makarova, Y.I. Wolf, O.S. Alkhnbashi, F. Costa, S.A. Shah, S.J. Saunders, et al., An updated evolutionary classification of CRISPR-Cas systems., Nat. Rev. Microbiol. 13 (2015) 722–736. doi:10.1038/nrmicro3569.

[13] P. Mohanraju, K.S. Makarova, B. Zetsche, F. Zhang, E.V. Koonin, J. Van der Oost, Diverse evolutionary roots and mechanistic variations of the CRISPR-Cas systems, Science (80-.). (2016).

[14] D. Haussecker, The Business of RNAi Therapeutics in 2012, Mol. Ther. — Nucleic Acids. 1 (2012) e8. doi:10.1038/mtna.2011.9.

[15] D. Haussecker, Current issues of RNAi therapeutics delivery and development, J. Control. Release. 195 (2014) 49–54. doi:10.1016/j.jconrel.2014.07.056.

[16] G. Silva, L. Poirot, R. Galetto, J. Smith, G. Montoya, P. Duchateau, et al., Meganucleases and other tools for targeted genome engineering: perspectives and challenges for gene therapy., Curr. Gene Ther. 11 (2011) 11–27. doi:10.2174/156652311794520111.

[17] J.K. Joung, J.D. Sander, TALENs: a widely applicable technology for targeted genome editing, Nat Rev Mol Cell Biol. 14 (2013) 49–55. doi:10.1038/nrm3486.

[18] F.D. Urnov, E.J. Rebar, M.C. Holmes, H.S. Zhang, P.D. Gregory, Genome editing with engineered zinc finger nucleases, Nat Rev Genet. 11 (2010) 636–646. doi:10.1038/nrg2842.

[19] T. Gaj, C.A. Gersbach, C.F. Barbas, ZFN, TALEN, and CRISPR/Cas-based methods for genome engineering, Trends Biotechnol. 31 (2013) 397–405. doi:10.1016/j.tibtech.2013.04.004.

[20] B. Wiedenheft, S.H. Sternberg, J. A. Doudna, RNA-guided genetic silencing systems in bacteria and archaea, Nature. 482 (2012) 331–338. doi:10.1038/nature10886.

[21] J. van der Oost, E.R. Westra, R.N. Jackson, B. Wiedenheft, Unravelling the structural and mechanistic basis of CRISPR-Cas systems., Nat. Rev. Microbiol. 12 (2014) 479–92. doi:10.1038/nrmicro3279.

[22] I. Mougiakos, E.F. Bosma, W.M. de Vos, R. van Kranenburg, J. van der Oost, Next Generation Prokaryotic Engineering: The CRISPR-Cas Toolkit, Trends Biotechnol. xx (2016) 1–13. doi:10.1016/j.tibtech.2016.02.004.

[23] A. V Wright, J.K. Nunez, J.A. Doudna, Review Biology and Applications of CRISPR Systems: Harnessing Nature's Toolbox for Genome Engineering, Cell. 164 (2016) 29–44. doi:10.1016/j.cell.2015.12.035.

[24] J. van der Oost, M.M. Jore, E.R. Westra, M. Lundgren, S.J.J. Brouns, CRISPR-based adaptive and heritable immunity in prokaryotes, Trends Biochem. Sci. 34 (2009) 401–407. doi:10.1016/j.tibs.2009.05.002.

[25] L.A. Marraffini, E.J. Sontheimer, Self versus non-self discrimination during CRISPR RNA-directed immunity., Nature. 463 (2010) 568–71. doi:10.1038/nature08703.

[26] F.J.M. Mojica, C. Díez-Villaseñor, J. García-Martínez, C. Almendros, Short motif sequences determine the targets of the prokaryotic CRISPR defence system, Microbiology. 155 (2009) 733–740. doi:10.1099/mic.0.023960-0.

[27] B. Shen, J. Zhang, H. Wu, J. Wang, K. Ma, Z. Li, et al., Generation of gene-modified mice via Cas9/RNA-mediated gene targeting., Cell Res. 23 (2013) 720–3. doi:10.1038/cr.2013.46.

[28] O. Shalem, N.E. Sanjana, F. Zhang, High-throughput functional genomics using CRISPR-Cas9., Nat. Rev. Genet. 16 (2015) 299–311. doi:10.1038/nrg3899.

[29] P.D. Hsu, E.S. Lander, F. Zhang, Development and applications of CRISPR-Cas9 for genome engineering, Cell. 157 (2014) 1262–1278. doi:10.1016/j.cell.2014.05.010.

[30] H. Yin, W. Xue, S. Chen, R.L. Bogorad, E. Benedetti, M. Grompe, et al., Genome editing with Cas9 in adult mice corrects a disease mutation and phenotype., Nat. Biotechnol. 32 (2014) 551–3. doi:10.1038/nbt.2884.

[31] J.A. Zuris, D.B. Thompson, Y. Shu, J.P. Guilinger, J.L. Bessen, J.H. Hu, et al., Cationic lipid-mediated delivery of proteins enables efficient protein-based genome editing in vitro and in vivo., Nat. Biotechnol. 33 (2014) 73–80. doi:10.1038/nbt.3081.

[32] H.L. Li, N. Fujimoto, N. Sasakawa, S. Shirai, T. Ohkame, T. Sakuma, et al., Precise correction of the dystrophin gene in duchenne muscular dystrophy patient induced pluripotent stem cells by TALEN and CRISPR-Cas9, Stem Cell Reports. 4 (2015) 143–154. doi:10.1016/j.stemcr.2014.10.013.

[33] P. Mali, L. Yang, K.M. Esvelt, J. Aach, M. Guell, J.E. DiCarlo, et al., RNA-Guided Human Genome Engineering via Cas9, Science (80-.). 339 (2013) 823–826. doi:10.1126/science.1232033.

[34] M. Jinek, A. East, A. Cheng, S. Lin, E. Ma, J. Doudna, RNA-programmed genome editing in human cells, Elife. 2013 (2013) 1–9. doi:10.7554/eLife.00471.

[35] S.W. Cho, S. Kim, J.M. Kim, J.-S. Kim, Targeted genome engineering in human cells with the Cas9 RNA-guided endonuclease., Nat. Biotechnol. 31 (2013) 230–2. doi:10.1038/nbt.2507.

[36] E.S. Lander, The Heroes of CRISPR, Cell. 164 (2016) 18–28. doi:10.1016/j.cell.2015.12.041.

[37] H. Ledford, Bitter fight over CRISPR patent heats up, 821 (2016) 1–5. doi:10.1038/nature.2015.17961.

[38] B. Zetsche, J.S. Gootenberg, O.O. Abudayyeh, I.M. Slaymaker, K.S. Makarova, P. Essletzbichler, et al., Cpf1 Is a Single RNA-Guided Endonuclease of a Class 2 CRISPR-Cas System, Cell. 163 (2015) 759–771. doi:10.1016/j.cell.2015.09.038.

[39] H. Wang, H. Yang, C.S. Shivalila, M.M. Dawlaty, A.W. Cheng, F. Zhang, et al., One-step generation of mice carrying mutations in multiple genes by CRISPR/cas-mediated genome engineering, Cell. 153 (2013) 910–918. doi:10.1016/j.cell.2013.04.025.

[40] W. Li, F. Teng, T. Li, Q. Zhou, Simultaneous generation and germline transmission of multiple gene mutations in rat using CRISPR-Cas systems, Nat. Biotechnol. 31 (2013) 684–686. doi:10.1038/nbt.2652.

[41] H. Yang, H. Wang, C.S. Shivalila, A.W. Cheng, L. Shi, R. Jaenisch, One-Step Generation of Mice Carrying Reporter and Conditional Alleles by CRISPR/Cas-Mediated Genome Engineering, Cell. 154 (2013) 1370–1379. doi:10.1016/j.cell.2013.08.022.

[42] Y. Ma, X. Zhang, B. Shen, Y. Lu, W. Chen, J. Ma, et al., Generating rats with conditional alleles using CRISPR/Cas9., Cell Res. 24 (2014) 122–5. doi:10.1038/cr.2013.157.

[43] V.T. Chu, T. Weber, R. Graf, T. Sommermann, K. Petsch, U. Sack, et al., Efficient generation of Rosa26 knock-in mice using CRISPR/Cas9 in C57BL/6 zygotes, BMC Biotechnol. 16 (2016) 4. doi:10.1186/s12896-016-0234-4.

[44] D. Yang, J. Xu, T. Zhu, J. Fan, L. Lai, J. Zhang, et al., Effective gene targeting in rabbits using RNA-guided Cas9 nucleases, J. Mol. Cell Biol. 6 (2014) 97–99. doi:10.1093/jmcb/mjt047.

[45] Y. Niu, B. Shen, Y. Cui, Y. Chen, J. Wang, L. Wang, et al., Generation of gene-modified cynomolgus monkey via Cas9/RNA-mediated gene targeting in one-cell embryos, Cell. 156 (2014) 836–843. doi:10.1016/j.cell.2014.01.027.

[46] J.D. Moore, The impact of CRISPR-Cas9 on target identification and validation, Drug Discov. Today. 20 (2015) 450–457. doi:10.1016/j.drudis.2014.12.016.

[47] S. Marine, A. Bahl, M. Ferrer, E. Buehler, Common seed analysis to identify off-target effects in siRNA screens., J. Biomol. Screen. 17 (2012) 370–8. doi:10.1177/1087057111427348.

[48] T. Wang, J.J. Wei, D.M. Sabatini, E.S. Lander, Genetic screens in human cells using the CRISPR-Cas9 system., Science. 343 (2014) 80–4. doi:10.1126/science.1246981.

[49] O. Shalem, E.N. Sanjana, E. Hartenian, F. Zhang, Genome-Scale CRISPR-Cas9 Knockout, Science (80-.). 343 (2014) 84–88. doi:10.1038/nbt.2647.

[50] J. Peng, Y. Zhou, S. Zhu, W. Wei, High-throughput screens in mammalian cells using the CRISPR-Cas9 system, FEBS J. 282 (2015) 2089–2096. doi:10.1111/febs.13251.

[51] P. Liang, Y. Xu, X. Zhang, C. Ding, R. Huang, Z. Zhang, et al., CRISPR/Cas9-mediated gene editing in human tripronuclear zygotes, Protein Cell. 6 (2015) 363–372. doi:10.1007/s13238-015-0153-5.

[52] K.S. Bosley, M. Botchan, A.L. Bredenoord, D. Carroll, R.A. Charo, E. Charpentier, et al., CRISPR germline engineering—the community speaks, Nat. Publ. Gr. 33 (2015) 478–486. doi:10.1038/nbt.3227.

[53] Y. Fu, J. A Foden, C. Khayter, M.L. Maeder, D. Reyon, J.K. Joung, et al., High-frequency off-target mutagenesis induced by CRISPR-Cas nucleases in human cells., Nat. Biotechnol. 31 (2013) 822–6. doi:10.1038/nbt.2623.

[54] P.D. Hsu, D.A. Scott, J.A. Weinstein, F.A. Ran, S. Konermann, V. Agarwala, et al., DNA targeting specificity of RNA-guided Cas9 nucleases., Nat. Biotechnol. 31 (2013) 827–32. doi:10.1038/nbt.2647.

[55] D.M. Barrett, S. A Grupp, C.H. June, Chimeric Antigen Receptor- and TCR-Modified T Cells Enter Main Street and Wall Street., J. Immunol. 195 (2015) 755–61. doi:10.4049/jimmunol.1500751.

[56] K. Schumann, S. Lin, E. Boyer, D.R. Simeonov, M. Subramaniam, R.E. Gate, et al., Generation of knock-in primary human T cells using Cas9 ribonucleoproteins, Proc. Natl. Acad. Sci. 112 (2015) 10437–10442. doi:10.1073/pnas.1512503112.

[57] P. Tebas, D. Stein, W.W. Tang, I. Frank, S.Q. Wang, G. Lee, et al., Gene editing of CCR5 in autologous CD4 T cells of persons infected with HIV., N. Engl. J. Med. 370 (2014) 901–10. doi:10.1056/NEJMoa1300662.

[58] S. Su, B. Hu, J. Shao, B. Shen, J. Du, Y. Du, et al., CRISPR-Cas9 mediated efficient PD-1 disruption on human primary T cells from cancer patients, Sci. Rep. 6 (2016) 20070. doi:10.1038/srep20070.

[59] M. V. Maus, D.J. Powell, Chimeric Antigen Receptor T-Cells - New Approaches to Improve Their Efficacy and Reduce Toxicity, Cancer J. 21 (2015) 475–479. doi:10.1097/PPO.0000000000000155.

[60] S.L. Maude, N. Frey, P.A. Shaw, R. Aplenc, D.M. Barrett, N.J. Bunin, et al., Chimeric Antigen Receptor T Cells for Sustained Remissions in Leukemia, N. Engl. J. Med. 371 (2014) 1507–1517. doi:10.1056/NEJMoa1407222.

[61] L.P.B. Philip, C. Schiffer-Mannioui, D. Le Clerre, I. Chion-Sotinel, S. Derniame, P. Potrel, et al., Multiplex genome-edited T-cell manufacturing platform for "off-the-shelf" adoptive T-cell immunotherapies, Cancer Res. 75 (2015) 3853–3864. doi:10.1158/0008-5472.CAN-14-3321.

[62] J.C. Cohen, E. Boerwinkle, T.H. Mosley, H.H. Hobbs, Sequence variations in PCSK9, low LDL, and protection against coronary heart disease., N. Engl. J. Med. 354 (2006) 1264–72. doi:10.1056/NEJMoa054013.

[63] K. Fitzgerald, M. Frank-Kamenetsky, S. Shulga-Morskaya, A. Liebow, B.R. Bettencourt, J.E. Sutherland, et al., Effect of an RNA interference drug on the synthesis of proprotein convertase subtilisin/kexin type 9 (PCSK9) and the concentration of serum LDL cholesterol in healthy volunteers: a randomised, single-blind, placebo-controlled, phase 1 trial., Lancet. 383 (2014) 60–8. doi:10.1016/S0140-6736(13)61914-5.

[64] Q. Ding, A. Strong, K.M. Patel, S.L. Ng, B.S. Gosis, S.N. Regan, et al., Permanent alteration of PCSK9 with in vivo CRISPR-Cas9 genome editing, Circ. Res. 115 (2014) 488–492. doi:10.1161/CIRCRESAHA.115.304351.

[65] N.K. Paulk, K. Wursthorn, Z. Wang, M.J. Finegold, M.A. Kay, M. Grompe, Adeno-associated virus gene repair corrects a mouse model of hereditary tyrosinemia in vivo, Hepatology. 51 (2010) 1200–1208. doi:10.1002/hep.23481.

[66] C. Long, J.R. McAnally, J.M. Shelton, A.A. Mireault, R. Bassel-Duby, E.N. Olson, Prevention of muscular dystrophy in mice by CRISPR/Cas9-mediated editing of germline DNA, Science. 345 (2014) 1184–8. doi:10.1126/science.1254445.

[67] M.C. Miceli, S.F. Nelson, The case for eteplirsen: Paving the way for precision medicine, Mol. Genet. Metab. (2016) 2015–2016. doi:10.1016/j.ymgme.2016.04.001.

[68] C. Long, L. Amoasii, A.A. Mireault, J.R. McAnally, H. Li, E. Sanchez-Ortiz, et al., Postnatal genome editing partially restores dystrophin expression in a mouse model of muscular dystrophy, Science (80-.). 351 (2016) 400–403. doi:10.1126/science.aad5725.

[69] C.E. Nelson, C.H. Hakim, D.G. Ousterout, P.I. Thakore, E.A. Moreb, R.M.C. Rivera, et al., In vivo genome editing improves muscle function in a mouse model of Duchenne muscular dystrophy, Science (80-.). 351 (2016) 403–407. doi:10.1126/science.aad5143.

[70] D. Haussecker, Stacking up CRISPR against RNAi for therapeutic gene inhibition, FEBS J. (2016). doi:10.1111/febs.13742.

[71] R.N. Cottle, C.M. Lee, D. Archer, G. Bao, Controlled delivery of β-globin-targeting TALENs and CRISPR/Cas9 into mammalian cells for genome editing using microinjection, Sci. Rep. 5 (2015) 16031. doi:10.1038/srep16031.

[72] W. Qin, S.L. Dion, P.M. Kutny, Y. Zhang, A.W. Cheng, N.L. Jillette, et al., Efficient CRISPR/Cas9-Mediated Genome Editing in Mice by Zygote Electroporation of Nuclease., Genetics. 200 (2015) 423–30. doi:10.1534/genetics.115.176594.

[73] M. Hashimoto, T. Takemoto, Electroporation enables the efficient mRNA delivery into the mouse zygotes and facilitates CRISPR/Cas9-based genome editing, Sci. Rep. 5 (2015) 11315. doi:10.1038/srep11315.

[74] T. Gaj, J. Guo, Y. Kato, S.J. Sirk, C.F. Barbas, Targeted gene knockout by direct delivery of zinc-finger nuclease proteins, Nat. Methods. 9 (2012) 805–807. doi:10.1038/nmeth.2030.

[75] S. Kim, D. Kim, S.W. Cho, J. Kim, J.-S. Kim, Highly efficient RNA-guided genome editing in human cells via delivery of purified Cas9 ribonucleoproteins, Genome Res. 24 (2014) 1012–1019. doi:10.1101/gr.171322.113.

[76] D.S. D'Astolfo, R.J. Pagliero, A. Pras, W.R. Karthaus, H. Clevers, V. Prasad, et al., Efficient intracellular delivery of native proteins, Cell. 161 (2015) 674–690. doi:10.1016/j.cell.2015.03.028.

[77] X. Han, Z. Liu, M. c. Jo, K. Zhang, Y. Li, Z. Zeng, et al., CRISPR-Cas9 delivery to hard-to-transfect cells via membrane deformation, Sci. Adv. 1 (2015) e1500454–e1500454. doi:10.1126/sciadv.1500454.

[78] S. Ramakrishna, A.-B. Kwaku Dad, J. Beloor, R. Gopalappa, S.-K. Lee, H. Kim, Gene disruption by cell-penetrating peptide-mediated delivery of Cas9 protein and guide RNA, Genome Res. 24 (2014) 1020–1027. doi:10.1101/gr.171264.113.

[79] W. Sun, W. Ji, J.M. Hall, Q. Hu, C. Wang, C.L. Beisel, et al., Self-Assembled DNA Nanoclews for the Efficient Delivery of CRISPR-Cas9 for Genome Editing, Angew. Chemie - Int. Ed. 54 (2015) 12029–12033. doi:10.1002/anie.201506030.

[80] F.A. Ran, L. Cong, W.X. Yan, D. A. Scott, J.S. Gootenberg, A.J. Kriz, et al., In vivo genome editing using Staphylococcus aureus Cas9, Nature. 520 (2015) 186–190. doi:10.1038/nature14299.

[81] N.E. Sanjana, O. Shalem, F. Zhang, Improved vectors and genome-wide libraries for CRISPR screening, Nat. Methods. 11 (2014) 006726. doi:10.1101/006726.

[82] E.J. Fine, C.M. Appleton, D.E. White, M.T. Brown, H. Deshmukh, M.L. Kemp, et al., Trans-spliced Cas9 allows cleavage of HBB and CCR5 genes in human cells using compact expression cassettes., Sci. Rep. 5 (2015) 10777. doi:10.1038/srep10777.

[83] H. Nishimasu, F.A. Ran, P.D. Hsu, S. Konermann, S.I. Shehata, N. Dohmae, et al., Crystal structure of Cas9 in complex with guide RNA and target DNA, Cell. 156 (2014) 935–949. doi:10.1016/j.cell.2014.02.001.

[84] H. Yin, C.-Q. Song, J.R. Dorkin, L.J. Zhu, Y. Li, Q. Wu, et al., Therapeutic genome editing by combined viral and non-viral delivery of CRISPR system components in vivo, Nat. Biotechnol. 34 (2016) 328–333. doi:10.1038/nbt.3471.

[85] K.T. Love, K.P. Mahon, C.G. Levins, K.A. Whitehead, W. Querbes, J.R. Dorkin, et al., Lipid-like materials for low-dose, in vivo gene silencing., Proc. Natl. Acad. Sci. U. S. A. 107 (2010) 1864–9. doi:10.1073/pnas.0910603106.

[86] P. Mali, J. Aach, P.B. Stranges, K.M. Esvelt, M. Moosburner, S. Kosuri, et al., CAS9 transcriptional activators for target specificity screening and paired nickases for cooperative genome engineering., Nat. Biotechnol. 31 (2013) 833–8. doi:10.1038/nbt.2675.

[87] F.A. Ran, P.D. Hsu, C.Y. Lin, J.S. Gootenberg, S. Konermann, A.E. Trevino, et al., Double nicking by RNA-guided CRISPR cas9 for enhanced genome editing specificity, Cell. 154 (2013) 1380–1389. doi:10.1016/j.cell.2013.08.021.

[88] Y. Fu, J.D. Sander, D. Reyon, V.M. Cascio, J.K. Joung, Improving CRISPR-Cas nuclease specificity using truncated guide RNAs, Nat Biotechnol. 32 (2014) 279–284. doi:10.1038/nbt.2808.

[89] I.M. Slaymaker, L. Gao, B. Zetsche, D.A. Scott, W.X. Yan, F. Zhang, Rationally engineered Cas9 nucleases with improved specificity, Science (80-.). 351 (2016) 84–88. doi:10.1126/science.aad5227.

[90] B.P. Kleinstiver, V. Pattanayak, M.S. Prew, S.Q. Tsai, N.T. Nguyen, Z. Zheng, et al., High-fidelity CRISPR–Cas9 nucleases with no detectable genome-wide off-target effects, Nature. 529 (2016) 490–495. doi:10.1038/nature16526.

[91] I. Fonfara, H. Richter, M. Bratovič, A. Le Rhun, E. Charpentier, The CRISPR-associated DNA-cleaving enzyme Cpf1 also processes precursor CRISPR RNA., Nature. (2016) 1–19. doi:10.1038/nature17945.

[92] B. Zetsche, P. Mohanraju, J. Van der Oost, F. Zhang, Multiplex gene editing by CRISPR-Cpf1 through autonomous processing of a single crRNA array., Nat. Biotechnol. (2016).

[93] S. Shmakov, O.O. Abudayyeh, K.S. Makarova, Y.I. Wolf, J.S. Gootenberg, E. Semenova, et al., Discovery and Functional Characterization of Diverse Class 2 CRISPR-Cas Systems, Mol. Cell. 60 (2015) 385–397. doi:10.1016/j.molcel.2015.10.008.

Chapter | 8

Summarizing discussion and perspectives

The slow start of RNA therapeutics development

As of early 2017, it is now 18 years since the discovery of RNA interference with double-stranded RNA by Andrew Fire and Craig Mello [1] and 15 years since the description of RNAi in human cells using the short 21-nucleotide duplexes that we now consider 'conventional' siRNAs [2]. This initiated a scramble of small, risk-prone biotech companies aiming to bring these siRNAs into the clinic in the period of 2002-2005. However, as of today, the first RNA based drug has yet to be admitted to the European market. Back then, leading companies marked their territory by securing IP on the RNA molecules to strengthen their strategic position. In reality, this was merely a way to finance their own R&D department by licensing the technology to other companies who also wanted a piece of the pie, while still figuring out how to deliver these molecules themselves [3]. Patents were filed on applications and design rules of siRNAs [2,4] but none on delivery technology. The wide variety of backbone modifications shown in Figure 1.2 is also a result of different companies each claiming their own piece of land without focusing on the delivery problem. When in 2005-2008 the large pharmaceutical companies like Merck, Novartis and Roche also jumped on the bandwagon, the field of RNA therapeutics gained momentum fast, accelerated even more by the award of the Nobel Prize to Fire and Mello in 2006. It seemed that also the big players were enticed by all the available well-characterized disease targets that were considered 'undruggable' by traditional small molecules before, without worrying about drug delivery. This forced them to make another round of investments to acquire enabling delivery technology, but with the majority of them not living up to the claims and with the expiration of the IP on the molecules looming, Roche decided to completely pull the plug from their RNA therapeutics development platform. Being considered one of the front-runners within Big Pharma, this also led other big companies to decide to withdraw, largely putting their combined investments of 2.5-3B$ to waste [3]. This was followed by a period (2008-2011) where RNA therapeutics were regarded with strong skepticism and RNAi in human patients was considered an elusive goal by some. It is now recognized that the delivery challenge of this new class of therapeutics had been heavily underestimated and that this is the main reason there are still no products on the market, despite considerable efforts. However, from 2011 onwards, the field seems to be recovering, backed by a heavy focus on delivery technology with a strong scientific foundation. Several types of delivery technology have enabled the 'rebirth' of RNA therapeutics, and it seems but a matter of time before the first RNA based product will finally reach the market [3,5].

Three main types of delivery systems have been established and clinically evaluated. Of the GalNAc-conjugates, Dynamic PolyConjugates (DPCs) and stable nucleic acid lipid nanoparticles (SNALPs), the SNALPs are clinically most advanced, with late-stage trials in multiple indications. All these indications are targeting the liver, showing that the promise that any gene can be targeted by simply changing the siRNA sequence is finally paying off, at least when the tissue and target cell are shared. The liver has proven to be an organ that is easy to access after intravenous administration, because it is highly vascularized and its main function is to screen the blood for foreign compounds or materials such as nanoparticles. The liver endothelium is naturally fenestrated, allowing passage of particles as large as ~80nm SNALPs to the hepatocyte.

Nevertheless, other tissues are difficult to reach. Adapting lipid nanoparticles (LNPs) to improve the delivery to other tissues has been the aim of this thesis. Those and other possible improvements will be discussed and summarized in this chapter.

Uptake mechanisms in the liver and beyond

Nanoparticles that are administered intravenously are typically cleared rapidly from the circulation by macrophages in the liver and spleen. To oppose this, nanoparticles are shielded with PEGylated lipids that allow them to circulate longer. However, this surface shielding also prevents contact with target membranes, which is crucial for uptake into the cell and escape from the endosome to achieve high transfection efficiencies. The effect of different PEG-lipids on transfection efficiency *in vitro* has been shown in **Chapter 2**, which is thought to correlate with the extent of PEG-shedding. It is demonstrated that PEG-lipids with more hydrophobic anchors and therefore low rates of dissociation prevent transfection, whereas more loosely anchored lipids dissociate from the surface of the particle and allow interaction with the target cells. Depending on the application, the PEG-shielding should be tuned in order to allow sufficiently long circulation to reach the target tissue but to dissociate in time to facilitate contact with the target cell, whilst still avoiding uptake by liver macrophages. This is the main challenge in adapting LNPs for transfection of other tissues.

The mechanism by which the clinically evaluated SNALPs are preferentially taken up in hepatocytes is elucidated in a paper by Alnylam Pharmaceuticals that also holds the key to reaching other target cells [6]. The clinically used PEG-lipids dissociate from the LNP quickly after intravenous administration, revealing the naked surface of the particle. In the case of particles containing the ionizable DLin-KC2-DMA this surface is close to neutrally charged. This neutral surface charge is important, as it allows Apolipoprotein E (ApoE) to adsorb to it, which did not occur when cationic LNPs were used as a control. ApoE then functions as an endogenous targeting ligand, resulting in uptake into the hepatocytes via the low-density lipoprotein (LDL) receptor (LDLR). This mechanism was validated by using ApoE deficient mice and LDLR deficient mice, in which the particles were not efficiently taken up. By using an exogenous targeting ligand in the form of a lipid-conjugated N-acetylgalactosamine (GalNAc) the uptake could be restored again and by using another strain of knock-out mice, this was verified to happen via the asialoglycoprotein receptor (ASGPR). Furthermore, when the endogenous uptake mechanism was inhibited completely by using high amounts of tightly anchored DSG-PEG lipid there was no liver specific delivery, neither in wild-type mice, but also here this could be restored by exogenous targeting with the GalNAc lipid [6]. This indicates that other exogenous targeting ligands could be used to target cells other than hepatocytes, provided that they are not taken up via endogenous ApoE/LDLR targeting to the liver first. To achieve this, other, more hydrophobic PEG-anchors can be used to extend the circulation time and avoid high first pass accumulation in the liver [7]. In this thesis, a couple of different approaches to conjugate targeting ligands to the LNPs have been explored. In **Chapter 3**, liposome functionalization using "click" chemistry has been described, employing copper-free cyclo-addition with a bicyclononyne(BCN)-lipid for the first time on the surface of liposomes. In **Chapter 6** a follow-up to this approach was investigated, using a dibenzocyclooctyl(DBCO)-phospholipid. Click conjugation via

this lipid was compared to the gold standard of maleimide-thiol coupling as well as a completely new strategy to couple a peptide in a reversible way, to release it at lower pH. In **Chapter 5** it is demonstrated that LNPs that are too heavily PEGylated indeed do not have any cell interaction and transfection efficiency, but when uptake is facilitated by using a coiled-coil forming peptide pair, transfection of the same particle is restored. This demonstrates the concept that cell type specificity can be introduced by a specific ligand, if the unspecific interaction is blocked by PEGs [8].

Still, the cell types that can be treated with nanocarriers is limited by the capacity of such nanocarriers to reach those target cells in the vascular or extravascular space. Fortunately, within the bloodstream itself, there is an important type of target cells, namely the leukocytes. The lab of Dan Peer has done a lot of work on targeting immune cells using SNALPs and the strategy outlined above, of using more hydrophobic PEG-anchors and active targeting ligands. T-helper cells could be targeted by using a CD4 monoclonal antibody conjugated to the SNALP [9] and B-cells could be targeted with anti-CD38 [10]. Doses required to show effective and therapeutic gene silencing were around 1 mg/kg of siRNA. Gene silencing in leukocytes with siRNAs could be beneficial in treating hematological malignancies and improving immunotherapy [11].

Recently, it was shown that by making the LNPs smaller, particles can extravasate easier and penetrate other tissues. The Cullis lab made LNPs of ~35nm in diameter that allowed them to penetrate into the bone marrow and silence the *SOST* gene (encoding the sclerostin protein) in osteocytes in the bones of mice. A complete biodistribution study was not performed, but it is likely that only a small fraction of the total dose ends up in the bone marrow. Indeed, to achieve 50% silencing in the osteocytes, 15 mg/kg of siRNA had to be dosed, as compared to 0.005 mg/kg to reach the same level of silencing in hepatocytes using LNPs with the same ionizable lipid. So although a large enough amount reaches the osteocytes to show an effect on sclerostin expression, it is likely that the vast majority of the dose eventually still goes to the liver. That does not have to lead to any problems if the *SOST* gene is not expressed there, but such high doses of LNPs can cause hepatotoxicity and with the high cost of goods of both the RNA molecules and the LNPs, dosing so high is not ideal [12]. On the other hand, given the architecture of the liver and its physiological function, it may not be realistic to expect that it can ever be completely bypassed. So perhaps, any new type of tissue in which genes can be silenced safely and effectively should be considered a big achievement, provided that it does not cause any hepatotoxicity.

Preparation of LNPs by microfluidic mixing methods

Chapter 2 describes the advancements made with the ionizable aminolipids but the potency of SNALPs can also be improved by using a different preparation method. The SNALPs currently used in clinics are prepared with a method called microfluidic mixing [13–15]. This does not only allow the formation of much smaller particles, like the 35 nm particles mentioned before, but also leads to a different organization of the lipids and RNAs in the formulation and encapsulation efficiencies of close to 100%. With this technique, two solutions of siRNA in aqueous buffer and lipids in ethanol are rapidly mixed using a microfluidic mixing device. This leads to an increase in polarity in the

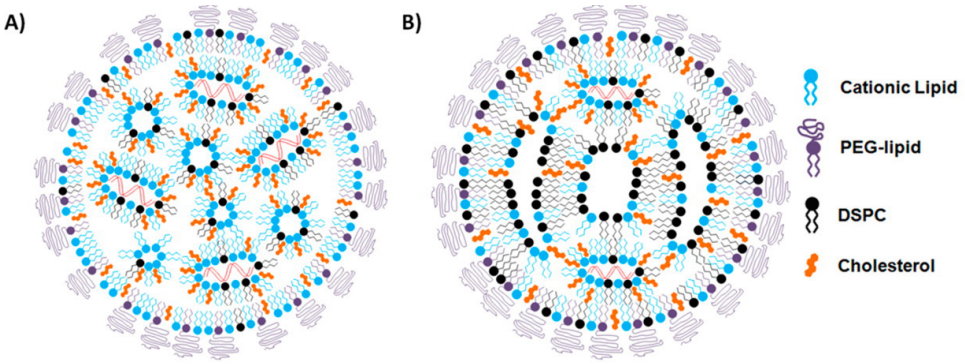

Figure 8.1 | Molecular organization of the clinically used SNALP formulation
RNA molecules are encapsulated in micellar structures, composed predominantly of cationic lipid. PEG-lipids are the last to precipitate during microfluidic synthesis and are therefore deposited on the outside.
A: With low amounts of bilayer-forming helper lipid (DSPC) the core consists only of micellar-like compartments, some of them empty.
B: With higher amounts of stabilizing lipid and cholesterol, more bilayer-like structures are formed, with compartments large enough to also encapsulate mRNA or plasmids. Figure adapted from REF. [15].

ethanolic lipid solution, causing the lipids to precipitate in order of hydrophobicity. The neutral aminolipid-RNA complex precipitates first, forming the core of the particle, followed by DSPC and finally the more hydrophilic PEG-lipids that therefore mainly reside on the outside of the particles. Smaller particles have a bigger surface-to-volume ratio, so when more PEG-lipid was added, smaller particles could be formed. This way, "limit-size" particles could be formed, that are as small as physically possible, considering the dimensions of all the components. For example, the absolute minimum size that can be obtained is a single inverted micelle encapsulating one siRNA molecule, covered with PEG-lipids that is approximately 20nm [13]. When examined by electron microscopy, the SNALPs prepared by microfluidic mixing exhibit an electron rich core with multiple compartments, consistent with the assumption that the siRNA is encapsulated in inverted micelles of the cationic lipid [15,16]. Such an organization explains also why stable particles can still be formed with the aminolipids despite their high propensity to adopt the hexagonal H_{II} phase. The ratio of aminolipid and helper lipid determines the balance between bilayer-like and hexagonal structures and particles with 'mixed phase' cores can also be made by increasing the amount of DSPC, for example to encapsulate bigger cargos like mRNA or plasmid DNA. See Figure 8.1.

LNPs containing nucleic acids prepared with extrusion techniques, similar to the formulations described in **Chapter 2** are organized in concentric bilayers with the nucleic acids sandwiched in between bilayers [17]. Such preparation techniques require higher PEG-lipid percentages to stabilize the particles during formation and are predominantly organized as non-fusogenic bilayers, two additional factors that are likely to decrease their transfection efficiency. So the clinically advanced LNP formulations are superior not only because of the optimized cationic lipids, but also because of the more favorable lipid organization in its core. Such structures cannot be

obtained by preparation with film hydration and extrusion, as LNPs hydrated by the conventional method rather than by microfluidic mixing are likely to aggregate. So the supreme potency of the clinically advanced SNALPs is a combined effect of optimized excipients (novel amino- and PEG-lipids) and an advanced formulation method.

There are several advantages of making smaller LNPs using microfluidic methods, primarily the extent of tissue penetration. The accumulation in bone marrow was already given as an example, but it was found that in general, smaller particles extravasate more and penetrate deeper into tissues. This is especially interesting for tumor tissue, which seems particularly suitable for treatment with nanoparticles because of the Enhanced Permeability and Retention (EPR) effect. This effect is caused by the inherent leakiness of tumor vasculature in fast-growing animal models, through which nanoparticles can extravasate. The true extent of the EPR effect in humans is much debated nowadays, after many nanoparticulate formulations failed to show a real benefit over free drug in human cancer patients [18,19]. Nevertheless, it seems logical that smaller particles can penetrate deeper into interstitial tissue than larger ones [20–22]. The concept of silencing the androgen growth factor receptors on a xenograft prostate tumor with i.v. administered SNALPs has already been demonstrated [23]. It is not certain how this model translates to the human situation, but these particles were ~80nm in diameter and particles smaller than that have not been tested in clinical trials so far.

Another advantage of smaller sized LNPs is that they can be administered via the subcutaneous (s.c.) route and still exhibit efficient gene silencing in the liver. To achieve this, the residence time of the PEG-lipids had to be increased, long enough for the particles to drain via the lymph nodes into the circulation. Particle size influences the degree of lymphatic drainage, as 120nm particles were not able to drain at all, whereas 40nm particles drained completely to the blood compartment. This is an important consideration for the applications targeting immune cells that reside in the lymph nodes. The other benefits of s.c. injection is self-administration by the patient and potentially a prolonged effect due to the depot effect [24]. This would have huge implications for the PCSK9 trial, in which plasma LDL cholesterol was lowered (and thereby the putative risk of coronary heart disease) [25]. If a single s.c. injection every 3 or 6 months could replace the oral intake of statins multiple times a day [26], even an expensive nanoformulation would be considered more attractive. An alternative administration route is a prerequisite for the treatment of chronic indications which would greatly improve the market potential, even if it would be used only in the most high-risk patients.

However, recent insights learned that the potency of LNPs also decreases when their size is reduced. It was found that also the aminolipid has the ability to dissociate from the lipid particle after the PEG-lipid has shedded when particles are beneath a certain size (<30nm). This could be prevented by using PEG-lipids that dissociate slower, but this compromised the transfection efficiency, as was also shown in **Chapter 2**. This once again demonstrates the delicate balance between the transfection potency of LNPs and the residence times of the lipid components and it turns out that particle size is another factor that should be taken into consideration [27,28].

More recent advancements are the co-encapsulation of small molecule drugs in the aqueous core of the LNPs using the same fluidics methods. In an attempt to avoid the high extent of recycling to the extracellular medium (around 70% of the endocytosed LNPs was found to be excreted again [29]) Niemann-Pick C inhibitor NP3.47 was co-encapsulated to inhibit maturation of the endosome after endocytosis [30]. Niemann-Pick C-1 (NPC1) is an important regulator of major recycling pathways of siRNA delivered by LNPs and intracellular retention and gene silencing were increased in NPC1 knockout cells [29]. Inhibition of NPC1 by the inhibitor 3.47 traps the LNPs in the late-endosomes, extending the timeframe in which the particles can escape and avoiding exocytosis. Of note, it is imperative that modified RNAs are used for this application if they are to survive the prolonged exposure to the degrading environment but this approach showed 3-fold higher retention and 4-fold higher gene silencing [30]. Other potential applications are the co-encapsulation of corticosteroids or other immune modulators to dampen the immune response to the LNPs or the co-encapsulation of cytostatic drugs when targeting tumors.

SNALPs already on their return?

The previous sections illustrate that SNALPs are a versatile and the most mature technology. They have convincingly demonstrated that RNAi in humans is feasible and the approval of the first RNAi drug seems within reach. There are several late-stage clinical trials for liver indications and pre-clinical evidence is emerging that there are even more targets than the liver. However, there are indications that industry is already moving away from SNALPs even before the first drug has reached the market, likely because of the complex production and regulatory issues. Such motivations are obviously not documented in scientific literature, but every now and then companies publish a paper that gives a hint as to which direction their R&D department is heading, or which problems they are trying to solve. For example, Arrowhead Pharmaceuticals published about their protease-triggered DPC variant, which could indicate they are facing problems with instability in the bloodstream or during storage with the acid-labile variant [31]. The acid-triggered DPC employs a mechanism for endosomal escape that is similar to the approach with LNPs described in **Chapter 6**. Also there, the acid-labile bond that was used to couple the endosomolytic peptide to the LNPs appeared to not be completely stable at physiological pH. A protease-cleavable bond was also considered in the work with the LNPs and could solve the instability problem there as well. Apart from the safety issues, increased stability is crucial for longer circulation and deposition in extrahepatic tissues. Furthermore it is clear that Arrowhead is also pursuing subcutaneous administration and that paper and others have hinted at the use of other ligands than GalNAcs to target e.g. tumor endothelial cells.

Alnylam has disclosed their on-going efforts to design simplified GalNAc-conjugates based on a linear instead of tri-antennary GalNAc orientation. For optimal recognition by the ASGPR a trivalent GalNAc ligand is crucial, but the redesigned linear variant maintained the same spatial orientation and distance between the sugar moieties but required much fewer synthesis steps. The GalNAc conjugates are produced by solid-phase synthesis which is obviously a huge advantage compared to the other two clinically advanced technologies and the new design further helps to streamline manufacturing and reduce the cost of goods [32,33].

This demonstrates that the competing technologies also keep improving and from the regulatory as well as the production point-of-view, small well-defined conjugates are preferred over large and complex particulate systems. However, there is one major limitation to the conjugate platforms and that is the size of the cargo they can deliver. For both the GalNAc-conjugates and the Dynamic PolyConjugates it is very unlikely that the technology can be adapted to deliver nucleic acids much larger than an siRNA. So although conjugates may gradually be replacing SNALP technology for small RNA therapeutics, there are no alternative synthetic delivery systems for the delivery of mRNA and plasmid DNA [34]. There is a plasmid/mRNA application that has been getting a tremendous amount of attention over the past few years and that is in desperate need of delivery technology: SNALPs may play a role in enabling CRISPR-Cas9 mediated gene editing in humans, similar as they have done in enabling siRNA gene silencing.

The rise of CRISPR-Cas9 gene editing

While the problem of delivering siRNA still has not been solved completely, companies and investors have already jumped on the next hype. The gene editing system CRISPR-Cas9 has made an impact even bigger than RNAi back in the days and there are many similarities between the two technologies. CRISPR is discussed in the context of this thesis because it can also be used to silence genes. However, CRISPR-Cas9 silences genes on the genomic, rather than the transcriptional level, so it has been argued that RNAi is redundant now that CRISPR can provide a permanent solution to what siRNAs can only temporarily (or transiently) address. This certainly has some advantages, for example in genome editing in crops or embryos, but for therapeutic applications in humans, for safety reasons a transient intervention is probably much preferred.

But before treating human patients, the CRISPR-Cas9 construct has to be delivered into the right target cell and another similarity to the RNAi field is that this aspect seems to be heavily underestimated. The mechanism of CRISPR-Cas9 gene editing and potential applications are reviewed in **Chapter 7**. Because it is so cheap, quick and easy to use, it has revolutionized the field of genome editing and keeps on breaking ground in different areas across biology. Similar to RNAi, therapeutic application in human patients is the "final frontier" and the expectations for CRISPR today may even exceed the exuberance about RNAi a decade ago [35]. The fact that Silicon Valley capital is now also flowing into companies dedicated to CRISPR therapeutics illustrates how widely anticipated this technology and its applications are. Napster co-founder and former Facebook president Sean Parker has recently invested 250M$ of his own money to fund the first CRISPR-based immunotherapy trial [36]. This new source of financing will likely benefit the CRISPR field, but the kind of high risk-high return investments that were previously only seen in the IT-sector were also the cause of the quick rise-and-fall of the RNAi field in 2005-2008 [3]. The biomedical field should be careful not to make the same mistake twice of fighting for applications and disease targets, but keeping a blind eye for the daunting challenge of delivery. Investors are easily tempted by promises based on progress made after manipulating cells in a petri-dish, without thinking about translation. And in the meantime, main-stream media are also not really helping to keep expectations realistic as they are also carried away by all the

Figure 8.2 | Altering animal traits using CRISPR-Cas9
CRISPR works well in several species of butterflies (*Papilla xuthus, Papilla machaon*) [39]. This visually appealing example illustrates the power and ease with which CRISPR-Cas can be used to alter genes in animal embryos and eggs. In this example, the wild type (bottom) is darker than the yellow gene knockout (top), and small patches of darker wild-type tissue are observed in the yellow knockout animal, while the wing pattern is maintained. Photo courtesy of Michael Perry and Claude Desplan, New York University, reproduced from REF. [40].

possible applications when the target cells can be manipulated under a microscope in a tissue culture lab, like curing malaria [37] genetically modifying embryos [38] and the captivating idea of changing animal appearances [39]. See Figure 8.2.

However, it is true that there is an incredible amount of applications that *are* possible with the current technology and perhaps human cells are the only ones that are still out of reach [40]. Human embryonal genome editing is impossible for ethical reasons [41,42] and therapeutic editing of somatic cells in the patient is still a technical challenge. Applications that are more feasible at this moment are discussed in **Chapter 7** but it is likely that *ex-vivo* editing applications are the first to move into the clinic.

The constructs that encode the Cas9 enzyme and the guide RNA(s) are fairly big and there is only one report of systemic administration with non-viral carriers so far, by Daniel Anderson's group, who used SNALPs to deliver the Cas9 mRNA to the liver of mice [43]. The CRISPR-Cas9 field is still too young to say whether this will be the go-to delivery method, but it is exemplary for how versatile and robust the SNALP

technology is. It also once again emphasizes the importance of delivery technology to unlock the potential of advanced therapeutics. The fast pace at which the gene editing and silencing systems are developing underscores the need to keep improving the enabling delivery systems. A lot of progress has already been made, but the combined complexity of nanoparticulate carriers and a drug with such intricate dynamics as RNA therapeutics make the safe and efficient application in human patients a significant challenge. New hurdles have been identified along the way and it appears that immunogenicity remains a considerable risk, as late-stage clinical trials still suffer unexpected setbacks [44,45]. However, now that it is generally recognized that RNA therapeutic development coincides with the development of advanced delivery technology, it seems but a matter of time before RNA therapeutics will finally be able to deliver.

References

[1] A. Fire, S. Xu, M.K. Montgomery, S.A. Kostas, S.E. Driver, C.C. Mello, Potent and specific genetic interference by double-stranded RNA in Caenorhabditis elegans., Nature. 391 (1998) 806–11. doi:10.1038/35888.

[2] S.M. Elbashir, J. Harborth, W. Lendeckel, A. Yalcin, K. Weber, T. Tuschl, Duplexes of 21 ± nucleotide RNAs mediate RNA interference in cultured mammalian cells, Nature. 411 (2001) 494–498. doi:10.1038/35078107.

[3] D. Haussecker, The Business of RNAi Therapeutics in 2012, Mol. Ther. — Nucleic Acids. 1 (2012) e8. doi:10.1038/mtna.2011.9.

[4] D.-H. Kim, M.A. Behlke, S.D. Rose, M.-S. Chang, S. Choi, J.J. Rossi, Synthetic dsRNA Dicer substrates enhance RNAi potency and efficacy., Nat. Biotechnol. 23 (2005) 222–226. doi:10.1038/nbt1051.

[5] D. Haussecker, Current issues of RNAi therapeutics delivery and development, J. Control. Release. 195 (2014) 49–54. doi:10.1016/j.jconrel.2014.07.056.

[6] A. Akinc, W. Querbes, S. De, J. Qin, M. Frank-Kamenetsky, K.N. Jayaprakash, et al., Targeted delivery of RNAi therapeutics with endogenous and exogenous ligand-based mechanisms., Mol. Ther. 18 (2010) 1357–1364. doi:10.1038/mt.2010.85.

[7] B.L. Mui, Y.K. Tam, M. Jayaraman, S.M. Ansell, X. Du, Y.Y.C. Tam, et al., Influence of polyethylene glycol lipid desorption rates on pharmacokinetics and pharmacodynamics of siRNA lipid nanoparticles., Mol. Ther. Nucleic Acids. 2 (2013) e139. doi:10.1038/mtna.2013.66.

[8] Y.Y.C. Tam, S. Chen, J. Zaifman, Y.K. Tam, P.J.C. Lin, S. Ansell, et al., Small molecule ligands for enhanced intracellular delivery of lipid nanoparticle formulations of siRNA, Nanomedicine Nanotechnology, Biol. Med. 9 (2013) 665–674. doi:10.1016/j.nano.2012.11.006.

[9] S. Ramishetti, R. Kedmi, M. Goldsmith, F. Leonard, A.G. Sprague, B. Godin, et al., Systemic Gene Silencing in Primary T Lymphocytes Using Targeted Lipid Nanoparticles, ACS Nano. 9 (2015) 6706–6716. doi:10.1021/acsnano.5b02796.

[10] S. Weinstein, I.A. Toker, R. Emmanuel, S. Ramishetti, I. Hazan-Halevy, D. Rosenblum, et al., Harnessing RNAi-based nanomedicines for therapeutic gene silencing in B-cell malignancies, Proc. Natl. Acad. Sci. (2015) 201519273. doi:10.1073/pnas.1519273113.

[11] I. Hazan-Halevy, D. Landesman-Milo, D. Rosenblum, S. Mizrahy, B.D. Ng, D. Peer, Immunomodulation of hematological malignancies using oligonucleotides based-nanomedicines, J. Control. Release. (2016). doi:10.1016/j.jconrel.2016.07.052.

[12] G. Basha, M. Ordobadi, W.R. Scott, A. Cottle, Y. Liu, H. Wang, et al., Lipid Nanoparticle Delivery of siRNA to Osteocytes Leads to Effective Silencing of SOST and Inhibition of Sclerostin In Vivo, Mol. Ther. Acids. 5 (2016) e363. doi:10.1038/mtna.2016.68.

[13] N.M. Belliveau, J. Huft, P.J. Lin, S. Chen, A.K. Leung, T.J. Leaver, et al., Microfluidic Synthesis of Highly Potent Limit-size Lipid Nanoparticles for In Vivo Delivery of siRNA., Mol. Ther. Nucleic Acids. 1 (2012) e37. doi:10.1038/mtna.2012.28.

[14] C. Walsh, K. Ou, N.M. Belliveau, T.J. Leaver, A.W. Wild, J. Huft, et al., Microfluidic-Based Manufacture of siRNA-Lipid Nanoparticles for Therapeutic Applications, in: 2014: pp. 109–120. doi:10.1007/978-1-4939-0363-4_6.

[15] A.K.K. Leung, Y.Y.C. Tam, S. Chen, I.M. Hafez, P.R. Cullis, Microfluidic Mixing: A General Method for Encapsulating Macromolecules in Lipid Nanoparticle Systems, J. Phys. Chem. B. 119 (2015) 8698–8706. doi:10.1021/acs.jpcb.5b02891.

[16] A.K.K. Leung, I.M. Hafez, S. Baoukina, N.M. Belliveau, I. V. Zhigaltsev, E. Afshinmanesh, et al., Lipid nanoparticles containing siRNA synthesized by microfluidic mixing exhibit an electron-dense nanostructured core, J. Phys. Chem. C. 116 (2012) 18440–18450. doi:10.1021/jp303267y.

[17] N. Maurer, K.F. Wong, H. Stark, L. Louie, D. McIntosh, T. Wong, et al., Spontaneous entrapment of polynucleotides upon electrostatic interaction with ethanol-destabilized cationic liposomes., Biophys. J. 80 (2001) 2310–2326. doi:10.1016/S0006-3495(01)76202-9.

[18] J.W. Nichols, Y.H. Bae, EPR: Evidence and fallacy., J. Control. Release. 190 (2014) 451–64. doi:10.1016/j.jconrel.2014.03.057.

[19] F. Danhier, To exploit the tumor microenvironment: Since the EPR effect fails in the clinic, what is the future of nanomedicine?, J. Control. Release. 244 (2016) 108–121. doi:10.1016/j.jconrel.2016.11.015.

[20] L. Huang, B. Sullenger, R. Juliano, The role of carrier size in the pharmacodynamics of antisense and siRNA oligonucleotides., J. Drug Target. 18 (2010) 567–74. doi:10.3109/10611861003734019.

[21] H. Cabral, Y. Matsumoto, K. Mizuno, Q. Chen, M. Murakami, M. Kimura, et al., Accumulation of sub-100 nm polymeric micelles in poorly permeable tumours depends on size, Nat. Nanotechnol. 6 (2011) 815–823. doi:10.1038/nnano.2011.166.

[22] A. Albanese, A.K. Lam, E.A. Sykes, J. V. Rocheleau, W.C.W. Chan, Tumour-on-a-chip provides an optical window into nanoparticle tissue transport, Nat. Commun. 4 (2013). doi:10.1038/ncomms3718.

[23] J.B. Lee, K. Zhang, Y.Y.C. Tam, Y.K. Tam, N.M. Belliveau, V.Y.C. Sung, et al., Lipid nanoparticle siRNA systems for silencing the androgen receptor in human prostate cancer in vivo, Int. J. Cancer. 131 (2012) 781–790. doi:10.1002/ijc.27361.

[24] S. Chen, Y.Y.C. Tam, P.J.C. Lin, A.K.K. Leung, Y.K. Tam, P.R. Cullis, Development of lipid nanoparticle formulations of siRNA for hepatocyte gene silencing following subcutaneous administration, J. Control. Release. 196 (2014) 106–112. doi:10.1016/j.jconrel.2014.09.025.

[25] K. Fitzgerald, M. Frank-Kamenetsky, S. Shulga-Morskaya, A. Liebow, B.R. Bettencourt, J.E. Sutherland, et al., Effect of an RNA interference drug on the synthesis of proprotein convertase subtilisin/kexin type 9 (PCSK9) and the concentration of serum LDL cholesterol in healthy volunteers: a randomised, single-blind, placebo-controlled, phase 1 trial., Lancet. 383 (2014) 60–8. doi:10.1016/S0140-6736(13)61914-5.

[26] K. Fitzgerald, S. White, A. Borodovsky, B.R. Bettencourt, A. Strahs, V. Clausen, et al., A Highly Durable RNAi Therapeutic Inhibitor of PCSK9, N. Engl. J. Med. (2016) NEJMoa1609243. doi:10.1056/NEJMoa1609243.

[27] S. Chen, Y.Y. Tam, P.J. Lin, M.M. Sung, Y.K. Tam, P.R. Cullis, Influence of particle Size on the in vivo potency of lipid nanoparticle formulations of siRNA, J Control Release. 235 (2016) 236–244. doi:10.1016/j.jconrel.2016.05.059.

[28] Y. Sato, Y. Note, M. Maeki, N. Kaji, Y. Baba, M. Tokeshi, et al., Elucidation of the physicochemical properties and potency of siRNA-loaded small-sized lipid nanoparticles for siRNA delivery, J. Control. Release. 229 (2016) 48–57. doi:10.1016/j.jconrel.2016.03.019.

[29] G. Sahay, W. Querbes, C. Alabi, A. Eltoukhy, S. Sarkar, C. Zurenko, et al., Efficiency of siRNA delivery by lipid nanoparticles is limited by endocytic recycling., Nat. Biotechnol. 31 (2013) 653–8. doi:10.1038/nbt.2614.

[30] H. Wang, Y.Y.C. Tam, S. Chen, J. Zaifman, R. van der Meel, M.A. Ciufolini, et al., The Niemann-Pick C1 Inhibitor NP3.47 Enhances Gene Silencing Potency of Lipid Nanoparticles Containing siRNA, Mol. Ther. (2016). doi:10.1038/mt.2016.179.

[31] D.B. Rozema, A. V. Blokhin, D.H. Wakefield, J.D. Benson, J.C. Carlson, J.J. Klein, et al., Protease-triggered siRNA delivery vehicles, J. Control. Release. 209 (2015) 57–66. doi:10.1016/j.jconrel.2015.04.012.

[32] S. Matsuda, K. Keiser, J.K. Nair, K. Charisse, R.M. Manoharan, P. Kretschmer, et al., siRNA Conjugates Carrying Sequentially Assembled Trivalent N- Acetylgalactosamine Linked Through Nucleosides Elicit Robust Gene Silencing In Vivo in Hepatocytes, ACS Chem. Biol. 10 (2015) 1181–1187. doi:10.1021/cb501028c.

[33] K.G. Rajeev, J.K. Nair, M. Jayaraman, K. Charisse, N. Taneja, J. O'Shea, et al., Hepatocyte-Specific Delivery of siRNAs Conjugated to Novel Non-nucleosidic Trivalent N -Acetylgalactosamine Elicits Robust Gene Silencing in Vivo, ChemBioChem. 16 (2015) 903–908. doi:10.1002/cbic.201500023.

[34] K.J. Kauffman, M.J. Webber, D.G. Anderson, Materials for non-viral intracellular delivery of messenger RNA therapeutics, J. Control. Release. 240 (2016) 227–234. doi:10.1016/j.jconrel.2015.12.032.

[35] D. Haussecker, Stacking up CRISPR against RNAi for therapeutic gene inhibition, FEBS J. (2016). doi:10.1111/febs.13742.

[36] S. Reardon, First CRISPR clinical trial gets green light from US panel, Nature. (2016). doi:10.1038/nature.2016.20137.

[37] A. Hammond, R. Galizi, K. Kyrou, A. Simoni, C. Siniscalchi, D. Katsanos, et al., A CRISPR-Cas9 gene drive system targeting female reproduction in the malaria mosquito vector Anopheles gambiae, Nat. Biotechnol. 34 (2016) 78–83. doi:10.1038/nbt.3439.

[38] P. Liang, Y. Xu, X. Zhang, C. Ding, R. Huang, Z. Zhang, et al., CRISPR/Cas9-mediated gene editing in human tripronuclear zygotes, Protein Cell. 6 (2015) 363–372. doi:10.1007/s13238-015-0153-5.

[39] X. Li, D. Fan, W. Zhang, G. Liu, L. Zhang, L. Zhao, et al., Outbred genome sequencing and CRISPR/Cas9 gene editing in butterflies, Nat. Commun. 6 (2015) 8212. doi:10.1038/ncomms9212.

[40] R. Barrangou, J.A. Doudna, Applications of CRISPR technologies in research and beyond, Nat. Biotechnol. 34 (2016) 933–941. doi:10.1038/nbt.3659.

[41] J. Travis, Germline editing dominates DNA summit, Science (80-.). 350 (2015) 1299–1300. doi:10.1126/science.350.6266.1299.

[42] K.S. Bosley, M. Botchan, A.L. Bredenoord, D. Carroll, R.A. Charo, E. Charpentier, et al., CRISPR germline engineering—the community speaks, Nat. Publ. Gr. 33 (2015) 478–486. doi:10.1038/nbt.3227.

[43] H. Yin, C.-Q. Song, J.R. Dorkin, L.J. Zhu, Y. Li, Q. Wu, et al., Therapeutic genome editing by combined viral and non-viral delivery of CRISPR system components in vivo, Nat. Biotechnol. 34 (2016) 328–333. doi:10.1038/nbt.3471.

[44] D. Lowe, Alnylam Blindsided, (2016). http://blogs.sciencemag.org/pipeline/archives/2016/10/06/alnylam-blindsided.

[45] H. Ledford, Investors flee as firm scraps RNA-interference drug candidate, Nature. (2016). doi:10.1038/nature.2016.20769.

Appendices

Nederlandse Samenvatting
Curriculum Vitae
List of Publications

RNA interferentie en lipide nanodeeltjes

Het onderzoek dat in dit proefschrift beschreven is richt zich op de toediening van RNA therapeutica met behulp van lipide nanodeeltjes. In 2006 ontvingen Craig Mello en Andrew Fire de Nobelprijs voor Fysiologie en Geneeskunde voor hun ontdekking van RNA interferentie (RNAi) met dubbelstrengs RNA (dsRNA), waarmee elk gewenst eiwit zeer specifiek geremd kan worden. Elk eiwit in de natuur is gecodeerd in het DNA, waar vervolgens een transcript van gemaakt wordt in de vorm van (m)RNA, wat op zijn beurt de blauwdruk vormt voor de productie van het eiwit via het proces van translatie. Mello en Fire ontdekten dat door een dubbelstrengs RNA molecuul (dsRNA) de cel in te brengen, met een antisense sequentie die complementair is aan het mRNA, dit mRNA afgebroken kan worden, waarmee de expressie van het eiwit geremd wordt. Dit mechanisme is van onschatbare waarde geweest in het ophelderen van allerlei cellulaire processen, door eiwitten één voor één uit te schakelen met behulp van RNAi en daar het effect van te bestuderen. Dit heeft geholpen allerlei nieuwe aangrijpingspunten voor geneesmiddelen te identificeren en al snel daarna werd voorgesteld om RNAi zélf als geneesmiddel te gebruiken om een eiwit dat een ziekte teweeg brengt, specifiek uit te schakelen.

Het bleek echter veel moeilijker dan gedacht om dit mechanisme dat in het lab slechts een simpele handeling vergt, om te vormen tot een succesvolle en veilige ingreep in menselijke patiënten. Dit komt vooral omdat RNA moleculen fysisch-chemische eigenschappen hebben die ze erg ongeschikt maakt als geneesmiddel. Zo zijn ze bijvoorbeeld vele malen groter dan een conventioneel therapeutisch molecuul en heeft een siRNA (van het Engelse small interfering RNA, het meest gebruikte RNA therapeuticum) 42 negatieve ladingen. Door deze grootte en negatieve lading kan het onmogelijk het membraan van de cel passeren waarin het moet werken en daarnaast wordt RNA afgebroken door nucleases als het in vrije vorm in de bloedbaan wordt toegediend. Bovendien kan het immuunsysteem geactiveerd worden door kleine RNA's, omdat deze in vrije vorm niet in het lichaam voor horen te komen en normaliter een teken zijn dat er een virusinfectie gaande is.

Om deze therapeutische RNA's te beschermen tegen afbraak en immuunreacties en om hun toegang tot de cel te faciliteren, worden nanotechnologische toedieningssystemen gebruikt. De systemen waar dit onderzoek zich op richt zijn lipide deeltjes. Dit zijn een soort capsules van vet-achtige stoffen van ongeveer honderd nanometer groot die via de bloedbaan toegediend worden. Hierin zitten de RNA therapeutica verpakt om ze te beschermen, totdat ze de cel bereikt hebben waarin ze moeten werken. Door deze lipide nanodeeltjes uit te rusten met specifieke herkenningsmoleculen kan het opnamepatroon gestuurd worden in de richting van de cellen waarin het eiwit dat geremd moet worden tot expressie komt. Na intracellulaire opname van het nanodeeltje komt het terecht in het endosoom, een compartiment dat opgenomen stoffen sorteert en ze weer uitscheidt of ze verplaatst naar het lysosoom, een ander intracellulair compartiment dat deze stoffen afbreekt. Dit is uiteraard niet het gewenste pad dat de nanodeeltjes moeten afleggen, dus na intracellulaire opname is ontsnapping uit het endosoom ook een barrière die overwonnen dient te worden. Aan deze uitdagingen is gewerkt en de bevindingen daarvan zijn opgeschreven in dit proefschrift. Het uiteindelijke doel is om de hoeveelheid therapeutisch RNA dat intact afgegeven wordt in de cel te verhogen.

Overzicht van dit proefschrift

In **Hoofdstuk 2** worden de componenten van een lipide nanodeeltje besproken, namelijk een cationisch 'fusogeen' lipide, een helper lipide, een gePEGyleerd lipide en cholesterol. Het helper lipide en cholesterol zorgen er voornamelijk voor dat het geheel zich tot een stabiel deeltje vormt. Het cationische lipide moet interactie aangaan met negatief geladen biologische membranen, zoals het celmembraan en het membraan van het endosoom. Het gePEGyleerde lipide zorgt ervoor dat de nanodeeltjes niet herkend worden door het immuunsysteem, maar dit zorgt er tevens voor dat de interactie met de biologische membranen verhinderd wordt. In dit hoofdstuk wordt experimenteel aangetoond dat succesvolle transfectie afhankelijk is van het tijdig dissocieren van het PEG-lipide, om de interactie met het celmembraan mogelijk te maken. Na toediening in de bloedbaan zal de situatie anders zijn dan de condities in een laboratoriumexperiment en de hoeveelheid en het type PEG-lipide zal hierop aangepast moeten worden. De lipide nanodeeltjes die op dit moment in de kliniek getest worden bevatten een geoptimaliseerd cationisch lipide dat ontwikkeld is om geladen te zijn in het zure milieu van het endosoom maar neutraal in de pH van de bloedbaan. Daarnaast zijn de vetzuurstaarten van dit lipide tweevoudig onverzadigd, waardoor het een conische vorm krijgt. Wanneer de kopgroep van het lipide geladen is gaat het een interactie aan met de veelal negatief geladen lipiden van biologische membranen en mede door deze conische vorm faciliteert dit ontsnapping uit het endosoom. De nanodeeltjes die dit geavanceerde lipide bevatten zijn daardoor vele malen efficienter dan de deeltjes die wij kunnen maken in het laboratorium. Om deze reden is er in dit proefschrift gezocht naar andere manieren om de opname en ontsnapping uit het endosoom te verbeteren en zo de afgifte van RNA therapeutica in de cel te verhogen.

In **Hoofdstuk 3** worden lipide nanodeeltjes uitgerust met een herkennings ligand om ze specifiek aan een bepaald type cel te laten binden. Hiervoor wordt kopervrije "klik-chemie" gebruikt, door een lipide te maken dat een reactieve bicyclononyne (BCN) groep bevat en een recombinant tot expressie gebracht 'DARPin'-ligand dat een azide bevat, door het inbouwen van een onnatuurlijke aminozuur. De BCN groep faciliteert de "klik"-reactie zonder toevoeging van Cu^+ ionen als katalysator, wat een voordeel is als deze lipide deeltjes in biologische systemen gebruikt moeten worden, aangezien Cu^+ daar toxisch kan zijn. Dit is de eerste keer dat de kopervrije variant van deze "klik"-reactie op het oppervlakte van lipide deeltjes is beschreven.

Om verschillende deeltjes op een eerlijke en structurele manier te kunnen vergelijken, moeten deze goed gekarakteriseerd zijn. Een belangrijk onderdeel van deze karakterisatie is het bepalen van de hoeveelheid RNA die in het deeltje zit en het vaststellen of deze daar daadwerkelijk in zit, of slechts aan het oppervlakte 'vastgeplakt' is. (In dat laatste geval is het alsnog gevoelig voor afbraak door nucleases en gaat het hoogstwaarschijnlijk niet intact mee de cel in als het deeltje wordt opgenomen). In **Hoofdstuk 4** werd vastgesteld dat in een groot deel van de wetenschappelijke publicaties over lipide nanodeeltjes voor RNA therapeutica, de karakterisatie van de RNA belading heel summier of zelfs helemaal niet beschreven is. Daar bovenop komt nog de grote variatie in de gebruikte methodes in de publicaties waar het wel beschreven staat en wordt er zelden rekening gehouden met eventuele verstoringen die

componenten van het toedieningssysteem (zoals lipiden) kunnen hebben op sommige analysemethodes. Daarom wordt in dit hoofdstuk een voorbeeld beschreven van hoe de analyse van de RNA belading op een herhaalbare en systematische manier gedaan zou kunnen worden. Om de grootste verontreiningen te verwijderen wordt het RNA geëxtraheerd van de lipiden en dat wordt vervolgens geanalyseerd met verschillende methoden. De resultaten in dit hoofdstuk kunnen als richtlijn dienen voor een meer gestandaardiseerde methode van analyse zodat bevindingen in wetenschappelijke publicaties beter gerapporteerd worden en dat resultaten van verschillende labs beter vergeleken kunnen worden.

Hoofdstuk 5 gaat wederom in op het specifiek sturen van lipide nanodeeltjes naar een bepaald celtype. In dit hoofdstuk wordt een peptide-paar gebruikt, dat aan elkaar plakt als een soort 'moleculair klittenband'. Het ene peptide is gekoppeld aan de nanodeeltjes en het andere is vastgezet op het membraan van de cel waaraan iets afgeleverd moet worden. De interactie tussen deze peptiden is zeer specifiek en maakt het mogelijk onderscheid te maken tussen cellen die wel en die niet met het peptide uitgerust zijn, los van bestaande oppervlakte eiwitten die normaal gesproken als herkenningsmolecuul worden gebruikt. Na binding van de nanodeeltjes aan de cellen via de peptide-interactie worden deze deeltjes opgenomen en zijn ze in staat twee verschillende soorten model RNA therapeutica intracellulair af te geven. Dit hoofdstuk toont ook aan dat nanodeeltjes die op zichzelf geen interactie hebben met de cel doordat ze te sterk gePEGyleerd zijn, wel specifieke interactie aangaan als ze uitgerust zijn met deze herkenningsmoleculen. Ongemodificeerde nanodeeltjes hebben geen interactie maar enkel als gevolg van de combinatie van de twee verschillende peptiden worden de deeltjes opgenomen en geven ze hun belading af in de cel.

In **Hoofdstuk 6** wordt een strategie onderzocht om de ontsnapping uit het endosoom efficiënter te maken. In plaats van herkenningsmoleculen worden membraan-actieve peptiden aan de lipide nanodeeltjes gekoppeld. Deze membraan-actieve peptiden zouden het endosomale membraan lek moeten prikken of zelfs op laten lossen, zodat de deeltjes vrij kunnen komen uit het endosoom. Hiervoor worden verschillende manieren van koppeling onderzocht, waaronder een nieuwe vorm van "klik"-chemie (als verbetering van de methode beschreven in **Hoofdstuk 3**). Daarnaast is een manier om het peptide reversibel te koppelen onderzocht, zodat het loskomt in zure omgeving. Het peptide dat gebruikt is, is melittine dat afkomstig is uit bijengif. Onze bevindingen toonden aan dat verankering van het peptide zijn membraan-actieve werking vermindert, waarschijnlijk omdat in vrije vorm moet clusteren met andere peptide-moleculen voor optimale werking. Bovendien ging de activiteit van melittine achteruit als de pH verlaagd werd, terwijl het juist actief zou moeten zijn in het zure milieu van het endosoom. Om dit op te lossen werd gekozen om een reversibele binding te gebruiken om melittine los te laten koppelen van het lipide deeltje als het de zure omgeving van het endosoom bereikt heeft zodat het daar in zijn meest actieve, vrije vorm is. Daarnaast werd een andere variant van melittine gezocht, waarvan de activiteit hersteld wordt in zuur milieu en dat juist veel minder krachtig is in neutrale pH. De combinatie van deze factoren zorgt ervoor dat melittine veel effectiever is in de endosomale omgeving waar we willen dat het werkt en dat het hele nanodeeltje een stuk veiliger is om toe te dienen in de bloedbaan waar de pH neutraal is, omdat het risico dat het peptide interactie aangaat met andere biologische membranen sterk verminderd is.

Hoofdstuk 7 is een literatuuroverzicht over CRISPR-Cas9, een nieuwe ontwikkeling in de biotechnologie, die het mogelijk maakt expressie van eiwitten te remmen op DNA-niveau en zelfs volledige genen te corrigeren. Er wordt nu al gezegd dat deze ontdekking van vergelijkbare waarde is als de ontdekking van RNA interferentie en er wordt zelfs al gespeculeerd dat ook hiervoor ooit een Nobelprijs wordt uitgereikt. Een andere vergelijking met RNAi is dat ook hier enorm hoog gespannen verwachtingen zijn over de mogelijkheid om dit systeem in te zetten als een geneesmiddel, maar wederom wordt de transitie naar toepassing van dit systeem in de mens ernstig onderschat. De genetische constructen die coderen voor het CRISPR-Cas9 systeem zijn vele malen groter dan RNA therapeutica en daardoor in theorie dus nog veel moeilijker om intracellulair af te geven. Lipide nanodeeltjes zijn voor RNA therapeutica een van de meest vergevorderde toedieningssystemen en het is al aangetoond dat ze ook aangepast zouden kunnen worden om CRISPR-Cas9 systemen af te geven. Desalniettemin lijkt het nog een behoorlijke uitdaging om CRISPR-Cas9 op therapeutische wijze te gebruiken in patiënten, al helemaal via systemische toediening, zoals besproken wordt in dit hoofdstuk. De meest voor de hand liggende toepassingen berusten op manipulatie van de cellen buiten het lichaam, dus in het lab, die daarna teruggespoten worden in de patiënt. Mogelijk zullen de eerste van deze toepassingen binnen enkele jaren getest kunnen worden in menselijke patiënten. Daarna zal blijken of toepassing van CRISPR-Cas9 als geneesmiddel net zo'n opgave is als de toepassing van RNAi.

Conclusies

RNA interferentie wordt al jaren gezien als een veelbelovende techniek om voorheen onbehandelbare ziekten te behandelen of te genezen. De toepassing ervan in patiënten wordt echter verhinderd door de ongunstige eigenschappen van de therapeutische RNA moleculen en te lang werd de noodzaak van geavanceerde toedieningsvormen om dit mogelijk te maken onderschat. Toediening met behulp van lipide nanodeeltjes is een geavanceerde techniek die hiervoor uitkomst biedt, maar er zijn nog verschillende verbeteringen mogelijk. In dit proefschrift worden verschillende strategieën onderzocht om zowel de opname van de deeltjes in de cel, als de ontsnapping ervan uit het endosoom te verbeteren. Klinisch onderzoek naar lipide nanodeeltjes voor RNA therapeutica is al vergevorderd en het valt te verwachten dat RNAi in menselijke patiënten binnen enkele jaren realiteit zal worden.

Curriculum vitae

Erik Oude Blenke was born on 31 October 1987 in Eindhoven, The Netherlands. After finishing his Gymnasium at the Van Maerlantlyceum, Eindhoven in 2006 he started his bachelor of Pharmacy at the University of Utrecht. During his master program Drug Innovation he performed a 9 month internship at the Department of Pharmaceutics at Utrecht University investigating the role of apolipoprotein C1 in the development of the inflammatory tumor microenvironment under the supervision of Prof. Dr. Raymond Schiffelers. After this, he did a 6 month internship at the Department of Pharmacy at the University of Copenhagen, Denmark. This work focused on CPP-functionalized lipid systems for siRNA delivery and was supervised by Dr. Hanne Mørck Nielsen and Dr. Camilla Foged. He received his MSc. diploma in 2012 and started his PhD project in 2013, at the Department of Pharmaceutics, Utrecht University supervised by Dr. Enrico Mastrobattista. This work was carried out in the EU Innovative Medicines Initiative (IMI) funded COMPACT consortium. This consortium aimed to Collaborate on the Optimization of Macromolecular Pharmaceutical Access to Cellular Targets and Erik's research project specifically focussed on the intracellular delivery of therapeutic nucleic acids. The results of this work are presented in this PhD thesis.

Publications from this thesis

E. Oude Blenke, G. Klaasse, H. Merten, A. Plückthun, E. Mastrobattista, N.I. Martin, Liposome functionalization with copper-free "click chemistry," J. Control. Release. 202 (2015) 14–20. doi:10.1016/j.jconrel.2015.01.027.

E. Oude Blenke, J. van den Dikkenberg, B. van Kolck, A. Kros, E. Mastrobattista, Coiled coil interactions for the targeting of liposomes for nucleic acid delivery, Nanoscale. 8 (2016) 8955–8965. doi:10.1039/C6NR00711B.

E. Oude Blenke, M.J.W. Evers, E. Mastrobattista, J. van der Oost, CRISPR-Cas9 gene editing: Delivery aspects and therapeutic potential, J. Control. Release. (2016) *in press* doi:10.1016/j.jconrel.2016.08.002.

E. Oude Blenke, M.J.W. Evers, V. Baumann, J. Winkler, G. Storm, E. Mastrobattista, Critical evaluation of quantification techniques for siRNA formulated in lipid nanoparticles, *submitted for publication*

E. Oude Blenke, M. Sleszynska, M.J.W. Evers, G. Storm, N.I. Martin, E. Mastrobattista, Strategies for the activation and release of the membranolytic peptide melittin from liposomes using endosomal pH as a trigger, *submitted for publication*

Other publications

E. Oude Blenke, E. Mastrobattista, R.M. Schiffelers, Strategies for triggered drug release from tumor targeted liposomes., Expert Opin. Drug Deliv. 10 (2013) 1399–410. doi:10.1517/17425247.2013.805742.

Y. Shi, R. van der Meel, B. Theek, **E. Oude Blenke**, E.H.E. Pieters, M.H.A.M. Fens, et al., Complete Regression of Xenograft Tumors upon Targeted Delivery of Paclitaxel via ∏–∏ Stacking Stabilized Polymeric Micelles, ACS Nano. 9 (2015) 3740–3752. doi:10.1021/acsnano.5b00929.

X. Zeng, A.M. de Groot, A.J.A.M. Sijts, F. Broere, **E. Oude Blenke**, S. Colombo, et al., Surface coating of siRNA–peptidomimetic nano-self-assemblies with anionic lipid bilayers: enhanced gene silencing and reduced adverse effects in vitro, Nanoscale. 7 (2015) 19687–19698. doi:10.1039/C5NR04807A.

“You mustn’t be afraid to dream a little bigger, darling.” - *Eames (Inception)*

Appendices

Acknowledgements / Dankwoord

Four years is a very long time to work on something with so much dedication that it occupies your mind day and night. Such an experience changes and shapes you as a person, but it is also inevitable that it eventually makes you grow weary of it. Sometimes I wish I could have back the passion that I had in the early years, but I think that if I hadn't learned so much along the way, I wouldn't feel so different about things now.

I am extremely grateful for all the things I've learned and experienced and for all the people that I've met and who taught me. I look back at these four years with gratitude and great satisfaction and I would like to use these final pages to thank the people who helped me accomplish this.

So thanks so very much, to all the people from Biopharmacy, my fellow PhD students, professors, staff, technicians and Master students. To all my friends within the group, and in the other UIPS groups and the UMC.

And thanks to all my friends and family outside science, it is good to get your mind on other things sometimes too!

The problem with these acknowledgements is that the more people I mention, the bigger the risk someone important feels forgotten or left out, but there are a couple of people that I *have* to thank with a personal note:

Enrico, bedankt voor de mooie (en minder mooie) tijden die we gehad hebben tijdens onze vele consortium trips en voor alles wat ik van je geleerd heb. Vooral in de eerste jaren hebben we veel wetenschappelijke discussies gehad en je was voor mij de ideale begeleider: je gaf me veel vrijheid op het lab en tijdens meetings was je kritisch als ik positief was en altijd opbeurend en vol met nieuwe ideeën als ik ergens negatief of teleurgesteld over was. In de laatste jaren hebben we het ook vaak gehad over de academische wereld en de verschillen met de industrie, de professionaliteit en omgang met mensen en over het publicatie/review proces. Ik denk dat we hier altijd grotendeels op één lijn zaten, maar dat we elk onze eigen conclusies daarover trokken. Je optimisme en welwillendheid zijn bewonderenswaardig en zullen een voorbeeld zijn voor de rest van mijn carrière. Bedankt voor de goede samenwerking!

Nathaniel, although you were only officially added to my supervising team in the latest stage, you were on board since my first year. I remember our projects as the most efficient collaborations ever, where there was a clear division in tasks and we knew each other's expertises very well. The publication of the "click liposomes" paper before the end of my second year really helped to boost my confidence that I could do this PhD-thing and paved the way for a pretty smooth ride until the end. I'm very happy to see things going so well for you and your group and I'm sure we will hear a lot more from you in the coming years. It was a pleasure to work with you! And I know this will look weird writing it here, but also thanks for all the drugs ;)

Beste Gert, vanaf het begin was duidelijk afgesproken dat Enrico de inhoudelijke begeleiding zou doen, dus aanvankelijk gingen onze gesprekken vooral over onze gedeelde liefde voor Carrie Mathison en Homeland. De 'supervisor meetings' met jou en Enrico kenmerkten zich door zoveel gezelligheid en sterke verhalen dat *ik* degene moest zijn die orde moest houden. Maar daarnaast waren deze meetings ook heel

effectief en was je er altijd als er belangrijke zaken geregeld moesten worden (in deze context ook dank aan Barbara voor het regelen van alle formulieren!). Bedankt voor de goede werksfeer en het vertrouwen en voor de vooral gezellige samenwerking!

Beste Wim, omdat we niet direct hebben samengewerkt moesten onze 'meetings' plaatsvinden onder het genot van een biertje of whisky, op vrijdag in het DDW, op congressen, of in het baseball-stadion in Seattle. Ondanks dat heb ik veel van je geleerd en ik heb me vaak afgevraagd hoe het zou zijn als we echte workmeetings gehad zouden hebben. Je directe en soms wat ongenuanceerde manier van benaderen heeft je een bepaalde reputatie gegeven, maar veel mensen hebben half niet door hoe goed je het met ze voor hebt. Wat dat betreft lijken we misschien wel wat op elkaar... Bedankt voor alle anekdotes over de academie, conferenties, hoogleraren, het review-proces en over voormalige AIOs van Biofarmacie...ik hoop dat ik er een paar aan toe heb kunnen voegen.

Mies, bedankt voor alle keren dat we samen hebben gegeten, gebarbecue't, bier of whisky hebben gedronken, een lam uit elkaar gehaald hebben en samen de UPLC vervloekt hebben. Joep, altijd goed om een analist in de buurt te hebben met verstand van goede muziek, speciaalbier en microscopie. Bedankt voor je hulp bij Hoofdstuk 5. Louis, bedankt voor het managen van het biochemielab, waar ik het grootste deel van mijn tijd de afgelopen jaren heb besteed. Roel, bedankt voor je hulp met van alles en nog wat, op het biochemielab, de celkweek of het HPLC lab. Ebel, al mijn *in vivo* skills heb ik van jou geleerd, bedankt voor alle tijd die we in het GDL door hebben gebracht voor Yang's studie.

En dan 'Team Erik', ofwel "de studenten die *wel* wat kunnen"...Floor en Martijn.
Bedankt voor het opheffen van mijn studentenvloek ;) Ik blijf me verbazen dat twee zulke verschillende personen zo goed met elkaar overweg kunnen en ook nog allebei met mij! Bedankt voor de leuke tijd. Ik heb veel van jullie geleerd en ik hoop dat jullie ook nog wat van mij hebben geleerd. Floor, supercool dat je op zo'n toplab stage loopt en dat je het zo naar je zin hebt in Zürich! Martijn, schiet nou toch eens op met het regelen van je eigen PhD, die volgende artikelen moet je echt zelf schrijven hoor ;) #GoTeamErik!!

And finally, my paranymphs. Lies, we kennen elkaar al sinds de bachelor Farmacie en daarna de master Drug Innovation. Leuk dat je na je stage in Kopenhagen ook mijn collega bij Biofarmacie was, met zo'n top-CV moet je haast wel een gouden toekomst tegemoet gaan ;) Fijn dat je ook bij mijn promotie naast me zal staan. Maria, my best buddy over the past year or so, and hopefully for a long time to come. Thanks for also being there with me on my promotion day!

And thanks to ALL the people that I did not mention...I did not forget you.
Without a doubt, the best memory of my PhD is meeting so many people from different countries, cultures and backgrounds and I am very proud and happy to call so many of you my friends.

I will not take this for granted. THANK YOU!!!

Erik